frontiers | Research Topics

Novel targets and state of the art therapies in ARDS and sepsis

Edited by
Shahd Horie, Emma Murphy and Daniel O'Toole

Published in
Frontiers in Medicine
Frontiers in Public Health

ISSN 1664-8714
ISBN 978-2-8325-5705-1
DOI 10.3389/978-2-8325-5705-1

About Frontiers

Frontiers is more than just an open access publisher of scholarly articles: it is a pioneering approach to the world of academia, radically improving the way scholarly research is managed. The grand vision of Frontiers is a world where all people have an equal opportunity to seek, share and generate knowledge. Frontiers provides immediate and permanent online open access to all its publications, but this alone is not enough to realize our grand goals.

Frontiers journal series

The Frontiers journal series is a multi-tier and interdisciplinary set of open-access, online journals, promising a paradigm shift from the current review, selection and dissemination processes in academic publishing. All Frontiers journals are driven by researchers for researchers; therefore, they constitute a service to the scholarly community. At the same time, the *Frontiers journal series* operates on a revolutionary invention, the tiered publishing system, initially addressing specific communities of scholars, and gradually climbing up to broader public understanding, thus serving the interests of the lay society, too.

Dedication to quality

Each Frontiers article is a landmark of the highest quality, thanks to genuinely collaborative interactions between authors and review editors, who include some of the world's best academicians. Research must be certified by peers before entering a stream of knowledge that may eventually reach the public - and shape society; therefore, Frontiers only applies the most rigorous and unbiased reviews. Frontiers revolutionizes research publishing by freely delivering the most outstanding research, evaluated with no bias from both the academic and social point of view. By applying the most advanced information technologies, Frontiers is catapulting scholarly publishing into a new generation.

What are Frontiers Research Topics?

Frontiers Research Topics are very popular trademarks of the *Frontiers journals series*: they are collections of at least ten articles, all centered on a particular subject. With their unique mix of varied contributions from Original Research to Review Articles, Frontiers Research Topics unify the most influential researchers, the latest key findings and historical advances in a hot research area.

Find out more on how to host your own Frontiers Research Topic or contribute to one as an author by contacting the Frontiers editorial office: frontiersin.org/about/contact

Novel targets and state of the art therapies in ARDS and sepsis

Topic editors
Shahd Horie — University of Galway, Ireland
Emma Murphy — Limerick Institute of Technology, Ireland
Daniel O'Toole — University of Galway, Ireland

Citation
Horie, S., Murphy, E., O'Toole, D., eds. (2024). *Novel targets and state of the art therapies in ARDS and sepsis*. Lausanne: Frontiers Media SA.
doi: 10.3389/978-2-8325-5705-1

Table of contents

frontiers | Frontiers in Medicine

TYPE Editorial
PUBLISHED 05 November 2024
DOI 10.3389/fmed.2024.1496821

OPEN ACCESS

EDITED AND REVIEWED BY
Marc Jean Struelens,
Université libre de Bruxelles, Belgium

*CORRESPONDENCE
Daniel O'Toole
✉ daniel.otoole@nuigalway.ie
Shahd Horie
✉ shahd.horie@nuigalway.ie
Emma Murphy
✉ emma.murphy@tus.ie

RECEIVED 15 September 2024
ACCEPTED 17 October 2024
PUBLISHED 05 November 2024

CITATION
O'Toole D, Horie S and Murphy E (2024) Editorial: Novel targets and state of the art therapies in ARDS and sepsis.
Front. Med. 11:1496821.
doi: 10.3389/fmed.2024.1496821

Editorial: Novel targets and state of the art therapies in ARDS and sepsis

Daniel O'Toole[1]*, Shahd Horie[2]* and Emma Murphy[3]*

[1]Discipline of Physiology, University of Galway, Galway, Ireland, [2]Discipline of Anaesthesia, University of Galway, Galway, Ireland, [3]PRISM Research Institute, Technological University of the Shannon, Athlone, Ireland

KEYWORDS

ARDS, sepsis, diagnostics, therapeutics, infection

Editorial on the Research Topic
Novel targets and state of the art therapies in ARDS and sepsis

Acute respiratory distress syndrome (ARDS) and sepsis remain leading causes of patient morbidity and mortality and the COVID-19 pandemic has highlighted the continuing lack of effective therapeutic options for these and other related acute inflammatory conditions. Among the problems facing ARDS researchers is that there is currently no specific biomarker for rapid diagnosis, and adhering to the Berlin consensus criteria (1) and therefore necessitates methods that are time consuming and expensive, particularly in the context of overloaded health care services. Recent hot topics are sub-phenotyping of patients, with clearly delineated hyper- and hypo-inflammatory versions of ARDS being more widely recognized (2) and emerging biomarkers of patient outcome giving clinicians the opportunity to treat these quite distinct disease variants with distinct therapeutic approaches. There are also still no licensed medicine specifically targeting ARDS or sepsis (3), a critical gap in the clinician's arsenal and individual organ and symptom support remains the mainstay (4).

Recently, a host of novel medicinal approaches have been investigated to address these problems, such as advances in the development of pharmacological agents, recombinant protein drugs, and cell and gene therapies. Bioinformatics based approaches and clinical profiling of patients are also paving the way for stratification, targeted therapies, and precision medicines. Here, we summarize breaking contributions to the field in a collection of articles published as part of the Research Topic entitled "*Novel targets and state of the art therapies in ARDS and sepsis*."

Our first review paper explores the utility of measuring mitochondrial markers of ARDS related disease (McClintock et al.). The summarized studies include assessments of mitochondrial DNA in blood, peroxidation markers and a range of metabolites such as glucose, lactate and xanthine and point to a future where simple point of care devices could instantly diagnose ARDS and ARDS severity based on minimal essential parameters. In a patient sample analysis study, Peng et al. have identified dysfunctional iron metabolism mediated via hepcidin as a predictor of patient outcome in COVID-19 ARDS, a finding which could ultimately be applicable to ARDS of any etiology. Finally in this group of manuscripts we have a study of immune cell subpopulations in ARDS patients where it was discovered that the ratio of CD4/CD8 markers was an effective predictor of disease severity and could assist in directing resources and appropriate care to specific sufferers (Pascual-Dapena et al.).

Our second thematic grouping of papers is a deep dive into the pathology and pathobiology of ARDS. Indeed, it could be argued that this Research Topic overlaps with and informs diagnostics and therapeutics and is fundamental to an intelligent approach to ARDS patient care. As well as the alveolar cells of the lung, acute lung injury is also associated with endothelial dysfunction and vascular thrombosis and we are provided with a comprehensive overview of how the Kallikrein-Kinin axis contributes to this disease process (Bailey et al.). Large datasets demand increasingly complex computational approaches to maximize the meaningful information extracted, and so we are happy to welcome from Parkinson et al. a machine learning assisted mRNA profiling of one of the more vulnerable patient populations, that of neonatal sepsis. We also see a single-cell analysis approach to assessment of risk factors for progression of shock to ARDS that has identified the importance of chromatin accessibility near a specific gene locus, CALCRL (Armstead et al.). To round off this section, we have two studies focusing on specific disease mechanisms and their involvement in ARDS and sepsis. Firstly, Liu et al. elucidates the contribution of the ferroptosis pathway in ischemia/reperfusion driven inflammation in a rat model and secondly we have from Hu et al. an intriguing paper detailing the involvement of the C-type lectin pancreatic stone protein in multiple organ dysfunction syndrome (MODS).

In our final subsection we explore approaches to ARDS and sepsis patient management and therapeutics, from refining traditional support protocols to cutting edge advanced therapeutic medicinal products (ATMPs). This theme includes a retrospective sepsis patient analysis comparing saline and Ringers solutions for resuscitation (Isha et al.), followed with a preclinical study from González et al. of a nebulizer delivered stem cell therapy for ARDS, this with the novelty of utilizing the secretome as opposed to the cell itself.

We, the editors of this special edition of Frontiers in Medicine, hope that you, the reader, find this Research Topic to be as informative and interesting as we did when assembling and curating it, and expect that it will spark future research into diagnosing and treating this devastating family of diseases.

Author contributions

DO'T: Writing – original draft, Writing – review & editing. SH: Writing – review & editing. EM: Writing – review & editing.

Conflict of interest

The authors declare that the research was conducted in the absence of any commercial or financial relationships that could be construed as a potential conflict of interest.

Publisher's note

References

1. ARDS Definition Task Force, Ranieri VM, Rubenfeld GD, Thompson B, Ferguson N, Caldwell E, et al. Acute respiratory distress syndrome. *JAMA*. (2012) 307:2526–33. doi: 10.1001/jama.2012.5669

2. Gordon AC, Alipanah-Lechner N, Bos LD, Dianti J, Diaz JV, Finfer S, et al. From ICU syndromes to ICU subphenotypes: consensus report and recommendations for developing precision medicine in the ICU. *Am J Respir Crit Care Med*. (2024) 210:155–166. doi: 10.1164/rccm.202311-2086SO

3. Battaglini D, Iavarone IG, Rocco PR. An update on the pharmacological management of acute respiratory distress syndrome. *Expert Opin Pharmacother*. (2024) 25:1229–1247. doi: 10.1080/14656566.2024.2374461

4. Battaglini D, Fazzini B, Silva PL, Cruz FF, Ball L, Robba C, et al. Challenges in ARDS definition, management, and identification of effective personalized therapies. *J Clin Med*. (2023) 12:1381. doi: 10.3390/jcm 12041381

frontiers | Frontiers in Public Health

SYSTEMATIC REVIEW
published: 26 April 2022
doi: 10.3389/fpubh.2022.881412

The Relationship Between Hepcidin-Mediated Iron Dysmetabolism and COVID-19 Severity: A Meta-Analysis

Denggao Peng[1,2], *Yanzhang Gao*[1], *Li Zhang*[1], *Zhichao Liu*[1], *Huan Wang*[1] and *Yingxia Liu*[1,2]*

[1] Shenzhen Third People's Hospital, Second Hospital Affiliated to Southern University of Science and Technology, Shenzhen, China, [2] Graduate Collaborative Training Base of Shenzhen Third People's Hospital, Hengyang Medical School, University of South China, Hengyang, China

OPEN ACCESS

Edited by:
Daniel O'Toole,
National University of Ireland
Galway, Ireland

Reviewed by:
Alessia Pagani,
San Raffaele Hospital (IRCCS), Italy
Somdet Srichairatanakool,
Chiang Mai University, Thailand

***Correspondence:**
Yingxia Liu
yingxialiu@hotmail.com

Specialty section:
This article was submitted to Infectious Diseases - Surveillance, Prevention and Treatment, a section of the journal Frontiers in Public Health

Received: 22 February 2022
Accepted: 30 March 2022
Published: 26 April 2022

Citation:
Peng D, Gao Y, Zhang L, Liu Z, Wang H and Liu Y (2022) The Relationship Between Hepcidin-Mediated Iron Dysmetabolism and COVID-19 Severity: A Meta-Analysis. Front. Public Health 10:881412. doi: 10.3389/fpubh.2022.881412

Backgrounds: Hepcidin has been identified as a systemic iron-regulatory hormone. Recent studies have suggested that iron metabolism disorders may be involved in the pathogenesis of acute respiratory distress syndrome and multiple organ dysfunction in coronavirus disease 2019 (COVID-19).

Objectives: To re-evaluate the hepcidin-related iron metabolism parameters and explore the relationship between hepcidin-mediated iron dysmetabolism and COVID-19 severity.

Methods: COVID-19 is classified as mild and moderate as non-severe, severe and critical as severe. A meta-analysis was conducted. Four bibliographic databases were comprehensively searched up to December 31st 2021.

Results: Six unique studies with data from 477 COVID-19 patients were included. Compared to non-severe cases, severe cases had higher hepcidin (standardized mean difference (SMD), −0.39; 95% Confidence Interval (CI) [−0.76, −0.03]; $P = 0.03$) and ferritin (SMD, −0.84; 95% CI [−1.30, −0.38]; $P = 0.0004$). In five out of six studies, a total of 427 patients were tested for serum iron, and there were significant differences in their levels between severe and non-severe cases (SMD, 0.22; 95% CI [0.02, 0.41]; $P = 0.03$). A total of 320 patients from four out of six studies were tested for transferrin saturation, and the statistical difference was not significant (SMD, 0.06; 95% CI [−0.17, 0.28]; $P = 0.64$).

Conclusion: Severe COVID-19 cases had higher serum levels of hepcidin and ferritin, and lower serum iron, without significant differences in transferrin saturation. Further studies are needed to verify whether targeting the hepcidin-mediated iron metabolism axis may influence the outcome and treatment of COVID-19.

Keywords: COVID-19, ferritin, hepcidin, iron metabolism, severity

INTRODUCTION

Since the outbreak of coronavirus disease 2019 (COVID-19) caused by severe acute respiratory syndrome coronavirus 2 (SARS-CoV-2) (1), the number of confirmed cases has increased rapidly around the world (2, 3). Acute respiratory distress syndrome (ARDS) and multiple organ dysfunction are the main clinical manifestations and leading causes of mortality in severe COVID-19 cases (4). Iron homeostasis is crucial for host immune defense and inflammatory response. Disorders of iron metabolism are mainly manifested as iron deficiency and/or overload, both of which can cause cellular and organ dysfunction (5). Low serum iron (SI) concentration restricts hemoglobin synthesis and causes anemia and systemic hypoxemia. Emerging data have found that hypoferremia is an independent risk factor for hypoxic respiratory failure and death in COVID-19 patients (6, 7). The rapid and excessive accumulation of intracellular iron, especially in macrophages, causes cell and tissue damage, presumably through the production of reactive oxygen species (ROS) catalyzed by iron. In addition, iron overload may also trigger a unique iron-dependent form of non-apoptotic cell death termed ferroptosis (8). Serum ferritin concentration has been proven to reflect the individual's iron storage status. Studies have found that increased serum ferritin levels are associated with adverse outcomes (9–11). Although studies on transferrin saturation (TSAT) have been far fewer than that of ferritin and hypoferritemia, low TSAT has been consistently reported in severe COVID-19, and significantly correlated to lung aeration loss, inflammatory markers and worse outcomes (7, 12–14).

The hepatic peptide hepcidin has been identified as the systemic iron-regulatory hormone and plays an important role in maintaining iron homeostasis (15). Hepcidin regulates intestinal iron absorption, SI concentrations, and tissue iron redistribution by inducing the degradation of its receptor, the sole iron exporter ferroportin (14, 16), and blocking ferroportin export activity (17). Serum hepcidin measurement may be a promising tool for assessing the status of iron metabolism (18), but has not been widely implemented in clinical practice (14, 19, 20). Notably, unlike serum ferritin testing that has been documented in guidelines, hepcidin has been rarely measured in COVID-19 patients (13, 21). As expected in severe inflammatory diseases, recent studies have reported that most COVID-19 patients showed varying degrees of upregulation of hepcidin levels (16, 21–25). More importantly, hepcidin levels have significantly negatively correlated with the ratio of arterial oxygen partial pressure (PaO_2) and fraction of inspired oxygen (FiO_2), which can be used to predict COVID-19 severity and mortality (22). To adopt the results for clinical use, these interesting findings need to be validated in wider cohorts, and the relationship between hepcidin-mediated iron dysmetabolism and COVID-19 severity also needs to be further analyzed. In view of the particularity of the prevention and control of the COVID-19 epidemic and the randomness of its incidence, large-scale, multi-center, prospective cohort studies are very difficult to achieve. Here we classify mild and moderate as non-severe, severe, and critical as severe, and conduct a meta-analysis to re-evaluate the hepcidin-related iron metabolism parameters (hepcidin, ferritin, iron, and TSAT) in COVID-19 patients and explore the relationship between iron dysmetabolism and severity.

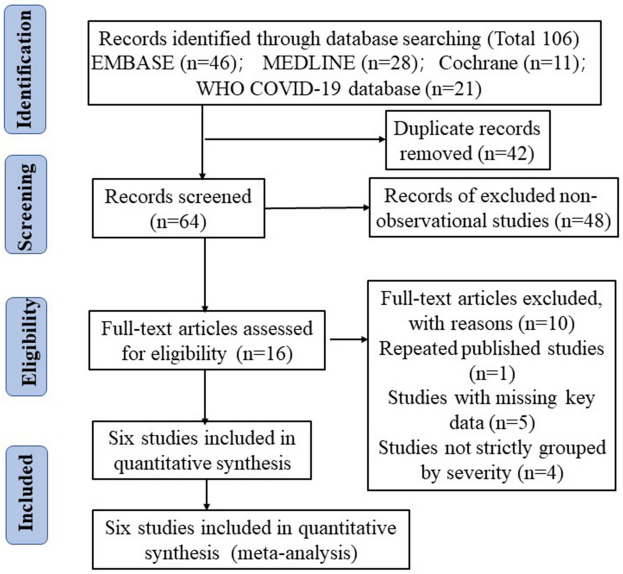

FIGURE 1 | The literature selection process based on the PRISMA flow diagram.

METHODS

Research Strategy

This meta-analysis was performed following a recently published guideline and reported according to PRISMA (Preferred Reporting Items for Systematic Reviews and Meta-Analyses) guidelines (26). We searched comprehensively MEDLINE (National Library of Medicine, US), EMBASE (Elsevier, Netherlands), Cochrane (Cochrane Collaboration, UK), and the WHO COVID-19 database to identify relevant articles up to December 31, 2021. Keywords include "COVID-19," "SARS-CoV-2," and iron metabolism biomarkers, including "hepcidin," "ferritin," "serum iron," "transferrin," "soluble transferrin receptor," "unsaturated iron binding capacity," and "transferrin saturation," The detailed search strategy is given in **Supplementary File 1**.

Study Selection and Eligibility Criteria

We follow the international guidelines for the diagnosis and treatment of COVID-19. The detailed severity classification criteria used in the evaluation of original studies and meta-analyses include: (1) Mild: asymptomatic or mild clinical symptoms, and no pneumonia on imaging, or outward

Abbreviations: ARDS, acute respiratory distress syndrome; CI, confidence interval; COVID-19, coronavirus disease 2019; FiO_2, fraction of inspired oxygen; HIF, hypoxia induced factor; NOS, Newcastle-Ottawa quality assessment scale; PaO_2, arterial oxygen partial pressure; SARS-CoV-2, severe acute respiratory syndrome coronavirus 2; SMD, standardized mean difference; SI, serum iron; TSAT, transferrin saturation.

treatment; (2) Moderate: fever, respiratory tract symptoms, pneumonia on imaging, and inward treatment; (3) Severe: dyspnea, or respiratory rate >30 breaths/min at rest, or oxygen saturation <93%, or PaO_2/FiO_2 < 300 mmHg; (4) Critical: respiratory failure and need for mechanical ventilation, or shock, or combined with other organ failure should be treated in the Intensive Care Unit. Severe and critical categories were defined as severe, mild, and moderate as non-severe in data analysis.

Inclusion criteria:

(1) All observational studies (e.g., cross-sectional, longitudinal, case-control, and cohort) with prospective or retrospective designs.
(2) Studies published in English, including preprints.
(3) Studies investigating hepcidin-mediated iron metabolism in COVID-19 cases.

Exclusion criteria:

(1) Duplicate studies, or repeated published studies.
(2) Studies in which accurate data cannot be obtained or some data are missing.
(3) Studies not strictly grouped by severity.

Data Extraction

The extraction methodology was discussed and formulated by the team. Two of us (ZL and HW) independently screened the full text according to the selection criteria, and recorded information about the author's name, publication time, study location, study design, sample size, laboratory results of iron metabolism parameters, and COVID-19 severity in the data file. All laboratory values were converted to conventional units based on the US National Institute of Standards and Technology conversion factors. For studies that only reported the median and interquartile range, we converted these values into mean and standard deviation according to the methods reported by Hozo et al. (27) and Wan et al. (28).

Risk of Bias Assessment

Two authors (LZ and YG) independently used the Newcastle-Ottawa scale to assess the quality of the included studies (29). A third author (DP) ruled in case consensus was not reached. The scale was developed for non-random and observational studies including case-control, cross-sectional, longitudinal, and cohort studies (if applicable). The quality was assessed using a 9-star system. Studies rated ≥6 stars were defined as "acceptable quality" and proceeded to the final meta-analysis step.

Statistical Analysis

This meta-analysis used RveMan5.4 (Cochrane Collaboration), with inverse variance as the statistical method to calculate standardized mean differences (SMDs) and corresponding 95% confidence intervals (CIs) for continuous variables. A $P < 0.05$ was determined to be statistically significant. The I^2 statistic was used to assess the heterogeneity among the analyzed studies. An $I^2 > 50\%$ or $P < 0.10$ indicated heterogeneity, for which the random effects model was used. Otherwise, the fixed effects model was used. In addition, visual inspection of funnel plots was used to evaluate publication bias.

RESULTS

Study Identification and Selection

Sixty-four unique citations were identified, of which 48 non-observational studies were excluded and 16 were selected for full-text eligibility assessment. Of these, six observational studies including 477 COVID-19 patients were included in the final data analysis and synthesis. The flow chart and details of study selection results can be found in **Figure 1** and **Supplementary File 1**. The detailed characteristics of the included studies were shown in **Table 1**.

Serum Levels of Iron Metabolism Parameters

Six unique studies with data from 477 COVID-19 patients were included. Hepcidin and ferritin were assessed in six out of six (100%) studies. Heterogeneity was assessed at $P = 0.006$, $I^2 = 70\%$ and $P = 0.0001$, $I^2 = 80\%$, respectively (**Figures 2A,B**). Both of them had significant heterogeneity, and the random effects model was used. Compared to non-severe cases, severe cases have higher hepcidin (SMD, −0.39; 95% CI [−0.76, −0.03]; $P = 0.03$) and ferritin (SMD, −0.84; 95% CI [−1.30, −0.38]; $P = 0.0004$). In five out of six (83.3%) studies, a total of 427 patients were tested for SI, and there were significant differences in their levels between severe and non-severe cases (SMD, 0.22; 95% CI [0.02, 0.41]; $P = 0.03$). A total of 320 patients from four out of six (66.7%) studies were tested for TSAT, and the statistical difference was insignificant (SMD, 0.06; 95% CI [−0.17, 0.28]; $P = 0.64$). Heterogeneity was assessed at $P = 0.38$, $I^2 = 4\%$ and $P = 0.66$, $I^2 = 0\%$, respectively (**Figures 2C,D**). Neither of them was significantly heterogenous, and the fixed effects model was used.

Quality of Studies and Publication Bias

All six included studies had NOS scores ≥6 stars, and their quality was acceptable. The funnel plots of SMDs in hepcidin and ferritin (both included six studies) were asymmetric, suggesting the possible presence of publication bias. For SI and TAST, five and four studies were included, respectively, and we found no evidence of publication bias (**Supplementary File 1**).

DISCUSSION

To our knowledge, this study is the first meta-analysis of the relationship between hepcidin-mediated iron dysmetabolism and COVID-19 severity. However, there is significant heterogeneity among six studies included in the data synthesis of hepcidin and ferritin. The possible reasons are analyzed as follows: (a) The time point and time course of laboratory testing were different. Some studies collected blood samples at admission (21–23), another 2 months after onset (16), and others throughout the hospital stay (24, 25). In addition, the detection methods and the reagents used were not the same. Enzyme-linked immunosorbent assay (ELISA) kits (16, 21–24) or competitive enzyme immunoassay (EIA) kits (25) were used to detect hepcidin. (b) Iron metabolism is strongly influenced by gender, with females generally having lower SI and hepcidin levels

TABLE 1 | Detailed characteristics of the eligible studies.

References	Region	Center	Design	Sample size	Cohort settings	Iron parameter	NOS score
Chakurkar et al. (24)	India	Single	Prospective, cohort, longitudinal	120	Mild ($n = 22$); Moderate ($n = 57$); Severe ($n = 41$)	Hepcidin, Ferritin, SI, TSAT	7*
Duca et al. (25)	Italy (Piacenza)	Single	Prospective, cohort, longitudinal	32	PaO_2/FiO_2 ratio: >300 mmHg ($n = 13$) >200, <300 ($n = 14$) <100 ($n = 5$)	Hepcidin, Ferritin, SI, TSAT	6*
Nai et al. (22)	Italy (Milano)	Single	Retrospective, cohort, cross -sectional	107	PaO_2/FiO_2 ratio: >300 ($n = 50$) <300 ($n = 57$)	Hepcidin, Ferritin, SI	7*
Sonnweber et al. (16)	Austria	Multiple	Prospective, cohort, cross -sectional	109	Mild ($n = 22$); Moderate ($n = 34$); Severe ($n = 53$)	Hepcidin, Ferritin, SI, TSAT	8*
Yagci et al. (23)	Turkey	Single	Retrospective, cohort, cross -sectional	59	Mild ($n = 18$); Severe ($n = 19$); Critical ($n = 22$)	Hepcidin, Ferritin, SI, TSAT	7*
Zhou et al. (21)	China	Single	Retrospective, cohort, cross -sectional	50	Mild ($n = 38$); Severe ($n = 12$)	Hepcidin, Ferritin	6*

*FiO_2, fraction of inspired oxygen; NOS, Newcastle-Ottawa quality assessment scale; PaO_2, arterial oxygen partial pressure; SI, serum iron; TSAT, transferrin saturation. The symbol * means stars.*

than males (22). Also, males have a higher ratio of severe COVID-19 cases. There were potential effects on heterogeneity due to differences in the composition of males and females between studies. (c) Our study classified mild and moderate as non-severe, severe and critical as severe. Differences in the proportions and sample sizes of cases of distinct severity between studies contributed to heterogeneity. Unfortunately, hepcidin and its related iron metabolism parameters are rarely tested simultaneously in COVID-19, and there are even fewer original studies analyzing the relationship between hepcidin and disease severity. Also, subgroup analysis could not be performed due to the lack of access to raw data. Furthermore, only the Sonnweber 2020 study tested hepcidin and ferritin 2 months after onset. We removed this study and performed a new meta-analysis and found no significant change in the final overall effect (**Supplementary Figure 1**). Therefore, from the results of the meta-analysis, differences in blood collection at different stages of COVID-19 between studies may not affect the fact that severe cases have higher levels of hepcidin and ferritin. This also suggests that hepcidin-mediated iron dysmetabolism throughout the course of COVID-19 may be some very promising therapeutic targets. Comprehensively, these studies met rigid criteria for inclusion and were homogeneous in terms of study design and objectives, as well as cohort settings. Therefore, the final overall effect generated by the random effects model brings novel insights into the biological effects of COVID-19.

Hepcidin, the key iron metabolism regulatory hormone, sequesters iron and prevents iron efflux in enterocytes and macrophages, resulting in increased intracellular ferritin and hypoferremia (30, 31). Physiologically, hepcidin synthesis by hepatocytes is reactively upregulated or downregulated by high or low SI, respectively. Other hepcidin agonists are inflammatory cytokines represented by interleukin-6 (IL-6). Conversely, hepcidin is antagonized by hypoxemia, with hypoxia induced factors (HIF) release (15, 32). Our study found that severe COVID-19 cases had higher serum levels of hepcidin and ferritin, and lower SI, without significant differences in TSAT.

These findings were consistent with most of other studies. Unexpectedly, hepcidin levels in severe COVID-19 cases did not appear to be downregulated by hypoferremia in a feedback manner and antagonized by systemic hypoxemia. Hyperferritinemia inevitably promotes the production of ROS and lipoperoxidation, which ultimately leads to extensive cell and tissue damage possibly through the ferroptosis pathway, and cascade-amplified inflammation (32, 33). In turn, hyperinflammation will transcriptionally upregulate hepcidin, further exacerbating iron dysmetabolism. We speculate that the potential intervention targets for this vicious circle may lie in the hepcidin-mediated iron metabolism axis.

Cytokine storm is a hallmark of the hyperinflammatory state of COVID-19 and is closely linked to disturbances in iron metabolism (30, 34). A growing body of studies have suggested that several components of elevated inflammatory status may be effective therapeutic targets, notably the administration of IL-6 receptor antagonists such as tocilizumab, which significantly reduces the mortality of severe COVID-19 cases (35, 36). However, the effective suppression of the excessive inflammatory response has also raised concerns about prolonged SARS-CoV-2 clearance. Furthermore, data on whether IL-6 receptor antagonists can correct hepcidin-mediated iron dysmetabolism in COVID-19 cases have been lacking to date.

Ehsani highlighted the striking similarity between the amino acid sequence of the SARS-CoV-2 spike glycoprotein and the hepcidin protein (37). This observation provides ideas for vaccine design and bioengineered antibody development for

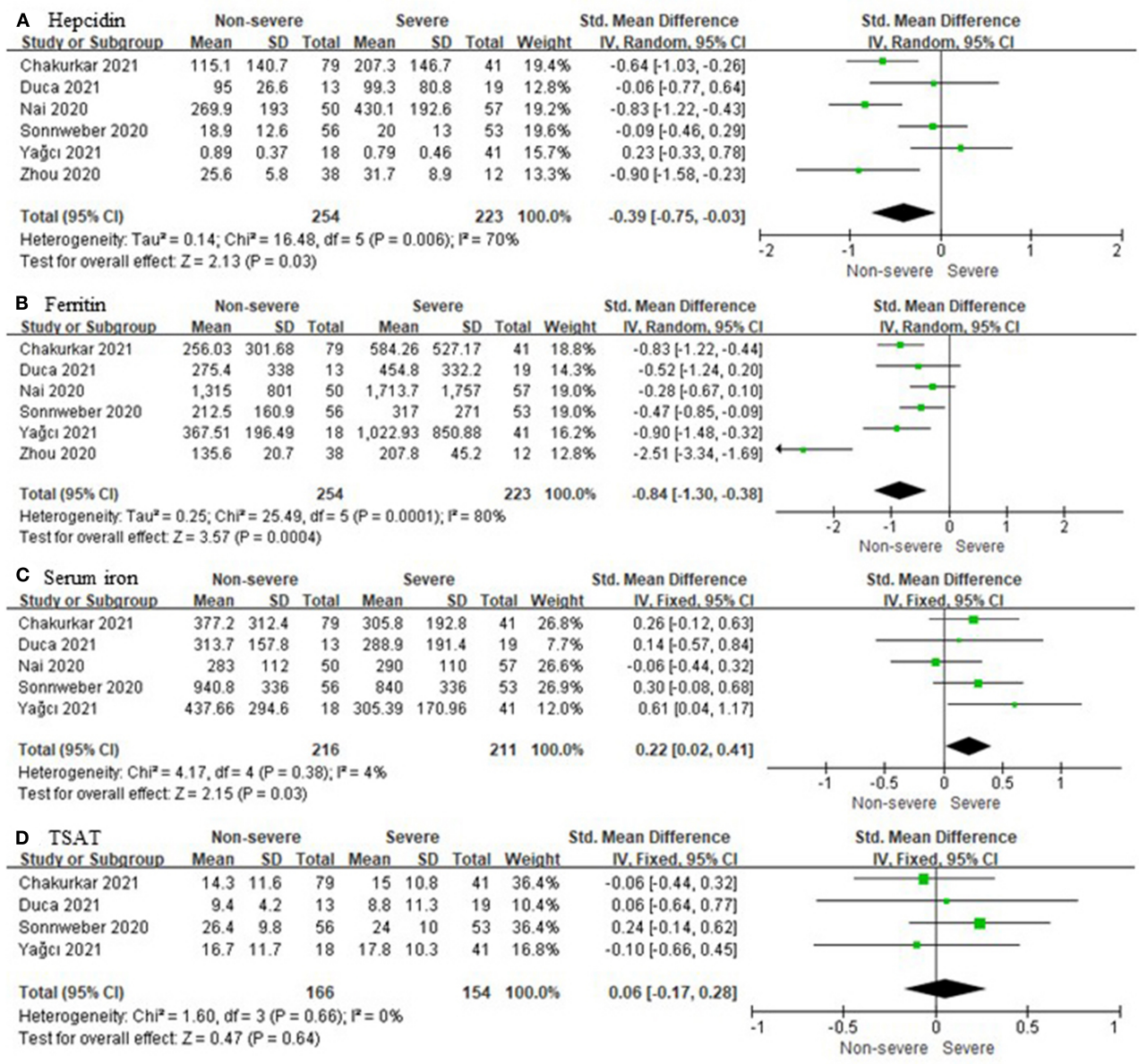

FIGURE 2 | Comparison of iron metabolism parameters between non-severe and severe COVID-19 cases. **(A)** Hepcidin; **(B)** Ferritin; **(C)** Serum iron; **(D)** Transferrin saturation (TSAT).

SARS-CoV-2. Hepcidin-mimetic action of SARS-CoV-2 may markedly increase circulating and tissue ferritin, while inducing SI deficiency (32, 33). However, whether SARS-CoV-2 utilizes ferroportin on the cell membrane as another binding receptor for the spike protein to invade host cells requires further analysis. Moreover, whether SARS-CoV-2 directly degrades ferroportin through mimicking hepcidin or indirectly upregulates hepcidin through inflammation to mediate iron dysmetabolism also needs to be carefully investigated. In animal models, hepcidin-neutralizing monoclonal antibodies have been shown to reverse inflammatory anemia (38). Recently, an antibody targeting ferroportin has been described and hypothesized to reduce ferroportin degradation by interfering with hepcidin binding, thereby increasing SI (39). The application of hepcidin antibodies to block viral entry and correct iron metabolism disturbances in COVID-19 cases may be a very promising therapeutic approach in the future.

Hyperferritinemia in COVID-19 lies downstream of the hepcidin-mediated iron metabolism axis. Iron chelation has been shown to reduce viral replication and exert anti-inflammatory effects in viral infections (32, 40, 41). Multiple evidences have shown that deferoxamine reduces the levels of IL-6, the main

inflammatory mediator that triggers cytokine storm, mimics HIF, and downregulates hepcidin (40, 42). However, the application of iron chelators in COVID-19 has brought great controversy (42–44). The iron dysmetabolism of COVID-19 is essentially abnormal iron distribution; the coexistence of low SI and local intracellular iron overload, and total iron in the body may not increase. Therefore, the safety and efficacy of systemic iron chelator administration has been challenged (43), and hepcidin antagonists may be preferred as supportive treatments for COVID-19 compared with iron chelators. Four clinical trials of iron chelation are currently underway (NCT04333550, NCT04361032, NCT04389801, IRCT20200506047323N4) and the results are pending.

There are some limitations to this study that need to be noted. First, most of the studies were single-center, retrospective, with small sample sizes, and may be subject to confounding and bias. Second, the six studies used for hepcidin and ferritin data synthesis were heterogeneous, subgroup analyses were not performed, and the results from random-effects models may be inaccurate. Third, the literature search may not be completely comprehensive, resulting in the omission of a few relevant studies. Fourth, this included preprint is a preliminary manuscript version. There are certain risks to the validity and applicability of the data it provides.

CONCLUSIONS

Severe COVID-19 cases had higher serum levels of hepcidin and ferritin, and lower SI, without significant differences in TSAT. Compared with other clinically applied therapeutic options targeting the iron metabolism axis, such as IL-6 receptor antagonists and iron chelators, hepcidin antibody may be more promising, but further studies are needed to verify whether targeting the hepcidin-mediated iron metabolism axis may influence the outcome and treatment of COVID-19.

DATA AVAILABILITY STATEMENT

The original contributions presented in the study are included in the article/**Supplementary Material**, further inquiries can be directed to the corresponding author/s.

AUTHOR CONTRIBUTIONS

DP was responsible for methodology, investigation, formal analysis, data curation, writing the original draft, and visualization. YG and LZ for investigation, formal analysis, and data curation. YL for conceptualization, investigation, review and editing, and supervision. ZL and HW worked on conceptualization, formal analysis, investigation, and data curation. All authors have read and approved the final manuscript version to be submitted.

ACKNOWLEDGMENTS

The authors thank Professor Hai Rao, School of Medicine, Southern University of Science and Technology, China, and Cindy Acon Chen, USA, for reviewing this manuscript.

SUPPLEMENTARY MATERIAL

The Supplementary Material for this article can be found online at: https://www.frontiersin.org/articles/10.3389/fpubh.2022.881412/full#supplementary-material

REFERENCES

1. Huang C, Wang Y, Li X, Ren L, Zhao J, Hu Y, et al. Clinical features of patients infected with 2019 novel coronavirus in Wuhan, China. *Lancet*. (2020) 395:497–506. doi: 10.1016/S0140-6736(20)30183-5
2. Li Q, Guan X, Wu P, Wang X, Zhou L, Tong Y, et al. Early Transmission dynamics in Wuhan, China, of novel coronavirus-infected pneumonia. *N Engl J Med*. (2020) 382:1199–207. doi: 10.1056/NEJMoa2001316
3. Wu C, Chen X, Cai Y, Xia J, Zhou X, Xu S, et al. Risk factors associated with acute respiratory distress syndrome and death in patients with coronavirus disease 2019 pneumonia in Wuhan, China. *JAMA Intern Med*. (2020) 180:934–43. doi: 10.1001/jamainternmed.2020.0994
4. Ruan Q, Yang K, Wang W, Jiang L, Song J. Clinical predictors of mortality due to COVID-19 based on an analysis of data of 150 patients from Wuhan, China. *Intensive Care Med*. (2020) 46:846–48. doi: 10.1007/s00134-020-05991-x
5. Ganz T, Nemeth E. Iron homeostasis in host defence and inflammation. *Nat Rev Immunol*. (2015) 15:500–10. doi: 10.1038/nri3863
6. Shah A, Frost JN, Aaron L, Donovan K, Drakesmith H. Systemic hypoferremia and severity of hypoxemic respiratory failure in COVID-19. *Crit Care*. (2020) 24:320. doi: 10.1186/s13054-020-03051-w
7. Zhao K, Huang J, Dai D, Feng Y, Liu L, Nie S. Serum iron level as a potential predictor of coronavirus disease 2019 severity and mortality: a retrospective study. *Open Forum Infect Dis*. (2020) 7:ofaa250. doi: 10.1093/ofid/ofaa250
8. Stockwell BR, Friedmann Angeli JP, Bayir H, Bush AI, Conrad M, Dixon SJ, et al. Ferroptosis: a regulated cell death nexus linking metabolism, redox biology, and disease. *Cell*. (2017) 171:273–85. doi: 10.1016/j.cell.2017.09.021
9. Lv Y, Chen L, Liang X, Liu X, Gao M, Wang Q, et al. Association between iron status and the risk of adverse outcomes in COVID-19. *Clin Nutr*. (2021) 40:3462–9. doi: 10.1016/j.clnu.2020.11.033
10. Huang I, Pranata R, Lim MA, Oehadian A, Alisjahbana B. C-reactive protein, procalcitonin, D-dimer, and ferritin in severe coronavirus disease-2019: a meta-analysis. *Ther Adv Respir Dis*. (2020) 14:1753466620937175. doi: 10.1177/1753466620937175
11. Kappert K, Jahić A, Tauber R. Assessment of serum ferritin as a biomarker in COVID-19: bystander or participant? Insights by comparison with other infectious and non-infectious diseases. *Biomarkers*. (2020) 25:616–25. doi: 10.1080/1354750X.2020.1797880
12. Bolondi G, Russo E, Gamberini E, Circelli A, Meca MCC, Brogi E, et al. Iron metabolism and lymphocyte char- acterisation during Covid-19 infection in ICU patients: an observational cohort study. *World J Emerg Surg*. (2020) 15:41. doi: 10.1186/s13017-020-00323-2
13. Hippchen T, Altamura S, Muckenthaler MU, Merle U. Hypoferremia is associated with increased hospitalization and oxygen demand in COVID-19 patients. *Hemasphere*. (2020) 4:e492. doi: 10.1097/HS9.0000000000000492
14. Girelli D, Marchi G, Busti F, Vianello A. Iron metabolism in infections: focus on COVID-19. *Semin Hematol*. (2021) 58:182–7. doi: 10.1053/j.seminhematol.2021.07.001

15. Ganz T, Nemeth E. Hepcidin and iron homeostasis. *Biochim Biophys Acta*. (2012) 1823:1434–43. doi: 10.1016/j.bbamcr.2012.01.014
16. Sonnweber T, Boehm A, Sahanic S, Pizzini A, Aichner M, Sonnweber B, et al. Persisting alterations of iron homeostasis in COVID-19 are associated with non-resolving lung pathologies and poor patients' performance: a prospective observational cohort study. *Respir Res*. (2020) 21:276. doi: 10.1186/s12931-020-01546-2
17. Aschemeyer S, Qiao B, Stefanova D, Valore EV, Sek AC, Ruwe TA, et al. Structure-function analysis of ferroportin defines the binding site and an alternative mechanism of action of hepcidin. *Blood*. (2018) 131:899–910. doi: 10.1182/blood-2017-05-786590
18. Stoffel NU, Lazrak M, Bellitir S, Mir NE, Hamdouchi AE, Barkat A, et al. The opposing effects of acute inflammation and iron deficiency anemia on serum hepcidin and iron absorption in young women. *Haematologica*. (2019) 104:1143–9. doi: 10.3324/haematol.2018.208645
19. Girelli D, Nemeth E, Swinkels DW. Hepcidin in the diagnosis of iron disorders. *Blood*. (2016) 127:2809–13. doi: 10.1182/blood-2015-12-639112
20. Lasocki S, Lefebvre T, Mayeur C, Mebazaa A, Gayat E; FROG-ICU study group. Iron deficiency diagnosed using hepcidin on critical care discharge is an independent risk factor for death and poor quality of life at one year: an observational prospective study on 1161 patients. *Crit Care*. (2018) 22:314. doi: 10.1186/s13054-018-2253-0
21. Zhou C, Chen Y, Ji Y, He X, Xue D. Increased serum levels of hepcidin and ferritin are associated with severity of COVID-19. *Med Sci Monit*. (2020) 26:e926178. doi: 10.12659/MSM.926178
22. Nai A, Lore NI, Pagani A, De Lorenzo R, Di Modica S, Saliu F, et al. Hepcidin levels predict Covid-19 severity and mortality in a cohort of hospitalized Italian patients. *Am J Hematol*. (2021) 96:E32–5. doi: 10.1002/ajh.26027
23. Yagci S, Serin E, Acicbe Ö, Zeren MI, Odabaşi MS. The relationship between serum erythropoietin, hepcidin, and haptoglobin levels with disease severity and other biochemical values in patients with COVID-19. *Int J Lab Hematol*. (2021) 43(Suppl. 1):142–51. doi: 10.1111/ijlh.13479
24. Chakurkar V, Rajapurkar M, Lele S, Mukhopadhyay B, Lobo V, Injarapu R, et al. Increased serum catalytic iron may mediate tissue injury and death in patients with COVID-19. *Sci Rep*. (2021) 11:19618. doi: 10.1038/s41598-021-99142-x
25. Duca L, Nava I, Vallisa D, Vadacca G, Magnacavallo A, Vercelli A, et al. *COVID-19, inflammatory response, iron homeostasis and toxicity: a prospective cohort study in the Emergency Department of Piacenza (Italy)*. Research Square (2021) (preprint). Available online: https://www.researchsquare.com/article/rs-1085949/v1
26. Muka T, Glisic M, Milic J, Verhoog S, Bohlius J, Bramer W, et al. A 24-step guide on how to design, conduct, and successfully publish a systematic review and meta-analysis in medical research. *Eur J Epidemiol*. (2020) 35:49–60. doi: 10.1007/s10654-019-00576-5
27. Hozo SP, Djulbegovic B, Hozo I. Estimating the mean and variance from the median, range, and the size of a sample. *BMC Med Res Methodol*. (2005) 5:13. doi: 10.1186/1471-2288-5-13
28. Wan X, Wang W, Liu J, Tong T. Estimating the sample mean and standard deviation from the sample size, median, range and/or interquartile range. *BMC Med Res Methodol*. (2014) 14:135. doi: 10.1186/1471-2288-14-135
29. Stang A. Critical evaluation of the Newcastle-Ottawa scale for the assessment of the quality of nonrandomized studies in meta-analyses. *Eur J Epidemiol*. (2010) 25:603–5. doi: 10.1007/s10654-010-9491-z
30. Edeas M, Saleh J, Peyssonnaux C. Iron: innocent bystander or vicious culprit in COVID-19 pathogenesis? *Int J Infect Dis*. (2020) 97:303–5. doi: 10.1016/j.ijid.2020.05.110
31. Daher R, Manceau H, Karim Z. Iron metabolism and the role of the iron-regulating hormone hepcidin in health and disease. *Presse Med*. (2017) 46(12 Pt 2):e272–8. doi: 10.1016/j.lpm.2017.10.006
32. Cavezzi A, Troiani E, Corrao S. COVID-19: hemoglobin, iron, and hypoxia beyond inflammation. A narrative review. *Clin Pract*. (2020) 10:1271. doi: 10.4081/cp.2020.1271
33. Hirschhorn T, Stockwell BR. The development of the concept of ferroptosis. *Free Radic Biol Med*. (2019) 133:130–43. doi: 10.1016/j.freeradbiomed.2018.09.043
34. Mehta P, McAuley DF, Brown M, Sanchez E, Tattersall RS, Manson JJ. COVID-19: consider cytokine storm syndromes and immunosuppression. *Lancet*. (2020) 395:1033–4. doi: 10.1016/S0140-6736(20)30628-0
35. Moore JB, June CH. Cytokine release syndrome in severe COVID-19. *Science*. (2020) 368:473–4. doi: 10.1126/science.abb8925
36. Zhang C, Wu Z, Li JW, Zhao H, Wang GQ. Cytokine release syndrome in severe COVID-19: interleukin-6 receptor antagonist tocilizumab may be the key to reduce mortality. *Int J Antimicrob Agents*. (2020) 55:105954. doi: 10.1016/j.ijantimicag.2020.105954
37. Ehsani S. COVID-19 and iron dysregulation: distant sequence similarity between hepcidin and the novel coronavirus spike glycoprotein. *Biol Direct*. (2020) 15:19. doi: 10.1186/s13062-020-00275-2
38. Sasu BJ, Cooke KS, Arvedson TL, Plewa C, Ellison AR, Sheng J, et al. Antihepcidin antibody treatment modulates iron metabolism and is effective in a mouse model of inflammation-induced anemia. *Blood*. (2010) 115:3616–24. doi: 10.1182/blood-2009-09-245977
39. Sheetz M, Barrington P, Callies S, Berg PH, McColm J, Marbury T, et al. Targeting the hepcidin-ferroportin pathway in anaemia of chronic kidney disease. *Br J Clin Pharmacol*. (2019) 85:935–48. doi: 10.1111/bcp.13877
40. Liu W, Zhang S, Nekhai S, Liu S. Depriving iron supply to the virus represents a promising adjuvant therapeutic against viral survival. *Curr Clin Microbiol Rep*. (2020) 20:1–7. doi: 10.1007/s40588-020-00140-w
41. Abobaker A. Can iron chelation as an adjunct treatment of COVID-19 improve the clinical outcome? *Eur J Clin Pharmacol*. (2020) 76:1619–20. doi: 10.1007/s00228-020-02942-9
42. Perricone C, Bartoloni E, Bursi R, Cafaro G, Guidelli GM, Shoenfeld Y, et al. COVID-19 as part of the hyperferritinemic syndromes: the role of iron depletion therapy. *Immunol Res*. (2020) 68:213–24. doi: 10.1007/s12026-020-09145-5
43. Garrick MD, Ghio AJ. Iron chelation may harm patients with COVID-19. *Eur J Clin Pharmacol*. (2021) 77:265–6. doi: 10.1007/s00228-020-02987-w
44. Abobaker A. Reply: iron chelation may harm patients with COVID-19. *Eur J Clin Pharmacol*. (2021) 77:267–8. doi: 10.1007/s00228-020-02988-9

Conflict of Interest: The authors declare that the research was conducted in the absence of any commercial or financial relationships that could be construed as a potential conflict of interest.

Publisher's Note: All claims expressed in this article are solely those of the authors and do not necessarily represent those of their affiliated organizations, or those of the publisher, the editors and the reviewers. Any product that may be evaluated in this article, or claim that may be made by its manufacturer, is not guaranteed or endorsed by the publisher.

frontiers | Frontiers in Medicine

ORIGINAL RESEARCH
published: 23 June 2022
doi: 10.3389/fmed.2022.924267

Individuals With Higher CD4/CD8 Ratio Exhibit Increased Risk of Acute Respiratory Distress Syndrome and In-Hospital Mortality During Acute SARS-CoV-2 Infection

*Ana Pascual-Dapena[1,2], Juan José Chillaron[3], Gemma Llauradó[3], Isabel Arnau-Barres[4], Juana Flores[3], Inmaculada Lopez-Montesinos[5], Luisa Sorlí[5], Juan Luis Martínez-Pérez[1,2], Silvia Gómez-Zorrilla[5], Juan Du[5], Natalia García-Giralt[5] and Robert Güerri-Fernández[1,5,6]**

[1] Medicine and Life Sciences Department, Pompeu Fabra University, Barcelona, Spain, [2] Departament de Medicina, Universitat Autonoma de Barcelona, Barcelona, Spain, [3] Endocrinology Department, Hospital del Mar Institute of Medical Research, Barcelona, Spain, [4] Geriatrics Department, Hospital del Mar Institute of Medical Research, Barcelona, Spain, [5] Infectious Diseases Department, Hospital del Mar Institute of Medical Research, Barcelona, Spain, [6] Centro de Investigación Biomédica en Red en Enfermedades Infecciosas, Ciberinfecc, Instituto de Salud Carlos III, Madrid, Spain

OPEN ACCESS

Edited by:
Sara Manti,
University of Catania, Italy

Reviewed by:
Jose Alberto Choreño-Parra,
Instituto Nacional de Enfermedades Respiratorias-México (INER), Mexico
Alejandro Vallejo,
Ramón y Cajal Institute for Health Research, Spain

***Correspondence:**
Robert Güerri-Fernández
rguerri@imim.es

Specialty section:
This article was submitted to Infectious Diseases – Surveillance, Prevention and Treatment, a section of the journal Frontiers in Medicine

Received: 20 April 2022
Accepted: 06 June 2022
Published: 23 June 2022

Citation:
Pascual-Dapena A, Chillaron JJ, Llauradó G, Arnau-Barres I, Flores J, Lopez-Montesinos I, Sorlí L, Luis Martínez-Pérez J, Gómez-Zorrilla S, Du J, García-Giralt N and Güerri-Fernández R (2022) Individuals With Higher CD4/CD8 Ratio Exhibit Increased Risk of Acute Respiratory Distress Syndrome and In-Hospital Mortality During Acute SARS-CoV-2 Infection. Front. Med. 9:924267. doi: 10.3389/fmed.2022.924267

Background: CD4/CD8 ratio has been used as a quantitative prognostic risk factor in patients with viral infections. This study aims to assess the association between in-hospital mortality and at admission CD4/CD8 ratio among individuals with acute SARS-CoV-2 infection.

Methods: This is a longitudinal cohort study with data of all consecutive patients admitted to the COVID-19 unit at Hospital del Mar, Barcelona, Spain for ≥48 h between March to May 2020. The CD4+ CD8+ T-cell subset differentiation was assessed by flow cytometry at admission as well as a complete blood test. Patients were classified according to CD4/CD8 ratio tertiles. The primary outcome was in-hospital mortality and the secondary outcome was acute respiratory distress (ARDS).

Results: A total of 338 patients were included in the cohort. A high CD4/CD8 ratio (third tertile) was associated with a higher in-hospital mortality [adjusted Cox model hazard ratio (HR) 4.68 (95%CI 1.56–14.04, p = 0.006), reference: second tertile HR 1]. Similarly, a high CD4/CD8 ratio (third tertile) was associated with a higher incidence of ARDS [adjusted logistic regression model OR 1.97 (95%CI 1.11–3.55, p = 0.022) reference: second tertile HR 1]. There was a trend of higher in-hospital mortality and incidence of ARDS in patients within the first tertile of CD4/CD8 ratio compared with the second one, but the difference was not significant. No associations were found with total lymphocyte count or inflammatory parameters, including D-dimer.

Conclusion: CD4/CD8 ratio is a prognostic factor for the severity of COVID-19, reflecting the negative impact on prognosis of those individuals whose immune response has abnormal CD8+ T-cell expansion during the early response to the infection.

Keywords: SARS-CoV-2, prognose, mortality, CD4/CD8 ratio, ARDS

INTRODUCTION

SARS-CoV-2 has caused a world-wide pandemic, with more than 400 million confirmed cases and over 5.8 million deaths until March 2022 (1).

Since its first detection in December of 2019, several prognosis factors have been described. Some of them are directly associated with uncontrolled immune response to the virus leading to a hyperinflammatory status, and some other ones such as hypoalbuminemia or myocardial injury, depend on the host clinical response (2, 3). The impact of the virus in the immune system can be summarized as lymphopenia, which has been widely reported as a notable aspect of SARS-CoV-2 infection. This is common to other respiratory viral infections, including influenza A H3N2 virus or human rhinovirus (4, 5). However, lymphopenia associated with SARS-CoV-2 infection is more intense, it lasts longer (5, 6) and it seems to be more selective in T cell lineages, with a higher impact on CD8+ T cells (7, 8). Notwithstanding, a larger wide-spread lymphopenia involving CD4+ T cells, CD8+ T cells, B cells and natural killer cells has also been reported (9, 10).

The CD4/CD8 ratio has shown relevance in chronic viral infections such as HIV infection, in which the CD4/CD8 ratio has been reported as a quantitative outcome reflecting the critical role of both T-cells subsets in the HIV pathogenesis or disease progression. Examination of CD4/CD8 ratio as a quantitative trait can be important to patient care as it might be used as a prognostic risk factor (11–13).

This study aims to assess the association between in-hospital mortality and at admission CD4/CD8 ratio in individuals with acute SARS-CoV-2 infection, to elucidate if a T-cell subset disbalance might be behind an abnormal response of the host against the virus.

MATERIALS AND METHODS

Study Design and Patient Selection

A longitudinal cohort study where data of all consecutive patients admitted to the COVID-19 unit at Hospital del Mar, Barcelona, Spain for ≥48 h between March to May 2020 were collected. The study procedures have previously been described (3, 14). As per protocol, the differentiation of CD4+ CD8+ T-cell subset was assessed in all admitted patients by flow cytometry at admission (day 1 of hospitalization), as well as a complete blood test.

The single-cell suspensions were stained with Aqua-viability dye and PacBlue-anti-CD3 and ECD-anti-CD4 from Beckman-Coulter (Brea, CA, United States); and APC-H7-anti-CD8 from Becton-Dickinson (San Jose, CA, United States) according to manufacturers' recommendations. Fluorescence-activated cell sorter analysis was performed on a custom Becton-Dickinson LSR II flow cytometer used for data acquisition and analyzed with FlowJo (TreeStar, Ashland, OR, United States). A representative example of the gating strategy for the lymphocyte subsets is shown in **Supplementary Figure 1**.

Patients were classified according to CD4/CD8 ratio tertiles. The primary outcome was in-hospital mortality and the secondary outcome was acute respiratory distress syndrome (ARDS) defined as a PaO_2-to-FiO_2 ratio < 200 and compatible alveolar X-Ray infiltrates.

Ethics Considerations

The Institutional Ethics Committee of Hospital del Mar of Barcelona approved the study and due to the nature of the retrospective data review and the emergent situation derived from the SARS-coV-2 pandemic, waived the need for informed consent from individual patients (CEIm 2020/9352).

Statistical Analysis

Continuous variables are expressed as mean and standard deviation or the median and interquartile range (IQR). Qualitative variables are presented as frequencies (percentages). Normality for baseline characteristics was evaluated by Shapiro–Wilk normality test. Quantitative data was analyzed by Kruskal–Wallis test and Dunn's test or Wilcoxon rank-sum (Mann–Whitney) test, and qualitative data was analyzed by chi-square test or Fisher exact test, as required. Appropriate coefficient tests were used for correlation among various continuous variables.

The association between the CD4/CD8 ratio and its tertiles and the primary outcome (in-hospital mortality) was assessed with unadjusted/adjusted Cox proportional hazards models. The reference group was the second tertile of CD4/CD8 ratio, for representing the most physiological range of values. Results are expressed as hazard ratio (HR) [95% confidence interval (CI)]. The same model was explored with tertiles of CD4+ T-cells and CD8+ T-cells. The association between the secondary end points and the CD4/CD8 ratio and its tertiles was assessed by logistic regression. The area under curve (AUC)-receiver operating characteristics (ROC) curve was obtained for the CD4/CD8 ratio analyzed as a continuous variable.

The level of significance in this study was set at a $p \leq 0.05$ and CI of 95%. All statistical analyses were performed using STATA/MP V.14.

RESULTS

A total of 388 individuals admitted to COVID-19 unit were included in the eligibility review, 210 (54%) males and 178 (46%) females. Median age was 63 years (IQR 52–75). Patients were divided into three groups according to the CD4/CD8 ratio tertile. Baseline characteristics of each group are shown in **Table 1**. Tertile 2 which encompasses the more physiological range of values (1.49–2.41; 15) was considered as reference for comparisons. This group showed the lowest rate of in-hospital mortality, the lowest intensive care unit admissions and the lowest acute respiratory distress syndrome (ARDS) incidence (**Table 1**).

Total lymphocyte count was not different between the three tertiles ($p = 0.679$), with a median in the lower limit of reference values of a normal hemogram (median 1.03 10^6 lymphocytes/ml, IQR 0.75–1.39), showing a common tendency to lymphopenia in all groups. The first tertile showed the lowest CD4+ T-cell count and the third tertile showed the lowest CD8+ T-cell

TABLE 1 | Baseline characteristics and the comparison according to the three different CD4/CD8 T-cell ratio tertiles.

	Overall	CD4/CD8 T-cell ratio			*p*-value
		First tertile (≤1.494)	second tertile (1.495–2.413)	Third tertile (≥2.414)	
n	388	130	129	129	
Age, median (IQR)	63 (52–75)	65 (53–77)	62 (50–74)	64 (53–73)	0.409
Male, *n* (%)	210 (54%)	80 (62%)	66 (51%)	64 (49%)	0.082
Current smoker, *n* (%)	28 (7%)	10 (7%)	6 (4.6%)	12 (9.3%)	0.347
Days of symptoms, median (IQR)	7 (4–9)	7 (5–9)	7 (4–9)	7 (5–9)	0.732
In-hospital stay, days, median (IQR)	9 (6–16)	9 (6–15)	9 (5–16)	9 (6.5–17)	0.843
Comorbidities, *n* (%)					
Hypertension	215 (55%)	69 (53%)	66 (51%)	80 (62%)	0.173
Diabetes mellitus	95 (24%)	32 (24%)	36 (28%)	27 (21%)	0.427
Cardiovascular disease	45 (11.6%)	12 (9.2%)	13 (10%)	20 (15.5%)	0.261
Chronic respiratory disease	34 (8.7%)	11 (8.4%)	13 (10%)	10 (7.7%)	0.812
Chronic kidney disease	120 (30%)	50 (38%)	38 (29.5%)	32 (24.5%)	0.052
Chronic liver disease	30 (7.7%)	15 (11.5%)	6 (4.6%)	9 (7%)	0.134
Immune condition	16 (4%)	4 (3%)	5 (4%)	7 (5%)	0.411
Charlson comorbidity index					
No comorbidity	171 (44%)	58 (44%)	54 (42%)	59 (45%)	0.933
Medium-low (1–2)	125 (32%)	35 (27%)	51 (39.5%)	39 (30%)	0.083
High (≥3)	92 (24%)	37 (28.5%)	23 (18%)	32 (25%)	0.118
Clinical markers at onset, median (IQR)					
C-Reactive protein mg/dl	7 (3.1–15.6)	6.8 (3.7–13.4)	6.1 (2.7–14.5)	7.8 (2.8–19.2)	0.772
IL-6 pg/ml	40 (13–83)	46.6 (19.9–75.7)	33.8 (13.2–83.8)	39.3 (10–92)	0.928
D-Dimer UI/l	765 (460–1,330)	870 (520–1,550)	650 (390–1,020)*	825 (460–1,520) ‡	0.018
Creatinin mg/dl	0.93 (0.73–1.12)	0.94 (0.74–1.14)	0.9 (0.73–1.07)	0.93 (0.73–1.14)	0.329
Hemogram, median (IQR)					
Lymphocyte 10^6 count/ml	1.03 (0.75–1.39)	1.04 (0.73–1.45)	1.09 (0.74–1.41)	0.98 (0.77–1.31)	0.679
CD4+ T-cell (10^6 cells/ml)	0.380 (0.250–0.609)	0.285 (0.179–0.416)	0.417 (0.280–0.609)*	0.492 (0.331–0.743) † ‡	<0.001
CD8+ T-cell (10^6 cells/ml)	0.199 (0.123–0.345)	0.295 (0.181–0.435)	0.211 (0.150–0.339)*	0.127 (0.079–0.191) † ‡	<0.001
Severity parameters, median (IQR)					
MEWS	2 (1–3)	2 (1–3)	2 (1–3)	2 (2–3)	0.401
PaO_2-to-FiO_2 ratio,	208 (112–310)	210 (132–317)	265 (92–316)	171 (108–278)	0.249
CURB-65	1 (0–2)	1 (0–2)	1 (0–2)	1 (0–2)	0.157
Outcomes, *n* (%)					
In-hospital Mortality	33 (8.5%)	12 (9%)	5 (4%)	16 (12%)‡	0.050
ARDS	99 (25%)	35 (27%)	24 (19%)	40 (31%)	0.078
ICU-Admission	85 (21%)	29 (22%)	25 (19%)	31 (24%)	0.674

Data are given as median (IQR) or n (%) unless otherwise indicated. CURB-65, confusion, urea >7 mmol/L, respiratory rate $30/min, low blood pressure #90/60 mm Hg, and age 65 years; FiO_2, fraction of inspired oxygen; MEWS, Modified Early Warning Score; PaO_2, arterial partial pressure of oxygen.

**P < 0.05 for second tertile compared with first tertile.*

†P < 0.05 for third tertile compared with first tertile.

‡P < 0.05 for third tertile compared with second tertile.

count, suggesting that the abnormal CD4/CD8 ratio was due to depletion of CD4+ T-cells or lack of expansion of CD8+ T-cells, respectively, and not because of an anomalous expansion of one of the cell-types. No significant differences in inflammatory markers were found among groups, except for D-dimer levels which were higher in first and third tertiles ($p = 0.018$), showing an increased underlying infection activity compared to the reference second tertile. However, these differences were not sustained after multivariate adjustment.

Additionally, no significant differences were observed among tertile groups in the severity scores at admission, nor in the main comorbidities. In spite of not being different across all tertiles, chronic kidney disease was significantly more prevalent in patients with lower ratios (first tertile) when compared to the

TABLE 2 | Adjusted models for in-hospital mortality and ARDS risk according to the CD4/CD8 T-cell ratio tertiles.

In-hospital mortality	**Hazard ratio**	**CI (95%)**		***p*-value**
First tertile (Ref: 1, second tertile)	2.16	0.71	6.58	0.175
Third tertile (Ref: 1, second tertile)	4.68	1.56	14.04	0.006
ARDS	**Odds ratio**	**CI (95%)**		***p*-value**
First tertile (Ref: 1, second tertile)	1.58	0.87	2.87	0.131
Third tertile (Ref: 1, second tertile)	1.97	1.11	3.55	0.022

ARDS: Acute respiratory distress syndrome.
Adjusted models. For In-hospital mortality we used a Cox Proportional Hazards model, adjusted for age, sex, comorbidity, and severity of the episode. For ARDS we applied a logistic regression model adjusted for age, sex, comorbidity, and severity.

highest ratios (third tertile; $p = 0.018$), but showed no differences when compared to the reference tertile.

We found a significant association between CD4/CD8 ratio and in-hospital mortality [HR1.08 (95%CI: 1.03–1.41); $p = 0.002$]. Each unit increase in the ratio was associated with an 8% increase in mortality. Thus, higher CD4/CD8 ratios (third tertile) was significantly associated with increased risk of in-hospital mortality [HR 4.42 (95% CI: 1.36–12.55); $p = 0.005$] respect to second tertile (**Table 2**). We also found this trend in lower ratios (first tertile), but without statistical significance as compared to the reference [HR 2.69 (95% CI: 0.94–7.69); $p = 0.064$]. This association presents a comprehensive Kaplan–Meier log rank of 8.75 ($p = 0.012$). After adjusting by age, sex, comorbidity, and severity of the episode, the third tertile remained significantly associated with in-hospital mortality [HR 4.68 (1.56–14.04); $p = 0.006$] (**Table 2**). No association was found with mortality and total lymphocyte count or inflammatory parameters, including D-dimer. No global differences between CD4/CD8 ratio and the incidence of ARDS were found ($p = 0.078$). However, when analyzing across tertiles, the third tertile with higher CD4/CD8 ratio showed an increased incidence of ARDS after adjusting by age, sex and comorbidity [OR 1.97 (95% CI: 1.11–3.55); $p = 0.022$] than the reference group. There was no association between ARDS and lower ratios ($p = 0.131$).

Several sensitivity analyses were performed, creating models that controlled for specific comorbidities like chronic kidney

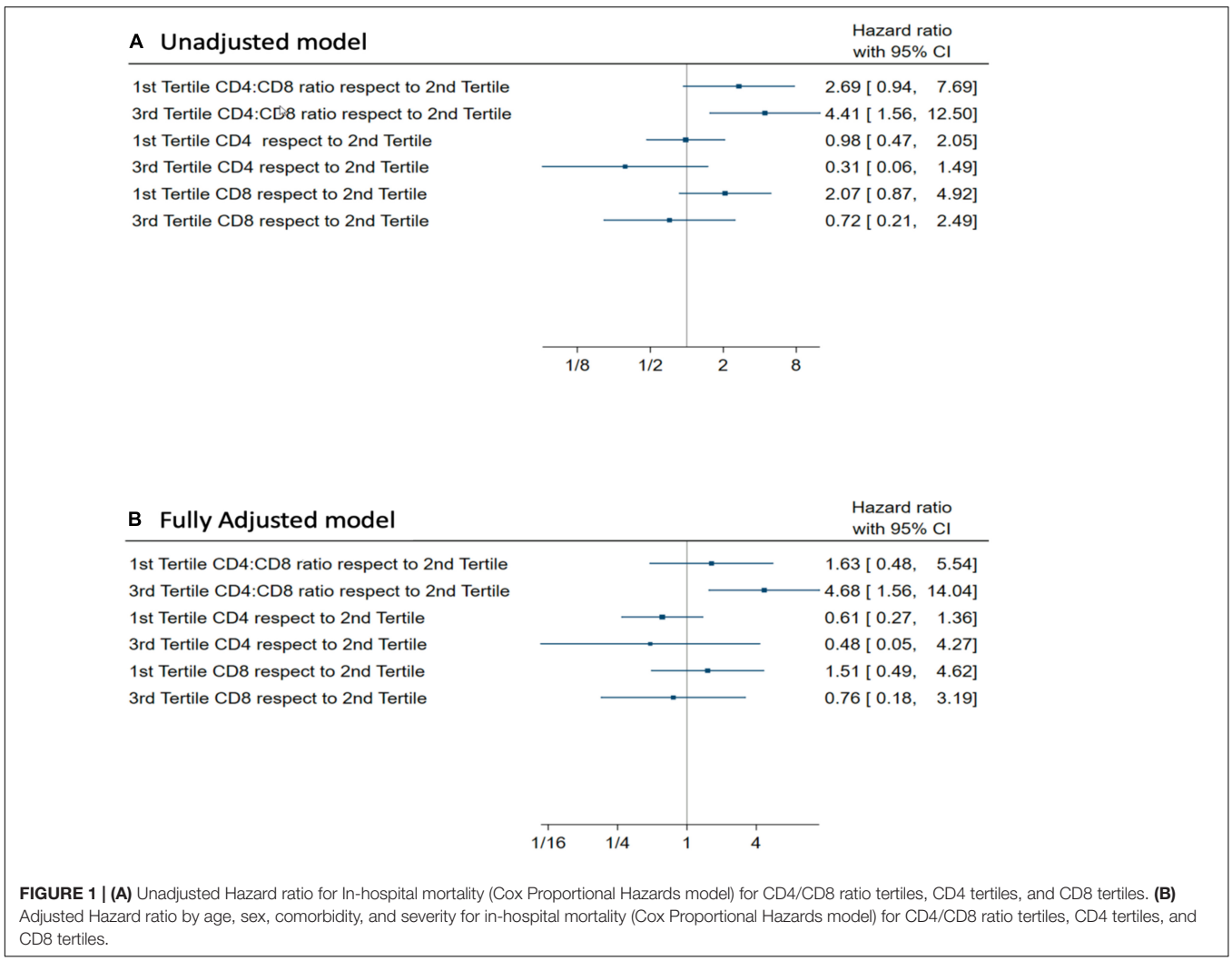

FIGURE 1 | (A) Unadjusted Hazard ratio for In-hospital mortality (Cox Proportional Hazards model) for CD4/CD8 ratio tertiles, CD4 tertiles, and CD8 tertiles. **(B)** Adjusted Hazard ratio by age, sex, comorbidity, and severity for in-hospital mortality (Cox Proportional Hazards model) for CD4/CD8 ratio tertiles, CD4 tertiles, and CD8 tertiles.

disease, inflammatory markers, as well as creating an alternative division of groups (considering standard measures of CD4/CD8 ratio: <1.0, 1.0–2.5, >2.5, instead of tertiles). All analyzes yielded similar findings that are in favor of those already presented (data not shown). In an alternative exploratory model with the same adjustment but considering CD4 and CD8 tertiles, no association was found with in-hospital mortality (**Figure 1**).

Receiver Operating Characteristics curves and AUCs were used to assess the discriminative accuracy of the CD4/CD8 ratio on mortality (**Figure 2A**) and ARDS (**Figure 2B**). In this case, the CD4/CD8 ratio was analyzed as a continuous variable. The AUC (95% CI) for discriminating mortality was 0.56 (0.44–0.68), standard error = 0.061. Using the best cut-off point of 2.027 in the CD4/CD8 ratio, the sensitivity was 57.6% with a specificity of 58.03%. The AUC (95% CI) for discriminating ARDS was 0.50 (0.43–0.57), standard error = 0.036, hence the model using lineal values of the CD4/CD8 ratio has no discrimination capacity to distinguish between patients with or without ARDS.

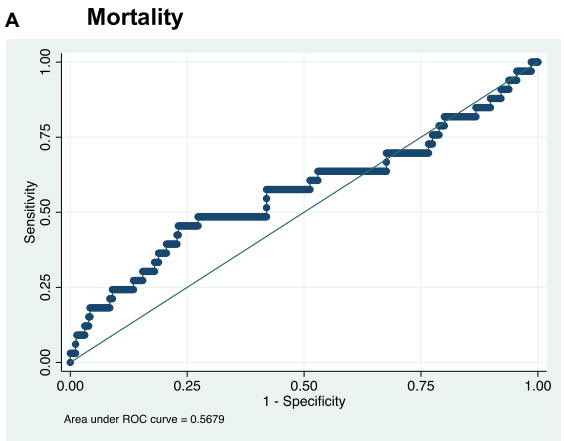

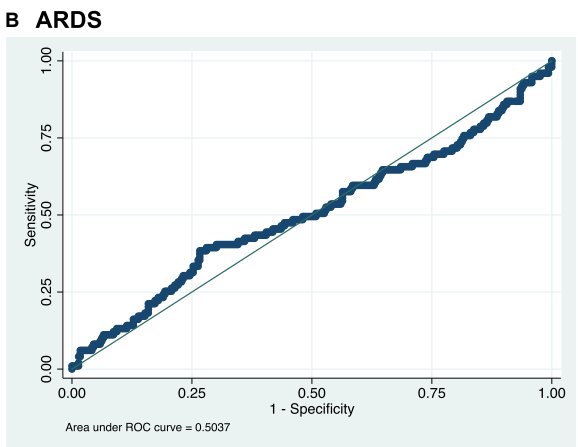

FIGURE 2 | ROC curve for the CD4/CD8 ratio: **(A)** The best cutoff for mortality discrimination is ≥ 2.027 Sensitivity: 57.58% Specificity: 58.03%; **(B)** the best cutoff for ARDS discrimination is ≥ 1.945 Sensitivity: 48.48% Specificity: 53.98%.

DISCUSSION

We report an association between the CD4/CD8 ratio and in-hospital mortality due to acute SARS-CoV-2 infection, regardeless of total lymphocyte count. Higher ratios (third tertile), which demonstrated lack of CD8+ T cell expansion, were significantly associated with mortality, but also lower ratios (first tertile) showed a trend to worse prognosis.

An abnormal CD4/CD8 ratio is often viewed as clinically relevant (16–18), it rarely measures below 1.0 or above 2.5 (15) and its disbalance by excess or defect always offers insights about immune malfunction. There is evidence that the CD4/CD8 ratio is genetically controlled in healthy humans (15, 19) and in the case of sarcoidosis, for example, a higher CD4+/CD8+ ratio is found in patients who carry HLA-DRB1*03 (19).

Indeed, the CD4/CD8 ratio has been used clinically in different scenarios: For example in the diagnosis of sarcoidosis and in chronic granulomatours diseases where a depletion in CD8+ T-cells leading to a higher CD4/CD8 ratio seems to be protective to worse disease presentations (19). Conversely, in HIV infection, the CD4/CD8 ratio is abnormally low (20). This shows on the one hand, the damage that the infection induces in the CD4+ T-cell compartment, and on the other hand, the restoration of the immune system after starting antiretroviral treatment, which sometimes restores CD4+ T-cells correctly but favors an over-expansion of CD8+ T-cell compartment (12, 21, 22). Thus, a CD4/CD8 ratio below 1 in individuals with HIV under antiretroviral therapy shows an incomplete and abnormal reconstitution of the immune system (12, 23, 24). These low ratios have been associated with worse outcomes like increased cardiovascular events, long-term complications, and all-cause mortality (18). Hence, there are clinical scenarios in which a depletion in CD8+ T-cells can be beneficial, and others where an expansion can be detrimental.

A particular scenario occurs in SARS-CoV-2 infection where, as we report, the highest tertile of CD4/CD8 ratio (with values > 2.4) is associated with a higher risk in-hospital death during the acute infection. There is also a trend in the case of the lower tertile of the CD4/CD8 ratio which could be taken into consideration.

In our cohort, individuals with higher CD4/CD8 ratio levels had lower CD8+ T-cell levels, showing an inadequate expansion of CD8+ cytotoxic T-cells, while those with lower CD4/CD8 ratio levels had lower CD4+ T-cell levels (not an abnormal expansion of CD8+ T-cells).

Therefore, the absence of an adequate expansion of CD8+ T-cells, leading to higher CD4/CD8 ratios, has a deleterious impact on the prognosis of the infection in terms of in-hospital mortality but also in ARDS incidence (13, 25).

This highlights the determining role of cytotoxic cellular immunity in the response in the acute phase of infection, setting its importance as keystone for a first line defense against SARS-CoV-2 infection. Although this fact has been reported by some authors, the evidence remained inconclusive (26, 27) or was based in small populations (28).

We can infer that an impaired CD8+ T-cell response with low cell clonal expansion, may lead to a poorer infection control and consequently worse prognosis, as opposed to a high and robust clonal expansion of this subset of T-cell that may be associated with milder forms of the disease (29, 30). In fact, an early development of a cytotoxic CD8+ T cell response, typically observed within 7 days of symptoms and peaking at 14 days, is correlated with effective viral clearance (7) and mild disease (31). In this line, Zuani et al. studied the T-cell subset composition in the peripheral blood of COVID-19 survivors and non-survivors (11). Analyzing CD8+ T-cell subpopulations, they observed lower counts in memory cells and effector memory cells re-expressing CD45RA (temra) among non-survivors with a lower absolute CD8+ T-cell count (11).

Notably, our patients with lower CD8 levels leading to a higher CD4/CD8 ratio did not present a more severe acute presentation of infection nor more inflammation at admission to the hospital when comparing to the other groups. It reflects the important role of the CD8+ T-cell subset in controlling the infection in its early stages, before an hyperinflammatory state has been established.

However, we also found a trend to a worse prognosis among the individuals in the lowest tertile of CD4/CD8 ratio. Similarly to what happens in HIV infection inadequate and persistent expansion of CD8+ T-cells can lead to an excessive uncontrolled immune response that can also affect the prognosis of the SARS-CoV-2 infection.

In fact, individuals with the lowest or highest CD4/CD8 ratio have worse prognosis than individuals within the second tertile. This could be related to the fact that patients within the lowest tertile also have a trend increased mortality. Hence, the risk of a poorer prognosis is determined by the fact of having an unbalanced CD4/CD8 out of the normal range.

This study has some limitations that must be stated. Firstly, it is a single-center study, with the consequent limited population. Also, the retrospective nature of the study does not allow us to establish causality between the CD4/CD8 ratio and the outcome. In addition, only CD4+ or CD8 T-cells global count were analyzed. Further studies to evaluate how naïve, effector memory cells and other subpopulations are associated with worse prognosis, pinpointing the underlaying mechanisms for the depletion of CD8+ Tcells and broadening our findings.

This study also presents some strengths. Importantly, samples are consistently collected at admission for all patients, therefore not generating bias and being a good representation of patients who need hospitalization due to COVID-19. Likewise, the healthcare was provided under the same guidelines by the same group of healthcare providers, eliminating variability that could lead to difference in outcomes.

In conclusion, CD4/CD8 ratio is a prognostic factor for acute SARS-CoV-2 infection independent of CD4 or CD8 alone, reflecting the negative impact on prognosis of those individuals whose immune response is disbalanced with an abnormal CD8+ T-cell depletion during the early response to the infection. This is different to other viral infections such as HIV, for which persistently low CD4/CD8 ratio is associated with worse outcome and increased risk of non-AIDS (18), or systemic diseases like sarcoidosis, for which lack of expansion and high ratios is advantageous.

DATA AVAILABILITY STATEMENT

Some or all datasets generated during and/or analyzed during the current study are not publicly available but could be available from the corresponding author on reasonable request.

ETHICS STATEMENT

The studies involving human participants were reviewed and approved by Ethics Committee PsMar CEIm 2020/9352. Written informed consent for participation was not required for this study in accordance with the national legislation and the institutional requirements.

AUTHOR CONTRIBUTIONS

RG-F, AP-D, and JC conceptualized and conducted the study. AP-D, RG-F, JC, and NG-G revised methodology and did data analysis. IA-B, IL-M, JL, SG-Z, GL, and JD contributed with recruitment and data curation. All authors have revised and edited the final manuscript.

FUNDING

This work received support and funding from Centro de Investigación Biomédica en Red de Fragilidad y Envejecimiento Saludable (CIBERFES; grant number CB16/10/00245), FEDER funds, and the FIS Project from Instituto de Salud Carlos III, Ministerio de Ciencia e Innovación (grant number PI16/01860 and PI19/00019). "PI19/00019" and "PI16/01860", funded by Instituto de Salud Carlos III (ISCIII) and co-funded by the European Union.

SUPPLEMENTARY MATERIAL

The Supplementary Material for this article can be found online at: https://www.frontiersin.org/articles/10.3389/fmed.2022.924267/full#supplementary-material

REFERENCES

1. World Health Organization [WHO]. *COVID-19 Weekly Epidemiological Update*. Geneva: World Health Organization (2022).

2. Arnau-Barrés I, Pascual-Dapena A, López-Montesinos I, Gómez-Zorrilla S, Sorlí L, Herrero M, et al. Prevalence and prognostic value of myocardial injury in the initial presentation of SARS-Cov-2 infection among older adults. *J Clin Med.* (2021) 10:3738. doi: 10.3390/jcm10163738

3. Arnau-Barrés I, Pascual-Dapena A, López-Montesinos I, Gómez-Zorrilla S, Sorlí L, Herrero M, et al. Severe hypoalbuminemia at admission is strongly associated with worse prognosis in older adults with sars-cov-2 infection. *J Clin Med.* (2021) 10:5134. doi: 10.3390/jcm10215134
4. Ziegler CGK, Allon SJ, Nyquist SK, Mbano IM, Miao VN, Tzouanas CN, et al. SARS-CoV-2 receptor ACE2 is an interferon-stimulated gene in human airway epithelial cells and is detected in specific cell subsets across tissues. *Cell.* (2020) 181:1016–35.e19. doi: 10.1016/j.cell.2020.04.035
5. Shah VK, Firmal P, Alam A, Ganguly D, Chattopadhyay S. Overview of immune response during SARS-CoV-2 infection: lessons from the past. *Front Immunol.* (2020) 11:1949. doi: 10.3389/fimmu.2020.01949
6. Wilk AJ, Rustagi A, Zhao NQ, Roque J, Martínez-Colón GJ, McKechnie JL, et al. A single-cell atlas of the peripheral immune response in patients with severe COVID-19. *Nat Med.* (2020) 26:1070–6. doi: 10.1038/s41591-020-0944-y
7. Notarbartolo S, Ranzani V, Bandera A, Gruarin P, Bevilacqua V, Putignano AR, et al. Integrated longitudinal immunophenotypic, transcriptional and repertoire analyses delineate immune responses in COVID-19 patients. *Sci Immunol.* (2021) 6:eabg5021. doi: 10.1126/sciimmunol.abg5021
8. Le Bert N, Tan AT, Kunasegaran K, Tham CYL, Hafezi M, Chia A, et al. SARS-CoV-2-specific T cell immunity in cases of COVID-19 and SARS, and uninfected controls. *Nature.* (2020) 584:457–62. doi: 10.1038/s41586-020-2550-z
9. De Biasi S, Meschiari M, Gibellini L, Bellinazzi C, Borella R, Fidanza L, et al. Marked T cell activation, senescence, exhaustion and skewing towards TH17 in patients with COVID-19 pneumonia. *Nat Commun.* (2020) 11:3434. doi: 10.1038/s41467-020-17292-4
10. Kared H, Redd AD, Bloch EM, Bonny TS, Sumatoh H, Kairi F, et al. SARS-CoV-2-specific CD8+ T cell responses in convalescent COVID-19 individuals. *J Clin Invest.* (2021) 131:e145476. doi: 10.1172/JCI145476
11. De Zuani M, Lazničková P, Tomašková V, Dvončová M, Forte G, Stokin GB, et al. High CD4-to-CD8 ratio identifies an at-risk population susceptible to lethal COVID-19. *Scand J Immunol.* (2021) 95:e13125. doi: 10.1111/sji.13125
12. Duffau P, Ozanne A, Bonnet F, Lazaro E, Cazanave C, Blanco P, et al. Multimorbidity, age-related comorbidities and mortality: association of activation, senescence and inflammation markers in HIV adults. *AIDS.* (2018) 32:1651–60. doi: 10.1097/QAD.0000000000001875
13. Pallotto C, Suardi LR, Esperti S, Tarquini R, Grifoni E, Meini S, et al. Increased CD4/CD8 ratio as a risk factor for critical illness in coronavirus disease 2019 (COVID-19): a retrospective multicentre study. *Infect Dis.* (2020) 52:675–7. doi: 10.1080/23744235.2020.1778178
14. Vogel-González M, Talló-Parra M, Herrera-Fernández V, Pérez-Vilaró G, Chillón M, Nogués X, et al. Low zinc levels at admission associates with poor clinical outcomes in sars-cov-2 infection. *Nutrients.* (2021) 13:562. doi: 10.3390/nu13020562
15. Amadori A, Zamarchi R, De Silvestro G, Forza G, Cavatton G, Danieli GA, et al. Genetic control of the CD4/CD8 T-cell ratio in humans. *Nat Med.* (1995) 1:1279–83. doi: 10.1038/nm1295-1279
16. Zaman MM, Recco RA, Raguthu L, Likki S, Reddy S. Characteristics of HIV-1-infected patients with CD4/CD8 lymphocyte ratio normalization on antiretroviral therapy. *AIDS Patient Care STDS.* (2000) 14:647–9. doi: 10.1089/10872910050206568
17. Pahwa S, Read JS, Yin W, Matthews Y, Shearer W, Diaz C, et al. CD4+/CD8 +T cell ratio for diagnosis of HIV-1 infection in infants: women and infants transmission study. *Pediatrics.* (2008) 122:331–9. doi: 10.1542/peds.2007-2308
18. Serrano-Villar S, Sainz T, Lee SA, Hunt PW, Sinclair E, Shacklett BL, et al. HIV-infected individuals with low CD4/CD8 ratio despite effective antiretroviral therapy exhibit altered T cell subsets, heightened CD8+ T Cell activation, and increased risk of non-AIDS morbidity and mortality. *PLoS Pathog.* (2014) 10:e1004078. doi: 10.1371/journal.ppat.1004078
19. Planck A, Eklund A, Grunewald J. Markers of activity in clinically recovered human leukocyte antigen-DR17-positive sarcoidosis patients. *Eur Respir J.* (2003) 21:52–7. doi: 10.1183/09031936.03.00059103
20. Serrano-Villar S, Pérez-Elías MJ, Dronda F, Casado JL, Moreno A, Royuela A, et al. Increased risk of serious non-AIDS-related events in HIV-infected subjects on antiretroviral therapy associated with a low CD4/CD8 ratio. *PLoS One.* (2014) 9:e85798. doi: 10.1371/journal.pone.0085798
21. Baker JV, Peng G, Rapkin J, Krason D, Reilly C, Cavert WP, et al. Poor initial CD4+ recovery with antiretroviral therapy prolongs immune depletion and increases risk for AIDS and non-AIDS diseases. *J Acquir Immune Defic Syndr.* (2008) 48:541–6. doi: 10.1097/QAI.0b013e31817bebb3
22. Jordan SC. Innate and adaptive immune responses to SARS-CoV-2 in humans: relevance to acquired immunity and vaccine responses. *Clin Exp Immunol.* (2021) 204:310–20. doi: 10.1111/cei.13582
23. De Paula HHS, Ferreira ACG, Caetano DG, Delatorre E, Teixeira SLM, Coelho LE, et al. Reduction of inflammation and T cell activation after 6 months of cART initiation during acute, but not in early chronic HIV-1 infection. *Retrovirology.* (2018) 15:76. doi: 10.1186/s12977-018-0458-6
24. Müller-Durovic B, Grählert J, Devine OP, Akbar AN, Hess C. CD56-negative NK cells with impaired effector function expand in CMV and EBV co-infected healthy donors with age. *Aging.* (2019) 11:724–40. doi: 10.18632/aging.101774
25. Lei C, Lin W, Deng X, Hu F, Chen F, Cai W, et al. Factors associated with clinical outcomes in patients with Coronavirus Disease 2019 in Guangzhou, China. *J Clin Virol.* (2020) 133:104661. doi: 10.1016/j.jcv.2020.104661
26. Westmeier J, Paniskaki K, Karaköse Z, Werner T, Sutter K, Dolff S, et al. Impaired cytotoxic CD8+ T cell response in elderly COVID-19 patients. *mBio.* (2020) 11:e02805–20.
27. Flament H, Rouland M, Beaudoin L, Toubal A, Bertrand L, Lebourgeois S, et al. Outcome of SARS-CoV-2 infection is linked to MAIT cell activation and cytotoxicity. *Nat Immunol.* (2021) 22:322–35. doi: 10.1038/s41590-021-00870-z
28. Rha MS, Shin EC. Activation or exhaustion of CD8+ T cells in patients with COVID-19. *Cell Mol Immunol.* (2021) 18:2325–33. doi: 10.1038/s41423-021-00750-4
29. Gallerani E, Proietto D, Dallan B, Campagnaro M, Pacifico S, Albanese V, et al. Impaired priming of SARS-CoV-2-specific naive CD8+ T cells in older subjects. *Front Immunol.* (2021) 12:693054. doi: 10.3389/fimmu.2021.693054
30. Stephens DS, McElrath MJ. COVID-19 and the path to immunity. *JAMA.* (2020) 324:1279–81.
31. Bergamaschi L, Mescia F, Turner L, Hanson AL, Kotagiri P, Dunmore BJ, et al. Longitudinal analysis reveals that delayed bystander CD8+ T cell activation and early immune pathology distinguish severe COVID-19 from mild disease. *Immunity.* (2021) 54:1257–75.e8. doi: 10.1016/j.immuni.2021.05.010

Conflict of Interest: The authors declare that the research was conducted in the absence of any commercial or financial relationships that could be construed as a potential conflict of interest.

frontiers | Frontiers in Medicine

TYPE Systematic Review
PUBLISHED 14 December 2022
DOI 10.3389/fmed.2022.1011819

OPEN ACCESS

EDITED BY
Shahd Horie,
University of Galway, Ireland

REVIEWED BY
Alejandro Pablo Adam,
Albany Medical College, United States
Daniel O'Toole,
University of Galway, Ireland

*CORRESPONDENCE
Catherine R. McClintock
cmcclintock05@qub.ac.uk

SPECIALTY SECTION
This article was submitted to Infectious Diseases: Pathogenesis and Therapy, a section of the journal Frontiers in Medicine

RECEIVED 04 August 2022
ACCEPTED 18 November 2022
PUBLISHED 14 December 2022

CITATION
McClintock CR, Mulholland N and Krasnodembskaya AD (2022) Biomarkers of mitochondrial dysfunction in acute respiratory distress syndrome: A systematic review and meta-analysis. *Front. Med.* 9:1011819. doi: 10.3389/fmed.2022.1011819

Biomarkers of mitochondrial dysfunction in acute respiratory distress syndrome: A systematic review and meta-analysis

Catherine R. McClintock*, Niamh Mulholland and Anna D. Krasnodembskaya

Wellcome-Wolfson Institute for Experimental Medicine, School of Medicine, Dentistry and Biomedical Sciences, Queen's University Belfast, Belfast, United Kingdom

Introduction: Acute respiratory distress syndrome (ARDS) is one of the main causes of Intensive Care Unit morbidity and mortality. Metabolic biomarkers of mitochondrial dysfunction are correlated with disease development and high mortality in many respiratory conditions, however it is not known if they can be used to assess risk of mortality in patients with ARDS.

Objectives: The aim of this systematic review was to examine the link between recorded biomarkers of mitochondrial dysfunction in ARDS and mortality.

Methods: A systematic review of CINAHL, EMBASE, MEDLINE, and Cochrane databases was performed. Studies had to include critically ill ARDS patients with reported biomarkers of mitochondrial dysfunction and mortality. Information on the levels of biomarkers reflective of energy metabolism and mitochondrial respiratory function, mitochondrial metabolites, coenzymes, and mitochondrial deoxyribonucleic acid (mtDNA) copy number was recorded. RevMan5.4 was used for meta-analysis. Biomarkers measured in the samples representative of systemic circulation were analyzed separately from the biomarkers measured in the samples representative of lung compartment. Cochrane risk of bias tool and Newcastle-Ottawa scale were used to evaluate publication bias (Prospero protocol: CRD42022288262).

Results: Twenty-five studies were included in the systematic review and nine had raw data available for follow up meta-analysis. Biomarkers of mitochondrial dysfunction included mtDNA, glutathione coupled mediators, lactate, malondialdehyde, mitochondrial genetic defects, oxidative stress associated markers. Biomarkers that were eligible for meta-analysis inclusion were: xanthine, hypoxanthine, acetone, *N*-pentane, isoprene and mtDNA. Levels of mitochondrial biomarkers were significantly higher in ARDS than in non-ARDS controls (P = 0.0008) in the blood-based samples, whereas in the BAL the difference did not reach statistical significance (P = 0.14).

mtDNA was the most frequently measured biomarker, its levels in the blood-based samples were significantly higher in ARDS compared to non-ARDS controls (P = 0.04). Difference between mtDNA levels in ARDS non-survivors compared to ARDS survivors did not reach statistical significance (P = 0.05).

Conclusion: Increased levels of biomarkers of mitochondrial dysfunction in the blood-based samples are positively associated with ARDS. Circulating mtDNA is the most frequently measured biomarker of mitochondrial dysfunction, with significantly elevated levels in ARDS patients compared to non-ARDS controls. Its potential to predict risk of ARDS mortality requires further investigation.

Systematic review registration: [https://www.crd.york.ac.uk/prospero], identifier [CRD42022288262].

KEYWORDS

acute respiratory distress syndrome, biomarker, mitochondrial dysfunction, mitochondrial DNA, mortality, systematic review, meta-analysis, ARDS

Introduction

Acute Respiratory Distress Syndrome is a principle cause of respiratory failure in critically ill patients requiring mechanical ventilation, characterized by severe pulmonary inflammation, diffuse alveolar damage and pulmonary edema (1). Due to a lack of effective treatment, ARDS results in substantial mortality of up to 30–40% (2). In addition to this, the current COVID-19 pandemic reports ARDS as one of the leading causes of ICU mortality, presenting an urgent need for advancement in ARDS research (3). ARDS pathogenesis remains nebulous; consequently, pharmacological therapies that reduce the severity of lung injury in preclinical models have not yet been translated into effective clinical treatment options. Therefore, further research into the mechanisms of ARDS pathogenesis and translational therapies is imperative.

Mitochondria are complex para-symbiotic organelles that perform a myriad of diverse yet interconnected functions, producing ATP and biosynthetic intermediates while also contributing to cellular stress responses such as autophagy and apoptosis (4). Acute inflammation can alter various mitochondrial functions, including reduced levels oxidative phosphorylation, and thus ATP production, increased mtROS production, increased apoptosis, as well as altered mitochondrial biogenesis and mitophagy (5). Dysfunctional mitochondria release multiple forms of damage-associated molecular patterns (DAMPs), such as ATP and mtDNA (6, 7). Similar to pathogenic stimuli, mitochondrial DAMPs can activate innate immunoreceptors, thus contributing to a vicious cycle of dysregulated inflammation. Other biochemical markers of mitochondrial dysfunction described in the literature include direct (lactate, pyruvate, lactate-to-pyruvate ratio, ubiquinone, alanine) and indirect markers (creatine kinase (CK), carnitine, aspartate aminotransferase (AST), alanine aminotransferase (ALT) and ammonia) (8). Clinical observational studies demonstrate that biochemical markers of mitochondrial dysfunction are associated with higher mortality and a higher risk of disease development in many respiratory conditions as well as sepsis (6, 9).

This review aims to assess the association between levels of biomarkers of mitochondrial dysfunction in any biological sample with mortality and other physiological and clinical outcomes in critically ill patients with ARDS. This will be carried out by presenting and appraising current research publications using standardized predefined assessable outcome measurements.

Methods

This systematic review was conducted in accordance to the Preferred Reporting Items for Systematic Reviews and Meta-Analyses (PRISMA) and Cochrane guidelines. Please see **Supplementary Methods 1** for extended explanations of search criterion.

Literature search

The databases CINAHL, EMBASE, MEDLINE, and Cochrane were systematically searched using predefined search terms for headings: Mitochondria, ARDS, and patient; synonyms and analogous terms of these headlines were defined in **Table 1**. In order to be eligible studies must include adult (18y/o) participants with ARDS in intensive care units (ICU) (critically ill patients). The severity, cause, and duration of

TABLE 1 Title and abstract article screening terms.

Mitochondrial search terms (35 terms)	ARDS search terms (10 terms)	Patient search terms (8 terms)
Mitochondria	Acute respiratory distress syndrome	Patient
Mitochondrial function	ARDS	Case report
Mitochondrial dysfunction	Infant respiratory distress syndrome	Case study
Mitochondrial disorder	Infantile respiratory distress syndrome	Human subject
Mitochondrial respiration	IRDS	Human
Mitochondrial biogenesis	Adult respiratory distress syndrome	Trial
Mitochondrial homeostasis	Respiratory distress syndrome adult	Human trial
Mitochondrial fitness	Respiratory insufficiency	Clinical trial
Mitochondrial DNA	Respiratory failure	
mtDNA	Respiratory distress syndrome	
Cytopathic hypoxia		
Mitochondrial RNA		
Mitochondrial miRNA		
mitoMIRs		
Aerobic metabolism		
ATP		
Adenosine triphosphate		
Tricarboxylic acid cycle		
TCA cycle		
Krebs cycle		
Electron transport chain		
ROS		
Reactive oxygen species		
Oxidative stress		
OXPHOS		
Oxidative phosphorylation		
Retrograde signaling		
Sirtuins		
SIRT		
Amino acid synthesis		
Fatty acid oxidation		
Mitophagy		
Biogenesis		
Fission		
Fusion		

ARDS will not be restricted. The definition of ARDS was not a limiting factor. Covid-ARDS was not included in this systematic review due to differences in disease pathophysiology. No other exclusion criteria was applied to patients. Published relevant studies up to a March 5, 2022 were searched. Full search code, database limitation and limits applied for each database search can be found on PROSPERO (CRD42022288262).

Study selection

Following the initial procurement of studies, by McClintock and Mulholland independently, from search databases, articles were retrieved in full text and stored on Endnote software. A 97% similarity in search results was obtained upon comparison of independent searches. Endnote enabled removal of duplicate articles. Those studies initially applicable were reviewed in full and criterion assessed, those failing to meet criterion were omitted.

Data extraction

The primary outcome was to assess the association between levels of biomarkers of mitochondrial dysfunction in clinical samples and ARDS patient mortality. The secondary outcome was to assess the association between levels of biomarkers of mitochondrial dysfunction in clinical samples and; (i) disease development and (ii) aggravation of ARDS disease severity. Alongside outcome data, the following information was also extracted: patient characteristics (age and sex), year of study publication, study design, sample size, characteristics of ARDS, type of biomarker, type of clinical sample, time of sampling, methods of biomarker measurement, concentration levels of the biomarkers.

All study designs were eligible for inclusion in this systematic review. Studies lacking a comparator/control, for example in the instance of retrospective case reports, were not eligible for meta-analysis inclusion. In the case of interventional studies, the data were extracted from the non-interventional/control arm of the study; this was to ensure that the mitochondrial biomarkers were not confounded by the intervention carried out.

Where possible biomarker concentration data for meta-analysis was collected in the form of mean, standardized mean difference (SMD) and "*N*" study participant. In the cases where median with interquartile range (IQR) were the only data provided, they were converted to Mean ± SD using the range rule (the standard deviation of a sample is approximately equal to one-fourth of the range of the data). Any standard errors provided were converted to standard deviation for consistency. RevMan software 5.4 was used to store and analyze data, as recommend by Cochrane guidelines. The random-effects model using the inverse- variance method was used on this statistical software, as this allowed for studies with the same biomarker lacking the same units to be compared. The I^2 statistics was used to analyze between-study heterogeneity, and values higher than 50% was considered as high heterogeneity. *P*-values less than 0.05 were considered significant.

Quality assessment

Given the inclusion of all study designs in this systematic review, the risk of bias assessment methods used to assess study quality were chosen based on applicable nature to study design. The study design was confirmed using the SIGN checklist prior to assessmen.[1] Randomized Control Trials (RCT) were grouped together and assessed using the Cochrane risk of bias tool[2] and non-randomized studies, were assessed using the Newcastle-Ottawa Scale (NOS).[3] Studies were considered high quality if the NOS score was more than six points.

1 https://www.sign.ac.uk/assets/study_design.pdf

2 https://methods.cochrane.org/bias/resources/rob-2-revised-cochrane-risk-bias-tool-randomized-trials

3 http://www.ohri.ca/programs/clinical_epidemiology/oxford.asp

Results

Study selection

A total of 3,029 articles were identified through search of the four databases. Twenty-six articles were included in the

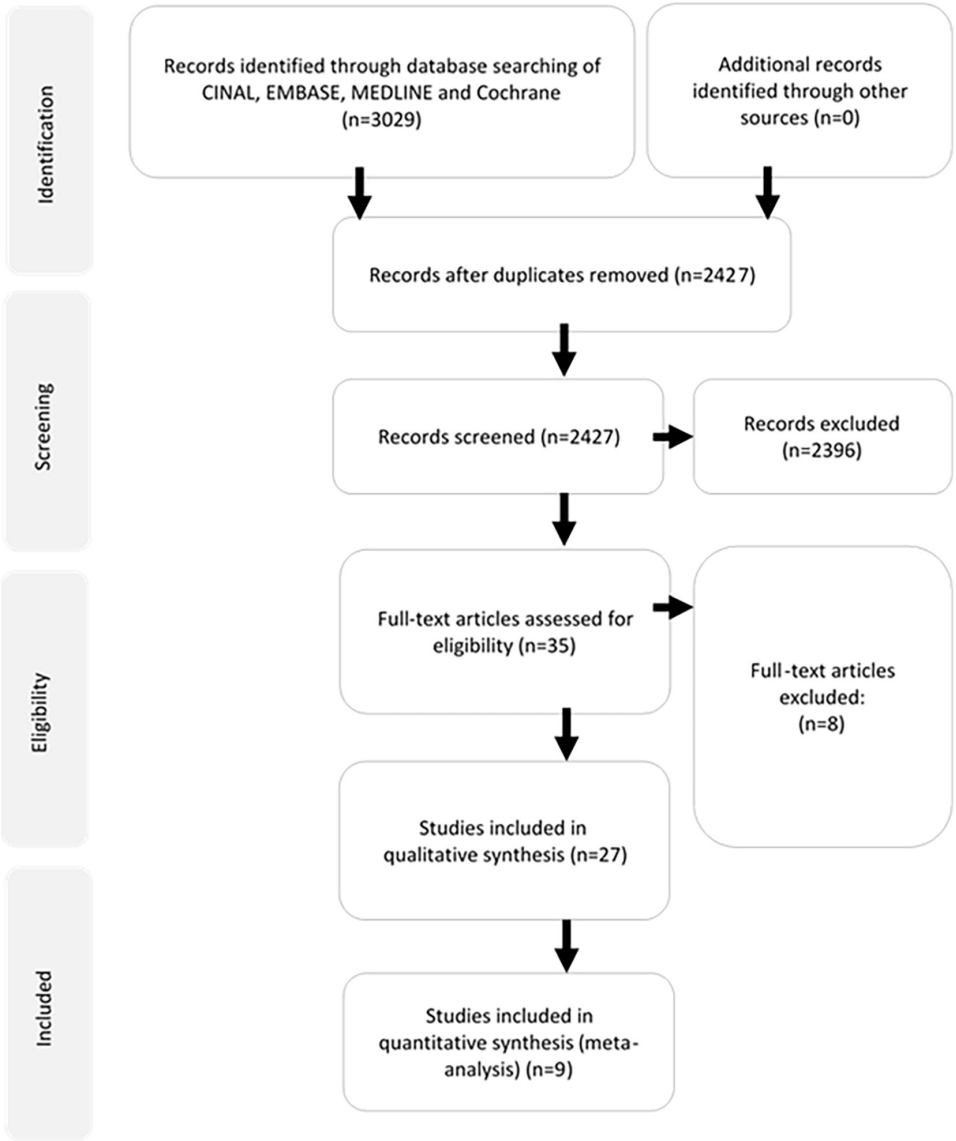

FIGURE 1
PRISMA flow diagram of literature search for studies included in this review.

TABLE 2 Summary of patient characteristics.

References	Patient sample size		Patient age		Patient sex		ARDS characteristic type/Cause
	ARDS	Non-ARDS	ARDS	Non-ARDS	ARDS male	Non-ARDS male	
Quinlan et al. (29)	29	6	35.9 ± 18	NR	14 (48.3)	NR	Trauma (24.1), pneumonia (10.3), sepsis (10.3), aspiration (10.3) and other (55.3)
Ortolani et al. (17)	12	0	55 ± 13	0 (0)	7 (58.3)	0 (0)	NR
Nathens et al. (30)	0	294	0	39 ± 15	0	222 (76)	NR
Scholpp et al. (24)	13	10	43.2 ± 12	44.1 ± 18	4 (5.3)	50 (66.7)	Pneumonia (30.7), sepsis (7.7) and other (61.6)
Nelson et al. (31)	94	62	NR	41 ± 1.22	NR	NR	NR
Soltan-Sharifi et al. (18)	10	0	52.7 ± 7.2	0	NR	0	NR
Moradi et al. (19)	13	0	49.2 ± 4.5	0	8 (61.5)	0	NR
Nakahira et al. (10)	134	309	49.5 ± ≈12.5*	275 (62.1)	NR		
Bhargava et al. (26)	22	0	49.4 ± ≈15.28*	0	16 (72.7)	0	Sepsis (27), pneumonia (59) and other (14)
Evans et al. (20)	18	8	46.1 ± 14.9	39.8 ± 11.0	9.9 (55)	4 (50)	Sepsis (39), aspiration (22), pneumonia (33) and other/unknown (5)
Liu et al. (25)	18	10	58.34 ± 8.25	57.93 ± 7.96	12 (66.7)	6 (60)	NR
Serpa et al. (22)	545	0	41.4 ± 14	0	331 (60.7)	0	Type: Pulmonary (92.4) and non-pulmonary (7.6) Cause: Pnemonia (83.8), non-pulmonary sepsis (1.8), trauma (8.9) and other (5.5)
Dorward et al. (27)	12 Divided into: 10 BAL and 7 serum sample for exp1 3 BAL and 6 serum samples for exp2	10 Divided into: 10 BAL and 8 serum samples 3 BAL and 6 serum samples	58 ± ≈30.5*	60 ± ≈30*	Calculation not available (64)	16.69 (79)	NR
Garramone et al. (11)	60	0	76.9 ± 13.0	0	34.2 (57)	0	NR
Fredenburgh et al. (33)	Cohort 1: 2 Cohort 2: 2	0	Cohort 1: 57 ± 19, Cohort 2: 49 ± 9	0 (0)	NR	0 (0)	NR
Mahmoodpoor et al. (21)	20	0	58 ± ≈10.5*	0 (0)	11 (55)	0 (0)	ARDS with comorbidities Sepsis (20) Surgery/Trauma (25) pneumonia (10)

(Continued)

TABLE 2 (Continued)

References	Patient sample size		Patient age		Patient sex		ARDS characteristic type/Cause
	ARDS	Non-ARDS	ARDS	Non-ARDS	ARDS male	Non-ARDS male	
Grazioli et al. (13)	8	3	NR	NR	NR	NR	NR
Bos et al. (28)	Phenotype one: 82 (uninflamed) ARDS with sepsis Phenotype two: 128 (reactive) ARDS with sepsis	547 sepsis 42 healthy control	64 ± ≈8*	62.258 ± ≈12.6*	121 (58)	323 (59)	Sepsis ARDS
Rosenberg et al. (32)	142	0	65 ± 0	0 (0)	64 (45.1)	0 (0)	NR
Blot et al. (14)	7 ARDS	14	60.5	50 (32–54 IQR)	17 (80.9)	5 (17.9)	NR
Huang et al. (15)	73	0	64	0	57 (78.1)	0 (0)	Pneumonia (57.53), aspiration (10/96), trauma (6.85), drowning (2.74), sepsis (16.44) and other (5.48)
Faust et al. (6)	PETROS: 41 MESSI: 45	PETROS: 183 MESSI: 75	44 ± 15≈* PETROS 62 ± 7.5≈* MESSI	33 ± 15≈18* PETROS 60 ± 18≈* MESSI	52 (15.1)	176 (51.2)	Trauma and sepsis
Korsunov et al. (23)	14	15	68 ± ≈7*	60.5 ± ≈14.25*	NR	NR	NR
Hernandez-Beeftink et al. (16)	264	423	63 ± 14	64 ± 15	175 (66)	255 (60)	Sepsis (100)

NR, not recorded; ARDS, acute respiratory distress syndrome; BAL, broncho-alveolar lavage; PETROS, Penn trauma organ dysfunction study; MESSI, molecular epidemiology of sepsis in the ICU; ICU, intensive care unit.
*Approximate range rule calculations.

review, nine of which contained sufficient information for meta-analysis. The selection process has been summarized according to the PRISMA guidelines in **Figure 1**. No potentially relevant papers were excluded from review.

Patient and study characteristics

Participant characteristics are summarized in the **Table 2**. The mean number of ARDS patients across all included articles was 79 and the mean non-ARDS was 148. In the ARDS studies there was a greater number of male participants (53.9% male), than in the non-ARDS (52.8% male). The mean ages of the ARDS participants was 55.4 and non-ARDS 51.3. The type and cause of ARDS varied, in the studies that provided this information, pneumonia and sepsis were the most prevalent causes of ARDS. There was a degree in variation of sample collection time, the majority of samples were collected upon enrollment or day 0 (52%) and the maximal collection time was 35 days. 29 sample sources across 25 studies. Sample sources were: blood (34.4%), plasma (34.4%), BAL (27.6%) and muscle tissue (3.45%).

Biomarkers of mitochondrial dysfunction reported in the included studies were: mitochondrial DNA (mtDNA) (eight studies) (6, 10–16) glutathione coupled mediators [(referenced retrospectively, glutathione, glutanation, glutathione *S*-transferase (GST), L-gluatamate and glutathione perosidase)] (five studies) (17–21), lactate (three studies) (20, 22, 23), malondialdehyde (MDA) (three studies) (17, 24, 25), metabolic signaling pathways and mediators [(referenced retrospectively: Nicotinamide adenine dinucleotide (NADH), N-terminal peptide FMNPLAQ - also known as NADH2, glyceraldehyde-3-phosphate dehydrogenase-like 6 (GAPDHL6), sirtuin enrichment, xanthine and hypoxanthine)] (four studies) (26–29), oxidative stress associated markers [(hydrogen peroxide (H_2O_2), super oxidase dismutase (SOD), ascorbate, alpha tocopherol, beta-carotene and retinol] (three studies) (24, 30, 31) (**Table 3**). Notably, multiple studies reported more than one biomarker, as recorded in **Tables 2–5**. Methods of sample analysis varied depending on the nature of sample biomarker. Mitochondrial DNA was recurrently analyzed using PCR (based

on mitochondrial copy number|), other markers were analyzed using HPLC, ELISA, enzyme immunoassay, mass spectrometry and GeneTitan Affymetrix (**Table 3**).

Mortality was recorded in seventeen of the twenty-five studies included in this review (**Table 4**). Mortality time point recording ranged from 4 to 60-day; however a number of studies failed to record a specific time point of mortality used in the analysis. Studies were examined for significant associations between raised biomarker levels and mortality outcomes, as well as non-significant trends. Due to a number of studies reporting multiple biomarkers, two studies fell into both of these categories (27, 30).

In the 17 studies which had recorded mortality, seven (41%) reported a significant association between elevated levels of mitochondrial biomarkers and higher mortality of ARDS patients (6, 15, 16, 19, 22, 27, 30). From these studies the significantly associated biomarkers were: hypoxanthine (30), GST isoform M1 (19), Thioredoxin (27), lactate (22) and mtDNA (6, 14–16). Due to the lack of provided numerical information only three studies were eligible for inclusion into the meta-analysis for association with mortality. Mitochondrial DNA was the only biomarker reported with significant association in more than one study.

Seven studies (41%) reported numerical trends toward association of higher levels of mitochondrial biomarkers with higher mortality, however the association did not reach statistical significance, or insufficient numerical information was provided (17, 23, 27, 29–32). Positively but non-significantly associated with mortality biomarkers consisted of: xanthine (30), glutathione, MDA (17), ascorbate, alpha-tocopherol (31), GAPDHL6 (27), glutathione peroxidase (selenium) (21), mediators of sirtuin signaling pathway, mediators of oxidative phosphorylation (29) and lactate (23).

The five (29%) remaining study biomarkers, from the 17 eligible for mortality association assessment, did not show any significant, nor general trend with biomarker levels and mortality (10, 14, 25, 27, 32). Of these five studies, two reported mortality of ARDS and non-ARDS groups together (10, 25), and two did not report mortality in non-ARDS group (14, 27), due to inability to draw comparisons between ARDS and non-ARDS cohorts for these four studies, no conclusions of association could be drawn. The remaining study has unclear findings. In Rosenberg et al., raised levels of GDF-19 were found in patients prior to hospital discharge, before declining in recovery. Whilst patient mortality was recorded, due to the temporary nature of increased biomarker levels no conclusive association can be drawn (33).

Development of other adverse clinical outcomes was recorded in five studies. These clinical outcomes included: multiple organ failure, renal failure, pulmonary fibrosis, atrial thrombus, hypotension and acute kidney injury. No statistical correlations of measured levels of mitochondrial biomarkers and development of other adverse clinical outcomes were performed (**Table 5**).

20 out of 25 studies assessed association of levels of mitochondrial biomarkers and risks of ARDS development or progression (**Table 5**). Eight studies (40%) reported a significant association between higher levels of mitochondrial biomarkers and the risk of developing ARDS or worsening of ARDS severity (6, 14, 15, 24, 27–29, 31). The biomarkers that indicated significant correlation with ARDS progression include; xanthine, hypoxanthine (29), N-pentane (24). Lipid peroxidation markers (31), NADH, NADH2 (27), sirtuin, mediators of oxidative phosphorylation (27), and mtDNA (6, 14, 15). Nine studies (45%) reported non-significant trend toward association between biomarker levels and risk of development or progression of ARDS (12, 13, 16–18, 20, 24, 30, 33). The biomarker are as follows: MDA (17, 24), glutathione (17), ascorbate, alpha-tocopherol (30), GSH, N-acetylcysteine (18), metabolite ion chromatograph (20), and mtDNA (12, 13, 16, 33). One study showed an opposing finding, with decreased biomarker levels in association with ARDS disease progression, reporting higher lactate levels in non-ARDS compare to ARDS (23).

Meta-analysis

Ten publications reported mean, standard deviation, and "*n*" number for inclusion in the meta-analysis. First, we compared the blood, plasma, broncho-alveolar lavage fluid (BAL), and lung epithelial lining fluid (ELF) levels of mitochondrial biomarkers between ARDS and non-ARDS subjects. To reflect the biological differences between biomarkers measured in the systemic circulation vs. lung compartment, peripheral blood, arterial blood and plasma were combined for comparison under the category "blood based biomarkers" and biomarkers measured in the BAL or ELF were combined under the category "BAL based biomarkers". Eight out of ten studies were eligible for this comparison (6, 10, 13, 14, 16, 23, 24, 29). Several studies provided information on multiple biomarkers, Faust et al., and Nakahira et al., reported data from two cohorts, the data on different biomarkers and different cohorts were included in meta-analysis separately (**Figure 2**). Collectively, 609ARDS patients and 1,054 non-ARDS were included in the comparison, of these 743 ARDS and 1,363 non-ARDS samples were blood based and the remainder were BAL. Biomarkers that were eligible for meta-analysis inclusion were: xanthine, hypoxanthine, (29), acetone, N-pentane, isoprene (24), lactate (23) and mtDNA (6, 10, 13, 14, 16). Xanthine and hypoxanthine are mediators involved in mitochondrial redox balance (34), acetone, isoprene and N-pentane are indicators of metabolic changes in association with oxidative stress (35–37) and accumulation of lactate is a metabolic indicator of oxidative phosphorylation impairment (38).

TABLE 3 Summary of study characteristics.

References	Study design	Sample size		Sample source	Sample moment	Sample analysis	Biomarker of mitochondrial dysfunction
		ARDS	Non-ARDS				
Quinlan et al. (29)	Observational study	29	6	Plasma and BAL	Plasma: 24 h after closure of venous catheter BAL: admission into ICU (from 11 ARDS patients)	HPLC analysis	Xanthine and hypoxanthine
Ortolani et al. (17)	RCT	12	0	BAL	Days 0,3,6 and 9 of placebo therapy	HPLC analysis	Glutathione and malondialdehyde (MDA)
Nathens et al. (30)	RCT	0	294	Plasma and BAL	Days 1,3,5,7,14 and 21 after admission	Enzyme immunoassay	Ascorbate and alpha tocopherol (metabolites)
Scholpp et al. (24)	Observational study	13	10	Plasma	Second day after admission to the intensive care unit (ICU)	HPLC analysis	Lipid peroxidation markers (acetone, isoprene and *n*-pentane) and MDA
Nelson et al. (31)	Permuted block randomized, single blinded trial	94	62	Plasma	Upon enrollment to study	HPLC analysis	Lipid peroxidation markers (beta-carotene, retinol, and α-tocopherol)
Soltan-Sharifi et al. (18)	Randomized interventional trial	10	0	Blood – red blood cells	(time 0), and times 24, 48, and 72 h post administration	GSH assay	Glutation (GSH) and *N*-acetylcysteine
Moradi et al. (9)	Prospective randomized single blinded trial	13	0	Peripheral blood	Administration of placebo day 0, samples taken day 2, 3, and 4	DNA genotyping via PCR	Three glutathione-*S*-transferase (GST) isoforms: GST m1, GST T1, GST P1
Nakahira et al. (10)	Retrospective study with two cohorts	134	309	Plasma	Upon initial enrollment of patients	qPCR	mtDNA copy number (NADH dehydrogenase 1 DNA level
Bhargava et al. (26)	Exploratory patient sample study	22	0	BAL	(Day 1–7) or the late phase (day 8–35)	iTRAQ labeling and 2D LC-Orbitrap M	Glycolysis protein expression and enrichment
Evans et al. (20)	Pre- RCT study	18	8	BAL	0–72 h of the diagnosis of ARDS	Chromatographic method	Metabolite ion chromatographs (L-glutamate, hypoxanthine, xanthine and L-lactate)
Liu et al. (25)	Case-control study	18	10	Arterial blood serum	T1,T2,T3, and T4	Assays for mediators of inflammation and oxidative stress	MDA, superoxide dismutase (SOD) and hydrogen peroxide (H_2O_2)
Serpa et al.(22)	Meta-analysis of observational studies	545	0	Arterial blood	Upon initial enrollment of patients	NR	Lactate measurement
Dorward et al. (27)	Retrospective study	12 Divided into: 10 BAL and 7 serum sample for exp1 3 BAL and 6 serum samples for exp2	10 Divided into: 10 BAL and 8 serum samples 3 BAL and 6 serum samples	BAL and blood	Upon initial enrollment of patients	Exp1: Liquid chromatography–tandem mass spectrometry Exp2: qPCR	Exp1: *N*-Formylated mitochondrial peptides: (*N*-formylated termini of NADH-ubiquinone oxidoreductase chain 2 (NADH2; fMNPLAQ) and NADH-ubiquinone oxidoreductase chain 4 L (NADH4L; fMPLIYM) Exp2: mtDNA

(Continued)

TABLE 3 (Continued)

References	Study design	Sample size		Sample source	Sample moment	Sample analysis	Biomarker of mitochondrial dysfunction
		ARDS	Non-ARDS				
Garramone et al. (11)	Cohort study	60	0	Blood plasma and serum	Upon initial enrollment of patients	ELIZA	Soluble Nox2-derived peptide (sNOX2-dp) a marker of NADPH-oxidase activity
Fredenburgh et al. (33)	Interventional double-blinded randomized parallel assigned trial	Cohort 1: 2 Cohort 2: 2	0	Plasma	Prior to treatment on day 1 and after treatment on days 1–5 and 7	Quantitative PCR of human NADH dehydrogenase 1 (MTND1)	mtDNA
Mahmoodpoor et al. (21)	Double-blind placebo-controlled randomized parallel clinical trial	20	0	Blood	Day 0,day 7, and day 14	Enzyme-linked immunosorent assay (EILZA)	Natural levels of selenium (glutathione peroxidase)
Pan et al. (12)	Case report	1	0	Muscle tissue	Upon admission to ICU	PCR	mtDNA
Grazioli et al. (13)	Observational	8	3	BAL	Day 1 and day 7	qRT-PCR	mtDNA
Bos et al. (28)	Observational prospective study	Phenotype one: 82 (uninflamed) ARDS with sepsis phenotype two: 128 (reactive) ARDS with sepsis	547 sepsis 42 healthy control	Whole blood	Within 24 h of ICU admission	Human genome U219 96-array plates and the GeneTitan instrument (Affymetrix)	mRNA
Rosenberg et al. (32)	Retrospective preliminary study	142	0	Blood	One week prior to hospital discharge	ELIZA	GDF-15
Blot et al. (14)	Observational case-control prospective study	7 ARDS	14	BAL and plasma	Upon enrollment	qPCR	mtDNA
Huang et al. (15)	Observational study	73	0	Plasma	Days 1, 3, and 7 after ICU admission	RT-qPCR	mtDNA
Faust et al. (6)	Two sided prospective study	41 PETROS cohort (trauma patients) 45 MESSI cohort (sepsis patients)	183 PETROS 75 MESSI	Plasma	At ED presentation and 48 h later	PCR	mtDNA
Korsunov et al. (23)	Single-center prospective comparative study	14	15	Arterial blood	Taken upon enrollment to study, over the period July–October 2021	Lactate = Chemray 120 Mindray biochemical analyser (China)	Lactate and oxygen transport
Hernandez-Beeftink et al. (16)	National, multicenter, observational study	264	423	Peripheral blood	24 h of sepsis diagnosis	mtDNA probes from the array data – CEU 1 array data	mtDNA

NR, not recorded; BAL, broncho-alveolar lavage; ICU, intensive care unit; HPLC, high-performance liquid chromatographic; RCT, randomized controlled trial; MDA, malondialdehyde; PCR, polymerase chain reaction; SNP, single nucleotide polymorphism; NAC, *N*-acetylcysteine; GST, glutathione-*S*-transferase; BWH RoCI, Brigham and Women's Hospital registry of critical illness; ME ARDS, molecular epidemiology of acute respiratory distress syndrome; mtDNA, mitochondrial deoxyribonucleic acid; ED, emergency department; ELISA, enzyme-linked immunosorbent assay; NIV, non-invasive ventilation; sNOX2-dp, Nox2-derived peptide; ARF, acute respiratory failure; NADPH, nicotinamide adenine dinucleotide phosphate; iCO, inhaled carbon monoxide; PETROS, Penn trauma organ dysfunction study; MESSI, molecular epidemiology of sepsis in the ICU; qRT-PCR, real-time quantitative reverse transcription; tRNA, transfer ribonucleic acid; GDF-15, growth differentiation factor-15; RCT, randomized controlled trial; mtDNA, mitochondrial deoxyribonucleic acid; MDA, malondialdehyde.

Mitochondrial biomarker levels in the blood based samples were significantly higher in ARDS than in non-ARDS controls. Standardized mean difference 0.66 [0.28,1.05], overall effect $Z = 3.36$, $P = 0.0008$. Heterogeneity, $I^2 = 88\%$, $P < 0.00001$. I^2 values show very large heterogeneity across non-ARDS and ARDS comparisons (**Figure 2A**).

Difference in the levels of the BAL based mitochondrial biomarkers did not reach statistical significance. Standardized mean difference 2.67 [−0.84,6.18], overall effect $Z = 1.49$, $P = 0.14$. Heterogeneity, $I^2 = 88\%$, $P = 0.004$. I^2 values also show very large heterogeneity across non-ARDS and ARDS BAL biomarker comparisons (**Figure 2B**).

Next, levels of blood based mitochondrial biomarkers were compared between survivors and those who died from ARDS. The blood biomarkers eligible for this analysis were, hypoxanthine, xanthine (31), mtDNA (6, 15, 16) and lactate (22). All these biomarkers were measured within 24-h of enrollment. Mortality was recorded at 7- (15), 28- (22)

TABLE 4 Primary outcome: Association of mitochondrial biomarker levels with ARDS mortality.

References	Biomarker	Mortality rates non-survivors		Biomarker summary		Summary of statistical comparison with mortality	Mortality time point	Association conclusion
		ARDS	Non-ARDS	ARDS	Non-ARDS			
Quinlan et al. (29)	Hypoxanthine and xanthine	14 (48.3)	0 (0)	Plasma Xanthine: $S = 13.3 \pm 2.01$ NS = 7.76 ± 0.09 Plasma Hypoxanthine: $S = (15.24 \pm 2.09)$ NS = (37.48 ± 3.1)	Plasma Xanthine: (9.4 ± 2.7) Plasma Hypoxanthine: (1.69 ± 0.76)	Plasma Xanthine: S vs NS $P = 0.68$ ARDS vs non = $P > 0.05$ Plasma Hypoxanthine: S vs NS $P = 0.001$ ARDS vs Non $P < 0.01$ No association with BAL	Time point unrecorded	Possible correlation Significant association No association
Ortolani et al. (17)	Glutathione and Malondialdehyde (MDA)	7 (58.3)	0 (0)	Glutathione (<450 μM to <550 nM) Malondialdehyde (<4 to >4 nM)	0	Both markers show non-significant positive association	28-day	Possible correlation
Nathens et al. (30)	Ascorbate and alpha tocopherol	0 (0) 0 (0)	7 (2.4) 9 (3.1) 9 (3.1)	Not applicable	Ascorbate: day-0 ≤ 0.5, day-21 ≤ 0.5 Alpha-tocopherol: day- <5, day-21 ≥ 10	53 (18) patients in non-ARDS cohort developed ARDS, statistics not carried out	28-day ICU Hospital	Possible correlation
Scholpp et al. (24)	MDA and lipid peroxidation markers (acetone, isoprene and pentane)	NR	NR	MDA: 0.55 Acetone: 1.32 Isoprene: 50.0 *n*-Petane: 1	MDA: 0.38 Acetone: 0.55 Isoprene: 33.2 *n*-Petane: 0.12	*n*-Petane statistically different in ARDS vs NON-ARDS	NR	Not applicable to this study
Nelson et al. (31)	Lipid peroxidation markers (beta-carotene, retinol, and α-tocopherol)	NR	NR	Exact values not provided: Beta carotene, retinol and α-tocopherol all significantly reduced in ARDS vs NON-ARDS			NR	Not applicable to this study
Soltan-Sharifi et al. (18)	Glutation (GSH) and *N*-acetylcysteine	NR	NR	GSH 0 h – <600 increased to <800 at 72 h	0	Not calculated, no trend of association with disease and time	NR	Not applicable to this study
Moradi et al. (19)	GST isoforms: M1, T1 and P1	10 (76.9)	0 (0)	Significant association of mortality with GST M1 null polymorphism and double deletion of both genes (M1, T1) in control ARDS placebo group of interest ($P < 0.05$). No significance for the GST P1 isoform with mortality. Absence of the GST M1 gene/deletion of both GTS M1 and GST T1 are more vulnerable to oxidative stress contributing to ARDS/ALI		Mortality with GST M1 $P < 0.05$ T1 and P1 non-significant	NR	Significant association
Nakahira et al. (10)	mtDNA copy number (NADH dehydrogenase 1 DNA level)	BWH 60 (30) ME 40 (16)		BWH [46,648 (14,468–63,510)] ME [29,828 (7,857–84,675)]	BWH [10,584 (3,992–41,466)] ME [8,771 (3,296–20,464)]	Only median and IQR provided – unable to calculate	28-day	Unclear correlation
Bhargava et al. (26)	Glycolysis protein expression & enrichment, and thioredoxin	15 (68.2)	0 (0)	Glycolysis is enriched in ARDS non-survivors with a fold change increase of 2.01 for GAPDHL6 (an example gene from the list of glycolytic proteins). This was not enriched in survivors. thioredoxin: S = apx. 2.5 NS = apx. 7.5	0	Significance was not provide with fold change thioredoxin $P < 0.05$	NR	Possible correlation Significant association

(Continued)

TABLE 4 (Continued)

References	Biomarker	Mortality rates non-survivors		Biomarker summary		Summary of statistical comparison with mortality	Mortality time point	Association conclusion
		ARDS	Non-ARDS	ARDS	Non-ARDS			
Evans et al. (20)	Metabolite ion chromatographs (L-glutamate, hypoxanthine, xanthine and L-lactate)	NR	NR	Metabolite fold change expression of ARDS vs healthy controls: L-Glutamate 7.94FC Hypoxanthine 40.96FC L-Lactate 3.49FC		L-Glutamate $P = 2.49E-06$ Hypoxanthine $P = 6.93E-10$ L-Lactate $P = 0.0437$	NR	Not applicable to this study
Liu et al. (25)	MDA, superoxide dismutase (SOD) and hydrogen peroxide (H_2O_2)	0 (0) Two patient mortality recorded – unclear as to which group		MDA = significantly higher in ARDS group ($P = 0.01$) SOD = significantly lower in ARDS group ($P < 0.01$) $H_2O_{2=}$ significantly higher in ARDS group ($P = 0.02$)			4-day One year follow up	Unclear findings
Serpa et al. (22)	Lactate measurement	192 (35.23)	0 (0)	Lactate: $S = (29.9 \pm 34.8)$ NS = (46.7 ± 43.0)	0	$P = 0.003$ Significant increase in lactate in non-survivors of ARDs	28-day	Significant association
Dorward et al. (27)	NADH, FMNPLAQ and NADH-	5 (42)	NR	Exact numbers not provided in text. Mitochondrial formylated peptides were elevated in BAL and serum from patients with ARDS. Bal and serum showed strong significant increase in markers in ARDS patients to healthy patient controls ($P < 0.001$) (Exp1). mtDNA recorded in BAL ($n = 3$ per group) and serum ($n = 6$ per group) showed $p < 0.05$ increase in mtDNA copy number in ARDS group compared to healthy control (Exp2).			NR	Unclear
Fredenburgh et al. (33)	mtDNA	NR	NR	Initial enrollment level: 7,218.0 End of study: 24,083.5	NR	Non-significant increase between biomarker levels, mortality not included in study	NR	Not applicable to this study
Mahmoodpoor et al. (21)	Natural levels of selenium (glutathione peroxidase)	16 (22.2)	0 (0)	Sele-: Day 0 – apx. > 75 Day 14 – apx > 75 Exact data values not available	0	Non-significant	14- day	Non-significant positive association
Pan et al. (12)	mtDNA	NR	NR	Patient was diagnosed with mitochondrial myopathy. Pathological findings of RRF in a muscle biopsy and genetic analysis of an A3243G point mutation in the tRNALEU (UUR) gene of mtDNA. Paper indicates a link between respiratory failure and mtDNA mutation in adult.			NR	Not applicable to this study
Grazioli et al. (13)	mtDNA	NR	NR	179.8583777	1.0	Not calculated	NR	Not applicable to this study
Bos et al. (28)	Mitochondrial canonical pathways based off mRNA expression	59 (28)	95 (17.4)	Pathway expression levels of mitochondrial function: SIRTUIN signaling and oxidative phosphorylation. ARDS fold change compared to Non-ARDS and significance presented in paper.		Statistical testing $P < 0.001$ Significant difference between mitochondrial dysfunctional genes/SIRTUIN pathway, oxidative phosphorylation in sepsis ARDS compared to sepsis. Mortality statistics not calculated.	60-day	Possible correlation
Rosenberg et al. (32)	GDF15	21 (14.8)	0 (0)	Raised levels of GDF-15 prior to discharge, and lower in recovery	NR	Not calculated	NR	Unclear
Blot et al. (14)	mtDNA	1 (14)	NR	0.1503	0.01546	No calculation available	30 day	Unclear
Huang et al. (15)	mtDNA	36 (49.3)	0 (0)	Severe: 1,230 (588–22,387) Moderate: 5,370 (628–13,052) Mild: 15,792 (1,623–186,814) *S*: 7,585 (1,717–15,792) NS: 67,608 (19,498–346,736)	NR	Severe ARDS vs Mild ARDS mtDNA levels $P = 0.03$ $P < 0.05$ – higher levels of mtDNA in ARDS survivors vs ARDS non-survivors	Day-7	Significant association

(Continued)

TABLE 4 (Continued)

References	Biomarker	Mortality rates non-survivors		Biomarker summary		Summary of statistical comparison with mortality	Mortality time point	Association conclusion
		ARDS	Non-ARDS	ARDS	Non-ARDS			
Faust et al. (6)	mtDNA	PETROS: 17 (7.6) MESSI: 50 (41.7)		PETROS: ARDS = 12.28 1.07 MESSI: ARDS = 11.06 1.31	PETROS: NON = 12.04 1.01 MESSI: NON = 11.25 1.20	PETROS: ARDS vs NON $P = 0.009$ S vs NS $P = 0.06$ MESSI: ARDS vs NON $P = 0.003$ S vs NS $P = 0.073$	30-day	Significant association
Korsunov et al. (23)	Lactate and oxygen transport	14 (100)	11 (73.3)	3.4 ± 3.75	5.3 ± 0.675	Not carried out, correlative trend evident in ARDS vs NON-ARDS	NR	Possible correlation
Hernandez-Beeftink et al. (16)	mtDNA	39 (82)	45 (174)	3.65 (1.39–9.59 (hazard ratio and 95% CL) 0.031 ± 0.2036 *S*: -0.0038 ± 0.2012 NS: 0.0702 ± 0.2001	1.24 (0.44–3.51) -0.0073 ± 0.2004	Non-ARDS $P = 0.683$ ARDS $P = 0.009$ mtDNA significantly associated with 28-day mortality	28-day	Significant association

S, survivor; NS, non-survivor; NR, not recorded; CL, confidence limit.

or 30-days (6), Quinlan et al., did not specify the time when mortality was recorded (31) (**Table 4**). By meta-analysis, levels of biomarkers were significantly higher in non-survivors compared to survivors of ARDS. Standardized mean difference 0.37 [0.11,0.62], overall effect $Z = 3.15$, $P = 0.002$. Heterogeneity, $I^2 = 90\%$, $P < 0.00001$. I^2 values show very large heterogeneity across non-ARDS and ARDS comparisons (**Figure 2C**).

Among the studies included in this review, mitochondrial DNA was the most frequently measured biomarker, therefore separate meta-analysis was performed on these studies. Three studies reported levels of mtDNA in plasma, serum or whole blood from ARDS and non-ARDS subjects (6, 10, 16). In the study of Nakahira et al., samples were collected upon enrollment into trial, Faust et al., collected samples upon arrival to emergency department (6, 10) and Hernández-Beeftink et al., recorded collection at 24 h after sepsis diagnosis (16). 484 ARDS patients and 990 non-ARDS patients were included in this comparison. Circulating mitochondrial DNA levels in patients with ARDS were significantly higher than in non-ARDS control groups. 0.50 [0.03,0.98], overall effect $Z = 2.07$, $P = 0.04$. Heterogeneity, $I^2 = 93\%$, $P < 0.00001$. Again, I^2 values show very large heterogeneity across non-ARDS and ARDS comparisons (**Figure 3A**). Although Blot et al., and Grazioli et al., reported significant elevation of mtDNA in the BAL samples of ARDS patients compared to healthy controls in small cohorts (5 ARDS vs.3 heathy and 7 ARDS vs. 3 healthy, respectively), numerical information provided in these studies was not sufficient to carry out meta-analysis. Also, Nakahira et al., displayed graphs with significant differences in mtDNA copy numbers between patients with and without ARDS however raw values were not provided and thus could not be included in meta-analysis.

Three studies also reported data on the levels of circulating mtDNA in ARDS survivors and non-survivors (6, 15, 16). Both Haung et al., and Hernandez-Beeftink et al., collected samples at 24 h or 1 day after presentation (15, 16), Faust et al., collected samples at presentation (**Table 3**). There were 489 ARDS survivors and 192 ARDS non-survivors included in the comparison. Mortality was recorded at 30 days (Faust et al.), 28 days (Hernandez-Beeftink et al.) and 7 days (Huang et al.) (**Table 4**). Results of meta-analysis did not allow to draw definitive conclusions about whether or not levels of mtDNA are elevated in non-survivors as overall P value is on the border of significance, although there is a numeric trend toward higher levels in non-survivors. Standardized mean difference 0.37 [0.01,0.73], overall effect $Z = 2.00$, $P = 0.05$. Heterogeneity, $I^2 = 72\%$, $P = 0.01$. I^2 values show large heterogeneity across ARDS survivor and non-survivor comparisons (**Figure 3B**).

Publication bias

The nine RCT trials were assessed using the Cochrane risk of bias charts. Five studies were classed as low risk, and two as high risks (**Figure 4** and **Table 6**) (17–21, 30–33). The remaining 16, cohort and case–control studies, were assessed by the Newcastle–Ottawa Scale (NOS) (10, 13–16, 20, 22–29). The mean score was 6. 12 out of 16 of studies were considered low risk (**Table 7**).

Discussion

Clinical and biological markers for prediction of ARDS outcomes are based upon inflammatory indicators, including

TABLE 5 Secondary outcome: Association between levels of mitochondrial biomarkers and risks of development of new complications of ARDS or worsening of severity or development of ARDS.

References	Biomarker	Biomarker summary		Association to disease presence/ progression	Association to other worse outcomes of ARDS
		ARDS	Non-ARDS		
Quinlan et al. (29)	Hypoxanthine and xanthine	Plasma xanthine: $S = 13.3 \pm 2.01$ NS = 7.76 ± 0.09 Plasma hypoxanthine: $S = (15.24 \pm 2.09)$ NS = (37.48 ± 3.1)	Plasma xanthine: (9.4 ± 2.7) Plasma hypoxanthine: (1.69 ± 0.76)	Significant association with both hypoxanthine (Plasma $P < 0.01$ and BAL $P < 0.02$). Xanthine (plasma $P < 0.05$ and BAL $P < 0.01$)	NR
Ortolani et al. (17)	Glutathione and malondialdehyde (MDA)	Glutathione (<450 μM to <550 nM) Malondialdehyde (<4 to>4 nM)	0	Non-significant trend increase with time (9 days) of both Glutathione and Malondialdehyde	NR
Nathens et al. (30)	Ascorbate and alpha tocopherol	Not applicable	Ascorbate: day-0 ≤ 0.5, day-21 ≤ 0.5 Alpha-tocopherol: day- < 5, day-21 ≥ 10	Non-significant positive association (18% developed ARDS)	Multiple organ failure in 6.1% of subjects. Pneumonia in 15% at 28-day follow up, and 1.3% had renal failure
Scholpp et al. (24)	MDA and lipid peroxidation markers (acetone, isoprene and pentane)	MDA: 0.55 Acetone: 1.32 Isoprene: 50.0 *n*-Petane: 1	MDA: 0.38 Acetone: 0.55 Isoprene: 33.2 *n*-Petane: 0.12	Significant positive association for *N*-pentane ($P < 0.05$) non-significant positive association for MDA acetone and isoprene	NR
Nelson et al. (31)	Lipid peroxidation markers (beta-carotene, retinol, and α-tocopherol)	Exact values not provided: Beta carotene, retinol and α- tocopherol all significantly reduced in ARDS vs NON-ARDS		Significant levels of lipid peroxidation markers in ARDS vs non-ARDS patients ($P > 0.05$)	NR
Soltan-Sharifi et al. (18)	Glutation (GSH) and *N*-acetylcysteine	GSH 0 h – <600 increased to <800 at 72 h	0	Non-significant trend of association with time (3-days) with ARDS disease	NR
Moradi et al. (19)	GST isoforms: M1, T1 and P1	Significant association of mortality with GST M1 null polymorphism and double deletion of both genes (M1, T1) in control ARDS placebo group of interest ($P < 0.05$). No significance for the GST P1 isoform with mortality. Absence of the GST M1 gene/deletion of both GTS M1 and GST T1 are more vulnerable to oxidative stress contributing to ARDS/ALI		No association with recorded factors of duration of mechanical ventilation or Length of ICU stay Not directly applicable (NR)	NR
Nakahira et al. (10)	mtDNA copy number (NADH dehydrogenase 1 DNA level	BWH [46,648 (14,468–63,510)] ME [29,828 (7,857–84,675)]	BWH [10,584 (3,992–41,466)] ME [8,771 (3,296–20,464)]	Non-significant trend in association	NR
Bhargava et al. (26)	Glycolysis protein expression & enrichment, and Thioredoxin	Glycolysis is enriched in ARDS non-survivors with a fold change increase of 2.01 for GAPDHL6 (an example gene from the list of glycolytic proteins). This was not enriched in survivors Thioredoxin: S = apx. 2.5 NS = apx. 7.5	0	NR	NR

(Continued)

TABLE 5 (Continued)

References	Biomarker	Biomarker summary		Association to disease presence/ progression	Association to other worse outcomes of ARDS
		ARDS	Non-ARDS		
Rosenberg et al. (32)	GDF15	Raised levels of GDF-15 prior to discharge, and lower in recovery	NR	NR	More comorbidities present in higher GDF-15 quartiles – non-significant association
Blot et al. (14)	mtDNA	0.1503	0.01546	mtDNA levels significantly raised in ARDS patients indicating association significant $P = 0.02$	NR
Huang et al. (15)	mtDNA	Severe: 1,230 (588–22,387) Moderate: 5,370 (628–13,052) Mild: 15,792 (1,623–186,814) *S*: 7,585 (1,717–15,792) NS: 67,608 (19,498–346,736)	NR	Significant association $p = 0.04$	NR
Faust et al. (6)	mtDNA	PETROS: ARDS = 12.28 1.07 MESSI: ARDS = 11.06 1.31	PETROS: NON = 12.04 1.01 MESSI: NON = 11.25 1.20	Significant positive association ($P = 0.009$) Pero S ($P = 0.003$)	NR
Korsunov et al. (23)	Lactate and oxygen transport	3.4	5.3	Moderate evidence to suggest lower levels of lactate in ARDS patients	In-group one AKI was diagnosed in 8 patients (57.14%) which is twice as much as group 2–4 (26.7%)
Hernández-Beeftink et al. (16)	mtDNA	3.65 (1.39–9.59 (hazard ratio and 95% CL) 0.031 ± 0.2036 *S*: -0.0038 ± 0.2012 NS: 0.0702 ± 0.2001	1.24 (0.44–3.51) -0.0073 ± 0.2004	Non-significant trend of association	NR

S, survivor; NS, non-survivor; NR, not recorded; CL, confidence limit.

IL-6, IL-8, RAGE, Ang-2, C-reactive protein and procalcitonin (39, 40). A systematic review by van der Zee et al. examined the multivariate biomarkers associated with ARDS disease, in which RAGE and Ang-2 showed significant association with the risk of ARDS development; yet none were significantly correlated to mortality (40). This likely is contingent on the heterogeneous nature of ARDS pathophysiology.

Pneumonia and sepsis were the top two the most frequent and most devastating causes of ARDS in the studies included in the review. Recently mitochondrial dysfunction, specifically ability of immune cells to switch between glycolytic and oxidative phosphorylation pathways has emerged as a mechanism of pathogenesis of sepsis (41). Patients with sepsis have been shown to have decreased expression of mitochondrial quality mitophagy markers PINK1 and PARKIN, elevated levels of mtDNA, dysfunctional mitochondrial morphology and decreased mitochondrial mass, as well as increased cell death due to calcium overload and raised levels of reactive oxygen species (42–44). The consolidated contribution of mitochondrial dysfunction with the pathogenesis of sepsis, alongside the well-established sepsis induction of ARDS; combined made it plausible to hypothesize that mitochondrial dysfunction might too contribute to ARDS (5, 45).

To our knowledge, this is the first systematic review with meta-analysis investigating association of levels of biomarkers of mitochondrial dysfunction with ARDS. Majority of studies included into this review reported positive trends toward association of elevated levels of biomarkers of mitochondria dysfunction with ARDS. These trends reached statistical significance in the cases of mtDNA, xanthine, hypoxanthine, lactate, isoprene and *n*-pentane in the blood based samples, however statistically significant difference is absent in BAL samples. Of note, levels of xanthine were not detectable in the BAL of non-ARDS patients which could have impacted the results of meta-analysis.

Importantly, levels of circulating hypoxanthine, xanthine, mtDNA and lactate measured at early time points after presentation were significantly elevated in those who survived

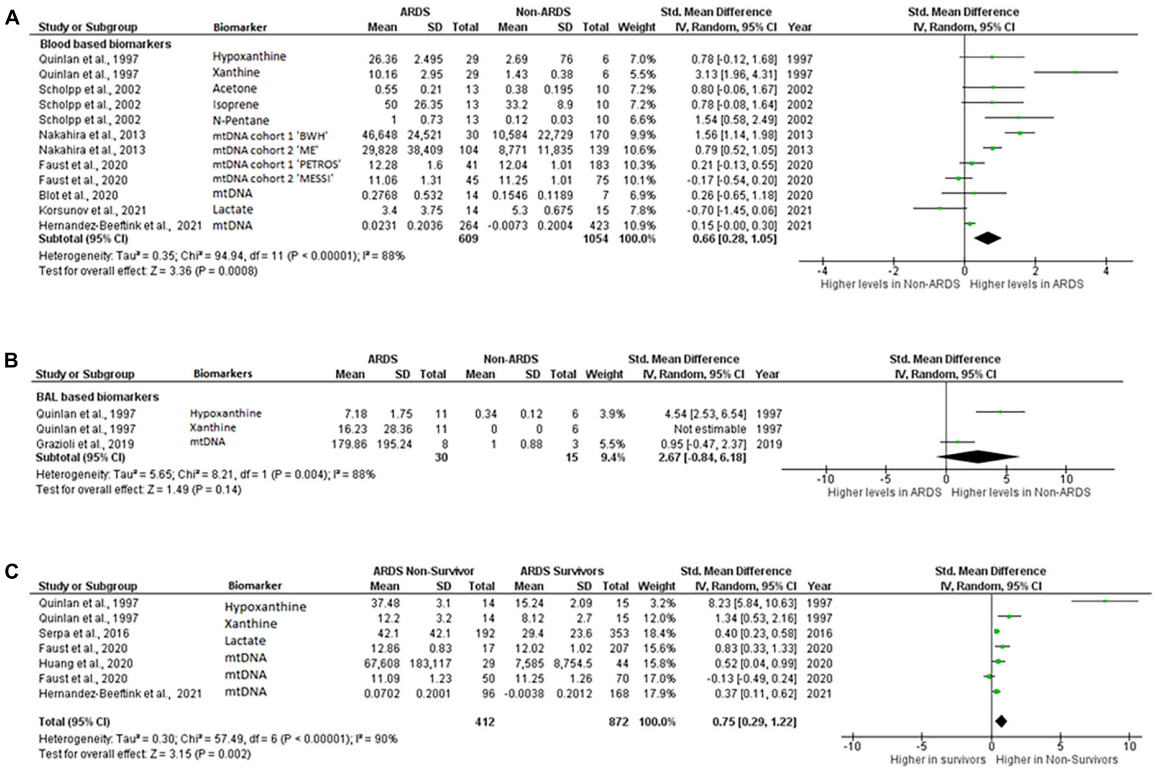

FIGURE 2
Levels of biomarkers of mitochondrial dysfunction. Forest plot meta-analysis of the levels of biomarkers in ARDS patients and non-ARDS controls in **(A)** blood samples $P = 0.008$ and **(B)** BAL samples $P = 0.14$ **(C)** ARDS survivors vs ARDS non-survivors, $P = 0.002$. Data analysis generated on RevMan 5.4.

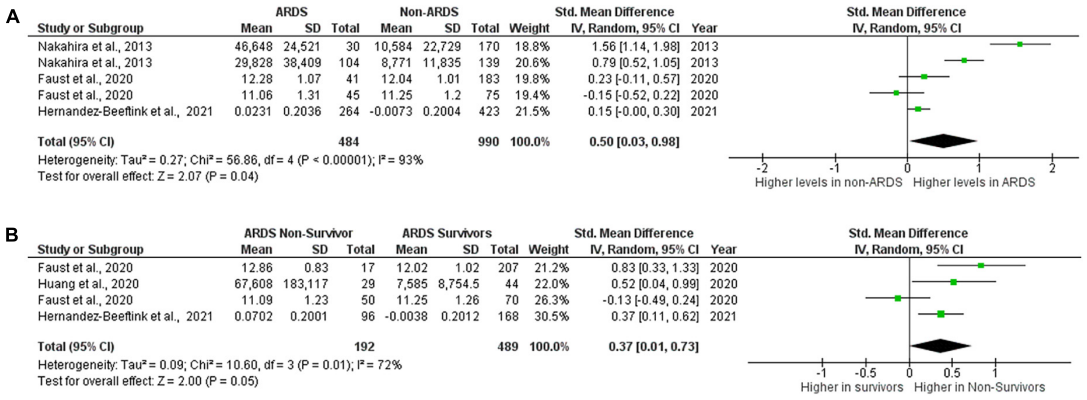

FIGURE 3
Levels of circulating mtDNA. Forest plot meta-analysis of the levels of circulating mtDNA in ARDS patients and non-ARDS controls, $P = 0.04$ **(A)** and in ARDS survivors vs ARDS non- survivors $P = 0.05$ **(B)**. Data analysis generated on RevMan 5.4.

ARDS compared to non-survivors, suggesting a potential role of mitochondrial dysfunction in ARDS pathogenesis.

MtDNA was the most frequently measured biomarker across the included studies. Levels of circulating cell-free mtDNA were significantly higher in ARDS patients compared to non-ARDS in six studies. This was further confirmed by meta-analysis of the three studies which have provided necessary raw values for comparison. Difference in mtDNA levels between ARDS survivors and non-survivors did not reach statistical significance by meta-analysis with overall $P = 0.05$, however there was strong trend toward higher levels in non-survivors. Interestingly, Faust et al., also reported mtDNA levels at 48 h

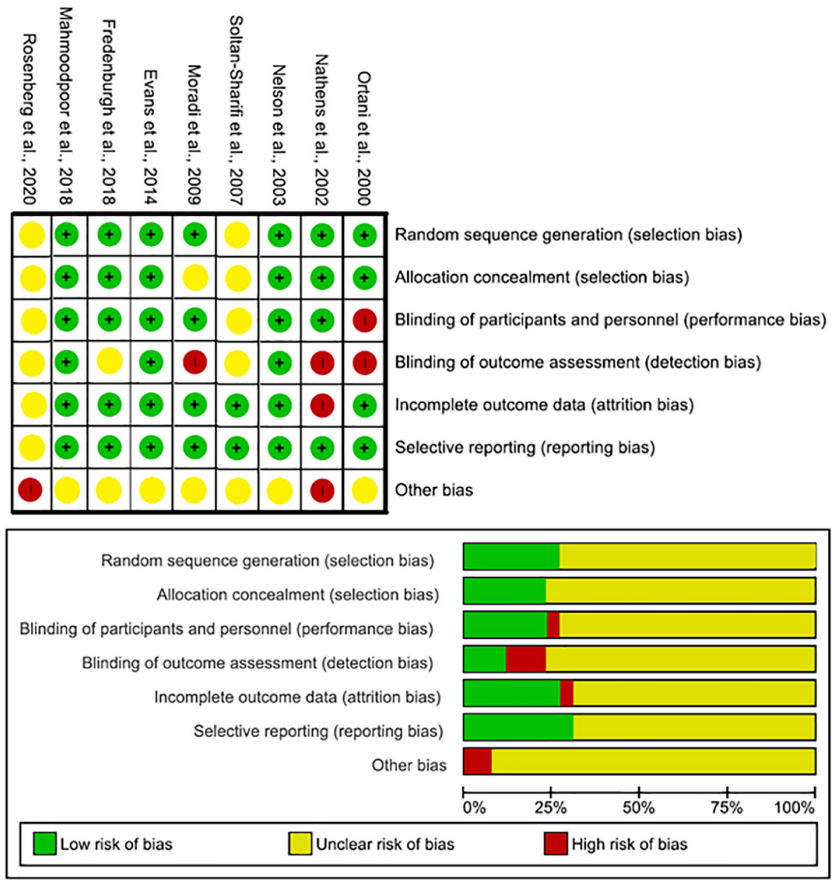

FIGURE 4
Quality assessment Cochrane risk of bias for RCT trial studies.

after presentation which were significantly higher in non-survivors than in survivors in both cohorts (6), suggesting that later time points might be more appropriate for measurements of mtDNA as predictor of mortality in ARDS. Taken together, these data indicate an association of mitochondrial dysfunction with ARDS pathophysiology and highlight blood mtDNA as important mediator of ARDS pathogenesis with the potential to serve as a biomarker for predicting the risk of mortality.

This systematic review identified ten different biomarkers of mitochondrial dysfunction measured in ARDS patients. Initial overview of mitochondrial biomarkers in ARDS vs non-ARDS patients showed significantly higher levels in the ARDS patient groups, regardless of the cause of ARDS (**Figure 2** and **Tables 4**, **5**). However, 6 of these biomarkers were only measured in one study; the top four most frequently measured biomarkers were (i) mtDNA, (ii) glutathione, (iii) lactate, and (iv) MDA. The study weighting of the meta-analysis was largely driven by blood mtDNA as the most frequently measured biomarker. Therefore, we carried out separate meta-analysis of the studies that reported levels of mtDNA. Plasma mtDNA levels were significantly higher in ARDS vs non-ARDS at time points from 0 to 24 h from presentation. Interestingly, Bolt et al., and Grazioli et al., also reported significant elevation in mtDNA levels in the BAL samples in ARDS patients compared to non-ARDS controls, although the information provided in these studies was not sufficient to run meta-analysis. However, the sample size was small in both studies (7 heathy vs. 7 ARDS and 3 healthy vs. 5ARDS BAL samples, respectively), therefore further studies are required to investigate the significance of alveolar release of mtDNA in ARDS, as a potential biomarker of lung injury.

Mitochondrial DNA levels are currently used as prognostic biomarker in a number of diseases such as Parkinson's disease and type two diabetes in combination with coronary heart disease (46). Hernandez-Beeftink et al., observed that mtDNA copies in the whole blood were significantly associated with 28-day survival in sepsis patients who developed ARDS (hazard ratio = 3.65, 95% confidence interval = 1.39–9.59, p = 0.009) but not in sepsis patients without ARDS. These findings support the hypothesis that cell free mtDNA copies at sepsis diagnosis could be considered an early prognostic biomarker in sepsis-associated ARDS patients. Results of this review support the potential use of mtDNA as ARDS biomarker; however, more

TABLE 6 Quality assessment Cochrane risk of bias table justifications for RCT trial studies.

	Random sequence generation (selection bias)	Allocation concealment (selection bias)	Blinding of participants and personnel (performance bias)	Blinding of outcome assessment (detection bias)	Incomplete outcome data (attrition bias)	Selective reporting (reporting bias)	Other bias
Ortolani et al. (17)	Random assignment of participants into treatment groups		Non-blinded study		Evenly assigned patient groups, no loose of patients in follow up	All outcome data reported	Other bias not discussed
Nathens et al. (30)	Random assignment of participants into treatment groups (1:1)		Personnel were blinded to grouping [carried out by computer and Pharmacy (non-investigators)]. Participants were non-blinded, but data taken from samples collected from blood thus removing this concern	Non-blinded for ease of care organization	High level of exclusion post trial administration	All outcome data reported	Lack of placebo for control group of inte rest for this SR and blinding for investigators post group assignment.
Nelson et al. (31)	Double blinded, controlled, randomized multicenter trial, permuted-block randomization design				Full patient follow up	All outcome data reported	Other bias not discussed
Soltan-Sharifi et al. (18)	Information not disclosed	Information not disclosed	Information not disclosed	Information not disclosed	Full patient follow up	All outcome data reported	Other bias not discussed
Moradi et al. (19)	Simple randomization was performed	Information not disclosed	Single blinding	Non-blinded	Full patient follow up	All outcomes set out, were recorded	Other bias not discussed
Evans et al. (20)	Randomized patients into treatment to control	Samples random order and were assigned to a random LC-MS run order using a computerized algorithm.	Agilent MassHunter Quantitative Analysis software, with the analyst blinded to the identity of the subjects.		Full patient follow up	All outcomes set out, were recorded	Other bias not discussed
Fredenburgh et al. (33)	Phase one unmasked for safety reasons, phase two was masked. Data taken only from phase two in relation for this SR.	Random allocation hidden from trial executives	Masking of which group participants where in as well as	Unclear	Full patient follow up	Data, even if unsuccessful reported	Other bias not discussed
Mahmoodpoor et al. (21)	Random assignment of participants into treatment groups (1:1)		Masking of which group participants where in as well as	Double blinded study	Full patient follow up	Data, even if unsuccessful reported	Other bias not discussed
Rosenberg et al. (32)	Information not disclosed	Information not disclosed	Information not disclosed	Information not disclosed	Information not disclosed	Information not disclosed	Potential recall bias

Risk of bias is higher with greater intensity of gray.

research would be required to determine the most appropriate sample (plasma or whole blood) as well as best time points for sample collection. Additionally, studies recorded mtDNA levels in different units (e.g., copy numbers per µl, µmol, intensities); although the meta-analysis model considers this factor, there is a need for standardization of the measurement units. Circulating mtDNA levels may facilitate the stratification of patients, however, future studies are necessary to standardize the technique and to define more accurate cut-off points.

Glutathione, and its downstream mediators, hypoxanthine and xanthine, follow a similar trend to mtDNA, with elevated levels in ARDS patients (**Tables 1**, **2**). Both hypoxanthine and xanthine are converted to uric acid through xanthine oxidase, resulting in ROS production and leading to oxidative stress (47, 48). In similar fashion, decreased glutathione reduction and increased redox imbalances are known to be associated with mitochondrial disorders (49). It is feasible that one, or both of these mediators could act as prognostic biomarkers for ARDS given the positive trends observed across the two studies (20, 21). Glutathione mediators were recorded in the blood and BAL samples, demonstrating similar trends. To further this avenue, measurement of all three ROS mediators in larger cohorts would be required.

Oxidative damage to lipids, amino acids, and DNA leads to accumulation of malondialdehyde (MDA) (**Tables 4**, **5**). MDA inhibits mitochondrial complex I, II and V, thus impacting the functionality of present mitochondria (50). Due to lack of control comparator for mortality/other worse outcomes, it was not possible to draw any definitive conclusions in regards to MDA. One out of three studies found significantly higher levels in ARDS compared to non-ARDS (17, 51), while the other two studies showed a non-significant trend with higher levels in ARDS (24). MDA was measured in both BAL and plasma; this variation could be driving the lack of conclusive results. Interestingly, studies which investigated the levels of lactate, another metabolite indirectly representative of mitochondrial

TABLE 7 Quality assessment Newcastle-Ottawa scale table for non-RCT studies.

Studies	Representativeness of the exposed cohort	Selection of the non-exposed cohort	Ascertainment of exposure	Demonstration that outcome of interest was not present at start of study	Comparability of cohorts on the basis of the design or analysis	Assessment of outcome	Was follow-up long enough for outcomes to occur	Adequacy of follow up of cohorts	Total
Quinlan et al. (29)	*	*	NR	*	*	*	NR	*	6
Scholpp et al. (24)	*	*	*	*	*	*	*	*	8
Nakahira et al. (10)	*	*	*	*	*	*	*	*	8
Bhargava et al. (26)	*	*	*	NA	*	*	*	NA	6
Evans et al. (20)	*		*	*					3
Liu et al. (25)	*		NR	*	*	*		*	5
Serpa et al. (22)	*	*	NR	*	*	*	*	*	7
Dorward et al. (27)	*	*	*	*	*	*	*	*	8
Garramone et al. (11)		*	NR	*		*	*		4
Grazioli et al. (13)		*	NR	*		*			3
Bos et al. (28)	*	*	Unclear	*	*	*	*	*	7
Blot et al. (14)		*	*	*	*	*	*	*	7
Huang et al. (15)	*	*	*	*	*	*	*	*	8
Faust et al. (6)	*	*	*	*	*	*	*	*	8
Korsunov et al. (23)		*	NR	*	*	*			4
Hernández -Beeftink et al. (16)	*	*	*	*	*	*			6

NR, not recorded. *One score.

dysfunction, also reported controversial findings (52). Evans et al., observed a fold-change increase in lactate in ARDS vs non-ARDS, while Serpa et al., demonstrated a higher level of lactate in ARDS non-survivors. On the contrary, Korsunov et al., reported higher levels of lactate in non-ARDS vs ARDS. No data comparisons around lactate were significant across the three studies (20, 22, 23). As there is no consistency across all three studies, it is plausible that metabolites such as MDA and lactate are not useful as prospective biomarkers for ARDS clinical outcomes (53).

One study examined a biomarker associated to mitochondria genetic defects; GDF-15 (**Tables 4**, **5**). GDF-15 is a secretory protein induced by mitochondrial stress, overexpressed in patients with mitochondrial point mutation syndromes (54, 55). The outcomes of this biomarker, as described in **Tables 4**, **5**, do indicate a possible link of association of mitochondrial dysfunction with ARDS, however the lack of raw numbers and limited size of the cohort did not allow for definitive conclusions; current evidence would not support the use of this genetic biomarker in ARDS.

The quality assessment imply a minimal risk of bias across the board of studies included. Main findings were drawn from meta-analysis, of which only one study, Korsunov et al., presented with NOS score of four, due to lack of provided information.

Limitations

This review had several limitations. First, the lack of global representation across study cohorts could influence the predictive power of the examined biomarkers. Secondly, a large variance in study size resulted in high I^2 values across all meta-analysis carried out; some of the smaller studies included less than 100 patients could be underpowered for significance calculations. Finally, regardless of standardized mean difference calculation weighting of studies, the inconsistency in biomarker units, as well as different methods of analysis of the same type of biomarkers could affect the statistical conclusions drawn from this small-scale meta-analysis.

Conclusion

This systematic review and meta-analysis suggest that increased levels of biomarkers of mitochondrial dysfunction are positively associated with ARDS. Blood-based biomarkers were the most appropriate for assessment of mitochondrial dysfunction. Circulating mtDNA is the most frequently measured biomarker of mitochondrial dysfunction; circulating mtDNA levels are significantly higher in ARDS patients compared to non-ARDS controls. Mitochondrial DNA is

a plausible biomarker candidate for further investigation of its role in ARDS pathogenesis. Further research is required to explore the role of mitochondrial biomarkers in greater populations of ARDS patients and between ARDS subphenotypes.

Data availability statement

The datasets presented in this study can be found in online repositories. The names of the repository/repositories and accession number(s) can be found in the article/**Supplementary material**.

Author contributions

AK designed the study, revised and independently checked the manuscript. CM and NM conducted the systematic searches and data extraction. CM merged the studies and wrote the manuscript. All authors approved the submitted version.

Funding

AK was supported by UKRI Medical Research Council Research (MR/R025096/1 and MR/S009426/1). CM was supported by Department for Economy Ph.D. studentship.

Acknowledgments

We are very grateful for Professor Danny McAuley and Dr. Bronwen Connolly for their guidance and professional advice during preparation of this systematic review.

Conflict of interest

The authors declare that the research was conducted in the absence of any commercial or financial relationships that could be construed as a potential conflict of interest.

Publisher's note

Supplementary material

The Supplementary Material for this article can be found online at: https://www.frontiersin.org/articles/10.3389/fmed.2022.1011819/full#supplementary-material

References

1. Sweeney RM, McAuley D. Acute respiratory distress syndrome. *Lancet.* (2016) 388:2416–30.

2. Matthay M, Zemans R, Zimmerman G, Arabi Y, Beitler J, Mercat A, et al. Acute respiratory distress syndrome. *Nat Rev Dis Prim.* (2018) 5:18. doi: 10.1038/s41572-019-0069-0

3. Fan E, Beitler J, Brochard L, Calfee C, Ferguson N, Slutsky A, et al. COVID-19-associated acute respiratory distress syndrome: is a different approach to management warranted? *Lancet Respir Med.* (2020) 8:816–21. doi: 10.1016/S2213-2600(20)30304-0

4. Schumacker P, Gillespie M, Nakahira K, Choi A, Crouser E, Piantadosi C, et al. Mitochondria in lung biology and pathology: more than just a powerhouse. *Am J Physiol Lung Cell Mol Physiol.* (2014) 306:962–74. doi: 10.1152/ajplung.00073.2014

5. Ten V, Ratner V. Mitochondrial bioenergetics and pulmonary dysfunction: current progress and future directions. *Paediatr Respir Rev.* (2020) 34:37–45. doi: 10.1016/j.prrv.2019.04.001

6. Faust H, Reilly J, Anderson B, Ittner C, Forker C, Zhang P, et al. Plasma mitochondrial DNA levels are associated with ARDS in trauma and sepsis patients. *Chest.* (2020) 157:67–76. doi: 10.1016/j.chest.2019.09.028

7. Simmons J, Lee Y, Pastukh V, Capley G, Muscat C, Muscat D, et al. Potential contribution of mitochondrial (mt) DNA damage associated molecular patterns (DAMPs) in transfusion products to the development of acute respiratory distress syndrome (ARDS) after multiple transfusions. *Physiol Behav.* (2017) 176:139–48. doi: 10.1097/TA.0000000000001421

8. Rossignol D, Frye R. Mitochondrial dysfunction in autism spectrum disorders: a systematic review and meta-analysis. *Mol Psychiatry.* (2012) 17:290–314. doi: 10.1038/mp.2010.136

9. Cloonan S, Kim K, Esteves P, Trian T, Barnes P. Mitochondrial dysfunction in lung ageing and disease. *Eur Respir Rev.* (2020) 29:200165.

10. Nakahira K, Kyung S, Rogers A, Gazourian L, Youn S, Massaro A, et al. Circulating mitochondrial DNA in patients in the ICU as a marker of mortality: derivation and validation. *PLoS Med.* (2013) 10:e1001577; discussione1001577. doi: 10.1371/journal.pmed.1001577

11. Garramone A, Cangemi R, Bresciani E, Carnevale R, Bartimoccia S, Fante E, et al. Early decrease of oxidative stress by non-invasive ventilation in patients with acute respiratory failure. *Intern Emerg Med.* (2018) 13:183–90. doi: 10.1007/s11739-017-1750-5

12. Pan X, Wang L, Fei G, Dong J, Zhong C, Lu J, et al. Acute respiratory failure is the initial manifestation in the adult-onset A3243G tRNALeu mtDNA mutation: a case report and the literature review. *Front Neurol.* (2019) 10:780. doi: 10.3389/fneur.2019.00780

13. Grazioli S, Dunn-Siegrist I, Pauchard L, Blot M, Charles P, Pugin J. Mitochondrial alarmins are tissue mediators of ventilator-induced lung injury and ARDS. *PLoS One.* (2019) 14:e0225468. doi: 10.1371/journal.pone.0225468

14. Blot M, Jacquier M, Aho Glele L, Beltramo G, Nguyen M, Bonniaud P, et al. CXCL10 could drive longer duration of mechanical ventilation during COVID-19 ARDS. *Crit Care.* (2020) 24:632.

15. Huang L, Chang W, Huang Y, Xu X, Yang Y, Qiu H. Prognostic value of plasma mitochondrial DNA in acute respiratory distress syndrome (ARDS): a single-center observational study. *J Thorac Dis.* (2020) 12:1320–8. doi: 10.21037/jtd.2020.02.49

16. Hernández-Beeftink T, Guillen-Guio B, Rodríguez-Pérez H, Marcelino-Rodríguez I, Lorenzo-Salazar J, Corrales A, et al. Whole-blood mitochondrial DNA

copies are associated with the prognosis of acute respiratory distress syndrome after sepsis. *Front Immunol.* (2021) 12:737369. doi: 10.3389/fimmu.2021.737369

17. Ortolani O, Conti A, De Gaudio A, Masoni M, Novelli G. Protective effects of N-Acetylcysteine and rutin on lipid peroxidation of the lung epithelium during the adult respiratory distress syndrome. *Shock.* (2000) 13:14–8. doi: 10.1097/00024382-200013010-00003

18. Soltan-Sharifi M, Mojtahedzadeh M, Najafi A, Khajavi M, Rouini M, Moradi M, et al. Improvement by N-acetylcysteine of acute respiratory distress syndrome through increasing intracellular glutathione, and extracellular thiol molecules and anti-oxidant power: evidence for underlying toxicological mechanisms. *Hum Exp Toxicol.* (2007) 26:697–703. doi: 10.1177/0960327107083452

19. Moradi M, Mojtahedzadeh M, Mandegari A, Soltan-Sharifi M, Najafi A, Khajavi M, et al. The role of glutathione-S-transferase polymorphisms on clinical outcome of ALI/ARDS patient treated with N-acetylcysteine. *Respir Med.* (2009) 103:434–41. doi: 10.1016/j.rmed.2008.09.013

20. Evans C, Karnovsky A, Kovach M, Standiford T, Burant C, Stringer K. Untargeted LC-MS metabolomics of bronchoalveolar lavage fluid differentiates acute respiratory distress syndrome from health. *J Proteome Res.* (2014) 13:640–9. doi: 10.1021/pr4007624

21. Mahmoodpoor A, Hamishehkar H, Shadvar K, Ostadi Z, Sanaie S, Saghaleini S, et al. The effect of intravenous selenium on oxidative stress in critically ill patients with acute respiratory distress syndrome. *Immunol Invest.* (2019) 48:147–59. doi: 10.1080/08820139.2018.1496098

22. Serpa Neto A, Schmidt M, Azevedo L, Bein T, Brochard L, Beutel G, et al. Associations between ventilator settings during extracorporeal membrane oxygenation for refractory hypoxemia and outcome in patients with acute respiratory distress syndrome: a pooled individual patient data analysis: mechanical ventilation during ECMO. *Intens Care Med.* (2016) 42:1672–84.

23. Korsunov, V, Georgiyants M, Skoryk V. Central hemodynamics and oxygen transport in patients with acute respiratory distress syndrome caused by Covid-19 and their impact on the course and outcomes of the disease. *EUREKA Heal Sci.* (2021) 1:3–11.

24. Scholpp J, Schubert J, Miekisch W, Geiger K. Breath markers and soluble lipid peroxidation markers in critically III patients. *Clin Chem Lab Med.* (2002) 40:587–94. doi: 10.1515/CCLM.2002.101

25. Liu D, Luo G, Luo C, Wang T, Sun G, Hei Z. Changes in the concentrations of mediators of inflammation and oxidative stress in exhaled breath condensate during liver transplantation and their relations with postoperative ARDS. *Respir Care.* (2015) 60:679–88. doi: 10.4187/respcare.03311

26. Bhargava M, Becker T, Viken K, Jagtap P, Dey S, Steinbach M, et al. Proteomic profiles in acute respiratory distress syndrome differentiates survivors from non-survivors. *PLoS One.* (2014) 9:e109713. doi: 10.1371/journal.pone.0109713

27. Dorward D, Lucas C, Doherty M, Chapman G, Scholefield E, Conway Morris A, et al. Novel role for endogenous mitochondrial formylated peptide-driven formyl peptide receptor 1 signalling in acute respiratory distress syndrome. *Thorax.* (2017) 72:928–36. doi: 10.1136/thoraxjnl-2017-210030

28. Bos L, Scicluna B, Ong D, Cremer O, Van Der Poll T, Schultz M. Understanding heterogeneity in biologic phenotypes of acute respiratory distress syndrome by leukocyte expression profiles. *Am J Respir Crit Care Med.* (2019) 200:42–50.

29. Quinlan G, Lamb N, Tilley R, Evans T, Gutteridge J. Plasma hypoxanthine levels in ARDS: implications for oxidative stress, morbidity, and mortality. *Am J Respir Crit Care Med.* (1997) 155:479–84. doi: 10.1164/ajrccm.155.2.9032182

30. Nathens A, Neff M, Jurkovich G, Klotz P, Farver K, Ruzinski J, et al. Randomized, prospective trial of antioxidant supplementation in critically III surgical patients. *Ann Surg.* (2002) 236:814–22. doi: 10.2174/138955707781024526

31. Nelson J, DeMichele S, Pacht E, Wennberg A, Gadek J, Drake J, et al. Effect of enteral feeding with eicosapentaenoic acid, γ-linolenic acid, and antioxidants on antioxidant status in patients with acute respiratory distress syndrome. *J Parenter Enter Nutr.* (2003) 27:98–104. doi: 10.1177/014860710302700298

32. Rosenberg B, Hirano M, Quinzii C, Colantuoni E, Needham D, Lederer D, et al. Growth differentiation factor-15 as a biomarker of strength and recovery in survivors of acute respiratory failure. *Thorax.* (2019) 74:1099–101. doi: 10.1136/thoraxjnl-2019-213621

33. Fredenburgh L, Perrella M, Barragan-Bradford D, Hess D, Peters E, Welty-Wolf K, et al. A phase I trial of low-dose inhaled carbon monoxide in sepsis-induced ARDS. *JCI Insight.* (2018) 3:e124039.

34. Gladden J, Zelickson B, Wei C, Ulasova E, Zheng J, Ahmed M, et al. Novel insights into interactions between mitochondria and xanthine oxidase in acute cardiac volume overload. *Free Radic Biol Med.* (2011) 51:1975–84. doi: 10.1016/j.freeradbiomed.2011.08.022

35. Tanda N, Hoshikawa Y, Sato T, Takahashi N, Koseki T. Exhaled acetone and isoprene in perioperative lung cancer patients under intensive oral care: possible indicators of inflammatory responses a nd metabolic changes. *Biomed Res.* (2019) 40:29–36. doi: 10.2220/biomedres.40.29

36. Hall J, Crane F. Disruption of mitochondrial membrane by acetone extraction. *Biochim Biophys Acta.* (1971) 2:682–6.

37. Akobsson-Borin A, Aberg F, Dallner G. Lipid peroxidation of microsomal and mitochondrial membranes extracted with n-pentane and reconstituted with ubiquinol, dolichol and cholesterol. *Biochim Biophys Acta.* (1994) 2:159–66. doi: 10.1016/0005-2760(94)90022-1

38. Villar J, Herrán-Monge R, González-Higueras E, Prieto-González M, Ambrós A, Rodríguez-Pérez A, et al. Clinical and biological markers for predicting ARDS and outcome in septic patients. *Sci Rep.* (2021) 11:22702.

39. Yan J, Rao Q. Biomarkers in the diagnosis and prognostic assessment of acute respiratory distress syndrome. *J Transl Intern Med.* (2014) 2:160–3.

40. Van Der Zee P, Rietdijk W, Somhorst P, Endeman H, Gommers D. A systematic review of biomarkers multivariately associated with acute respiratory distress syndrome development and mortality. *Crit Care.* (2020) 24:243. doi: 10.1186/s13054-020-02913-7

41. Rahmel T, Marko B, Nowak H, Bergmann L, Thon P, Rump K, et al. Mitochondrial dysfunction in sepsis is associated with diminished intramitochondrial TFAM despite its increased cellular expression. *Sci Rep.* (2020) 10:21029. doi: 10.1038/s41598-020-78195-4

42. Knutie S, Gabor C, Kohl K, Rohr J. Mitochondrial DNA in Sepsis. *Physiol Behav.* (2017) 176:139–48.

43. van der Slikke E, Star B, van Meurs M, Henning R, Moser J, Bouma H. Sepsis is associated with mitochondrial DNA damage and a reduced mitochondrial mass in the kidney of patients with sepsis-AKI. *Crit Care.* (2021) 25:36. doi: 10.1186/s13054-020-03424-1

44. Preau S, Vodovar D, Jung B, Lancel S, Zafrani L, Flatres A, et al. Energetic dysfunction in sepsis: a narrative review. *Ann Intens Care.* (2021) 11:104. doi: 10.1186/s13613-021-00893-7

45. Robinson MJ, Krasnodembskaya AD. Therapeutic targeting of metabolic alterations in acute respiratory distress syndrome. *Eur Respir Rev.* (2020) 29:200114. doi: 10.1183/16000617.0114-2020

46. Lowes H, Pyle A, Santibanez-Koref M, Hudson G. Circulating cell-free mitochondrial DNA levels in Parkinson's disease are influenced by treatment. *Mol Neurodegener.* (2020) 15:10. doi: 10.1186/s13024-020-00362-y

47. Kristal B, Vigneau-Callahan K, Moskowitz A, Matson W. Purine catabolism: links to mitochondrial respiration and antioxidant defenses? *Arch Biochem Biophys.* (1999) 370:22–33.

48. Vergeade A, Mulder P, Vendeville C, Ventura-Clapier R, Thuillez C, Monteil C. Xanthine oxidase contributes to mitochondrial ROS generation in an experimental model of cocaine-induced diastolic dysfunction. *J Cardiovasc Pharmacol.* (2012) 60:538–43. doi: 10.1097/FJC.0b013e318271223c

49. Enns G, Cowan T. Glutathione as a redox biomarker in mitochondrial disease—implications for therapy. *J Clin Med.* (2017) 6:50. doi: 10.3390/jcm6050050

50. Long J, Liu C, Sun L, Gao H, Liu J. Neuronal mitochondrial toxicity of malondialdehyde: inhibitory effects on respiratory function and enzyme activities in rat brain mitochondria. *Neurochem Res.* (2009) 34:786–94. doi: 10.1007/s11064-008-9882-7

51. Liu J, Zou Y, Tang Y, Xi M, Xie L, Zhang Q, et al. Circulating cell-free mitochondrial deoxyribonucleic acid is increased in coronary heart disease patients with diabetes mellitus. *J Diabetes Investig.* (2016) 7:109–14. doi: 10.1111/jdi.12366

52. Glancy B, Kane D, Kavazis A, Goodwin M, Willis W, Gladden L. Mitochondrial lactate metabolism: history and implications for exercise and disease. *J Physiol.* (2021) 599:863–88.

53. Metwaly S, Winston B. Systems biology ARDS research with a focus on metabolomics. *Metabolites.* (2020) 10:207. doi: 10.3390/metabo10050207

54. Ayuso P, Martínez C, Pastor P, Lorenzo-Betancor O, Luengo A, Jiménez-Jiménez F, et al. An association study between heme oxygenase-1 genetic variants and Parkinson's disease. *Front Cell Neurosci.* (2014) 8:298. doi: 10.3389/fncel.2014.00298

55. Fujita Y, Ito M, Ohsawa I. Mitochondrial stress and GDF15 in the pathophysiology of sepsis. *Arch Biochem Biophys.* (2020) 696:108668. doi: 10.1016/j.abb.2020.108668

frontiers | Frontiers in Medicine

TYPE Original Research
PUBLISHED 06 April 2023
DOI 10.3389/fmed.2023.1071741

OPEN ACCESS

EDITED BY
Emma Murphy,
Limerick Institute of Technology, Ireland

REVIEWED BY
Liu Chunfeng,
China Medical University, China
Artur Delgado,
São Paulo University, Brazil

*CORRESPONDENCE
Devang K. Sanghavi
✉ sanghavi.devang@mayo.edu

†These authors have contributed equally to this work and share first authorship

SPECIALTY SECTION
This article was submitted to Pulmonary Medicine, a section of the journal Frontiers in Medicine

RECEIVED 16 October 2022
ACCEPTED 20 March 2023
PUBLISHED 06 April 2023

CITATION
Isha S, Satashia PH, Yarrarapu SNS, Govero AB, Harrison MF, Baig HZ, Guru P, Bhattacharyya A, Ball CT, Caples SM, Grek AA, Vizzini MR, Khan SA, Heise KJ, Sekiguchi H, Cantrell WL, Smith JD, Chaudhary S, Gnanapandithan K, Thompson KM, Graham CG, Cowdell JC, Murawska Baptista A, Libertin CR, Moreno Franco P and Sanghavi DK (2023) A retrospective analysis of normal saline and lactated ringers as resuscitation fluid in sepsis.
Front. Med. 10:1071741.
doi: 10.3389/fmed.2023.1071741

A retrospective analysis of normal saline and lactated ringers as resuscitation fluid in sepsis

Shahin Isha[1†], Parthkumar H. Satashia[1†], Siva Naga S. Yarrarapu[1], Austin B. Govero[1], Michael F. Harrison[1,2], Hassan Z. Baig[1], Pramod Guru[1], Anirban Bhattacharyya[1], Colleen T. Ball[3], Sean M. Caples[4], Ami A. Grek[1], Michael R. Vizzini[1], Syed Anjum Khan[5], Katherine J. Heise[1], Hiroshi Sekiguchi[6], Warren L. Cantrell[1], Jeffrey D. Smith[1], Sanjay Chaudhary[1], Karthik Gnanapandithan[7], Kristine M. Thompson[2], Charles G. Graham[2], Jed C. Cowdell[7], Aleksandra Murawska Baptista[7], Claudia R. Libertin[8], Pablo Moreno Franco[1] and Devang K. Sanghavi[1*]

[1]Department of Critical Care Medicine, Mayo Clinic, Jacksonville, FL, United States, [2]Department of Emergency Medicine, Mayo Clinic, Jacksonville, FL, United States, [3]Department of Quantitative Health Sciences, Mayo Clinic, Jacksonville, FL, United States, [4]Division of Pulmonary and Critical Care Medicine, Mayo Clinic, Rochester, MN, United States, [5]Department of Critical Care Medicine, Mayo Clinic Health System Mankato, Mankato, MN, United States, [6]Department of Critical Care Medicine, Mayo Clinic, Phoenix, AZ, United States, [7]Division of Hospital Internal Medicine, Mayo Clinic, Jacksonville, FL, United States, [8]Division of Infectious Diseases, Mayo Clinic, Jacksonville, FL, United States

Background: The Surviving Sepsis Campaign suggested preferential resuscitation with balanced crystalloids, such as Lactated Ringer's (LR), although the level of recommendation was weak, and the quality of evidence was low. Past studies reported an association of unbalanced solutions, such as normal saline (NS), with increased AKI risks, metabolic acidosis, and prolonged ICU stay, although some of the findings are conflicting. We have compared the outcomes with the preferential use of normal saline vs. ringer's lactate in a cohort of sepsis patients.

Method: We performed a retrospective cohort analysis of patients visiting the ED of 19 different Mayo Clinic sites between August 2018 to November 2020 with sepsis and receiving at least 30 mL/kg fluid in the first 6 h. Patients were divided into two cohorts based on the type of resuscitation fluid (LR vs. NS) and propensity-matching was done based on clinical characteristics as well as fluid amount (with 5 ml/kg). Single variable logistic regression (categorical outcomes) and Cox proportional hazards regression models were used to compare the primary and secondary outcomes between the 2 groups.

Results: Out of 2022 patients meeting our inclusion criteria; 1,428 (70.6%) received NS, and 594 (29.4%) received LR as the predominant fluid (>30 mL/kg). Patients receiving predominantly NS were more likely to be male and older in age. The LR cohort had a higher BMI, lactate level and incidence of septic shock. Propensity-matched analysis did not show a difference in 30-day and in-hospital mortality rate, mechanical ventilation, oxygen therapy, or CRRT requirement. We did observe longer hospital LOS in the LR group (median 5 vs. 4 days, p = 0.047 and higher requirement for ICU post-admission (OR: 0.70; 95% CI: 0.51–0.96;

p = 0.026) in the NS group. However, these did not remain statistically significant after adjustment for multiple testing.

Conclusion: In our matched cohort, we did not show any statistically significant difference in mortality rates, hospital LOS, ICU admission after diagnosis, mechanical ventilation, oxygen therapy and RRT between sepsis patients receiving lactated ringers and normal saline as predominant resuscitation fluid. Further large-scale prospective studies are needed to solidify the current guidelines on the use of balanced crystalloids.

KEYWORDS

sepsis, fluid dose, balanced solution, ringers lactate, normal saline, resuscitation

1. Introduction

The Third International Consensus Guidelines defined sepsis as a "life-threatening organ dysfunction caused by a dysregulated host immune response to infection." On the other hand, septic shock has been defined as "a vasopressor requirement to maintain a mean arterial pressure of 65 mmHg or greater and serum lactate level greater than 2 mmol/L in the absence of hypovolemia" in a patient with suspected or confirmed sepsis (1). Sepsis and septic shock as a disease entity confer a major burden on the healthcare system and rigorous attempts have been made to improve the overall mortality and morbidity by adjusting the guidelines as per existing evidence (2, 3).

Early diagnosis and initiation treatment, which comprises of antibiotics and judicious fluid therapy during the initial phase of resuscitation have received strong recommendations. The 2021 updates on International Guidelines for Management of Sepsis and Septic Shock strongly recommended the use of crystalloids as first-line fluid therapy during the initial resuscitation phase of sepsis or septic shock. Moreover, for adults with sepsis or septic shock, the use of balanced crystalloids over normal saline was suggested by the guideline although the quality of evidence was reported to be "low" and the recommendation was "weak" (4).

Balanced crystalloid solutions, such as lactated Ringer's solution (LR), Ringer Acetate, Plasmalyte, etc., are usually normotonic and have a lower tendency to cause hyperchloremic acidosis (5, 6). On the other hand, the normal saline (NS) solution is an unbalanced solution and has been associated with hyperchloremic metabolic acidosis (7, 8). A large volume of NS infusion may also cause coagulopathy, renal dysfunction, and impaired immunological response (9). Despite significant work that has been done on the use of balanced crystalloids in critically ill patients, the data regarding the crystalloid of choice in sepsis is conflicting.

A large retrospective cohort study done by Raghunathan et al. (10) on patients admitted with sepsis failed to demonstrate any difference in the incidence of AKI and in-hospital and ICU length of stay, although the mortality rates were lower in the balanced crystalloid cohort. The SMART trial also showed favorable outcomes (lower rates of mortality, renal replacement therapy, or persistent renal dysfunction) in critically ill patients treated with balanced crystalloid use compared to normal saline (11). A network meta-analysis done by Rochwerg et al. (12) revealed that fluid resuscitation with balanced crystalloids was associated with lower mortality compared to normal saline in patients with sepsis, based on an indirect comparison. On the other hand, a chloride-restrictive strategy during fluid resuscitation of critically ill patients was shown to have a lower incidence of acute kidney injury (AKI) and renal replacement therapy requirement in a sequential prospective study conducted by Yunos et al. (13) however, no difference in mortality, hospital stay, or ICU stay was noted.

In the background of conflicting evidence, we have tried to compare the outcomes associated with NS and LR as a resuscitation fluid in patients who presented to the emergency department and were subsequently diagnosed with sepsis.

2. Materials and methods

Our automated data pull identified 2,899 hospitalization in 2,751 sepsis patients who presented to the Emergency Departments of 19 different Mayo Clinic sites between August 2018 to November 2020 with a diagnosis of sepsis and were treated with ≥30 mL/kg of either NS or LR during the first 6 h. Patients were excluded (n = 221) if they declined research authorization, were under 18 years old at the time of presentation to the ED or if the date of diagnosis was missing. Patients were also excluded (n = 571) they received >30 ml/kg of both fluid type or, received <30 ml/kg of each fluid type during the first 6 h. If a patient had more than one hospitalization with a diagnosis of sepsis during the study period, then we selected the first encounter per patient for inclusion in the study. Our final analysis included 2022 unique patients of these, 1,428 (70.6%) received NS, and 594 (29.4%) received LR as the predominant fluid. Patient information and relevant data were collected from the Electronic Health record. The time of diagnosis was determined by either time of antibiotic administration or the time of a lactic acid draw, not the result. Primary outcomes include in-hospital death, and secondary outcomes include in-hospital length-of-stay, 30-day mortality, ICU admission after diagnosis, ventilator use, and CRRT use. We used mean arterial pressure (MAP), vasopressor requirement and lactate level to define septic shock retrospectively. Any patient with a vasopressor requirement to maintain a mean arterial pressure of 65 mm Hg or greater and serum lactate level greater than 2 mmol/L was identified to have

TABLE 1A Baseline characteristics before and after matching according to fluid type among those who received 30 ml/kg or more.

	Before matching			After matching		
	Normal saline (*N* = 1,428)	Lactated ringers (*N* = 594)	SMD	Normal saline (*N* = 436)	Lactated ringers (*N* = 436)	SMD
Age at diagnosis (years)	71 (60, 81)	68 (58, 79)	0.11	69 (59, 79)	69 (59, 80)	0.04
Male sex	640 (44.8%)	238 (40.1%)	0.10	170 (39.0%)	188 (43.1%)	0.08
Race			0.13			0.06
American Indian/Alaskan Native	10 (0.7%)	3 (0.5%)		4 (0.9%)	3 (0.7%)	
Asian	32 (2.2%)	14 (2.4%)		11 (2.5%)	12 (2.8%)	
Black	33 (2.3%)	22 (3.7%)		13 (3.0%)	15 (3.4%)	
Native Hawaiian/Pacific Islander	3 (0.2%)	2 (0.3%)		1 (0.2%)	1 (0.2%)	
White	1,312 (91.9%)	528 (88.9%)		390 (89.4%)	392 (89.9%)	
Other/unknown	38 (2.7%)	25 (4.2%)		17 (3.9%)	13 (3.0%)	
Ethnicity			0.08			0.03
Not Hispanic or Latino	1,353 (94.7%)	554 (93.3%)		411 (94.3%)	409 (93.8%)	
Hispanic or Latino	41 (2.9%)	18 (3.0%)		14 (3.2%)	14 (3.2%)	
Other/Unknown	34 (2.4%)	22 (3.7%)		11 (2.5%)	13 (3.0%)	
Body mass index	24.6 (21.5, 28.7)	28.7 (23.9, 34.9)	0.60	26.2 (23.0, 30.6)	26.8 (23.2, 31.5)	0.02
COPD	173 (12.1%)	62 (10.4%)	0.05	40 (9.2%)	43 (9.9%)	0.02
Hypertension	530 (37.1%)	225 (37.9%)	0.02	171 (39.2%)	161 (36.9%)	0.05
CKD	236 (16.5%)	103 (17.3%)	0.02	74 (17.0%)	75 (17.2%)	0.01
Diabetes	276 (19.3%)	101 (17.0%)	0.06	85 (19.5%)	71 (16.3%)	0.08
CAD	254 (17.8%)	88 (14.8%)	0.08	69 (15.8%)	73 (16.7%)	0.03
CHF	154 (10.8%)	62 (10.4%)	0.01	47 (10.8%)	41 (9.4%)	0.05
Obesity	231 (16.2%)	184 (31.0%)	0.35	100 (22.9%)	107 (24.5%)	0.04
Dialysis	48 (3.4%)	19 (3.2%)	0.01	11 (2.5%)	13 (3.0%)	0.03
Type of diagnosis: lactate-draw	806 (56.4%)	434 (73.1%)	0.35	311 (71.3%)	304 (69.7%)	0.04
Hospital type (destination)	834 (58.4%)	469 (79.0%)	0.45	338 (77.5%)	344 (78.9%)	0.03
MAP	90.2 (81.3, 99.3)	88.7 (79.0, 98.3)	0.14	89.0 (80.0, 99.1)	88.7 (79.3, 98.3)	0.03
Septic shock	95 (6.7%)	113 (19.0%)	0.38	64 (14.7%)	67 (15.4%)	0.02
Blood culture positive	94 (6.6%)	58 (9.8%)	0.12	41 (9.4%)	44 (10.1%)	0.04
Maximum lactate	3.3 (2.6, 4.6)	3.8 (2.9, 5.7)	0.30	3.9 (2.9, 5.5)	3.7 (2.9, 5.8)	0.07
Total fluid amount (ml/kg)	40.3 (33.8, 50.9)	49.6 (39.9, 63.0)	0.04	44.7 (37.2, 55.2)	45.4 (37.7, 55.9)	0.05

SMD, standardized mean difference; COPD, chronic obstructive pulmonary disease; CKD, chronic kidney disease; CAD, coronary artery disease; CHF, congestive heart failure; MAP, mean arterial pressure. Numerical characteristics are given as median (interquartile range), while categorical characteristics are given as the percentage of patients. Overall maximum lactate was not available 740 patients before matching and 252 patients after matching.

septic shock, as per the "Third International Consensus Definitions for Sepsis and Septic Shock" guidelines (1).

Mayo Clinic Institutional Review Board (IRB) granted an exemption (application number 20-008691) from the need for approval for our study on 3 September 2020. The need for informed consent was waived by our IRB. Procedures were followed in accordance with the ethical standards of the committee responsible for human experimentation and with the Helsinki Declaration of 1975.

2.1. Statistical analysis

Continuous characteristics were summarized with the sample median and interquartile range. Categorical characteristics were summarized with the frequency and percentage of patients. Characteristics known at the time of sepsis diagnosis were summarized according to fluid type among the cohort of patients who received 30 ml/kg or more of fluid. We aimed to estimate the effect of fluid type on outcomes (in-hospital mortality (primary), hospital LOS (secondary), death within 30 days of diagnosis (secondary), ICU admission after diagnosis (secondary), mechanical ventilator (secondary), adult oxygen therapy (secondary), and CRRT (secondary). To control confounding, propensity score matching was used to identify a cohort of patients with similar baseline characteristics. Propensity score is defined here as the conditional probability of a patient diagnosed with sepsis receiving predominantly lactated ringers vs. normal saline given a set of covariates known at the time of sepsis diagnosis (baseline).

A logistic regression model with fluid type as the dependent variable and all the baseline characteristics displayed in Table 1A

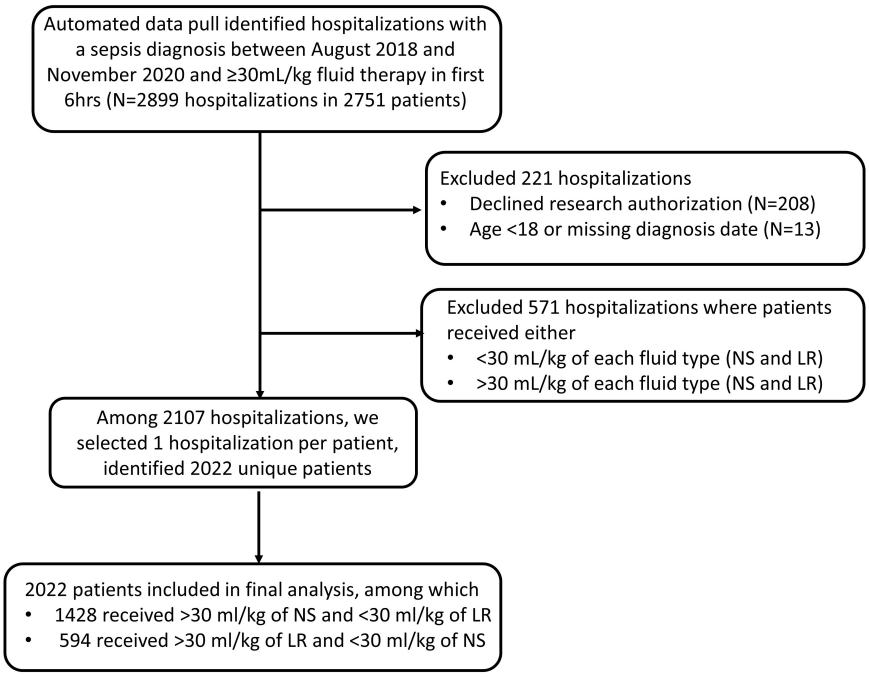

FIGURE 1
Flowchart showing inclusion and exclusion of patients in the study cohort.

as covariates was used to estimate the propensity score. Due to missingness, MAP was categorized based on tertiles and missing values were assigned to as separate category to estimate the propensity score. The nearest neighbor matching algorithm was used to select one patient who received normal saline to each patient who received lactated ringers with a caliper width equal to 0.2 of the standard deviation (SD) of the logit of the propensity score. The matching algorithm additionally included body mass index with a caliper width of 5 kg/m^2 and total fluid amount with a caliper width of 5 ml/kg. Standardized differences were estimated before and after matching using the tableone R package to assess potential imbalance in baseline characteristics between the 2 groups (14). A standardized difference less than 0.10 for a given baseline characteristic was considered a negligible imbalance between groups (substantial imbalance was defined as a standardize difference >0.2). Odds ratios (OR) and Hazard ratios (HR) were estimated from single variable logistic regression (categorical outcomes) and Cox proportional hazards regression (hospital length of stay). For hospital LOS, censoring occurred at the date of death for those who had an inpatient death and the Kaplan-Meier method was used to estimate median (25th percentile, 75th percentile); an HR less than 1.00 indicates a worse outcome (longer length of stay) for patients who were given LR compared to patients who were given NS. For categorical outcomes, ORs greater than 1.00 indicate a worse outcome for patients who were given >30 ml/kg of LR compared to patients who were given >30 ml/kg of NS. All statistical tests were two-sided. For our primary outcome, $p > 0.05$ was considered statistically significant without adjustment for multiple testing. For our secondary outcomes, $p < 0.05$ was considered statistically significant after adjustment for multiple testing using the Holm method, however, we do note unadjusted p-values in the results and tables. Adjusted p-values will be labeled as such. Statistical analyses were performed using R version 4.0.3 (R Foundation for Statistical Computing, Vienna, Austria).

3. Results

Our retrospective analysis included 2022 patients; of these, 1,428 (70.6%) received NS, and 594 (29.4%) received LR as the predominant fluid (Figure 1). Baseline patient characteristics are summarized in Table 1A before and after propensity score matching. Before matching, there were substantial baseline differences (standardized difference >0.2) between LR and NS, where patients who received predominantly LR were more likely to have had a higher body mass index and/or history of obesity, a lactate draw diagnosis, treated at a destination hospital, had septic shock, and a higher overall maximum lactate. After matching, all standardized differences were 0.08 or less and considered negligible. Table 1B shows baseline vital signs and laboratory information according to fluid type after matching. We did not observe any substantial imbalance in baseline vital signs and labs after matching (all standardized differences ≤0.18).

Table 2 summarizes the outcomes according to the fluid category. In our matched cohort, 8.0% died in-hospital among those who predominantly received >30 mL/kg of NS, and 8.5% died in-hospital among the group who predominantly received >30 mL/kg of LR. We did not find evidence of an association of fluid type (LR vs. NS) with in-hospital mortality (OR 1.06; 95% CI 0.66–1.73; $p = 0.81$) (primary outcome). The median hospital LOS after diagnosis was 1 day longer for those who received LR vs. NS (5 vs. 4 days; $p = 0.046$) (secondary outcome). In the subset of patients not in the ICU at the time

TABLE 1B Baseline vital signs and laboratory information of RL and NS cohorts after matching.

	Normal saline > 30 ml/kg (*N* = 436)	Lactated ringers > 30 ml/kg (*N* = 436)	SMD
Temperature (F)	*n* = 436	*n* = 435	
	98.1 (97.5, 98.4)	98.1 (97.5, 98.4)	0.13
Systolic blood pressure (mmHg)	*n* = 436	*n* = 436	
	123 (110, 138)	123 (111, 137)	0.02
Diastolic blood pressure (mmHg)	*n* = 436	*n* = 436	
	71 (62, 80)	71 (61, 80)	0.06
Pulse (beats per minute)	*n* = 435	*n* = 435	
	82 (71, 94)	81 (71, 92)	0.06
Respirations (breaths per minute)	*n* = 431	*n* = 427	
	18 (16, 20)	18 (16, 19)	0.03
Oxygen saturation (%)	*n* = 65	*n* = 61	
	95.1 (92.6, 97.0)	95.2 (92.8, 97.4)	0.08
Hemoglobin (g/dL)	*n* = 436	*n* = 435	
	11.9 (10.0, 13.7)	11.4 (9.6, 12.9)	0.18
White blood cell count (x10^3/mcL)	*n* = 436	*n* = 435	
	13.4 (8.4, 18.2)	12.4 (7.2, 17.4)	0.07
Platelets (x10^3/mcL)	*n* = 436	*n* = 435	
	208 (139, 280)	213 (149, 282)	0.06
Sodium P (mmol/L)	*n* = 301	*n* = 294	
	135 (132, 139)	136 (133, 139)	0.15
Potassium P (mmol/L)	*n* = 299	*n* = 295	
	4.0 (3.7, 4.5)	4.1 (3.7, 4.5)	0.02
BUN P (mg/dL)	*n* = 301	*n* = 293	
	22 (15, 33)	25 (16, 39)	0.18
Creatinine P (mg/dL)	*n* = 301	*n* = 293	
	1.2 (0.8, 1.6)	1.2 (0.8, 1.9)	0.11
Lactate P (mmol/L)	*n* = 320	*n* = 321	
	2.3 (1.6, 3.7)	2.1 (1.4, 3.2)	0.14
Bicarbonate P (mmol/L)	*n* = 301	*n* = 294	
	22 (19, 25)	22 (19, 24)	0.06

SMD, standardized difference. The number of available observations and median (25th percentile, 75th percentile) are shown.

of diagnosis, we found those who received LR were less likely to be admitted to the ICU after diagnosis compared to those who received NS (36.5% vs. 45.2%; OR 0.70; 95% CI 0.51–0.96; $p = 0.026$) (secondary outcome). We did not find evidence of differences in 30-day mortality or requirements for mechanical ventilator, adult oxygen therapy, or CRRT (all $p \geq 0.066$). After adjustment for multiple testing, associations of fluid type with hospital LOS and ICU admission after diagnosis were no longer statistically significant (adjusted $p = 0.28$ and 0.18, respectively).

4. Discussion

In our original cohort, we noted that most of the patients (1,428/2,022) were predominantly treated with >30 mL/kg of NS. Those treated with LR tended to have a higher BMI and were sicker with 19.0% having septic shock vs. 6.7% among those who received NS. Prior to matching patients on baseline characteristics and fluid amount, we observed in-patient mortality rates of 10.9% among those who received LR and 6.4% among those who received NS. After matching, in-patient mortality rates were similar (8.5 and 8.0%, respectively). For our secondary outcomes, after matching we observed a slight increase in hospital LOS and lower rate of ICU admission after diagnosis among those who had LR vs. NS, but these would not be considered statistically significant after adjustment for multiple testing based on 8 hypothesis tests of secondary outcomes. Such study findings contrast with some of the prior studies that reported favorable outcomes with balanced crystalloids (10, 13, 15).

While most of these studies were limited by their retrospective design, findings from the recent clinical trials have tried to shed more light on this domain. The SPLIT multicenter, double-blinded, cluster randomized, double-crossover clinical trial on 2,278 eligible medical and surgical ICU patients did not demonstrate any difference in AKI-related outcomes and mortality rate between buffered crystalloid and normal saline as fluid therapy (16). Although the SPLIT trial did not focus on sepsis patients, a similar finding was reported by the SALT pilot trial comprising of 974 patients with septic patients comprising 25 and 28% of balanced crystalloid and normal saline groups, respectively, in line with the findings of our study (17). On the other hand, the SMART single-center, randomized trial reported a lower rates of 30-day inpatient mortality and adverse renal outcome with the use of balanced crystalloid in their subgroup analysis of sepsis patients (18).

Limitations related to patient demographics and site-specific variations in outcome may be present in some of these past literatures. In that aspect, this study has several strengths. With more than 2,000 patients from 19 sites, both academic and community, from across multiple regions, including the Southeast, Southwest, and Midwestern United States adds to the generalizability. We have large sample size in our original cohort and even our sample size after matching would have at least 80% power at the two-sided 5% significance level to detect a difference of at least 6% in in-patient mortality (for example, 5% vs. 10%, 10% vs. 16%). Considering the current evidence on varying patient outcomes based on culture-status and fluid overload, our propensity-matched analysis addresses potential confounders and strengthens the overall methodology (19, 20).

The is a retrospective analysis, which comes with inherent limitations. We did not stratify our cohort based on the site of infection and origin of sepsis, which can obscure some of the findings. Also, there was no standardization of rate, type, or mode of delivery of fluid resuscitation among our patients, all of which could have a significant impact on the outcome. Particularly, the lack of information on infusion rate is a salient limitation, as previous studies have shown better survival with quicker rates (21, 22). Additionally, we could not account for prehospital fluid administration and partial administration of different fluid types leading to potential mixed effects. Finally, our study cohort had

TABLE 2 Association of fluid type with outcomes in the matched LR and NS cohorts.

Outcome	Normal saline (N = 436)[a]	Lactated ringers (N = 436)[a]	OR or HR (95% CI), LR vs. NS[b]	Unadjusted p-value
Primary outcome				
In-hospital mortality	35 (8.0%)	37 (8.5%)	1.06 (0.66–1.73)	0.81
Secondary outcomes				
Hospital LOS	4 (3, 7)	5 (3, 8)	0.87 (0.76–1.00)	**0.047**
Death within 30 days of diagnosis	69 (15.8%)	76 (17.4%)	1.12 (0.79–1.61)	0.52
ICU admission after diagnosis[c]	159/352 (45.2%)	107/293 (36.5%)	0.70 (0.51–0.96)	**0.026**
Mechanical ventilator	39 (8.9%)	56 (12.8%)	1.50 (0.98–2.32)	0.066
Adult oxygen therapy	187/326 (57.4%)	178/323 (55.1%)	0.91 (0.67–1.24)	0.56
CRRT	13/326 (4.0%)	12/323 (3.7%)	0.93 (0.41–2.08)	0.86

P-value of 0.05 was considered to be cut-off for statistical significance. Values shown in bold font represent statistical significance.
OR, odds ratio; HR, hazard ratio; CI, confidence interval; LOS, length of stay.
[a]Number (percent) or sample median (25th percentile, 75th percentile). Median hospital LOS was estimated using the Kaplan-Meier method censoring at the day of death for those patients who died in-hospital.
[b]ORs and HRs were estimated from single variable logistic regression (categorical outcomes) and Cox proportional hazards regression (hospital length of stay). For hospital length of stay, censoring occurred at the date of death for those who had an inpatient death and an HR less than 1.00 indicates a worse outcome (longer length of stay) for patients who were given LR compared to patients who were given NS. For categorical outcomes, ORs greater than 1.00 indicate a worse outcome for patients who were given >30 ml/kg of LR compared to patients who were given >30 ml/kg of NS.
[c]In subset of patients not admitted to the ICU prior to diagnosis.

more than 90% of white patients, which is non-representative of the overall US population, although the collection of data from 19 different sites provides generalizability. With the contrasting pieces of data, a further large-scale study is needed on the outcome of different types of resuscitation fluid in sepsis.

5. Conclusion

In our study, we did not show any difference in outcomes with LR as a predominant fluid for sepsis resuscitation compared to NS. Additional evidence is warranted to solidify the current guidelines on the use of balanced crystalloids.

Data availability statement

The original contributions presented in this study are included in the article/supplementary material, further inquiries can be directed to the corresponding author.

Ethics statement

Mayo Clinic Institutional Review Board (IRB) granted an exemption (application number 20-116 008691) from the need for approval for our study. The need for informed consent was waived by our IRB. The study was conducted in accordance with national and international guidelines.

Author contributions

SI: conceptualization, writing–original draft, writing–review and editing, visualization, supervision, and project administration. PS: conceptualization, writing–original draft, writing–review and editing, investigation, and visualization. SY: conceptualization, writing–review and editing, visualization, and data curation. AG and MH: methodology, writing–review and editing, visualization, investigation, and data curation. HB, PG, and AB: conceptualization, writing–original draft, writing–review and editing, visualization, and supervision. CB: methodology, writing–review and editing, data curation, and formal analysis. SMC, AG, MV, SK, KH, HS, WC, JS, SC, KG, KT, CG, JC, and AM: conceptualization, writing–original draft, and writing–review and editing. CL and PM: conceptualization, writing–original draft, writing–review and editing, and supervision. DS: conceptualization, writing–original draft, writing–review and editing, visualization, supervision, and project administration. All authors contributed to the article and approved the submitted version.

Acknowledgments

We would like to thank all the co-authors involved in this study for their useful contributions.

Conflict of interest

The authors declare that the research was conducted in the absence of any commercial or financial relationships that could be construed as a potential conflict of interest.

Publisher's note

References

1. Singer M, Deutschman C, Seymour C, Shankar-Hari M, Annane D, Bauer M, et al. The third international consensus definitions for sepsis and septic shock (sepsis-3). *JAMA*. (2016) 315:801. doi: 10.1001/jama.2016.0287

2. Fleischmann C, Scherag A, Adhikari N, Hartog C, Tsaganos T, Schlattmann P, et al. Assessment of global incidence and mortality of hospital-treated sepsis. current estimates and limitations. *Am J Respir Crit Care Med.* (2016) 193:259–72. doi: 10.1164/rccm.201504-0781OC

3. Fleischmann-Struzek C, Mellhammar L, Rose N, Cassini A, Rudd K, Schlattmann P, et al. Incidence and mortality of hospital- and ICU-treated sepsis: results from an updated and expanded systematic review and meta-analysis. *Intensive Care Med.* (2020) 46:1552–62. doi: 10.1007/s00134-020-06151-x

4. Evans L, Rhodes A, Alhazzani W, Antonelli M, Coopersmith C, French C, et al. Surviving sepsis campaign: international guidelines for management of sepsis and septic shock 2021. *Intensive Care Med.* (2021) 47:1181–247.

5. Morgan T. The ideal crystalloid - what is "balanced"? *Curr Opin Crit Care.* (2013) 19:299–307. doi: 10.1097/MCC.0b013e3283632d46

6. Corrêa T, Rocha L, Pessoa C, Silva E, de Assuncao M. Fluid therapy for septic shock resuscitation: which fluid should be used? *Einstein (Sao Paulo).* (2015) 13:462–8. doi: 10.1590/S1679-45082015RW3273

7. Astapenko D, Navratil P, Pouska J, Cerny V. Clinical physiology aspects of chloremia in fluid therapy: a systematic review. *Perioper Med (Lond).* (2020) 9:40. doi: 10.1186/s13741-020-00171-3

8. Hammond D, Lam S, Rech M, Smith M, Westrick J, Trivedi A, et al. Balanced crystalloids versus saline in critically Ill adults: a systematic review and meta-analysis. *Ann Pharmacother.* (2020) 54:5–13. doi: 10.1177/1060028019866420

9. Smorenberg A, Ince C, Groeneveld A. Dose and type of crystalloid fluid therapy in adult hospitalized patients. *Perioper Med (Lond).* (2013) 2:17. doi: 10.1186/2047-0525-2-17

10. Raghunathan K, Bonavia A, Nathanson B, Beadles C, Shaw A, Brookhart M, et al. Association between initial fluid choice and subsequent in-hospital mortality during the resuscitation of adults with septic shock. *Anesthesiology.* (2015) 123:1385–93. doi: 10.1097/ALN.0000000000000861

11. Semler M, Self W, Wanderer J, Ehrenfeld J, Wang L, Byrne D, et al. Balanced crystalloids versus saline in critically Ill adults. *N Engl J Med.* (2018) 378:829–39. doi: 10.1056/NEJMoa1711584

12. Rochwerg B, Alhazzani W, Sindi A, Heels-Ansdell D, Thabane L, Fox-Robichaud A, et al. Fluid resuscitation in sepsis: a systematic review and network meta-analysis. *Ann Intern Med.* (2014) 161:347–55. doi: 10.7326/M14-0178

13. Yunos N, Bellomo R, Hegarty C, Story D, Ho L, Bailey M. Association between a chloride-liberal vs chloride-restrictive intravenous fluid administration strategy and kidney injury in critically ill adults. *JAMA.* (2012) 308:1566–72. doi: 10.1001/jama.2012.13356

14. RDocumentation. *Tableone (version 0.13.2) [Internet].* (2022). Available online at: https://www.rdocumentation.org/packages/tableone/versions/0.13.2 (accessed March 15, 2022).

15. Raghunathan K, Shaw A, Nathanson B, Stürmer T, Brookhart A, Stefan M, et al. Association between the choice of IV crystalloid and in-hospital mortality among critically ill adults with sepsis*. *Crit Care Med.* (2014) 42:1585–91. doi: 10.1097/CCM.0000000000000305

16. Young P, Bailey M, Beasley R, Henderson S, Mackle D, McArthur C, et al. Effect of a buffered crystalloid solution vs. saline on acute kidney injury among patients in the Intensive Care Unit. *JAMA.* (2015) 314:1701. doi: 10.1001/jama.2015.12334

17. Semler M, Wanderer J, Ehrenfeld J, Stollings J, Self W, Siew E, et al. Balanced crystalloids versus saline in the intensive care unit. The salt randomized trial. *Am J Respir Crit Care Med.* (2017) 195:1362–72. doi: 10.1164/rccm.201607-1345OC

18. Brown R, Wang L, Coston T, Krishnan N, Casey J, Wanderer J, et al. Balanced crystalloids versus saline in sepsis. A secondary analysis of the smart clinical trial. *Am J Respir Crit Care Med.* (2019) 200:1487–95. doi: 10.1164/rccm.201903-0557OC

19. Gupta S, Sakhuja A, Kumar G, McGrath E, Nanchal R, Kashani K. Culture-negative severe sepsis. *Chest.* (2016) 150:1251–9. doi: 10.1016/j.chest.2016.08.1460

20. Silversides J, Major E, Ferguson A, Mann E, McAuley D, Marshall J, et al. Conservative fluid management or deresuscitation for patients with sepsis or acute respiratory distress syndrome following the resuscitation phase of critical illness: a systematic review and meta-analysis. *Intensive Care Med.* (2016) 43:155–70. doi: 10.1007/s00134-016-4573-3

21. Meyhoff, T, Møller M, Hjortrup P, Cronhjort M, Perner A, Wetterslev J. Lower vs. higher fluid volumes during initial management of sepsis: a systematic review with meta-analysis and trial sequential analysis. *Chest.* (2020) 157:1478–96. doi: 10.1016/j.chest.2019.11.050

22. Hu B, Chen J, Dong Y, Frank R, Passe M, Portner E, et al. Effect of initial infusion rates of fluid resuscitation on outcomes in patients with septic shock: a historical cohort study. *Crit Care.* (2020) 24:137. doi: 10.1186/s13054-020-2819-5

frontiers | Frontiers in Genetics

TYPE Original Research
PUBLISHED 11 April 2023
DOI 10.3389/fgene.2023.1158352

OPEN ACCESS

EDITED BY
Wanjun Gu,
Nanjing University of Chinese Medicine, China

REVIEWED BY
Li Guo,
Nanjing University of Posts and Telecommunications, China
Shanshan Zhu,
Southeast University, China

*CORRESPONDENCE
Edward Parkinson,
parkinsone@cardiff.ac.uk

SPECIALTY SECTION
This article was submitted to Computational Genomics, a section of the journal Frontiers in Genetics

RECEIVED 10 February 2023
ACCEPTED 29 March 2023
PUBLISHED 11 April 2023

CITATION
Parkinson E, Liberatore F, Watkins WJ, Andrews R, Edkins S, Hibbert J, Strunk T, Currie A and Ghazal P (2023), Gene filtering strategies for machine learning guided biomarker discovery using neonatal sepsis RNA-seq data. *Front. Genet.* 14:1158352. doi: 10.3389/fgene.2023.1158352

Gene filtering strategies for machine learning guided biomarker discovery using neonatal sepsis RNA-seq data

Edward Parkinson[1]*, Federico Liberatore [1], W. John Watkins [2], Robert Andrews [2], Sarah Edkins [2], Julie Hibbert [3,4,5], Tobias Strunk [3,4,6], Andrew Currie [3,5] and Peter Ghazal [2]

[1]Department of Computer Science and Informatics, Cardiff University, Cardiff, United Kingdom, [2]Project Sepsis, Systems Immunity Research Institute, Cardiff University, Cardiff, United Kingdom, [3]Wesfarmers Centre of Vaccines and Infectious Diseases, Telethon Kids Institute, Perth, WA, Australia, [4]Medical School, University of Western Australia, Perth, WA, Australia, [5]Centre for Molecular Medicine and Innovative Therapeutics, Murdoch University, Perth, WA, Australia, [6]Neonatal Directorate, Child and Adolescent Health Service, Perth, WA, Australia

Machine learning (ML) algorithms are powerful tools that are increasingly being used for sepsis biomarker discovery in RNA-Seq data. RNA-Seq datasets contain multiple sources and types of noise (operator, technical and non-systematic) that may bias ML classification. Normalisation and independent gene filtering approaches described in RNA-Seq workflows account for some of this variability and are typically only targeted at differential expression analysis rather than ML applications. Pre-processing normalisation steps significantly reduce the number of variables in the data and thereby increase the power of statistical testing, but can potentially discard valuable and insightful classification features. A systematic assessment of applying transcript level filtering on the robustness and stability of ML based RNA-seq classification remains to be fully explored. In this report we examine the impact of filtering out low count transcripts and those with influential outliers read counts on downstream ML analysis for sepsis biomarker discovery using elastic net regularised logistic regression, L1-reguarlised support vector machines and random forests. We demonstrate that applying a systematic objective strategy for removal of uninformative and potentially biasing biomarkers representing up to 60% of transcripts in different sample size datasets, including two illustrative neonatal sepsis cohorts, leads to substantial improvements in classification performance, higher stability of the resulting gene signatures, and better agreement with previously reported sepsis biomarkers. We also demonstrate that the performance uplift from gene filtering depends on the ML classifier chosen, with L1-regularlised support vector machines showing the greatest performance improvements with our experimental data.

KEYWORDS

neonatal sepsis, machine learning with RNA-seq, transcriptomic sepsis biomarkers, independent gene filtering, gene signature stability

Abbreviations: ML, Machine Learning; IBD, Inflammatory Bowel Disease; PAX, Potassium Amyl Xanthate; GLM, Generalised Linear Model; eNet, Elastic Net Regularised Logistic Regression; L1-SVM, L1 penalised Support Vector Machine; RF, Random Forest; PPV, Positive Predictive Value.

1 Introduction

Supervised machine learning (ML) analysis of gene expression data is a widely used AI approach to derive informative gene subsets with potential utility as diagnostic and prognostic clinical biomarkers (Liu et al., 2014; Lin et al., 2017; Zhang et al., 2021). These ML based feature selection algorithms have the power to both eliminate redundant genes, and identify relevant genes that both discriminate between clinical conditions of interest, and that generalise over the relevant patient populations (Mahendran et al., 2020). These techniques are referred to as ML gene selection or simply gene selection throughout this work. To date, the majority of validated sepsis biomarkers have been derived from microarray gene expression data (Smith et al., 2014; McHugh et al., 2015; Sweeney et al., 2015). In recent years RNA-Seq has largely replaced microarray as the preferred technology for generating gene expression data, given the higher resolution and decreasing cost of sequencing (Wang et al., 2009; Stark et al., 2019). The combination of ML gene selection with richer RNA-Seq data presents the opportunity to discover previously unidentified sepsis biomarkers. ML classification algorithms are however highly sensitive to any feature data characteristic, regardless of scale, that may differ between experimental groups, and will exploit these data characteristic differences in gene selection. Systematically adding noise to feature data has been shown to significantly degrade classification performance across a range of ML classification algorithms (Zhu and Wu, 2004; Hasan and Chu, 2022). It is therefore desirable to minimise this interference to ensure patterns detected have biological relevancy. To date the impact of applying independent filtering and pre-processing strategies to eliminate noise on the performance of ML approaches to biomarker discovery with RNA-Seq data has not been fully investigated.

Here we consider two sources of noise inherent in RNA-Seq data that may negatively impact ML gene selection. Firstly low read counts. Genes with consistently low read count values across all replicates may be technical or biological stochastic artefacts such as the detection of a transcript from a gene that is not uniformly active in a heterogeneous cell population or as the result of a transcriptional error (Wagner et al., 2013). Below some count threshold, genes with low read counts are subject to greater dispersion (variability) with greater false negatives (zero inflation) and false positives (outliers) that are not representative of true biological differences related to the condition of interest. The filtering out of low read count genes from RNA-Seq data in differential expression analyses is reported to improve detection of differentially expressed genes by reducing the impact of multiple testing corrections (Bourgon et al., 2010). A wide variety of approaches to filtering low count genes have been proposed, the most common being maximum-based filters, where genes with a maximum normalised count over all samples below a threshold t are filtered out (Rau et al., 2013). At a lower threshold t, the number of genes retained after filtering is expected to be more variable between samples, given differences in low count noise between samples. As t increases, the number of genes retained is expected to converge as the read counts increasingly represent the true biological signal, which is more consistent across samples (Koch et al., 2018). To avoid setting arbitrary thresholds, multiple authors have proposed approaches to setting the filter threshold based on the data. Rau et al. (2013) determine the optimal threshold based on maximising the similarity of expression between samples. Love et al. (2014) implement gene filtering in the R package DESeq2 to maximise the number of genes found to be significantly differentially expressed based on a user-specified target false discovery rate (FDR). Deyneko et al. (2022) derive a sample specific threshold by separately modelling the random (low count noise) and true biological signal, and subtracting the low count noise component from the reads of each sample. Zehetmayer et al. (2022) propose an adaptive approach, testing the impact of multiple filters and selecting the filter that maximises the power of a hypothesis test in the given data set. In all these approaches, the goal of independent gene filtering is to reduce the impact of multiple testing correction in gene by gene hypothesis testing. In a multivariate supervised learning setting, it is well known that features may have significant effects in combination despite having weak effects individually (Guyon and Elisseeff, 2003). This raises the question of whether and how low count filtering should be performed. Filtering out genes based on arbitrary thresholds risks discarding valuable biomarkers that may have discriminate power in combination with other genes and provide useful insights into underlying biology.

A second source of noise are influential outlier read counts. Relatively high read counts occurring in only a very small number of samples relative to the size of each patient group are unlikely to be representative of the general population and a result of biological heterogeneity and technical effects. These gene values may bias feature selection algorithms as they discriminate between examples in a training set, leading to model overfitting. Such influential outliers may be the result of natural variation between individuals or they may have been introduced during sample preparation. cDNA libraries require PCR amplification prior to sequencing to achieve sufficient sequence depth. This clonal amplification by PCR is stochastic in nature; different fragments may be amplified with different probabilities. This leaves the possibility of outlier read counts having resulted from bias introduced by amplification, rather than biological differences between samples (Fu et al., 2018; Stark et al., 2019). As with low count genes, in the context of differential expression analyses, hypothesis testing based on the negative binomial distribution, extreme outlier read counts can have a disproportionate effect on the results, increasing false positives and false negatives, and inflating the observed association between particular genes and the condition of interest (Mangiola et al., 2021). Multiple approaches to identify and remove outliers have been proposed in this context (Love et al., 2014; Brechtmann et al., 2018; Mangiola et al., 2021).

Despite significant work in the area of differential expression analysis, to our knowledge, there is a lack of analysis of the impact of gene filtering on downstream ML analysis, specifically in gene selection for biomarker discovery. Although multiple software pipelines have been developed to aid researchers in conducting this type of analysis using high-throughput sequence data (Chiesa et al., 2018; Goksuluk et al., 2019; Dag et al., 2022), gene filtering features are limited to removing low count and low variance genes and typically require users to provide their own arbitrary thresholds. Previous authors provide little justification for the use of these filters, nor do they provide recommended thresholds or guidance on how these might be adjusted to the ML algorithm being employed.

Evaluation of the impact of gene filtering in ML gene selection requires a success measure equivalent to the number of significant genes identified by a series of hypothesis tests in the differential expression analysis setting. In the task of biomarker discovery, the chosen set of genes effectively form an hypothesis on the underlying biological mechanisms of disease. The ability of the selected genes to discriminate between disease states is of primary importance if the biomarkers are to be translated into a clinical setting. Perhaps equally important to their predictive power is the stability of the chosen gene set in the event of changes to the training dataset (Jurman et al., 2008; Sechidis et al., 2019). An unstable gene selection procedure can be thought of as one where small changes to the training data result in large changes to the chosen gene set (Nogueira et al., 2018). We propose therefore that the appropriate way to evaluate the impact of gene filtering is to measure the relative classification performance of a derived gene set *and* the stability of the gene set to perturbation of the training data with and without gene filtering employed. A stability measure quantifies the similarity of a group of gene sets, often giving a value between zero and one, where zero implies a random choice of genes in each set, and one implies identical sets. A wide variety of stability measures have been proposed, and a comprehensive review is provided by Bommert et al. (2017) and Nogueira et al. (2018). Where existing biomarkers have been validated, as in the case of sepsis, an additional measure is the level of agreement of a new gene set with existing validated biomarkers.

In this article, we examine the impact of gene filtering on the performance and stability of three common ML algorithms for sepsis biomarker discovery using bulk RNA-Seq data. The motivation of this article is to assess the need to perform independent gene filtering in preparation for a ML analysis, the implications of not doing so, and the impact of gene filtering on the downstream classification performance and stability to changes in experimental data. We provide practical guidelines on the gene filtering steps needed in ML analysis of RNA-Seq data absent in the existing literature. The rest of this article is organised as follows: In the Materials and Methods section we summarise the data processing pipeline, the datasets used and the nature of the gene filters and ML classifiers applied. The Results and Discussion section demonstrates the impact of gene filtering on feature selection and the classification performance of the resulting gene sets, as well as their stability, and agreement with previously validated sepsis biomarkers. Finally, the Conclusion summarises the rationale for gene filtering prior to ML gene selection and outlines areas for future investigation.

2 Materials and methods

This section introduces the datasets used in this work and provides a brief theoretical background to the gene filter methods and supervised ML approaches employed.

2.1 Data processing pipeline overview

A schematic overview of the data processing and analysis pipeline used in this work is depicted in Figure 1. A detailed description of each stage of the pipeline is provided in the following sections.

2.2 Test datasets

The impact of gene filtering on ML performance is demonstrated using three experimental bulk RNA-Seq datasets. To the best of our knowledge, there are a limited number of RNA-Seq datasets profiling sepsis patients, and those that exist contain a small number of samples. We therefore conduct our analysis using two relatively small cohorts of neonatal infants containing sepsis cases, supplemented by a publicly available dataset of inflammatory bowel disease patients containing a far larger number of samples, to assess generality as well as increase confidence in the results.

2.2.1 Inflammatory bowel disease ("IBD") dataset

The IBD data is taken from the recent study by Nowak et al. (2022) who deposited 590 pediatric and adult patient samples in the EMBL-EBI ArrayExpress database (E-MTAB-11349). The data used in this work include the raw count data from 434 patients recruited at six gastrointestinal clinics across Europe between 2012 and 2016, with 167 patients diagnosed with ulcerative colitis and 267 controls. 49% of the patients are female and they range in age from 3 to 79. Details of the sequencing whole-blood RNA for this cohort using the Ion Torrent sequencing platform are given by Nowak et al. (2022).

2.2.2 Neonatal sepsis datasets

The first neonatal sepsis dataset (referred to as Sepsis 1 below) derives from a 2020 study by Ng et al. (2020) of 18 very preterm neonatal infants, deposited in the NCBI GEO omnibus gene expression database (GSE138712). Infants are classified based on a positive blood culture and elevated C-reactive protein concentrations as having confirmed late onset sepsis ($n = 5$), clinical late onset sepsis ($n = 4$) or no late onset sepsis ($n = 9$). Suspicion of sepsis in premature infants has a low threshold and there is a good possibility that they will not have sepsis. For the purposes of this work we have tested this assumption using neonatal sepsis biomarkers described by Smith et al. (2014), hereafter referred to as the "Sep3" gene signature. Accordingly, all clinical late onset sepsis cases are considered to have no late onset sepsis, with the exception of a single sample, classified as confirmed sepsis based on clear discrimination from PCA analysis using neonatal sepsis biomarkers and illustrated in Supplementary Figure S1. The retention of the clinical late onset sepsis group and allocation between confirmed and no sepsis is further justified by the need maintain the sample size and class balance to aid the performance of ML classification algorithms in what is already a very small dataset. Details of the sequencing whole-blood RNA procedure are provided by Ng et al. (2020).

The second sepsis dataset (referred to as Sepsis 2 below) derives from a cohort of 45 very preterm infants recruited from the neonatal intensive care unit of King Edward Memorial Hospital, Perth, Australia, a sub-study of The PROTECT Trial (Simmer et al., 2016), a pragmatic randomised placebo-controlled clinical trial evaluating the effectiveness of intravenous pentoxifylline for improving long-term outcomes in preterm infants with late onset sepsis or necrotising enterocolitis. The PROTECT study was approved

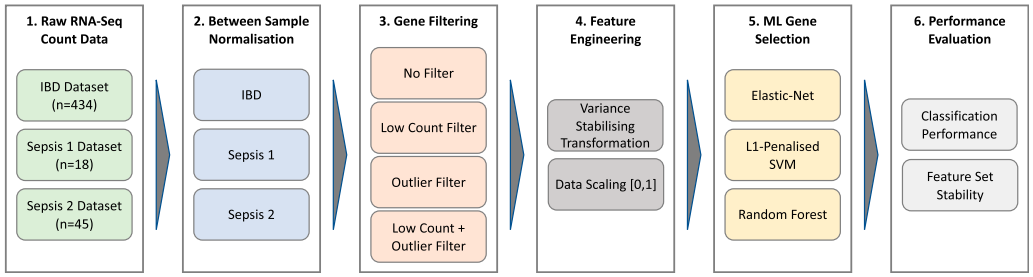

FIGURE 1
Data processing and analysis pipeline.

by the institutional Human Research Ethics Committee at King Edward Memorial Hospital, Perth, Australia (RGS0000002684). Written, informed consent was obtained by the Principal Investigator or delegate from the parent(s) prior to study participation. Infants with suspected late onset sepsis (> 72 hours after birth) were enrolled in the sub-study between 2016 and 2019.12 of the 45 infants were classified as having confirmed late onset sepsis in the event of a positive blood culture and the causative pathogen identified, two or more serial CRP measurements of > 20 mg/L within 72 h of blood culture and having been treated with antibiotics for five or more consecutive days. The remaining 33 infants are classified as no late onset sepsis, with negative blood culture, all CRP measurements below 20 mg/L and not more than 3 days of treatment with antibiotics. A peripheral whole blood sample was taken near the time of blood culture sampling for suspected late onset sepsis and prior to administration of study treatment. RNA was stabilised in PAX and stored at −80C until extraction. Total RNA quality and quantity was assessed using Agilent 4,200 TapeStation and a High Sensitivity RNA kit (Agilent Technologies). 75–100 ng of Total RNA with a RIN value > 7 was depleted of ribosomal RNA using the NEBNext® Globin and rRNA Depletion Kit (Human/Mouse/Rat) (New England BioLabs, NEB) and the sequencing libraries were prepared using the NEB® Ultra™ II Directional RNA Library Prep Kit for Illumina® (NEB). The steps included RNA fragmentation and priming, first strand cDNA synthesis, 2nd strand cDNA synthesis, adenylation of 3′ ends, adapter ligation, PCR amplification (16-cycles) and validation. The manufacturer's instructions were followed. The libraries were validated using the Agilent 4,200 TapeStation and a DNA1000 tape (Agilent Technologies) to ascertain the insert size, and the CLARIOstar® (BMG Labtech) was used to perform the fluorometric quantitation. Following validation, the libraries were normalized to 3nM, pooled together and sequenced using a 100-base paired-end (2 × 100bp PE) dual index read format on the Illumina® NovaSeq™6000 according to the manufacturer's instructions. Paired-end reads from Illumina sequencing were trimmed with Trim Galore (Babraham Bioinformatics Group, 2019a) and assessed for quality using FastQC (Babraham Bioinformatics Group, 2019b), using default parameters. Reads were mapped to the human GRCh38 reference genome using STAR (Dobin et al., 2013) and counts were assigned to transcripts using featureCounts (Liao et al., 2014) with the GRCh38.96 Ensembl gene build GTF. Both the reference genome and GTF were downloaded from the Ensembl FTP site (Ensembl, 2021).

2.3 Between sample normalisation

Raw read counts for each dataset are scaled using the median-of-ratios method described by Anders and Huber (2010) (often referred to as "normalisation" in bioinformatics literature) to account for systematic differences between samples resulting from technical factors, namely sequence depth (total number of aligned reads) and sample composition (relative proportion of transcripts for a given number of reads). These normalised read counts allow comparison of the relative expression level for each gene between samples. Filtering to identify genes with relatively low and extreme outlier read count genes is conducted using these normalised counts as described below.

2.4 Gene filtering

To demonstrate the impact of filtering low count and influential outlier genes on feature selection in a supervised ML setting, we apply two widely used filtering methods to each datasets. For the remainder of this work, the term gene is used as a shorthand to refer to an RNA transcript with a unique EBI Ensembl or NCBI RefSeq accession number; the level at which filtering is implemented.

2.4.1 Low count genes

To filter out low expression genes, we apply the data-based maximum filter approach proposed by Rau et al. (2013) and demonstrated to be superior to other maximum based filters for filtering out low count noise in a differential expression analysis setting. This approach derives a filter threshold t that maximises the similarity between samples using the Jaccard index (Jaccard, 1901). The vector of read counts for all genes in a given sample j with experimental condition $c(j)$ is given by $\mathbf{s}_j$. $\mathbf{s}_j$ is binarised for a given threshold t ($\mathbf{s}_j > t$ is 1, otherwise 0). The Jaccard similarity index between the binary vectors for each pair of samples j and j' from the same experimental condition ($c(j) = c(j')$) is given by Eq. 1.

$$J_S(\mathbf{s}_j, \mathbf{s}_{j'}) = \frac{\mathbf{s}_j \bigcap \mathbf{s}_{j'}}{\mathbf{s}_j \bigcup \mathbf{s}_{j'}} \tag{1}$$

The optimum threshold t^* is defined as the threshold that maximises the similarity between samples, corresponding to the maximum average Jaccard index over all pairs in each experimental condition, as in Eq. 2.

$$t^{\star} = \arg\max_{t} \text{ mean } \left\{ J_S\left(\mathbf{s}_j, \mathbf{s}_{j'}\right) :\ j < j' \text{ and } c\left(j\right) = c\left(j'\right) \right\} \quad (2)$$

2.4.2 Influential outlier genes

To identify sample gene pairs with influential outlier read counts, we implement the approach used in DESeq2 (Love et al., 2014) that uses Cook's distance (Cook, 1977a). Briefly, Cook's distance is a measure of influential points in a generalised linear regression model (GLM). In the context of the negative binomial distribution most frequently used to model RNA-Seq count data, Cook's distance is given by Eq. 3, where R_{ij} is the Pearson residual of sample j, a measure of the extent to which an observed value differs from the predicted value in the model; h_{ii} is the leverage of each count, which can be thought of as the weighted distance the values of the independent variables vary from the mean, τ is an over dispersion parameter that is set to 1 in the GLM, and p is the number of parameters. The Cook's distance D_{ij} is the scaled distance that the coefficient vector β_i of the GLM for gene i would change if the sample j were removed and the model refit. Counts with larger values of D_{ij} therefore have a greater influence on the model parameters.

$$D_{ij} = \frac{R_{ij}^2}{\tau p} \frac{h_{jj}}{\left(1 - h_{jj}\right)^2} \quad (3)$$

Influential outliers are defined by transforming the values of D_{ij} to points on the $F\left(p, m - p\right)$ distribution where the p is the number of model parameters and m is the number of samples, and defining a threshold by an arbitrary quantile q (Cook, 1977b). In this work q is set to 0.95, and a gene is filtered out if an influential outlier read count is present in one or more samples.

Following filtering, the filtered genes are removed from the raw count data and the raw counts are re-normalised by the median-of-ratios method.

2.5 Feature engineering

The skewed and heteroskedastic nature of RNA-Seq count data means that certain machine learning algorithms, in particular those such as support vector machines employing distance based measures, may be disproportionately influenced by the genes with the highest mean counts, due to the larger variance (absolute distances) between samples. To overcome this potential issue, the median-ratio scaled data is further pre-processed with the variance stabilising transformation described by Love et al. (2014) to reduce both the skewness and the mean-variance relationship and scaled to values between 0 and 1 to ensure all genes are on a comparable scale.

2.6 Gene selection with supervised machine learning

Gene selection is performed using supervised ML classification algorithms with embedded feature selection and computationally efficient implementations in R, henceforth referred to as classifiers or models interchangeably. The overall scheme for model training is illustrated in Figure 2.

2.6.1 Choice of machine learning classifiers

The classifiers selected are elastic net regularised logistic regression (eNet) (Zou and Hastie, 2005; Friedman et al., 2010), L1 regularised Support Vector Machines using the LIBLINEAR library (L1-SVM) (Fan et al., 2008) and Random Forest (RF) (Breiman, 2001). These methods are chosen for several reasons. Firstly because they are widely known and frequently used in gene selection applications (Mahendran et al., 2020). Secondly because each of these ML methods applies fundamentally different principles to fit the data, including linear (eNet, L1-SVM) and non-linear (RF) models, allowing us to investigate whether gene filtering approaches are applicable over a diverse set of ML approaches. Thirdly and perhaps most importantly because feature selection is embedded within these three methods. eNet and L1-SVM implicitly perform feature selection as a result of the L1 penalty shrinking the coefficients of the least important features to zero during the optimisation. In the case of Random Forest, the relative importance of features can be calculated following model training, and features ranked by importance. Other machine learning approaches without this property of embedded feature selection would require either a gene selection filter method to be applied prior to training the classifier, or a wrapper method such as recursive feature elimination (Guyon et al., 2002) to be applied during model training. Both these alternatives are deemed to complicate the analysis unnecessarily, and in the case of recursively searching for an optimum feature set, to increase the computational complexity so as to make the analysis impractical given the high dimensionality of the datasets.

2.6.2 Model training and gene selection

The procedure used to train each classifier and extract a gene set is illustrated in the central panel of Figure 2. The eNet and L1-SVM models are trained with a range of values of their respective regularisation hyperparameters in a k-fold cross validation scheme (k = 10 for the IBD dataset and 'leave-one-out' for the sepsis datasets) to provide a validation set for classification performance evaluation. Hyperparameter values are selected to yield a gene set of similar size for each model, targeting 30 genes for the IBD and Sepsis 2 datasets and 10 genes for the Sepsis 1 dataset, given the smaller number of samples in this case. Fixing the model hyperparameters to yield gene sets of a similar size is important to ensure gene set stability measures are broadly comparable between the models. A final model is trained on the full dataset, without cross validation, using the selected hyperparameter values, and the set of selected genes identified. The model predictions on the cross validation set at the chosen hyperparameter values are used to evaluate the classification performance[1].

The RF classifier is implemented with fixed hyperparameters (1,000 trees and $\sqrt{p}$ randomly selected genes per tree, where p is the total number of genes in the training set). Feature importance based on maximum decrease in Gini coefficient is used to manually select

1 Given the same cross validation scheme is used to both select the hyperparameter values that provide the desired number of genes and to evaluate classification performance, it is acknowledged the performance estimate is biased as a result, however given the low sample sizes of the Neonatal Sepsis datasets, a hold out test set is deemed impractical

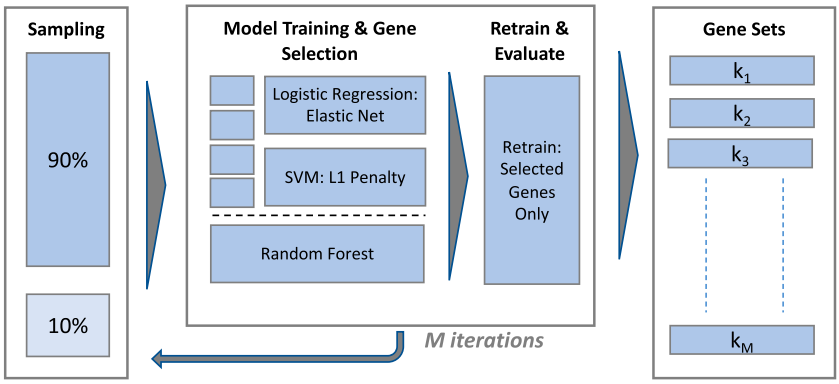

FIGURE 2
Gene selection performance and stability evaluation.

the most discriminative genes with respect to the target condition (Bommert et al., 2020). The top 30 genes by feature importance are selected for the IBD and Sepsis 2 datasets, and the top 10 are selected for the Sepsis 1 dataset. A final model is retrained on the full dataset using only the selected features, and the predictions on the out-of-bag samples used to evaluate classification performance.

2.7 Performance evaluation

2.7.1 Classification performance measurement

Classification performance is evaluated using the F_1 score (Chinchor, 1992), a widely used metric for evaluating ML classification performance, in particular where the two experimental groups under consideration are of different sizes, as is the case here. F_1 score is the harmonic mean of the Sensitivity (also known as Recall) and Positive Predictive Value (PPV, also known as Precision), as defined in Eq. 4, and gives a value in the range 0–1.

$$F_1 = 2 \cdot \frac{Sensitivity \cdot PPV}{Sensitivity + PPV} \tag{4}$$

A baseline F_1 score can be derived by assuming that a 'dumb' classifier predicts all patients to be the positive class (e.g., sepsis), in which case the F_1 score simplifies to $2p/(p + 1)$, where p is the probability of a positive example in a given dataset.

2.7.2 Feature stability measurement

To estimate gene set stability with and without gene filtering, training and gene selection was repeated on M 90% random stratified sub-samples of the unfiltered and filtered data (with $M = 100$), producing gene sets $k_1, k_1, \ldots, k_M$ in each case.

In the context of transcriptomic biomarker discovery, given the high level of correlation between features, two feature sets may contain different genes that are however correlated as a result of related biological function. Feature selection algorithms may only select one of a number of correlated features, and therefore if these correlations are not taken into account, stability may be underestimated (Sechidis et al., 2019). The recently reported stability measure by Sechidis et al. (2019) was considered for this work, however was found to be computationally expensive to compute using our very high dimensional datasets. Thus, gene set stability over the M gene sets is calculated using the measure proposed by Zucknick et al. (2008) that meets the majority of desirable properties of a stability measure (Nogueira et al., 2018; Bommert, 2020), takes into account the correlation between genes in the dataset and is bounded between 0 and 1, aiding comparisons between datasets. The Zucknick stability over M gene sets is the mean pairwise correlation-extended Jaccard index between set V_i and V_j, defined in Equation 5. The intersection term is supplemented by a correlation factor $C(V_i, V_j)$ defined as the mean absolute correlation $R_{(x,y)}$ of all genes selected in V_i with all genes selected in V_j but not in V_i. $R_{(x,y)}$ is thresholded on parameter $\tau = 0.5$, to avoid computing the effect of a large number of weak correlations.

$$\hat{\Phi}(Z) = \frac{2}{M(M-1)} \sum_{i=1}^{M-1} \sum_{j=i+1}^{M} \frac{|V_i \cap V_j| + C(V_i, V_j) + C(V_j, V_i)}{|V_i \cup V_j|}$$
$$C(V_k, V_l) = \frac{1}{|V_l|} \sum_{(x,y) \in V_k \times (V_l \setminus V_k)} \mathbb{1}(R_{(x,y)} > \tau) |R_{(x,y)}|$$
$$\mathbb{1}(R_{(x,y)} > \tau) = \begin{cases} 1, & \text{if } R_{(x,y)} > \tau \\ 0, & \text{otherwise} \end{cases} \tag{5}$$

3 Results and discussion

The experimental results describe how gene filtering impacts the classification performance and stability of the gene sets selected by the three supervised ML approaches (eNet, L1-SVM and RF), and evaluates the biological relevance of the resulting sepsis biomarkers in the context of previously validated gene signatures.

3.1 Filtered genes

The derived low counts maximum filter thresholds for the IBD, Sepsis 1 and Sepsis 2 datasets were calculated as $t^* = 13$, $t^* = 11$, and $t^* = 60$ respectively. The corresponding number of genes filtered out by the low counts, influential outlier and combined low counts and influential outlier filters are given in Table 1. The notable differences in the original number of genes reflects the different sequencing depths and technologies used for these cohorts.

TABLE 1 Filtered genes.

	Original	Retained	Filtered	% filtered
IBD				
Low Count	22,656	18,278	4,378	19
Outlier	22,656	21,052	1,604	7
Low Count + Outlier	22,656	16,674	5,982	26
Sepsis 1				
Low Count	28,325	13,361	14,964	53
Outlier	28,325	28,111	214	1
Low Count + Outlier	28,325	13,173	15,152	54
Sepsis 2				
Low Count	55,574	20,606	34,968	63
Outlier	55,574	54,942	632	1
Low Count + Outlier	55,574	20,176	35,398	64

The three datasets illustrate the potential variability in the proportion of genes that may be removed by filtering. The Sepsis 1 and Sepsis 2 datasets have a higher proportion of genes with low counts with 53% and 63% of the genes removed by the low counts filter respectively, compared with only 19% for the IBD dataset. The IBD dataset has a proportionally higher number of genes with influential outlier values, with 7% of genes removed by the outlier filter.

3.2 Gene Selection Frequency of low count and outlier genes

Figures 3, 4, 5 show the frequency of selection of all genes over $M = 100$ sub-samples of the three unfiltered datasets for each of the three ML gene selection approaches. In each plot, a bar on the horizontal axis represents a gene ID that is selected at least once over all sub-samples. The vertical axis gives the frequency that each gene is selected over 100 sub-samples. Genes selected by classifiers in the unfiltered dataset that would have passed both filters are labelled in red (Retained), selected genes that would have been filtered out by applying a low counts filter are labelled in green (Low Count), while those that would have been filtered out by the outlier filter are labelled in blue (Outlier).

It is striking that low count genes are selected in all datasets and by all classifiers, with the exception of RF with the IBD dataset. In both of the sepsis datasets, the majority of L1-SVM gene selections are low count genes, and low count genes represent the most frequently selected gene in the by eNet in the Sepsis 1 dataset and by L1-SVM in the Sepsis 2 dataset. RF appears to be the most robust to low count genes across all datasets. Influential outlier genes are also selected by the eNet and RF classifiers in both of the sepsis datasets, albeit at a lower frequency compared with low count genes likely due to the small number of genes identified as containing outlier read counts. These results clearly illustrate how, without prior filtering out of low count and influential outlier genes, ML gene selection is at risk of actively selecting non-informative and biasing genes that happen to be statistically useful in classifying the training examples, and as illustrated here, these non-informative genes can dominate the resultant patterns. This highlights the need for a considered and objective approach to filtering prior to conducting ML analysis.

3.3 Performance impact of gene filters

Table 2 outlines the F_1 scores achieved on classifying the validation set (eNet and L1-SVM) or out-of-bag samples (RF) without filtering, with each filter applied independently and with the combined filters. The F_1 scores for the L1-SVM and RF models are a mean value over ten repeated measures, and the mean and standard deviation are given, along with p-values of a t-test of mean F_1 score for filtered vs. unfiltered cases, with the null hypothesis of equal means. The baseline F_1 scores achieved by a dumb model predicting all examples as positive are 0.56 for IBD, 0.50 for Sepsis 1, 0.42 for Sepsis 2.

All three classifiers achieve significantly higher than baseline performance on the IBD dataset, and classification performance is significantly improved by both the low counts and outlier filters. The performance scores for the Sepsis 1 dataset should be treated with some caution, given the small number of examples, with only

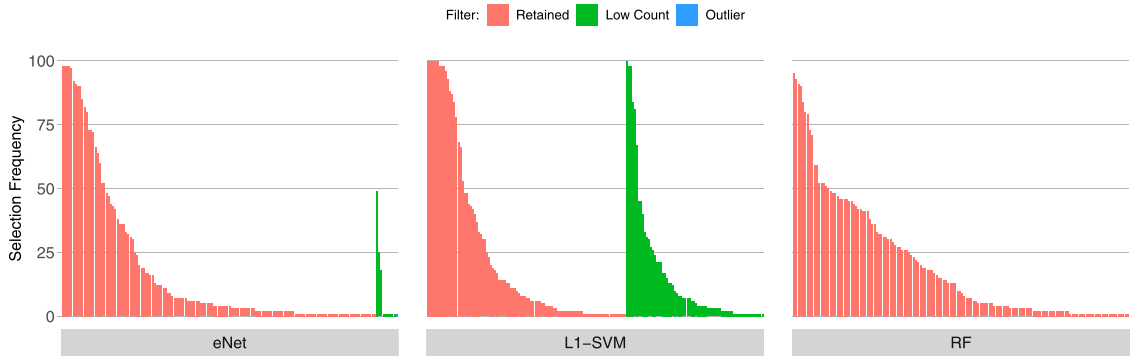

FIGURE 3
Gene selection frequency: IBD

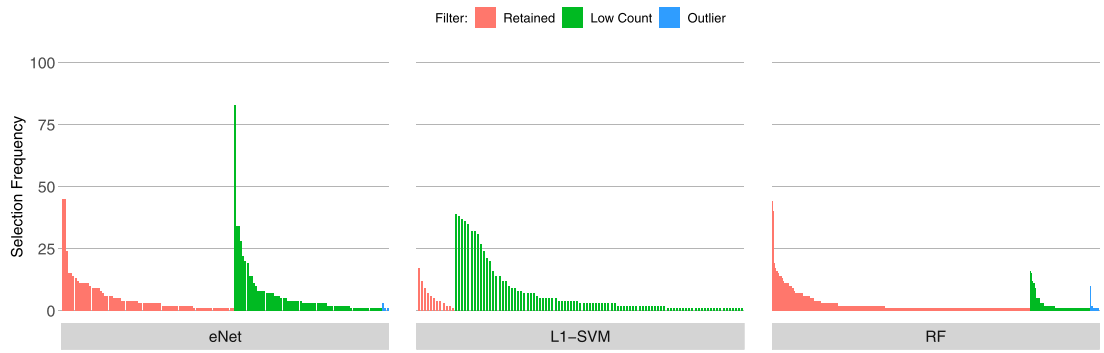

FIGURE 4
Gene selection frequency: Sepsis 1.

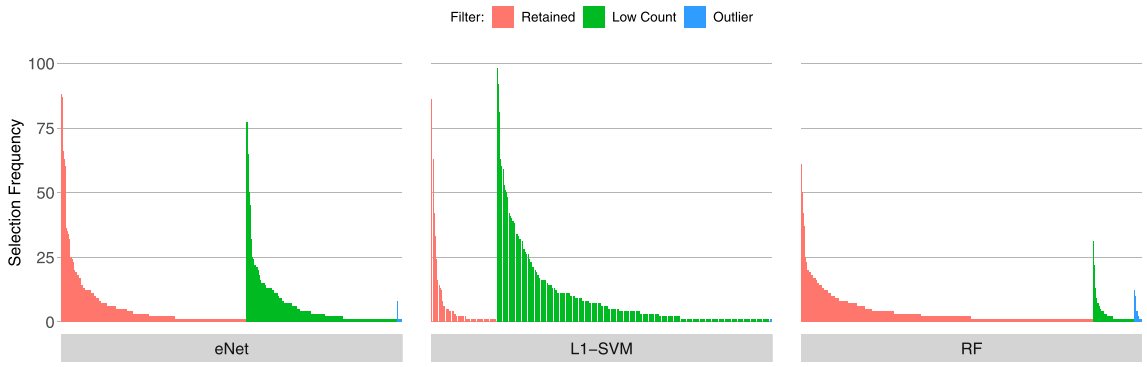

FIGURE 5
Gene selection frequency: Sepsis 2.

6 infants in the sepsis group. However, despite the eNet and L1-SVM models failing to perform better than the baseline in the unfiltered data, filtering again appears to improve performance. RF performance appears unchanged by gene filtering. Nevertheless, it can be said that removing over 50% of the genes in the Sepsis 1 dataset has not detrimentally impacted RF performance (all *p*-values are much greater than 0.05). Similarly, in the Sepsis 2 dataset, all models achieve above baseline performance, and the performance of eNet and L1-SVM is significantly improved by low count filtering and not negatively impacted by outlier filtering. Again RF performance is not significantly impacted by filtering. These results are consistent with previous studies on the impact of noise in feature data on machine learning classification performance. Zhu and Wu (2004) and Hasan and Chu (2022) both demonstrate that ML classification performance is materially improved by systematic removal of noise in feature data. By removing non-informative and biasing genes, the risk that such genes are used to construct a model is reduced, resulting in models that are better able to generalise to unseen patient data. In short, gene filtering reduces the risk of overfitting.

The consistent performance improvements across all three datasets using the eNet and L1-SVM models also indicate that gene filtering strategies are relevant to datasets with very different sample sizes (n = 434 for IBD compared with n = 18 for Sepsis 1), including datasets with very small sample sizes.

Comparing the performance of the three classifiers, in the Sepsis 1 and Sepsis 2 datasets, where 50%–60% of genes are removed by the low counts filter, RF achieves significantly better classification performance than eNet and L1-SVM, in particular where no filtering is applied. This result is consistent with the findings of (Hasan and Chu, 2022) that RF achieves relatively higher classification performance than a range of other classifiers in the presence of high levels of feature noise over a range of datasets.

One point of caution in interpreting these results: although the dimensionality of the datasets have been significantly reduced by gene filtering, and classification performance is improved on the validation set in the majority of cases, the F_1 scores should be interpreted in relative terms only. The risk remains that these classifiers are somewhat over fit to these relatively small datasets, and further work is required using a larger number of samples to characterise the true classification performance on new data.

A similar picture is seen in relation to gene set stability as outlined in Table 3.

For the L1-SVM and RF classifiers, feature set stability is shown increase in all three datasets when genes are filtered prior to model

TABLE 2 Gene filter impact on classification performance.

	eNET	L1-SVM			RF		
Filter	F_1	Mean F_1	Sd	*p*-value	Mean F_1	Sd	*p*-value
IBD							
None	0.885	0.703	0.005	—	0.703	0.007	—
Low Count	0.891	0.728	0.005	< 0.001	**0.724**	0.011	< 0.001
Outlier	0.895	0.725	0.002	< 0.001	0.718	0.008	< 0.001
Low Count + Outlier	**0.898**	**0.735**	0.002	< 0.001	0.718	0.010	0.0014
Sepsis 1							
None	0.500	0.286	0.000	—	0.982	0.038	—
Low Count	**0.667**	**0.800**	0.000	—	**1.000**	0.000	0.168
Outlier	0.500	0.286	0.000	—	0.992	0.029	0.556
Low Count + Outlier	**0.667**	**0.800**	0.000	—	0.973	0.044	0.628
Sepsis 2							
None	0.762	0.671	0.071	—	0.944	0.021	—
Low Count	0.818	0.731	0.011	0.026	0.949	0.017	0.580
Outlier	0.762	0.709	0.036	0.154	0.949	0.017	0.580
Low Count + Outlier	**0.870**	**0.734**	0.015	0.021	**0.957**	0.000	0.082

The bold values are the highest scoring filter for each dataset.

TABLE 3 Gene filter impact on feature stability.

	eNET		L1-SVM		RF	
Filter	Avg. No. Selected	Stability	Avg. No. Selected	Stability	Avg. No. Selected	Stability
IBD						
None	27.8	0.470	35.6	0.491	30	0.835
Low Count	27.9	**0.474**	24.7	0.545	30	**0.841**
Outlier	27.9	0.449	28.4	**0.559**	30	0.833
Low Count + Outlier	27.7	0.458	25.0	0.548	30	0.839
Sepsis 1						
None	11.6	0.581	6.400	0.479	10	0.410
Low Count	9.7	0.548	5.646	**0.549**	10	0.462
Outlier	9.7	**0.583**	6.121	0.510	10	0.430
Low Count + Outlier	9.7	0.547	5.485	0.544	10	**0.485**
Sepsis 2						
None	27.6	0.369	26.8	0.278	30	0.552
Low Count	25.3	**0.426**	22.7	**0.392**	30	0.588
Outlier	27.2	0.377	27.8	0.268	30	0.562
Low Count + Outlier	25.0	0.424	21.9	0.382	30	**0.603**

The bold values are the highest scoring filter for each dataset.

TABLE 4 Mean correlation between genes identified and known sepsis biomarker signatures.

Gene signature	Sep3			Sepsis meta score			SRSq-extended		
Filter	eNet	L1-SVM	RF	eNet	L1-SVM	RF	eNet	L1-SVM	RF
None	0.319	0.279	0.432	0.404	0.351	0.52	0.270	0.232	0.336
Low Count + Outlier	0.340	0.322	0.415	0.408	0.397	0.51	0.276	0.294	0.326
Difference	0.021	0.043	(0.017)	0.004	0.046	(0.010)	0.006	0.062	(0.010)

training. This is particularly clear for the low counts filter. The stability of the genes selected by eNet show conflicting results, with stability decreasing with the application of the outlier filter in the IBD dataset, and with the application of the low count filter in the Sepsis 1 dataset. The overall trend however is that filtering out uninformative genes results in gene sets that are less sensitive to changes in the data, and therefore likely to be more generalisable to new patient populations.

Beyond the improvements to classification performance and feature stability, filtering to remove uninformative and potentially biasing genes has reduced the dimensionality of the dataset. This has the further benefits of reducing data storage requirements and leading to a simpler optimisation of the model parameters, reducing the computational time required for analysis.

3.4 Correspondence with known sepsis biomarkers

A final evaluation of the impact of gene filtering is to determine the consistency of the genes identified by ML gene selection with known biomarkers for sepsis. Here, we compare the top 20 most frequently selected genes over the 100 random sub-samples of the Sepsis 2 dataset to each of three validated transcriptomic biomarker signatures. The signatures used are the Sep3 signature identified by Smith et al. (2014), the 12 gene signature used to compute the "Sepsis Meta Score" (SMS) reported by Sweeney et al. (2015) and the 19 gene "Extended Signature" used to derive the quantitative sepsis response signature (SRSq) reported by Cano-Gamez et al. (2022). A preliminary check is performed to determine whether any of the genes in these signatures are filtered out by applying the low count and outlier filters to the datasets. All genes are retained in the filtered dataset, with the exception of MMP9, removed on the basis of an outlier read count.

Given the small sample sizes and imbalanced nature of the neonatal sepsis datasets, any significance or inference from these investigations with regard new biomarkers cannot be made. However, the correlation between the biomarkers identified before and after gene filtering with validated sepsis biomarkers provides a proxy for biological relevance of the selected genes, and how this is impacted by gene filtering. The Pearson correlation coefficient between all pairs of genes in the normalised and unfiltered data set is calculated. The mean correlation between the top 20 genes identified by each classifier using unfiltered and filtered data, and the genes in the three signatures is calculated for each classifier gene signature pair. The results are shown in Table 4, and heat maps illustrating the individual correlations are provided Supplementary Figures S2—S4.

Both the eNet and L1-SVM classifiers select genes that are more highly correlated with the three known sepsis biomarker signatures after gene filtering; the difference is marginal for eNet but notably different for L1-SVM. These results are consistent with the above observation that the eNet and L1-SVM classifiers selected a significant proportion of uninformative low count genes when applied to the unfiltered dataset. Gene filtering improved classification performance, the stability of the selected genes, and the correlation of the selected genes with known biomarkers. In the case of RF, the average correlations of the identified genes with known biomarkers are lower after gene filtering, consistent with the observations above RF is more robust to low count genes in particular, and material improvements in performance are not observed when gene filtering is applied.

4 Conclusion

Biological data is noisy. RNA-Seq count data contains multiple sources of technical and biological noise that can bias ML classification algorithms used in biomarker discovery, resulting in misleading conclusions. In this short study, we have empirically demonstrated the value of independent filtering of genes in RNA-Seq data sets prior to ML gene selection. We have shown that three popular ML algorithms used for gene selection, eNet, L1-SVM, and RF all selected low count and influential outlier genes without filtering first being applied in a range of experimental datasets. We have also demonstrated that gene filtering can improve the classification performance and stability of the resulting gene signature, despite eliminating over 50% of the initial variables. In the case of L1-SVM, we have demonstrated that classification performance is especially improved by employing a low counts filter. Filtering out unnecessary genes brings the additional benefit of working with smaller data sets, reducing computational time and data storage requirements. We also find in the data sets analysed in this study that RF is more robust with small sample sizes to the presence of low counts genes, although this requires further validation to assess generality. In the light of these findings, we offer a number of guidelines on gene filtering to researchers using ML for sepsis biomarker discovery using RNA-Seq data.

1. The performance of gene selection models is very likely to be improved by removing technical and biological stochastic noise from RNA-Seq data, such as very low and outlier read counts. A systematic objective approach should be adopted to filter

transcripts to remove such effects, identifying as best as possible the boundary between noise and true biological signal in preference to applying arbitrary thresholds.
2. Include feature set stability in the evaluation metrics for any biomarker discovery analysis. Use stability improvements as well as classification performance to refine gene filtering thresholds and approaches.
3. Compare genes that are filtered out with validated biomarkers for the condition of interest and use this to sense check filter thresholds.
4. In noisy datasets, and where gene filtering appears to remove potentially relevant biomarkers, employ classifiers such as Random Forest, more likely to be robust to the noise in the data

A number of areas are identified for further work. Firstly, this work only considers a single approach for low count gene filtering and influential outlier detection. Multiple other methodologies exist in the literature, and further work is needed to evaluate their impact on ML classification performance, and how best to set a filter threshold in the context of ML gene selection analysis. Secondly, the impact of additional filters, whether to reduce other sources of technical noise and bias beyond low and outlier counts, and gene filters based on biological criteria should be investigated for their impact on ML performance. Thirdly, the work should be extended to a broader range of ML classifiers and datasets to be able to draw firmer conclusions on the level of gene filtering required for a specific class of classifier. Finally, in the case of sepsis biomarker discovery, a broader patient population is required for analysis to be able to confidently declare novel discriminate biomarkers for sepsis using the approaches described here.

Data availability statement

The IBD dataset can be found in the EMBL-EBI ArrayExpress database (E-MTAB-11349). The Sepsis 1 dataset can be found in the NCBI GEO Omnibus database (GSE138712). A copy of the Sepsis 2 dataset, with transcripts and patients de-identified can be found at https://github.com/parkyed/SepsisClassifiers. The analysis is implemented in R and the code is freely available at https://github.com/parkyed/SepsisClassifiers.

Ethics statement

Ethical review and approval was not required for the study using E-MTAB-11349 and GSE138712 in accordance with the local legislation and institutional requirements. The PROTECT study was approved by the institutional Human Research Ethics Committee at King Edward Memorial Hospital, Perth, Australia (RGS0000002684). Written, informed consent was obtained by the Principal Investigator or delegate from the parent(s) prior to study participation.

Author contributions

EP designed and implemented the analysis, conducted literature searches, researched data and selected relevant articles. EP also created figures and tables, and wrote, formatted and finalized the article for submission. FL, WJW, and PG supervised and reviewed the design and implementation of the study. SE conducted RNA extraction, quality assurance and library preparation for the Sepsis 2 dataset. RA conducted bioinformatics analysis to generate read counts for the Sepsis 2 dataset and guided RNA-Seq data pre-processing. TS, JH, and AC provided the dataset for the Sepsis 2 study and provided guidance on the clinical phenotyping of patients for both sepsis datasets. All authors contributed to writing and reviewing the manuscript.

Funding

Project Sepsis is funded by a Ser Cymru grant from Welsh Government and EU/ERDF funds to PG. PROTECT was funded by the NHMRC and Perth Children's Hospital Foundation. JH supported by the Wesfarmers Centre of Vaccines and Infectious Diseases.

Conflict of interest

PG is Founder and non-executive board member of Fios Genomics Ltd., and member of the development board of Sepsis Trust UK Ltd., without renumeration.

The remaining authors declare that the research was conducted in the absence of any commercial or financial relationships that could be construed as a potential conflict of interest.

Publisher's note

Supplementary material

The Supplementary Material for this article can be found online at: https://www.frontiersin.org/articles/10.3389/fgene.2023.1158352/full#supplementary-material

References

Anders, S., and Huber, W. (2010). Differential expression analysis for sequence count data. *Genome Biol.* 11, R106. doi:10.1186/gb-2010-11-10-r106

Babraham Bioinformatics Group (2019). Fastqc. Available at: https://www.bioinformatics.babraham.ac.uk/projects/fastqc/(Accessed 12 31, 2022).

Babraham Bioinformatics Group (2019). Trim galore. Available at: https://www.bioinformatics.babraham.ac.uk/projects/trim_galore/(Accessed 12 31, 2022).

Bommert, A., Rahnenführer, J., and Lang, M. (2017). A multicriteria approach to find predictive and sparse models with stable feature selection for high-dimensional data. *Comput. Math. Methods Med.* 2017, 7907163. doi:10.1155/2017/7907163

Bommert, A., Sun, X., Bischl, B., Rahnenführer, J., and Lang, M. (2020). Benchmark for filter methods for feature selection in high-dimensional classification data. *Comput. Statistics Data Analysis* 143, 106839. doi:10.1016/j.csda.2019.106839

Bommert, A. M. (2020). "Integration of feature selection stability in model fitting,". Ph.D. thesis (Dortmund: TU Dortmund University).

Bourgon, R., Gentleman, R., Huber, W., and Fienberg, S. E. (2010). Independent filtering increases detection power for high-throughput experiments. *Proc. Natl. Acad. Sci.* 107, 9546–9551. doi:10.1073/pnas.0914005107

Brechtmann, F., Mertes, C., Matusevičiūtė, A., Yepez, V. A., Avsec, Ž., Herzog, M., et al. (2018). Outrider: A statistical method for detecting aberrantly expressed genes in RNA sequencing data. *Am. J. Hum. Genet.* 103, 907–917. doi:10.1016/j.ajhg.2018.10.025

Breiman, L. (2001). Random forests. *Mach. Learn.* 45, 5–32. doi:10.1023/a:1010933404324

Cano-Gamez, E., Burnham, K. L., Goh, C., Allcock, A., Malick, Z. H., Overend, L., et al. (2022). An immune dysfunction score for stratification of patients with acute infection based on whole-blood gene expression. *Sci. Transl. Med.* 14, eabq4433. doi:10.1126/scitranslmed.abq4433

Chiesa, M., Colombo, G. I., and Piacentini, L. (2018). Damirseq -an r/bioconductor package for data mining of rna-seq data: Normalization, feature selection and classification. *Bioinformatics* 34, 1416–1418. doi:10.1093/bioinformatics/btx795

Chinchor, N. (1992). Muc-4 evaluation metrics. in *Proceedings of the 4th conference on Message understanding - muc4 '92*. Morristown, NJ: Association for Computational Linguistics, 22. doi:10.3115/1072064.1072067

Cook, R. D. (1977). Detection of influential observation in linear regression. *Technometrics* 19, 15. doi:10.2307/1268249

Cook, R. D. (1977). The Editor*Technometrics*. *Technometrics* 19, 349–350. doi:10.1080/00401706.1977.10489570

Dag, O., Kasikci, M., Ilk, O., and Yesiltepe, M. (2022). Geneselectml: A comprehensive way of gene selection for rna-seq data via machine learning algorithms. *Med. Biol. Eng. Comput.* 61, 229–241. doi:10.1007/s11517-022-02695-w

Deyneko, I. V., Mustafaev, O. N., Tyurin, A., Zhukova, K. V., Varzari, A., and Goldenkova-Pavlova, I. V. (2022). Modeling and cleaning rna-seq data significantly improve detection of differentially expressed genes. *BMC Bioinforma.* 23, 488. doi:10.1186/s12859-022-05023-z

Dobin, A., Davis, C. A., Schlesinger, F., Drenkow, J., Zaleski, C., Jha, S., et al. (2013). Star: Ultrafast universal rna-seq aligner. *Bioinformatics* 29, 15–21. doi:10.1093/bioinformatics/bts635

Ensembl (2021). Ensembl project. Available at: http://www.ensembl.org/info/data/ftp/index.html/(Accessed 12 31, 2022).

Fan, R. E., Chang, K. W., Hsieh, C. J., Wang, X. R., and Lin, C. J. (2008). Liblinear: A library for large linear classification. *J. Mach. Learn. Res.* 9, 1871–1874.

Friedman, J., Hastie, T., and Tibshirani, R. (2010). Regularization paths for generalized linear models via coordinate descent. *J. Stat. Softw.* 33, 1–22. doi:10.18637/jss.v033.i01

Fu, Y., Wu, P. H., Beane, T., Zamore, P. D., and Weng, Z. (2018). Elimination of pcr duplicates in rna-seq and small rna-seq using unique molecular identifiers. *BMC Genomics* 19, 531. doi:10.1186/s12864-018-4933-1

Goksuluk, D., Zararsiz, G., Korkmaz, S., Eldem, V., Zararsiz, G. E., Ozcetin, E., et al. (2019). Mlseq: Machine learning interface for rna-sequencing data. *Comput. Methods Programs Biomed.* 175, 223–231. doi:10.1016/j.cmpb.2019.04.007

Guyon, I., and Elisseeff, A. (2003). An introduction to variable and feature selection andré elisseeff. *J. Mach. Learn. Res.* 3, 1157–1182.

Guyon, I., Weston, J., Barnhill, S., and Vapnik, V. (2002). Gene selection for cancer classification using support vector machines. *Mach. Learn.* 46, 389–422. doi:10.1023/a:1012487302797

Hasan, R., and Chu, C. (2022). "Noise in datasets: What are the impacts on classification performance?," in Proceedings of the 11th International Conference on Pattern Recognition Applications and Methods (ICPRAM 2022), Feb 3, 2022 - Feb 5, 2022, 163–170. (Scitepress). doi:10.5220/0010782200003122

Jaccard, P. (1901). Etude de la distribution florale dans une portion des alpes et du jura. *Bull. Soc. Vaudoise Sci. Nat.* 37, 547–579. doi:10.5169/seals-266450

Jurman, G., Merler, S., Barla, A., Paoli, S., Galea, A., and Furlanello, C. (2008). Algebraic stability indicators for ranked lists in molecular profiling. *Bioinformatics* 24, 258–264. doi:10.1093/bioinformatics/btm550

Koch, C. M., Chiu, S. F., Akbarpour, M., Bharat, A., Ridge, K. M., Bartom, E. T., et al. (2018). A beginner's guide to analysis of rna sequencing data. *Am. J. Respir. Cell. Mol. Biol.* 59, 145–157. doi:10.1165/rcmb.2017-0430TR

Liao, Y., Smyth, G. K., and Shi, W. (2014). Featurecounts: An efficient general purpose program for assigning sequence reads to genomic features. *Bioinformatics* 30, 923–930. doi:10.1093/bioinformatics/btt656

Lin, Y., Qian, F., Shen, L., Chen, F., Chen, J., and Shen, B. (2017). Computer-aided biomarker discovery for precision medicine: Data resources, models and applications. *Briefings Bioinforma.* 20, 952–975. doi:10.1093/bib/bbx158

Liu, R., Wang, X., Aihara, K., and Chen, L. (2014). Early diagnosis of complex diseases by molecular biomarkers, network biomarkers, and dynamical network biomarkers. *Med. Res. Rev.* 34, 455–478. doi:10.1002/med.21293

Love, M. I., Huber, W., and Anders, S. (2014). Moderated estimation of fold change and dispersion for rna-seq data with deseq2. *Genome Biol.* 15, 550. doi:10.1186/s13059-014-0550-8

Mahendran, N., Vincent, P. M. D. R., Srinivasan, K., and Chang, C. Y. (2020). Machine learning based computational gene selection models: A survey, performance evaluation, open issues, and future research directions. *Front. Genet.* 11, 603808. doi:10.3389/fgene.2020.603808

Mangiola, S., Thomas, E. A., Modrák, M., Vehtari, A., and Papenfuss, A. (2021). Probabilistic outlier identification for rna sequencing generalized linear models. *NAR Genomics Bioinforma.* 3, lqab005. doi:10.1093/nargab/lqab005

McHugh, L., Seldon, T. A., Brandon, R. A., Kirk, J. T., Rapisarda, A., Sutherland, A. J., et al. (2015). A molecular host response assay to discriminate between sepsis and infection-negative systemic inflammation in critically ill patients: Discovery and validation in independent cohorts. *PLOS Med.* 12, e1001916. doi:10.1371/journal.pmed.1001916

Ng, S., Strunk, T., Lee, A. H., Gill, E. E., Falsafi, R., Woodman, T., et al. (2020). Whole blood transcriptional responses of very preterm infants during late-onset sepsis. *PLOS ONE* 15, e0233841. doi:10.1371/journal.pone.0233841

Nogueira, S., Sechidis, K., and Brown, G. (2018). On the stability of feature selection algorithms. *J. Mach. Learn. Res.* 18, 1–54.

Nowak, J. K., Adams, A. T., Kalla, R., Lindstrøm, J. C., Vatn, S., Bergemalm, D., et al. (2022). Characterisation of the circulating transcriptomic landscape in inflammatory bowel disease provides evidence for dysregulation of multiple transcription factors including nfe2, spi1, cebpb, and irf2. *J. Crohn's colitis* 16, 1255–1268. doi:10.1093/ecco-jcc/jjac033

Rau, A., Gallopin, M., Celeux, G., and Jaffrézic, F. (2013). Data-based filtering for replicated high-throughput transcriptome sequencing experiments. *Bioinformatics* 29, 2146–2152. doi:10.1093/bioinformatics/btt350

Sechidis, K., Papangelou, K., Nogueira, S., Weatherall, J., and Brown, G. (2019). "On the stability of feature selection in the presence of feature correlations," in European Conference on Machine Learning and Principles and Practice of Knowledge Discovery in Databases, Würzburg, Germany, September 16–20, 2019.

Simmer, K., Strunk, T., and Patole, S. (2016). Intravenous pentoxifylline as adjunct therapy to improve long-term disability in preterm infants. [Online]. Available at: https://www.anzctr.org.au/Trial/Registration/TrialReview.aspx?id=370404 (Accessed January 25, 2023).

Smith, C. L., Dickinson, P., Forster, T., Craigon, M., Ross, A., Khondoker, M. R., et al. (2014). Identification of a human neonatal immune-metabolic network associated with bacterial infection. *Nat. Commun.* 5, 4649. doi:10.1038/ncomms5649

Stark, R., Grzelak, M., and Hadfield, J. (2019). Rna sequencing: The teenage years. *Nat. Rev. Genet.* 20, 631–656. doi:10.1038/s41576-019-0150-2

Sweeney, T. E., Shidham, A., Wong, H. R., and Khatri, P. (2015). A comprehensive time-course-based multicohort analysis of sepsis and sterile inflammation reveals a robust diagnostic gene set. *Sci. Transl. Med.* 7, 287ra71. doi:10.1126/scitranslmed.aaa5993

Wagner, G. P., Kin, K., and Lynch, V. J. (2013). A model based criterion for gene expression calls using rna-seq data. *Theory Biosci.* 132, 159–164. doi:10.1007/s12064-013-0178-3

Wang, Z., Gerstein, M., and Snyder, M. (2009). Rna-seq: A revolutionary tool for transcriptomics. *Nat. Rev. Genet.* 10, 57–63. doi:10.1038/nrg2484

Zehetmayer, S., Posch, M., and Graf, A. (2022). Impact of adaptive filtering on power and false discovery rate in rna-seq experiments. *BMC Bioinforma.* 23, 388. doi:10.1186/s12859-022-04928-z

Zhang, X., Jonassen, I., and Goksøyr, A. (2021). *Bioinformatics: 4. Machine learning approaches for biomarker discovery using gene expression data*. Australia: Exon Publications. doi:10.36255/exonpublications.bioinformatics.2021

Zhu, X., and Wu, X. (2004). Class noise vs. Attribute noise: A quantitative study. *Artif. Intell. Rev.* 22, 177–210. doi:10.1007/s10462-004-0751-8

Zou, H., and Hastie, T. (2005). Regularization and variable selection via the elastic net. *J. R. Stat. Soc. B* 67, 301–320. doi:10.1111/j.1467-9868.2005.00503.x

Zucknick, M., Richardson, S., and Stronach, E. A. (2008). Comparing the characteristics of gene expression profiles derived by univariate and multivariate classification methods. *Stat. Appl. Genet. Mol. Biol.* 7, Article7. doi:10.2202/1544-6115.1307

frontiers | Frontiers in Medicine

TYPE Original Research
PUBLISHED 11 April 2023
DOI 10.3389/fmed.2023.1003121

OPEN ACCESS

EDITED BY
Emma Murphy,
Limerick Institute of Technology, Ireland

REVIEWED BY
Ziwen Zhu,
University of Missouri, United States
Monowar Aziz,
The Feinstein Institutes for Medical Research, United States

*CORRESPONDENCE
Alfred Ayala
✉ aayala@lifespan.org

SPECIALTY SECTION
This article was submitted to Infectious Diseases: Pathogenesis and Therapy, a section of the journal Frontiers in Medicine

RECEIVED 25 July 2022
ACCEPTED 21 March 2023
PUBLISHED 11 April 2023

CITATION
Armstead BE, Lee CS, Chen Y, Zhao R, Chung C-S, Fredericks AM, Monaghan SF and Ayala A (2023) Application of single cell multiomics points to changes in chromatin accessibility near calcitonin receptor like receptor and a possible role for adrenomedullin in the post-shock lung. *Front. Med.* 10:1003121. doi: 10.3389/fmed.2023.1003121

Application of single cell multiomics points to changes in chromatin accessibility near calcitonin receptor like receptor and a possible role for adrenomedullin in the post-shock lung

Brandon E. Armstead[1,2,3], Chung Sunny Lee[1,2], Yaping Chen[1,2], Runping Zhao[1,2], Chun-Shiang Chung[1,2], Alger M. Fredericks[1,2,4,5], Sean F. Monaghan[1,2,3,5] and Alfred Ayala[1,2,3,5]*

[1]Lifespan-Rhode Island Hospital, Providence, RI, United States, [2]Division of Surgical Research, Department of Surgery, Brown University, Providence, RI, United States, [3]Pathobiology Graduate Program, Brown University, Providence, RI, United States, [4]The Miriam Hospital, Providence, RI, United States, [5]The Warren Alpert Medical School, Brown University, Providence, RI, United States

Introduction: Acute lung injury (ALI)/acute respiratory distress syndrome (ARDS) is a commonly occurring sequelae of traumatic injury resulting from indirect insults like hypovolemic shock and/or extrapulmonary sepsis. The high lethality rate associated with these pathologies outlines the importance of clarifying the "priming" effects seen in the post-shock lung microenvironment, which are understood to bring about a dysregulated or overt immune response when triggered by a secondary systemic infectious/septic challenge culminating in ALI. In this pilot project, we test the hypothesis that application of a single cell multiomics approach can elucidate novel phenotype specific pathways potentially contributing to shock-induced ALI/ARDS.

Methods: Hypovolemic shock was induced in C57BL/6 (wild-type), PD-1, PD-L1, or VISTA gene deficient male mice, 8–12 weeks old. Wild-type sham surgeries function as negative controls. A total of 24-h post-shock rodents were sacrificed, their lungs harvested and sectioned, with pools prepared from 2 mice per background, and flash frozen on liquid nitrogen. N = 2 biological replicates (representing 4 mice total) were achieved for all treatment groups across genetic backgrounds. Samples were received by the Boas Center for Genomics and Human Genetics, where single cell multiomics libraries were prepared for RNA/ATAC sequencing. The analysis pipeline Cell Ranger ARC was implemented to attain feature linkage assessments across genes of interest.

Results: Sham (pre-shock) results suggest high chromatin accessibility around calcitonin receptor like receptor (CALCRL) across cellular phenotypes with 17 and 18 feature links, exhibiting positive correlation with gene expression between biological replicates. Similarity between both sample chromatin profiles/linkage arcs is evident. Post-shock wild-type accessibility is starkly reduced across replicates where the number of feature links drops to 1 and 3, again

presenting similar replicate profiles. Samples from shocked gene deficient backgrounds displayed high accessibility and similar profiles to the pre-shock lung microenvironment.

Conclusion: High pre-shock availability of DNA segments and their positive correlation with CALCRL gene expression suggests an apparent regulatory capacity on transcription. Post-shock gene deficient chromatin profiles presented similar results to that of pre-shock wild-type samples, suggesting an influence on CALCRL accessibility. Key changes illustrated in the pre-ALI context of shock may allow for additional resolution of "priming" and "cellular pre-activation/pre-disposition" processes within the lung microenvironment.

KEYWORDS

shock, sepsis, trauma, single cell, multiomics, ALI, ARDS

1. Introduction

1.1. Severe shock as a driver of ALI/ARDS

The altered cellular microenvironment resultant from severe blood loss has proven to be an important pre-dispositional contributor to downstream injury or organ failure (1–3). This is often characteristic of individuals who have undergone traumatic injury and reduced systemic blood volume resulting in sustained reduced mean arterial blood pressure (hypovolemic/hemorrhagic shock). Shock initially primes a variety of organ compartments, especially the lung, and results in a hyper-sensitive state for all cells within these tissues, a.k.a., priming, predisposition, re-programming, innate immune memory, etc. (1, 4–6). Oftentimes, surgical intervention corrects the injuries associated with the traumatic event. However, damage to the bowel-a reservoir of pathogens capable of causing severe infections-may be disseminated during surgery. A septic event may occur, which is characterized as the host dysregulated immune response to systemic infection (7). This infectious challenge then triggers the priming seen after shock and may result in varying severe pathologies which may contribute to acute lung injury (ALI).

One form of ALI, acute respiratory distress syndrome (ARDS), is commonly seen in patients who have undergone shock and/or sepsis (1, 2). The high mortality associated with ARDS (approximately 40% lethality) further highlights the importance of additional characterization and phenotypic identification of the pre-disease state elicited by shock in the lung (8). While targeted therapeutics have yet to offer considerable benefits in treating ARDS patients, the post-shock lung microenvironment has provided an important landscape worthy of survey and putative therapeutic targeting.

1.2. ALI pre-disease states

Acute lung injury is resultant from a variety of pre-injury or pre-disease states all of which culminate in tissue damage and eventual organ failure (1, 2, 8). These contributing factors are often characterized as either direct or indirect sources of ALI (8). Pulmonary contusion, or injury to the lung itself is an example of direct ALI. Other sources include, aspiration on gastric/bowel contents and pneumonia. Indirect sources of ALI include extrapulmonary septic events, shock, and massive blood transfusion. Additional characterization of these causative factors to ALI provides further clarity on molecular mechanisms important to disease predisposition, and may further improve currently exasperated and somewhat ineffective treatment modalities (9, 10).

1.3. Novel methods in transcriptional and chromatin profiling

Single cell or single nuclei methods for analyzing the transcriptional milieu and chromatin landscape have provided useful tools for clarifying and validating phenotype specific alterations in gene expression (11–13). Transcriptional assessments through single cell methods alone offer useful and informative conclusions not available through the implementation of bulk sequencing methods (11, 14). However, there remains some ambiguity in these analyses. The confidence in accurate evaluation of relevant biological phenomena has necessitated use of other assays such as flow cytometry analysis or qPCR as validation steps. Another helpful approach has been use of the assay for transposase accessible chromatin (ATAC) sequencing (15). This allows for the identification of changes in chromatin availability to transcription factors and key regulatory proteins, which importantly bind promoter regions or enhancer/silencer elements of transcribed genes (16, 17). Open or accessible regions of chromatin are understood to be positions of these important regulatory interactions. Such regions influence transcription of genes upstream or downstream of their location. Therefore, implementation of ATAC sequencing allows for the identification of regulatory elements influencing expression of genes enriched and detected through RNA sequencing.

Generating both RNA and ATAC sequencing readouts from a single cell offers an extremely useful means of corroborating data. This was recently adopted as a multiomics technique providing

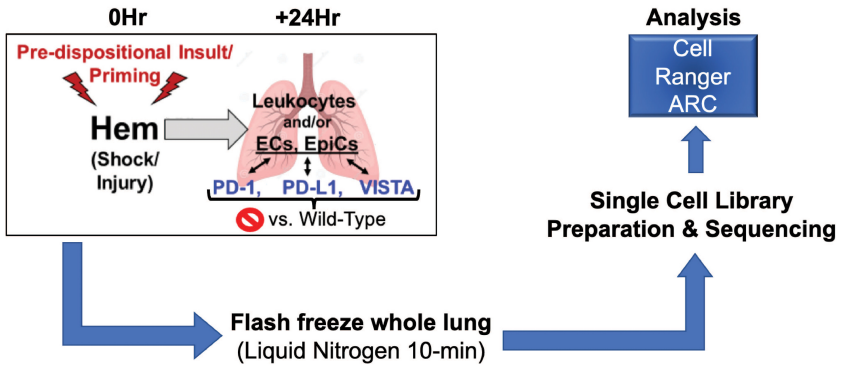

FIGURE 1
Illustrates workflow involved in data acquisition. Surgical techniques, sample harvesting, sequencing library preparation, and data analysis make up this process (*N* = 2/group).

information on correlation strength between accessible chromatin as well as transcript abundance at single cell resolution (18). Despite these advancements in technology, there remains the burden of further confirmation of multiomics datasets. However, through the novel incorporation of both transcriptomics and identification of chromatin landscape alterations, an initial level of confidence may be assigned to such analyses due to their tightly linked regulatory nature.

The most important aspect of the Cell Ranger ARC analysis pipeline used for this multiomics approach is the delineation of correlation strength between transcript abundance and accessible chromatin. These are referred to as linked features (19). Default pipeline settings allowed for the identification of links within 1 Mb. The stronger this relationship, the more likely an accessible locus possesses some regulatory capacity. Positive correlation beyond a pre-determined significance threshold aids in identifying enhancer elements, which drive transcription of linked genes. Anticorrelation is also detectable and occurs in the event of low transcript abundance and highly accessible chromatin, which indicates silencer elements that suppress transcription of linked genes. Silencers and enhancers are important regulatory genomic elements that will be discussed later. Both can be identified through this single cell multiomics approach.

1.4. Checkpoint proteins as immunomodulators of ALI

Signaling interactions between immunomodulatory receptors and ligands expressed across cellular phenotypes have recently been leveraged for immunotherapeutic benefits (20, 21). These regulators referred to as checkpoint proteins, have offered considerable benefits pertaining to tumor resolution and attenuating dysregulated immune responses leading to severe pathologies. Several of these proteins of particular importance serve as suppressors of the immune response. Following the initial signals required for lymphocyte activation which include antigen presentation *via* MHC I/II to the T-cell receptor, and co-stimulation by B-7 family/CD28 interactions, checkpoint proteins serves to either exacerbate or suppress subsequent immune activation.

Interactions between programmed cell death receptor 1 (PD-1) and its ligands (PD-L1/L2) importantly serve to suppress the immune response by blocking the activity of several key adaptor molecules, which normally act to stimulate T-cell activation (22–25). PD-1 is mainly expressed on lymphocytes and antigen presenting cells, but also across the endothelium/epithelium. These checkpoint proteins have been targeted clinically for oncogenic clearance (26), and an understanding of these benefits may be useful for other maladies of immune dysregulation pertaining to ALI/ARDS.

Another checkpoint protein providing putative utility in curtailing an aberrant immune response is the B-7 Ig superfamily member V-domain immunoglobulin suppressor of T-cell activation (VISTA) (27), which is primarily expressed on hematopoietic lineages (20, 28, 29). Myeloid populations possess higher VISTA expression than lymphoid groups, but among lymphocytes it is most highly expressed on regulatory T-cells. Interestingly, VISTA behaves as either a receptor or ligand and the outcome of its signaling is strongly tied to the cell and tissue specific context of these interactions. Ultimately, VISTA signaling suppresses the immune response and may drive other outcomes related to the development of ALI. Important therapeutic potential may be available through targeted stimulation or antagonism of VISTA signaling in the pre-development of lung inflammation, endothelial barrier dysfunction and/or fibrosis.

1.5. Disparate sepsis survival outcomes in the context of specific gene deficiencies

Sepsis is the most commonly seen pre-disease state for ALI (8). It is important to further characterize this relevant disease phenotype, especially in the context of checkpoint proteins and their impact on sepsis mortality. In experimental sepsis induced *via* the cecal ligation and puncture method, C57BL/6 mice deficient in PD-1 or PD-L1 expression relative to wild-type counterparts display improved survival (30, 31). However, mice deficient in VISTA expression are imparted a survival disadvantage relative to the wild-type background (32). Despite the shared co-inhibitory nature of their signaling,

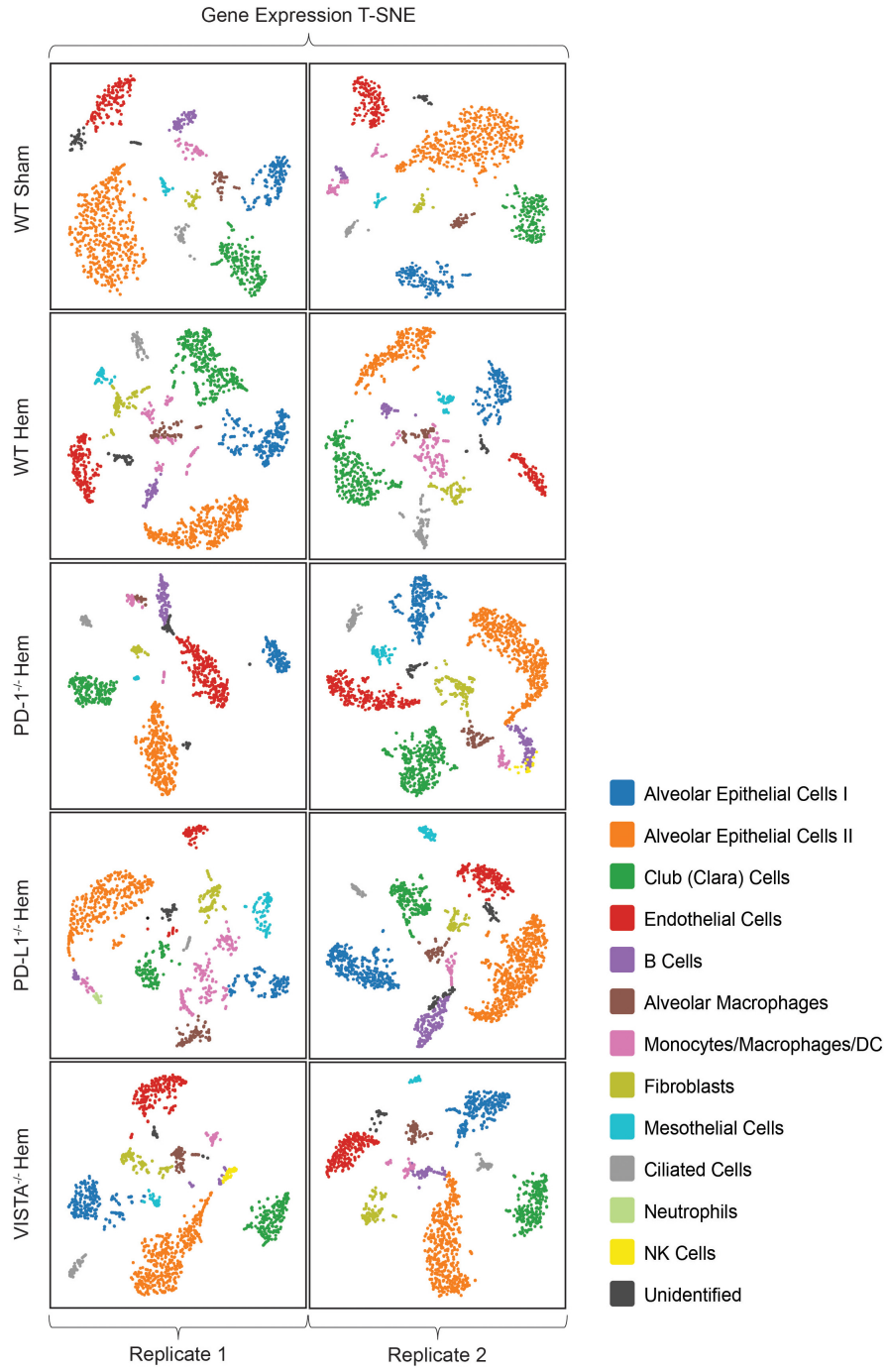

FIGURE 2
All samples in this multiomics approach are presented here in T-SNE plot format from Loupe Browser data visualization software. Wild-type sham/hemorrhaged as well as gene deficient hemorrhaged profiles are depicted. Samples are bracketed by individual biological replicates. Colored datapoints are clustered according to similarities in transcriptional profiles (*N* = 2/group).

these distinct mortality events in the context of experimental sepsis offer novel insights on the complex nature of checkpoint protein biology and specific impacts on pre-ALI disease states worthy of additional clarification. Shock presents another pre-dispositional insult for the development of ALI. Such checkpoint protein deficiencies are important and may create unique microenvironments within the lung concurrent with altered priming states.

1.6. Hypothesis

Taken together, we posit that the application of a single cell multiomics approach should allow us to begin to elucidate novel phenotype specific pathways potentially contributing to shock-induced priming/reprograming/predisposition to the development of ALI/ARDS in the face of a subsequent septic insult. Presented here is a multiomics analysis of wild-type vs. gene deficient murine

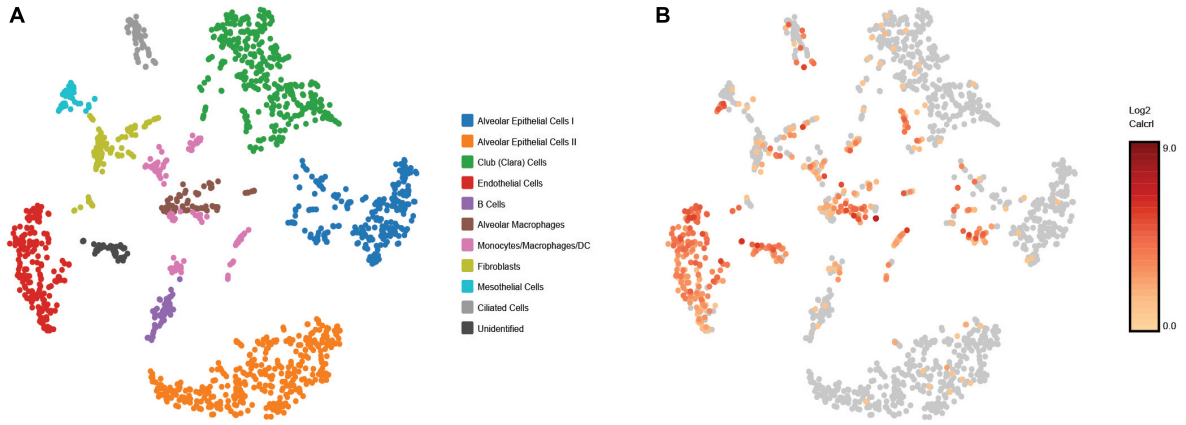

FIGURE 3
Depicts graph based projections **(A)** for all clusters in a representative sample [wild-type hem (1)], and its log2 fold change expression profile **(B)** for *Calcrl*.

lungs in the context of hemorrhage (hem) computed through Cell Ranger ARC (33), as depicted in Figure 1.

2. Results

2.1. Unsupervised analysis

Following implementation of the analysis pipeline Cell Ranger ARC on all 10 multiomics datasets, graph based clustering results were filtered/re-clustered based on cells falling within the linear distribution cut-off range of unique molecular identifiers (UMI's), features per barcode and a threshold of mitochondrial reads through the Loupe Browser data visualization platform (34). Clusters from the gene expression plot were identified based on similar patterns from referenced murine lung NGS (35–37) genes and others found in the online reference BioGPS (38) (**Supplementary Table 1**). Sample plots are shown in T-SNE (39) format, as presented in Figure 2. Identities included type 1 (ATI) and type II (ATII) alveolar epithelial cells, club (clara) cells, endothelial cells, B cells, alveolar macrophages, a mixed population of monocytes/macrophages/dendritic cells, fibroblasts, mesothelial cells, ciliated cells and an unidentified population of cells with overlapping expression from both endothelial and ATII cells. NK cells were only detected as a sizable cluster amongst PD-$1^{-/-}$ hem (2) and VISTA$^{-/-}$ hem (1). Neutrophils were unexpectedly detected in PD-$L1^{-/-}$ hem (1), as they are polymorphonuclear cells that should not have been captured. The sample preparation workflow applied here targets single nuclei. Neutrophils have proven difficult to detect in other single cell methods due to several factors, including their relatively low content of RNA and high amount of RNases (40).

Representative images from sample WT hem (1) are shown to depict unique cellular identities (Figure 3A) alongside the log2 fold change expression profiles of Calcitonin receptor like receptor *(Calcrl)* (Figure 3B), one of several markers used to identify endothelial cells. A heat map from this sample (Figure 4A) depicts some of the top upregulated genes expressed per cluster identity (log2 fold change) shown in T-SNE format, as well as *Calcrl* (Figure 4B), and the remaining endothelial markers *Tek* (Figure 4C) and *TMEM100* (Figure 4D) in violin plots.

2.2. Feature linkage assessment

In an attempt to discover genes with consistent expression and chromatin accessibility between biological replicates in the sham (wild-type) background, profiles for targets of interest were compared. These were then compared to hemorrhaged wild-type samples with distinct alterations in accessibility, and similarly for consistency between replicates. The third approach was surveying accessibility and expression across hemorrhaged samples gene deficient in global PD-1, PD-L1, or VISTA expression. Replicate consistency was again taken into account.

Representative images from one sample (Figure 5) are shown to illustrate global links for *Calcrl* (Figure 5A), a single (highlighted) link (Figure 5B), and higher resolution at this specific chromosome locus of accessibility (Figure 5C). The average number of single cell RNA-seq UMI's detected per cluster for *Calcrl* (Figure 5D), and average number of single cell ATAC-seq cut sites per cell at this specific locus (Figure 5E) are presented in bar graph format for all cells identified in this sample. The relative strength of correlation between linked features is indicated by the height of blue linkage arcs (19). Higher amplification arcs indicate strong correlation between transcript abundance and detectable accessible chromatin. Below each set of linkage arcs is pertinent gene information. Below this, is a representation of peak accessibility colored by the associated cluster. The height of each peak indicates the proportion of cells with accessible chromatin at that particular locus.

By totaling the number of feature links for specific genes in a given sample, the process of clarifying regulatory networks is somewhat expedited. *Calcrl* was found to be significantly enriched across clusters in both sham samples. Importantly, there was a similar number of feature links between replicates, with 18 in sample 1 (Figure 6A and Table 1) and 17 in sample 2. These loci were similarly positioned both upstream and downstream the *Calcrl* gene on Chromosome 2, and also exhibited positive

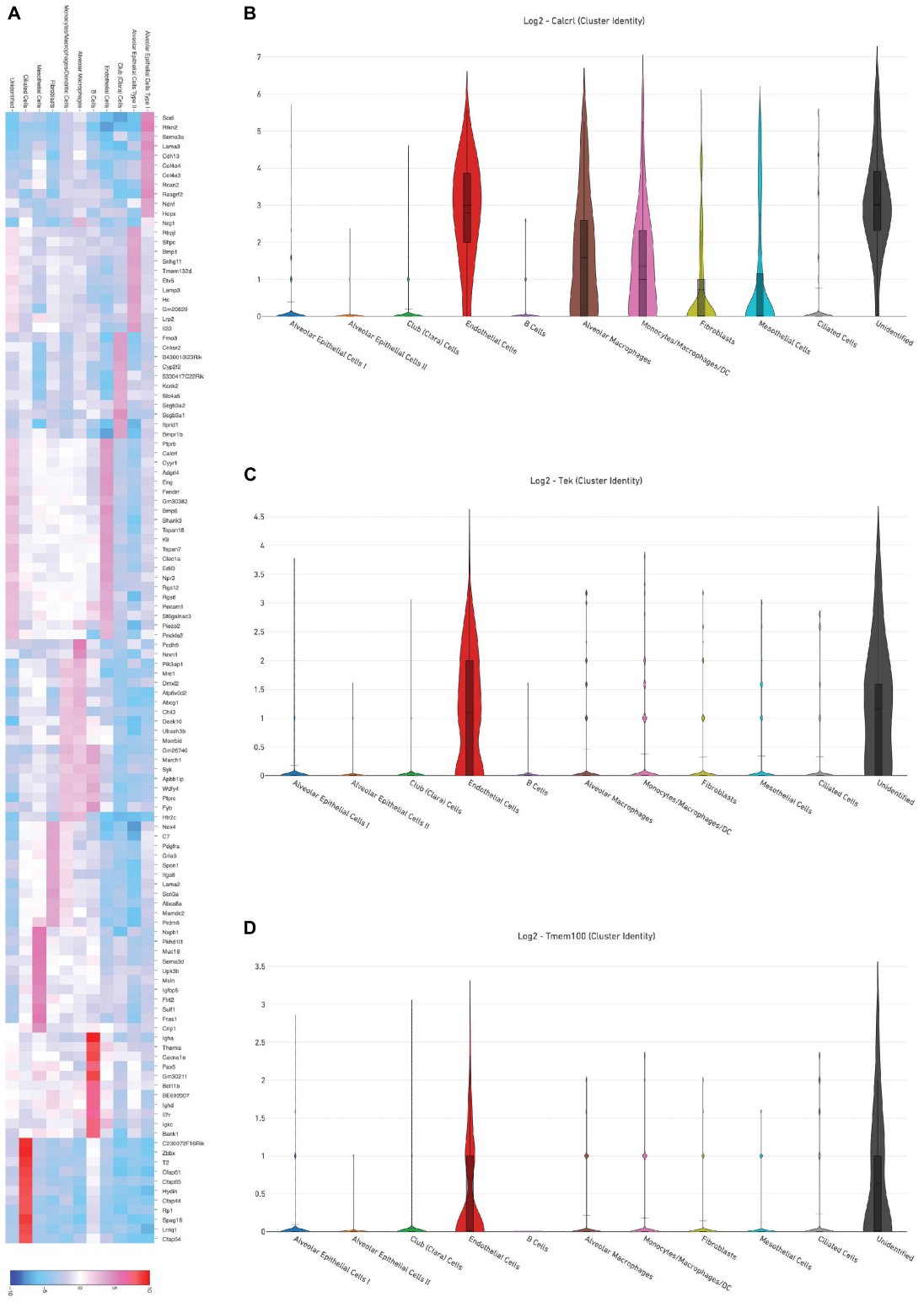

FIGURE 4
(A) Depicts a heat map of top significant genes upregulated per cluster (log2 fold change) in a representative sample [wild-type hem (1)]. Violin plots show relative log2 fold change expression profiles for markers used to identify endothelial cells in this sample: *Calcrl* **(B)**, *Tek* **(C)**, and *Tmem100* **(D)**.

correlation. In the hemorrhaged wild-type background, feature linkages were starkly reduced and consistent between replicates (Figure 6B and Table 1) as illustrated by 3 links and 1 link in samples 1 and 2, respectively. All were positively correlated. These data are also depicted in Supplementary Tables 2–5. In the context of specific gene deficiencies following hemorrhage shown in Figure 7 and Table 1, PD-1$^{-/-}$ (Figure 7A) featured strong consistency between replicates with 15 and 13 feature

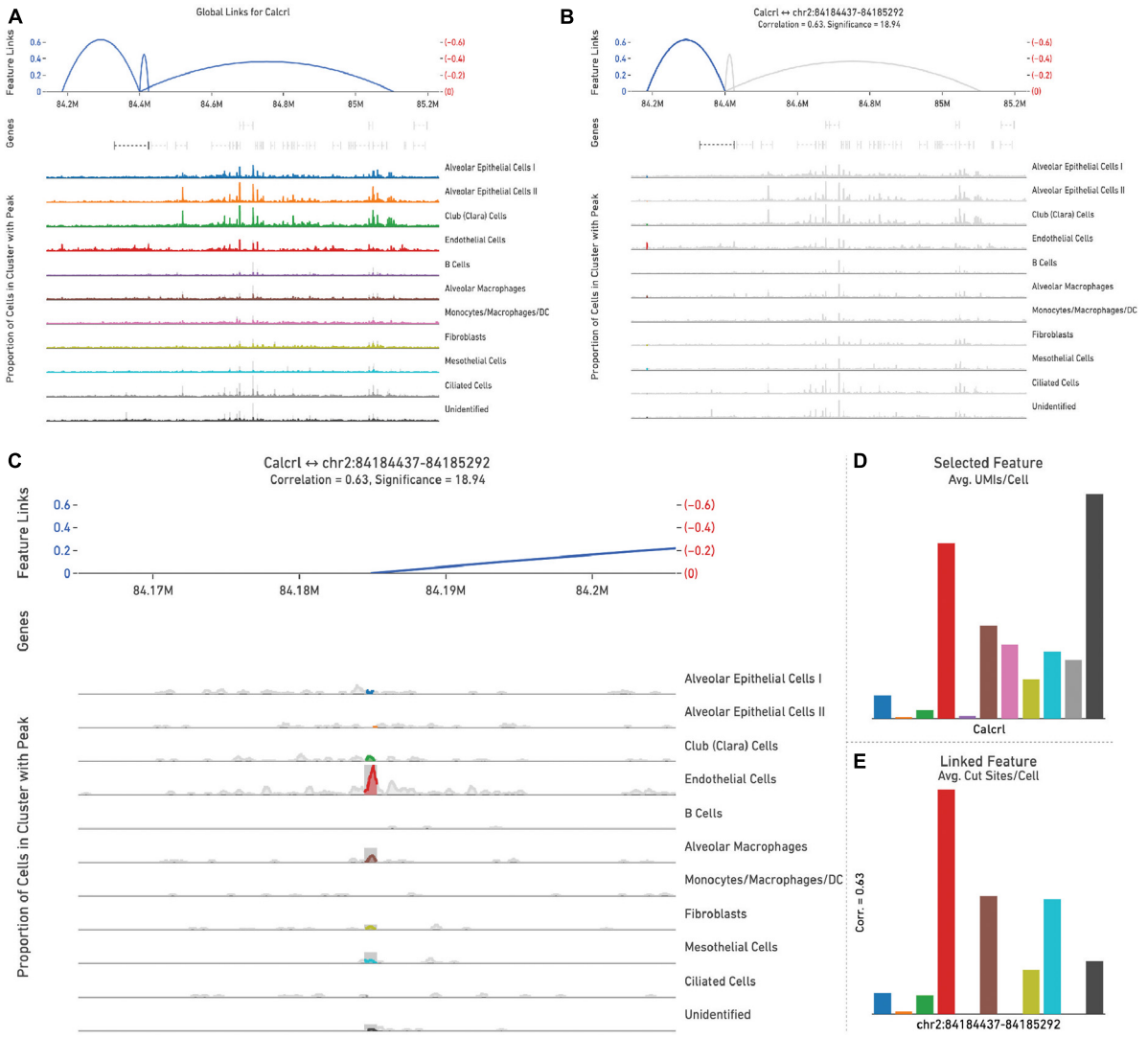

FIGURE 5
All feature links are depicted (within 1 Mb of *Calcrl*) **(A)** for representative sample wild-type hem (1). A single feature link is highlighted **(B)**, then shown at higher resolution at this specific locus chr2:84184437-84185292 **(C)**. The genomic location of *Calcrl* is denoted by the bracketed dashed line below the linkage arcs. **(D)** Displays average number of *Calcrl* unique molecular identifiers (UMIs), or cut sites per cell at this locus **(E)** for cells within each identified phenotype, presented in bar graph format.

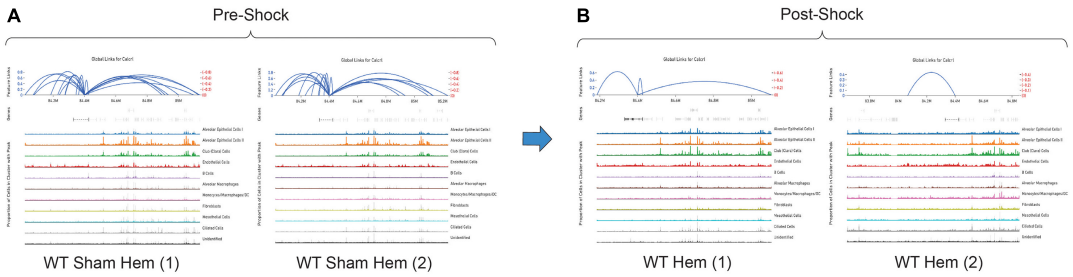

FIGURE 6
Feature linkage assessment of wild-type pre **(A)** and post-shock **(B)** lung microenvironments of *Calcrl*. Blue linkage arcs are displayed at the top of each sample plot; relative strength of correlation between accessible loci and *Calcrl* enrichment is conveyed *via* arc height. Colored peak information below arcs displays accessibility based on cells in individual clusters. The abundance of cells with accessible chromatin is represented by peak heights (*N* = 2/group).

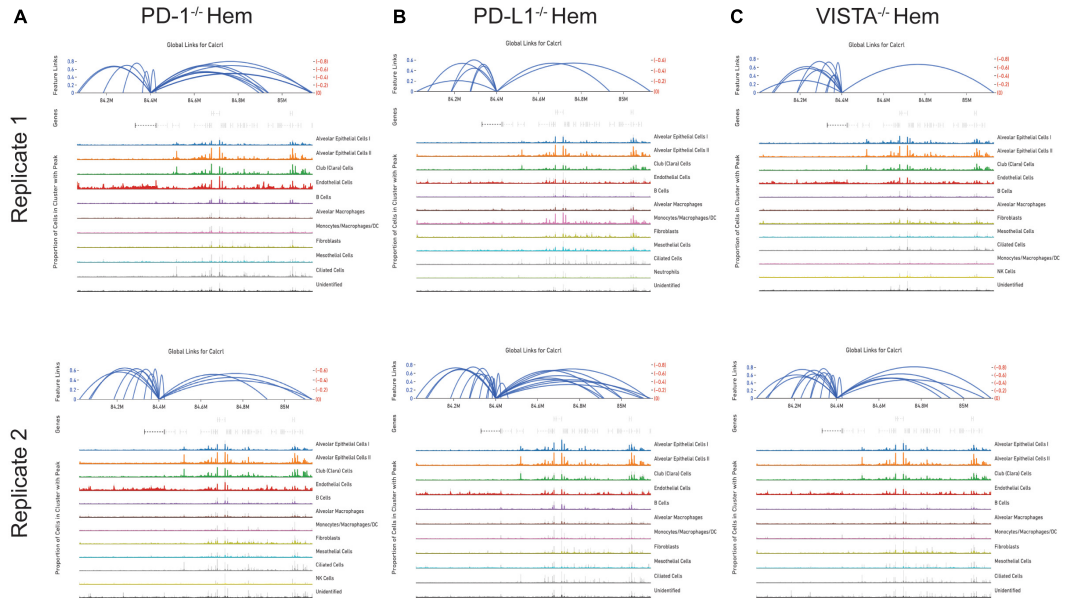

FIGURE 7
Feature linkage assessment of hemorrhaged gene deficient backgrounds. PD-1$^{-/-}$ **(A)**, PD-L1$^{-/-}$ **(B)** and VISTA$^{-/-}$ **(C)**. Data is displayed as represented in Figure 6.

TABLE 1 Total numbers of feature linkages are listed for each sample/replicate (*N* = 2/group).

	Total feature links				
Sample	WT sham hem	WT hem	PD-1$^{-/-}$ hem	PD-L1$^{-/-}$ hem	VISTA$^{-/-}$ hem
Replicate 1	18	3	15	8	10
Replicate 2	17	1	13	22	16

links. PD-L1$^{-/-}$ (Figure 7B) was less consistent, as shown by 8 and 22 feature links. VISTA$^{-/-}$ featured somewhat greater consistency (Figure 7C) with 10 and 16 feature links. These were also all positively correlated; data are tabulated in Supplementary Tables 6–11.

While the hemorrhaged wild-type backgrounds displayed reduced feature links, individual deficiencies in costimulatory checkpoint proteins appeared to maintain high accessibility around this particular gene. These profiles appeared more similar to sham controls than hemorrhaged wild-type samples.

3. Discussion

3.1. Genomic regulatory elements and transcription

Distally dispersed genomic loci can influence the transcription of linked genes following the binding of relevant adaptor molecules (15). A conformational change occurs within the chromatin structure once these proteins bind to such regulatory regions (16, 17). Proteins bound to this locus may then interact with transcription factors bound to the promoter region of a relevant gene, further influencing its transcription. In this way, such structural changes allow the bound regulatory region to subsequently influence gene regulation. As mentioned in the description of feature linkage assessments, elements that increase or upregulate transcription are referred to as enhancers. Those that suppress transcription are known as silencers. The nature of key modifications at the chromatin level allows for increased availability of these regulatory loci to adaptor binding. Through silencer or enhancer activity and subsequent chromatin folding, linked genes undergo altered transcription. These important dynamics serve to further illustrate the relationship between chromatin accessibility and transcriptional networks.

3.2. Cellular phenotypes amongst lung datasets

A broad distribution of identities from referenced datasets were detected throughout the samples represented here (35–37). The frequencies at which these were found across each sample somewhat varied, although this analysis was completed by one individual. That may account for some of these apparent disparities between calls made in the determination of cluster identities. Additional heat maps are provided illustrating each sample and the top enriched genes per cluster (Supplementary Figures 1–10).

An inherent inability to identify a prevalent neutrophil (polymorphonuclear) signal amongst this dataset due to single nuclei workflow limitations, particularly in hemorrhaged samples

where a high proportion of neutrophils is expected (1) has confounded certain aspects of this analysis, including an identification of their specific genomic alterations. This is with the exception of one sample detailed previously. The library preparation protocol for the datasets presented here relies on whole nuclei as an input material. Polymorphonuclear cells do not feature the typical single nucleus seen in other phenotypes (41) and, thus, are not expected to be captured through these methods due to sample sorting prior to library preparation.

3.3. *Calcrl* accessibility

As detected by the multiomics approach employed in this analysis, the receptor CALCRL exhibited altered chromatin profiles following shock. CALCRL provides a quality marker for endothelial cells (36), which serve an important role in the development of ALI/ARDS. A strong result in peak accessibility was notable amongst endothelial cells and several other phenotypes across all feature linkage profiles presented (**Figures 5**–**7**). This appears to echo the expression profile *Calcrl* exhibited in **Figures 3B**, **4B**, in which positive signal was detected predominantly in endothelial cells and scattered across several other phenotypes including alveolar macrophages and the mixed population of monocytes, macrophages and dendritic cells.

The deterioration of endothelial barrier function signals a hallmark characteristic of ARDS (42, 43). It is currently unclear whether this reduced accessibility near *Calcrl* in experimental shock offers potential as a clinical biomarker for this pre-disease state. The means by which such selective gene deficiencies maintain their sham profile of high accessibility also remains uncertain. Wild-type accessibility around *Calcrl* was high in sham backgrounds as noted by total feature linkages, with strong positive correlation. The strength of this correlation indicated that the relationship between transcripts detected by RNA sequencing relative to accessible genomic loci from ATAC sequencing was nearly 1:1. This indicates these regions were tightly regulating the transcription of this gene. The reduced accessibility near *Calcrl* in the wild-type hemorrhaged background is an interesting biological result. Of further importance is the outcome of maintained accessibility following hemorrhage in the context of individual checkpoint protein deficiencies. These profiles were more similar to sham results than hemorrhaged wild-type type profiles. Following sepsis modeling it was predicted that VISTA and PD-1/L1 uniquely contributed to pre-ALI priming and/or disease states given the disparate experimental sepsis mortality seen in gene deficient backgrounds relative to wild-type counterparts (30–32). Unexpectedly, all three gene deficiencies somewhat similarly featured accessible chromatin near *Calcrl*. Albeit this was less conserved between PD-L1$^{-/-}$ samples. Further work is necessary to clarify *Calcrl* and its role in the hemorrhaged lung microenvironment. Additional functional assays in cell types of interest may validate a defined role for this gene across hemorrhaged wild-type or deficient backgrounds.

3.4. Adrenomedullin signaling in sepsis and acute lung injury

CALCRL serves as a receptor for the peptide adrenomedullin (AM), along with receptor activity-modifying protein 2 (RAMP2) and RAMP3 as co-receptors (44–47). Not addressed within this manuscript is calcitonin gene-related peptide (CGRP), which binds a complex of RAMP1 and CALCRL (44, 48). Experimental data has identified multiple roles for this key ligand. In rats it has been shown that delivery of adrenomedullin binding protein-1 (AMBP-1) once sepsis was initiated, along with delivery of AM peptide prior to and throughout induction slowed the shift from hyperdynamic to hypodynamic sepsis, improved survival and reduced tissue damage associated with the insult (46). Furthermore, administering AM and AMBP-1 following sepsis induction in rats reduced inflammatory indices including circulating TNF-α, IL-6, and IL-1β (47). Importantly, circulating levels of AM are increased in septic patients (49). Such conflicting outcomes of AM activity in sepsis associated pathologies begets a murky role for this peptide in disease progression.

Experimental modeling has shown that the effects of adrenomedullin are favorable for a variety of lung injury indices, including endothelial permeability (50). It has also been confirmed that the signaling from CALCRL/AM ligation and endothelial nitric oxide synthase activity is important for the resolution of experimental bronchopulmonary dysplasia associated with pulmonary hypertension, clinically seen amongst infants (51). As others have shown, this activity is important for development of the murine lymphatic vascular system (45). These results may further suggest that the CALCRL/RAMP2 signaling axis *via* adrenomedullin ligation impacts the lung vascular endothelium in clinical contexts, and possibly the associated effects of ALI. Experimental data shared here in the context of shock induced by sustained hemorrhage highlights a potential role for this activity in the pre-ALI microenvironment.

This analysis posits similarities in *Calcrl* accessibility in the hemorrhaged lung microenvironment across cellular phenotypes of coinhibitory gene deficient backgrounds. Sham conditions appeared to present a baseline of high chromatin availability near *Calcrl* relative to an apparent reduction or loss in wild-type backgrounds, characterizing a primed state or altered predisposition of cells in the lung microenvironment. This begets the development of ALI/ARDS, whereas gene deficiencies seem to maintain homeostatic levels and mitigate priming. These data support viability of *Calcrl* as a therapeutic target for such diseases. Another consideration to be made is regarding the availability of the AM peptide across each deficient background. Of note, the PD-1/L1 deficiency offers a survival benefit in experimental ALI (52, 53). This is consistent with the aforementioned results in experimental sepsis (30–32). Additional work is planned to survey across each (post-hemorrhage) gene deficient group in order to determine whether AM levels are variable, as its ability to interact with the CALCRL endothelial receptor may play a role in either the septic immune response or shock-induced ALI priming.

3.5. Novel regulatory elements

The implementation of such methods for chromatin landscape profiling serves as an identifier of novel regulatory sites dispersed throughout the genome. These previously undescribed loci offer insights on the means by which widely dispersed enhancers/silencers seem to influence transcription. Correlation scores provide additional clarity on the likelihood of regulatory influence imparted by these loci. The specificity provided in this analysis is at chromosomal base pair resolution, which may be used to reference commonly occurring polymorphisms or genomic abnormalities leading to pathogenesis. While complexities in deciphering these details remain, the increased ubiquity of single cell multiomics approaches continues to favor iterative and accessible options for tailored analysis. The suite of tools for enhanced visualization offered by Loupe Browser are often modified and updated, providing the field with new and improved means of identifying highly specific druggable genomic targets.

4. Conclusion

The primary drivers of ALI and ARDS predispositional priming have required an additional degree of resolution not previously achieved. The complex lung microenvironment is composed of various immune/non-immune phenotypes involved in the associated hypersensitive state seen after shock. The methods presented in this pilot study offer a glimpse at clarifying altered cell specific roles resultant from shock-induced priming. The two-pronged multiomics approach of RNA/ATAC sequencing at single cell resolution has provided putative molecular target and genomic loci worthy of further analysis.

The work presented here has addressed the priming response concurrent with critical illness across backgrounds deficient in several key immunotherapeutic coinhibitory targets. This has resulted in identification of interesting alterations near the gene *Calcrl* following shock, which was significantly enriched across individual lung phenotypes. The peptide adrenomedullin AM, which binds CALCRL (44–47), has been implicated in the pathogenesis of sepsis and the immune response (46, 47). These interactions have implicated the vascular endothelium as it pertains to experimental lung injury (45, 50, 51). Despite the small sample size of this project, alterations made at the chromatin level during the pre-ALI state of shock induced priming were evident. The nature by which such reduced accessibility near CALCRL might pre-dispose to ALI/ARDS elicits additional questions pertaining to pre-transcriptional chromatin modifications. High pre-shock availability of DNA segments near CALCRL and their positive correlation with its expression suggest an apparent regulatory capacity on transcription. Post-shock coinhibitory gene deficient chromatin profiles presented similar results to that of pre-shock wild-type samples, suggesting an influence on CALCRL accessibility. Key changes illustrated in the pre-ALI context of hypovolemic/hemorrhagic shock may allow for additional resolution of "priming" and "cellular pre-activation/pre-disposition" processes within the lung microenvironment.

5. Materials and methods

5.1. Murine backgrounds

Mice deficient in PD-1 (PD-1$^{-/-}$) or PD-L1 (PD-L1$^{-/-}$) were used to breed the knock-out pups (provided by Tasuku Honjo, Kyoto University, Kyoto, Japan, through Megan Sykes at Massachusetts General Hospital, Boston, MA, USA) here at Lifespan-Rhode Island Hospital. VISTA deficient mice were generated through use of the CRISPR Cas9 system also in the C57BL/6 background as previously described by Gray et al. (32). Mice were genotyped to confirm global loss of expression per relevant receptor or ligand. All mice used in experimental shock modeling were aged 8–12 weeks (12: 12-h light/dark cycle, 68–72°F, 30–70% humidity).

5.2. Experimental model of shock

A model of hypovolemic shock was implemented, whereby a fixed-pressure hemorrhage was utilized to achieved sustained reduced mean arterial blood pressure in male C57BL/6 murine hosts aged 8–12 weeks. This choice was made so as to maximize our ability to initially see an experimental difference in the ALI/ARDS response based on previous reports that male mice did poorer in response to these experimental stressors of shock (hemorrhage) and/or septic (CLP) challenge than pro-estrus stratified females (54, 55). In brief, an isoflurane/oxygen gas mixture was used as anesthesia under the Rhode Island Hospital IACUC approved protocol for animal safety (AWC# 5064-18 and 5054-21). Bi-lateral arteriotomies were catheterized and used to monitor blood pressure and draw blood throughout the procedure. Mice were kept in this state for a 90-min duration, during which additional blood was drawn to maintain reduced blood pressure ∼40 mmHg (±5 mmHg). This provides a standardized and effective mimic of severely injured hypovolemic patients. Immediately following this experimental insult, mice were administered a crystalloid solution of lactated ringer's equivalent to 4× the volume of blood hemorrhaged. Sham surgeries were performed under anesthesia by which both femoral arteries were ligated. However, blood was not drawn and these serve as negative controls in this analysis.

5.3. Preparation of samples for sequencing libraries

An $N = 2$ was established in order to compare consistencies between chromatin alterations between biological replicates. A total of 24-h post-resuscitation, mice were euthanized and lungs were harvested. Tissue was pooled from 2 mice per treatment group/genotype for all samples prepared, and flash frozen on liquid nitrogen for 10 min. These were then stored at −80°C and shipped on dry ice to the Robert Boas Center for Genomics and Human Genetics within the Feinstein Institute for Medical Research-Northwell Health, Manhasset, NY, USA, where single cell (single nucleus) multiomics libraries from 4,000 cells/sample were prepared from lysed tissue. This was then filtered and washed,

followed by nuclear 7AAD exclusion staining. These were sorted and permeabilized, then washed and counted for use in subsequent steps. The 10× Genomics Chromium Next GEM Single Cell Multiome ATAC + Gene Expression library preparation kit was implemented (Product Code 1000285). Libraries were loaded and run on a Nextseq 500.

5.4. Single cell multiomics analysis pipeline and unsupervised analysis

Cell Ranger ARC was utilized for all pertinent pre-processing of multiomics datasets including mouse reference genome alignment (mm10), transcript counting (33). During additional pre-processing, all sample datasets were filtered and re-clustered based on cells falling within the linear distribution cut-off range of UMI's (unique molecular identifiers) (20–20,000) per barcode and (1–30,001) features per barcode and a maximum threshold of 5% mitochondrial reads (56) through the Loupe Browser data visualization platform (34). An unsupervised analysis was performed through which clusters from the gene expression plot were identified by patterns of positive signal detected. These profiled similarly to general expression patterns in referenced murine lung NGS (35–37) datasets and others found in the online reference BioGPS (38) (**Supplementary Table 1**).

5.5. Feature linkage assessment

Linked features provide a better understanding of the correlation between significantly enriched genes per cluster relative to altered chromatin accessibility and the likely presence of regulatory genomic elements (19). These were identified for *Calcrl* across all samples. The default settings for Cell Ranger ARC were implemented in which all resolved linked features fell within 1 Mb of *Calcrl*. The total number of links for each sample is provided in **Table 1**.

Data availability statement

The data presented in this study are deposited in the Brown Digital Repository, https://doi.org/10.26300/dm01-zr98.

Ethics statement

This animal study was reviewed and approved by the Rhode Island Hospital IACUC approved protocol for animal safety (AWC# 5064-18 and 5054-21).

Author contributions

BA initially drafted and revised this submission. BA, CL, YC, RZ, and C-SC performed the surgical techniques. BA and CL completed the sample collection. AF and SM helped BA to complete the RNA-seq and ATAC-seq analysis. YC performed the routine genotyping and husbandry of PD-1$^{-/-}$, PD-L1$^{-/-}$, and VISTA$^{-/-}$ mice. AA provided guidance throughout the conception and execution of this project. All authors reviewed this manuscript.

Funding

This study was supported by the National Institutes of Health [T32 HL134625 (BA and AF), R35 GM118097 (AA, C-SC, and YC), R35 GM142638 (SM), and P20 GM121344 (AF)], and funding from the Brown University "Karen T. Romer" Undergraduate Teaching and Research Award (CL).

Acknowledgments

We thank the staff of the Brown Center for Computation and Visualization and the Brown Computational Biology Core for their assistance in pertinent understanding of computational approaches related to these analyses. Figures were compiled in Adobe Illustrator 2021 (57).

Conflict of interest

SM is founder of Alcini, LLC.

The remaining authors declare that the research was conducted in the absence of any commercial or financial relationships that could be construed as a potential conflict of interest.

Publisher's note

Supplementary material

The Supplementary Material for this article can be found online at: https://www.frontiersin.org/articles/10.3389/fmed.2023.1003121/full#supplementary-material

References

1. Ayala A, Chung CS, Lomas JL, Song GY, Doughty LA, Gregory SH, et al. Shock-induced neutrophil mediated priming for acute lung injury in mice: divergent effects of TLR-4 and TLR-4/FasL deficiency. *Am J Pathol.* (2002) 161:2283–94. doi: 10.1016/S0002-9440(10)64504-X

2. Kauvar DS, Lefering R, Wade CE. Impact of hemorrhage on trauma outcome: an overview of epidemiology, clinical presentations, and therapeutic considerations. *J Trauma.* (2006) 60(6 Suppl):S3–11. doi: 10.1097/01.ta.0000199961.02677.19

3. Lomas-Neira J, Chung CS, Perl M, Gregory S, Biffl W, Ayala A. Role of alveolar macrophage and migrating neutrophils in hemorrhage-induced priming for ALI subsequent to septic challenge. *Am J Physiol Lung Cell Mol Physiol.* (2006) 290:L51–8. doi: 10.1152/ajplung.00028.2005

4. Lomas JL, Chung CS, Grutkoski PS, LeBlanc BW, Lavigne L, Reichner J, et al. Differential effects of macrophage inflammatory chemokine-2 and keratinocyte-derived chemokine on hemorrhage-induced neutrophil priming for lung inflammation: assessment by adoptive cells transfer in mice. *Shock.* (2003) 19:358–65. doi: 10.1097/00024382-200304000-00011

5. Sherwood ER, Burelbach KR, McBride MA, Stothers CL, Owen AM, Hernandez A, et al. Innate Immune Memory and the Host Response to Infection. *J Immunol.* (2022) 208:785–92. doi: 10.4049/jimmunol.2101058

6. Morris MC, Gilliam EA, Li L. Innate immune programing by endotoxin and its pathological consequences. *Front Immunol.* (2015) 5:680. doi: 10.3389/fimmu.2014.00680

7. Singer M, Deutschman CS, Seymour CW, Shankar-Hari M, Annane D, Bauer M, et al. The third international consensus definitions for sepsis and septic shock (sepsis-3). *JAMA.* (2016) 315:801–10. doi: 10.1001/jama.2016.0287

8. Perl M, Lomas-Neira J, Venet F, Chung CS, Ayala A. Pathogenesis of indirect (secondary) acute lung injury. *Expert Rev Respir Med.* (2011) 5:115–26. doi: 10.1586/ers.10.92

9. Calfee CS, Matthay MA. Nonventilatory treatments for acute lung injury and ARDS. *Chest.* (2007) 131:913–20. doi: 10.1378/chest.06-1743

10. Matthay MA, Zemans RL, Zimmerman GA, Arabi YM, Beitler JR, Mercat A, et al. Acute respiratory distress syndrome. *Nat Rev Dis Prim.* (2019) 5:18. doi: 10.1038/s41572-019-0069-0

11. Kulkarni A, Anderson AG, Merullo DP, Konopka G. Beyond bulk: a review of single cell transcriptomics methodologies and applications. *Curr Opin Biotechnol.* (2019) 58:129–36. doi: 10.1016/j.copbio.2019.03.001

12. Stuart T, Satija R. Integrative single-cell analysis. *Nat Rev Genet.* (2019) 20:257–72. doi: 10.1038/s41576-019-0093-7

13. Slovin S, Carissimo A, Panariello F, Grimaldi A, Bouché V, Gambardella G, et al. Single-cell RNA sequencing analysis: a step-by-step overview. *Methods Mol Biol.* (2021) 2284:343–65. doi: 10.1007/978-1-0716-1307-8_19

14. Li X, Wang CY. From bulk, single-cell to spatial RNA sequencing. *Int J Oral Sci.* (2021) 13:36. doi: 10.1038/s41368-021-00146-0

15. Buenrostro JD, Wu B, Chang HY, Greenleaf WJ. ATAC-seq: a method for assaying chromatin accessibility genome-wide. *Curr Protoc Mol Biol.* (2015) 109:21.29.1–21.29.9. doi: 10.1002/0471142727.mb2129s109

16. Kolovos P, Knoch TA, Grosveld FG, Cook PR, Papantonis A. Enhancers and silencers: an integrated and simple model for their function. *Epigenet Chromatin.* (2012) 5:1. doi: 10.1186/1756-8935-5-1

17. Panigrahi A, O'Malley BW. Mechanisms of enhancer action: the known and the unknown. *Genome Biol.* (2021) 22:108. doi: 10.1186/s13059-021-02322-1

18. 10x Genomics. Simultaneous Profiling of the Transcriptome and Epigenome from the Same cell. Document Number LIT000099 – Rev C – Product Sheet. (2021).

19. 10x Genomics. *Algorithms for Computation of Feature Linkages. Software -Single Cell Multiome ATAC + Gene Exp. -Official 10x Genomics Support*. (2022). Available online at: https://support.10xgenomics.com/single-cell-multiome-atac-gex/software/pipelines/latest/algorithms/feature-linkage (accessed July 19, 2022).

20. Wakeley ME, Gray CC, Monaghan SF, Heffernan DS, Ayala A. Check point inhibitors and their role in immunosuppression in sepsis. *Crit Care Clin.* (2020) 36:69–88. doi: 10.1016/j.ccc.2019.08.006

21. Boomer JS, Green JM, Hotchkiss RS. The changing immune system in sepsis: is individualized immunomodulatory therapy the answer? *Virulence.* (2014) 5:45–56. doi: 10.4161/viru.26516

22. Bardhan K, Anagnostou T, Boussiotis VA. The PD1:PD-L1/2 pathway from discovery to clinical implementation. *Front Immunol.* (2016) 7:550. doi: 10.3389/fimmu.2016.00550

23. Yokosuka T, Takamatsu M, Kobayashi-Imanishi W, Hashimoto-Tane A, Azuma M, Saito T. Programmed cell death 1 forms negative costimulatory microclusters that directly inhibit T cell receptor signaling by recruiting phosphatase SHP2. *J Exp Med.* (2012) 209:1201–17. doi: 10.1084/jem.20112741

24. Arasanz H, Gato-Cañas M, Zuazo M, Ibañez-Vea M, Breckpot K, Kochan G, et al. PD1 signal transduction pathways in T cells. *Oncotarget.* (2017) 8:51936–45. doi: 10.18632/oncotarget.17232

25. Patsoukis N, Wang Q, Strauss L, Boussiotis VA. Revisiting the PD-1 pathway. *Sci Adv.* (2020) 6:eabd2712. doi: 10.1126/sciadv.abd2712

26. Topalian SL, Drake CG, Pardoll DM. Targeting the PD-1/B7-H1(PD-L1) pathway to activate anti-tumor immunity. *Curr Opin Immunol.* (2012) 24:207–12. doi: 10.1016/j.coi.2011.12.009

27. Wang L, Rubinstein R, Lines JL, Wasiuk A, Ahonen C, Guo Y, et al. VISTA, a novel mouse Ig superfamily ligand that negatively regulates T cell responses. *J Exp Med.* (2011) 208:577–92. doi: 10.1084/jem.20100619

28. Liu J, Yuan Y, Chen W, Putra J, Suriawinata AA, Schenk AD, et al. Immune-checkpoint proteins VISTA and PD-1 nonredundantly regulate murine T-cell responses. *Proc Natl Acad Sci USA.* (2015) 112:6682–7. doi: 10.1073/pnas.1420370112

29. Huang X, Zhang X, Li E, Zhang G, Wang X, Tang T, et al. VISTA: an immune regulatory protein checking tumor and immune cells in cancer immunotherapy. *J Hematol Oncol.* (2020) 13:83. doi: 10.1186/s13045-020-00917-y

30. Huang X, Venet F, Wang YL, Lepape A, Yuan Z, Chen Y, et al. PD-1 expression by macrophages plays a pathologic role in altering microbial clearance and the innate inflammatory response to sepsis. *Proc Natl Acad Sci USA.* (2009) 106:6303–8. doi: 10.1073/pnas.0809422106

31. Huang X, Chen Y, Chung CS, Yuan Z, Monaghan SF, Wang F, et al. Identification of B7-H1 as a novel mediator of the innate immune/proinflammatory response as well as a possible myeloid cell prognostic biomarker in sepsis. *J Immunol.* (2014) 192:1091–9. doi: 10.4049/jimmunol.1302252

32. Gray CC, Biron-Girard B, Wakeley ME, Chung CS, Chen Y, Quiles-Ramirez Y, et al. Negative immune checkpoint protein, VISTA, regulates the CD4+ treg population during sepsis progression to promote acute sepsis recovery and survival. *Front Immunol.* (2022) 13:861670. doi: 10.3389/fimmu.2022.861670

33. 10x Genomics. *Cell Ranger ARC 2.0.1*. (2022).

34. 10x Genomics. Loupe Browser 6.0.0. (2022).

35. Angelidis I, Simon LM, Fernandez IE, Strunz M, Mayr CH, Greiffo FR, et al. An atlas of the aging lung mapped by single cell transcriptomics and deep tissue proteomics. *Nat Commun.* (2019) 10:963. doi: 10.1038/s41467-019-08831-9

36. Zhang L, Gao S, White Z, Dai Y, Malik AB, Rehman J. Single-cell transcriptomic profiling of lung endothelial cells identifies dynamic inflammatory and regenerative subpopulations. *JCI Insight.* (2022) 7:e158079. doi: 10.1172/jci.insight.158079

37. Hsu KS, Goodale BC, Ely KH, Hampton TH, Stanton BA, Enelow RI. Single-cell RNA-seq analysis reveals that prenatal arsenic exposure results in long-term, adverse effects on immune gene expression in response to influenza A infection. *Toxicol Sci.* (2020) 176:312–28. doi: 10.1093/toxsci/kfaa080

38. Wu C, Orozco C, Boyer J, Leglise M, Goodale J, Batalov S, et al. BioGPS: an extensible and customizable portal for querying and organizing gene annotation resources. *Genome Biol.* (2009) 10:R130. doi: 10.1186/gb-2009-10-11-r130

39. van der Maaten L, Hinton G. Visualizing data using t-SNE. *J Mach Learn Res.* (2008) 9:2579—-2605.

40. 10x Genomics. *Neutrophil Analysis in 10x Genomics Single Cell Gene Expression Assays. Document Number CG000444–Rev A–Technical Note*. (2021).

41. Skinner BM, Johnson EE. Nuclear morphologies: their diversity and functional relevance. *Chromosoma.* (2017) 126:195–212. doi: 10.1007/s00412-016-0614-5

42. Matthay MA, Ware LB, Zimmerman GA. The acute respiratory distress syndrome. *J Clin Invest.* (2012) 122:2731–40. doi: 10.1172/JCI60331

43. Gonzales JN, Lucas R, Verin AD. The acute respiratory distress syndrome: mechanisms and perspective therapeutic approaches. *Austin J Vasc Med.* (2015) 2:1009.

44. Larrue C, Guiraud N, Mouchel P, Dubois M, Farge T, Gotanègre M, et al. Adrenomedullin-CALCRL axis controls relapse-initiating drug tolerant acute myeloid leukemia cells. *Nat Commun.* (2021) 12:422. doi: 10.1038/s41467-020-20717-9

45. Fritz-Six K, Dunworth W, Li M, Caron K. Adrenomedullin signaling is necessary for murine lymphatic vascular development. *J Clin Invest.* (2008) 118:40–50. doi: 10.1172/JCI33302

46. Yang S, Zhou M, Chaudry IH, Wang P. Novel approach to prevent the transition from the hyperdynamic phase to the hypodynamic phase of sepsis: role of adrenomedullin and adrenomedullin binding protein-1. *Ann Surg.* (2002) 236:625–33. doi: 10.1097/00000658-200211000-00013

47. Yang S, Zhou M, Fowler DE, Wang P. Mechanisms of the beneficial effect of adrenomedullin and adrenomedullin-binding protein-1 in sepsis: down-regulation of proinflammatory cytokines. *Criti Care Med.* (2002) 30:2729–35. doi: 10.1097/00003246-200212000-00018

48. Lee S. Peptide ligand interaction with maltose-binding protein tagged to the calcitonin gene-related peptide receptor: The inhibitory role of receptor N-glycosylation. *Peptides.* (2022) 150:170735. doi: 10.1016/j.peptides.2022.170735

49. Hirata Y, Mitaka C, Sato K, Nagura T, Tsunoda Y, Amaha K, et al. Increased circulating adrenomedullin, a novel vasodilatory peptide, in sepsis. *J Clin Endocrinol Metab.* (1996) 81:1449–53. doi: 10.1210/jcem.81.4.8636349

50. Geven C, Kox M, Pickkers P. Adrenomedullin and adrenomedullin-targeted therapy as treatment strategies relevant for sepsis. *Front Immunol.* (2018) 9:292. doi: 10.3389/fimmu.2018.00292

51. Menon R, Shrestha A, Reynolds C, Barrios R, Caron K, Shivanna B. Adrenomedullin is necessary to resolve hyperoxia-induced experimental bronchopulmonary dysplasia and pulmonary hypertension in mice. *Am J Pathol.* (2020) 190:711–22. doi: 10.1016/j.ajpath.2019.11.011

52. Monaghan SF, Thakkar RK, Heffernan DS, Huang X, Chung CS, Lomas-Neira J, et al. Mechanisms of indirect acute lung injury: a novel role for the coinhibitory receptor, programmed death-1. *Ann Surg.* (2012) 255:158–64. doi: 10.1097/SLA.0b013e31823433ca

53. Lomas-Neira J, Monaghan SF, Huang X, Fallon EA, Chung CS, Ayala A. Novel role for PD-1:PD-L1 as mediator of pulmonary vascular endothelial cell functions in pathogenesis of indirect ARDS in mice. *Front Immunol.* (2018) 9:3030. doi: 10.3389/fimmu.2018.03030

54. Wichmann MW, Ayala A, Chaudry IH. Male sex steroids are responsible for depressing macrophage immune function after trauma-hemorrhage. *Am J Physiol.* (1997) 273:C1335–40. doi: 10.1152/ajpcell.1997.273.4.C1335

55. Zellweger R, Wichmann MW, Ayala A, Stein S, DeMaso CM, Chaudry IH. Females in proestrus state maintain splenic immune functions and tolerate sepsis better than males. *Crit Care Med.* (1997) 25:106–10. doi: 10.1097/00003246-199701000-00021

56. Osorio D, Cai JJ. Systematic determination of the mitochondrial proportion in human and mice tissues for single-cell RNA-sequencing data quality control. *Bioinformatics.* (2021) 37:963–7. doi: 10.1093/bioinformatics/btaa751

57. Adobe Inc. *Adobe Illustrator*. Mountain View, CA: Adobe Inc (2021).

frontiers | Frontiers in Medicine

TYPE Original Research
PUBLISHED 05 May 2023
DOI 10.3389/fmed.2023.1172529

OPEN ACCESS

EDITED BY
Daniel O'Toole,
University of Galway, Ireland

REVIEWED BY
Jianfeng Wu,
The First Affiliated Hospital of Sun Yat-sen University, China
Natalia Garcia-Giralt,
Carlos III Health Institute (ISCIII), Spain

*CORRESPONDENCE
Fen Liu
✉ liufen9934@163.com

RECEIVED 23 February 2023
ACCEPTED 13 April 2023
PUBLISHED 05 May 2023

CITATION
Hu P, Lu Yh, Deng W, Li Q, Zhao N, Shao Q, Wu L, Wang Xz, Qian Kj and Liu F (2023) The critical role of pancreatic stone protein/regenerating protein in sepsis-related multiorgan failure.
Front. Med. 10:1172529.
doi: 10.3389/fmed.2023.1172529

The critical role of pancreatic stone protein/regenerating protein in sepsis-related multiorgan failure

Ping Hu[1,2], Yuan hua Lu[1], Wei Deng[1,2], Qi Li[1], Ning Zhao[1], Qiang Shao[1], Ling Wu[1], Xu zhen Wang[1,2], Ke jian Qian[1] and Fen Liu[1,2]*

[1]Department of Critical Care Medicine, The First Affiliated Hospital of Nanchang University, Nanchang, Jiangxi, China, [2]Medical Innovation Center, The First Affiliated Hospital of Nanchang University, Nanchang, Jiangxi, China

Introduction: Multiple organ dysfunction syndrome (MODS) is common in patients with sepsistic admitted to an intensive care unit (ICU) and greatly increases mortality. Pancreatic stone protein/regenerating protein (PSP/Reg) is a type of C-type lectin protein that is overexpressed during sepsis. This study aimed to evaluate the potential involvement of PSP/Reg in MODS development in patients with sepsis.

Materials and methods: The relationship between circulating PSP/Reg levels, patient prognosis, and progression to MODS was analyzed in patients with sepsis admitted to the ICU of a general tertiary hospital. Furthermore, to examine the potential involvement of PSP/Reg in sepsis-induced MODS, a septic mouse model was established per the cecal ligation and puncture procedure, randomized into three groups, and subjected to a caudal vein injection of recombinant PSP/Reg at two different doses and phosphate-buffered saline. Survival analyses and disease severity scoring were performed to evaluate the survival status of the mice; enzyme-linked immunosorbent assays were performed to detect the levels of inflammatory factors and organ-damage markers in murine peripheral blood; terminal deoxynucleotidyl transferase dUTP nick end labeling (TUNEL) staining was performed to measure apoptosis levels in lung, heart, liver, and kidney tissue sections and to visualize the degree of organ damage in the mouse model; myeloperoxidase activity assay, immunofluorescence staining, and flow cytometry were performed to detect neutrophil infiltration levels in vital murine organs and the activation indexes of neutrophils.

Results and discussion: Our findings indicated that Circulating PSP/Reg levels were correlated with patient prognosis and sequential organ failure assessment scores. Furthermore, PSP/Reg administration increased disease severity scores, shortened survival time, increased the TUNEL-positive staining rate, and increased the levels of inflammatory factors, organ-damage markers, and neutrophil infiltration in the organs. Neutrophils can be activated by PSP/Reg to an inflammatory state, both *in vivo* and *in vitro*, which is characterized by the increased levels of intercellular adhesion molecule 1 and CD29.

Conclusion: Patient prognosis and progression to MODS can be visualized by monitoring PSP/Reg levels upon ICU admission. Additionally, PSP/Reg administration in animal models exacerbates the inflammatory response and severity of multiorgan damage, which may be accomplished by promoting the inflammatory state of neutrophils.

KEYWORDS

sepsis, neutrophils, infiltration, pancreatic stone protein, multiple organ dysfunction syndrome

1. Introduction

Sepsis was initially considered a systemic inflammatory response syndrome mediated by the release of massive amounts of inflammatory mediators; however, subsequent clinical trials targeting inflammatory suppression failed to reduce the mortality associated with sepsis (1–3). This failure has prompted a re-evaluation of the underlying mechanisms of sepsis and led to a growing appreciation of the complex interplay between host defense mechanisms, immune activation, and tissue injury that contributes to the development of sepsis and multiple organ dysfunction syndrome (MODS). The Third International Consensus Definitions for Sepsis and Septic Shock (Sepsis-3), published in 2016, defines sepsis as a life-threatening organ dysfunction induced by a dysregulated host response to infections, reaffirming the significance of the development of organ dysfunction (4) because the severity of organ dysfunction and the number of failed organs are closely correlated with the survival probability of patients. It has been estimated that 15% of patients admitted to an intensive care unit (ICU) experience MODS, which, depending on the number of dysfunctional organs, is associated with a mortality rate as high as 30–100% (5). However, the mechanism by which of sepsis triggers organ dysfunction is not fully understood, making MODS the leading cause of morbidity and mortality in patients admitted to the ICU (5).

2. Materials and methods

2.1. Study design and patients

In the current prospective study, adult patients with sepsis admitted to the ICU of the First Affiliated Hospital of Nanchang University from September 2021 to October 2022 were included, and some patients with potential bias were excluded (Supplementary Figure S1). Clinical data and blood samples were collected upon admission. The blood samples were centrifuged at 4°C (1,000 × *g*, 15 min) within 30 min of the collection to get the serum, which was then stored at −80°C for subsequent analysis. The study endpoints were mortality 28 days after admission and progression to MODS 48–72 h after admission. MODS was identified when the Sequential Organ Failure Assessment (SOFA) score was ≥5 points.

This study was approved by the Ethics Committee of the First Affiliated Hospital of Nanchang University (approval number: NC-2022-1-004), and each patient signed an informed consent form prior to participation.

2.2. Mice and septic model

C57BL/6 male mice aged 8–10 weeks and weighing 20–24 g were purchased from Vital River Lab Rotary (Zhejiang, China) and housed under specific pathogen-free conditions. All the experiments were performed in accordance with the regulations of the Experimental Animal Welfare and Ethics Committee of the First Affiliated Hospital of Nanchang University. Prior to the experiment, the mice were acclimated to a controlled indoor environment for over 1 week without food or water restrictions, followed by cecal ligation and puncture (CLP) for sepsis induction (6). The specific steps are briefly described below. After pentobarbital anesthesia, a midline incision of 1–2 cm was made under sterile conditions to expose the cecum, followed by the ligation of the cecal ileocecal valve using 6–0 nonabsorbable sutures between the third and fourth caudal vessels of the cecum. Subsequently, the cecum was punctured with an 18G needle to gently squeeze a small amount of intestinal content into the murine abdominal cavity, which was then closed with sutures after the intestine was incorporated. Postoperatively, the mice were placed on a heating pad, injected with 1 mL saline, and observed until the emergence of anesthesia.

Twenty-four hours after CLP, the health status of the mice was evaluated in a blinded manner based on the murine sepsis score (7). The scoring system comprises seven elements: appearance, level of consciousness, activity, response to stimuli, eyes, respiration rate, and respiration quality.

2.3. Animal treatments

Following CLP, the mice were randomized into phosphate-buffered saline (PBS) (control), PSP-40, and PSP-400 groups ($n = 5$ per group). Recombinant pancreatic stone protein/regenerating protein (PSP/Reg) (Sino Biological) was dissolved in PBS of 100 μL, and the solution was injected into the caudal vein 30 min after CLP at 40 and 400 ng/kg. Mice injected with low-dose PSP/Reg corresponded to patients with systemic infections, whereas high-dose PSP/Reg was the median amount in patients with sepsis (8). Control mice were administered PBS of the same volume, and all mice were euthanized 24 h post-treatment, and plasma, lung, liver, heart, and kidney samples were collected. A portion of the samples was utilized for immediate tissue myeloperoxidase (MPO) activity testing, whereas the remaining portion was promptly frozen and stored at −80°C for subsequent analysis.

2.4. Survival study

To evaluate the effect of PSP/Reg in a septic mouse model, 26 mice were randomized into three groups 30 min after CLP and injected with PSP/Reg (40 ng/kg) ($n = 10$), PSP/Reg (400 ng/kg) ($n = 10$), or an equivalent volume of PBS ($n = 6$) in the caudal vein. Over the subsequent 7 days, the survival rate was assessed every 2 h.

2.5. Measurement of PSP/Reg, cytokines, and organ-damage markers

The concentration of PSP/Reg in the serum samples was determined using a commercially available Human REG1α ELISA Kit (Wuhan Fine Biotech) according to the manufacturer's protocol. The laboratory technicians who performed the assays were blinded to the clinical information. The levels of cytokines (tumor necrosis factor-α, interleukin [IL]-6, and IL-1β) and organ-damage markers (lactate dehydrogenase, creatinine, and troponin I) were quantified using ELISA assay kits from R&D Systems and BD Life Science, respectively, following the manufacturer's instructions.

2.6. Immunofluorescence staining and terminal deoxynucleotidyl transferase dUTP nick end labeling (TUNEL)

Tissue samples were fixed in 4% paraformaldehyde, embedded into the optimal-cutting-temperature compound, and cut into 5-μm sections. The sections were then incubated in a blocking solution (PBS containing 10% goat serum and 1% bovine serum albumin) for 30 min, followed by overnight co-incubation at 4°C with the anti-LY6G antibody (Abcam). After washing, the sections were incubated with the fluorescein isothiocyanate-conjugated secondary antibody (Proteintech) for 2 h, and the cell nuclei were labeled with 4′,6-diamidino-2-phenylindole (Bioss).

The TUNEL assay was performed using One-Step TUNEL Apoptosis Assay Kit (Beyotime Biotechnology) following the manufacturer's instructions. Tissue sections were fixed in 4% paraformaldehyde, permeabilized with 0.1% Triton X-100 for 10 min, and incubated with the TUNEL reaction mixture for 1 h at 37°C in the dark. Cell nuclei were visualized with 4′,6-diamidino-2-phenylindole. Images were captured using an Olympus IX71 microscope and quantified using the ImageJ software.

2.7. MPO activity assay

MPO activity in murine lungs, hearts, livers, and kidneys was evaluated by performing a tissue MPO activity assay (Elabscience Biotechnology Co. Ltd.) according to the manufacturer's instructions. MPO activity was expressed as the optical density at 460 nm per mg of protein.

2.8. Determination of wet/dry ratio in lung tissue

Fresh lung tissue was placed on sterile gauze and weighed to obtain the wet weight. The tissue was then placed in an oven at 60°C for 72 h to obtain the dry weight, which was measured three times. The wet/dry ratio was calculated as the ratio of the wet weight to the dry weight.

2.9. Neutrophil isolation and culture

A mouse bone marrow neutrophil isolation kit (Solarbio) was used to isolate neutrophils from the mouse bone marrow. The specific steps are as follows. The mouse thigh bone was first rinsed with 75% ethanol and PBS and then with the 10% fetal bovine serum-supplemented Roswell Park Memorial Institute 1,640 medium after both ends of the thigh bone were sheared to obtain bone cells. Next, density gradient centrifugation was performed according to the manufacturer's instructions after erythrocyte lysis to obtain neutrophils, the morphology of which was observed by performing Wright-Giemsa staining. Flow cytometry (FCM) analysis revealed that the purity of the neutrophils was >90%. Subsequently, the isolated neutrophils were cultured in the complete Roswell Park Memorial Institute medium (10% PBS, 1% penicillin/streptomycin, 1% glutamine), and equivalent amounts of 40 ng/mL or 400 ng/ml PSP/Reg or PBS for 24 h of stimulation. The next day the Neutrophils were collected for further analysis.

2.10. FCM

Phycoerythrin-conjugated anti-intercellular adhesion molecule 1 (ICAM-1) (BD Biosciences) and fluorescein isothiocyanate-conjugated anti-CD29 antibodies (BD Biosciences) were used to detect the levels of surface antigens on neutrophils. After co-incubation at room temperature for 30 min, the cells were washed thrice with PBS containing 2% bovine serum albumin. FCM analysis was performed using an LSRFortessa cell analyzer (BD Biosciences), and the samples were analyzed using the FlowJo software.

2.11. Statistical analysis

Continuous variables in the clinical data were non-parametrically distributed and are, therefore, represented as the median (interquartile range [IQR]) or number (percentage). The Mann–Whitney U test was performed to compare differences in the median values of continuous clinical variables between the two groups, and the Kruskal–Wallis test was performed to compare PSP/Reg levels among the groups according to the SOFA score. The Spearman rank correlation test was performed to analyze the correlation between circulating PSP/Reg levels and organ support therapy using human data. Logistic regression and receiver operating characteristic (ROC) analyses were performed to assess whether circulating PSP/Reg was a predictive factor for MODS development (48–72 h after ICU admission) and 28-day mortality. Continuous variables in the *in vitro* and *in vivo* experiments were normally distributed and are described as the mean ± standard error of the mean. Statistical significance was assessed using Student's *t*-test or one- or two-way analysis of variance, as appropriate, to identify any differences within the groups. Kaplan–Meier survival curves were used to compare survival times, and the log-rank test was performed to compare differences between the groups.

3. Results

3.1. Increased circulating PSP/Reg levels in patients with sepsis admitted to the ICU were associated with MODS

To determine the clinical relevance of circulating PSP/Reg levels, 141 adult patients with sepsis who were admitted to the ICU were prospectively recruited. The patients' clinical characteristics are

TABLE 1 Baseline characteristics of patients included in the study.

Characteristic	Total (*n*=141)	Survivors (*n*=102)	Non-survivors (*n*=39)	*p*-values
Age (years)	61 (50–72)	60 (49–71)	63 (51–74)	0.80
Male, *n* (%)	91 (64)	69 (68)	22 (57)	0.21
ICU stay (days)	11 (9–14)	9 (7–11)	12 (10–14)	0.001
Site of infection, *n* (%)				
Abdomen	35 (25)	25 (25)	10 (26)	0.88
Respiratory tract	89 (63)	67 (66)	22 (56)	0.307
Urinary tract	2 (2)	2 (2)	None	–
Skin/Soft tissue	5 (4)	3 (3)	2 (5)	0.53
Others	10 (7)	5 (5)	5 (13)	0.1
Community/Hospital infections, *n* (%)	72 (51)	65 (64)	7 (18)	<0.001
Pathogen, *n* (%)				
Gram-positive	50 (35)	39 (38)	11 (28)	0.26
Gram-negative	78 (55)	56 (55)	22 (56)	0.872
Both	7 (5)	3 (3)	4 (10)	0.07
Fungi	6 (4)	4 (4)	2 (1)	0.75
Score (IQR)				
APACHE II	23 (16–33)	21 (16–31)	24 (19–36)	<0.001
SOFA (day 1)	6 (3–10)	4 (3–8)	7 (4–10)	<0.001
Organ failure, *n* (%)	87 (62)	57 (56)	30 (77)	0.028
Renal replacement therapy, *n* (%)	12 (9)	6 (6)	6 (15)	0.07
Vasopressors, *n* (%)	85 (60)	66 (65)	19 (49)	0.08
Mechanical ventilation, *n* (%)	93 (66)	71 (69)	22 (56)	0.139
AKI within 7 days, *n* (%)	43 (30)	28 (27)	15 (38)	0.204

presented in Table 1. Among the included patients, 102 (72%) survived (survival group) and 39 (28%) died (death group), with males outnumbering females in each subgroup. A total of 72 cases (51%) presented with community-acquired infections, whereas 69 (49%) with hospital-acquired infections. Most patients (55%) had Gram-negative infections, and the most common site of infection was the lungs (63%). The average length of ICU stay was 11 days (9–14 days).

Overall, the data revealed that the circulating PSP/Reg levels in patients with septic shock improved significantly compared with those in patients with severe sepsis (median, 347.1 ng/mL; [IQR, 179.1–665.2 ng/mL] vs. 82 ng/mL [IQR, 62–297.7 ng/mL]; $p < 0.001$) (Figure 1A). In addition, initial PSP/Reg levels correlated with initial SOFA scores ($p < 0.001$) (Figure 1B).

The Spearman rank correlation test showed a strong correlation between circulating PSP/Reg levels and dependence on organ support therapies among patients with a high demand for vasopressors at admission ($r = 0.496$; $p < 0.001$) and those who needed the long-term administration of vasopressors ($r = 0.545$; $p < 0.001$), mechanical ventilation ($r = 0.607$; $p < 0.01$), or renal replacement therapy ($r = 0.360$; $p = 0.015$).

Patients with MODS (SOFA scores ≥5) exhibited higher circulating PSP/Reg levels compared with patients without MODS (median, 427.2 ng/mL [IQR, 268–951.2 ng/mL] vs. 213.8 ng/mL [IQR, 136.8–536.4 ng/mL]; $p = 0.001$) (Figure 1C). Similarly, patients who died within 28 days of ICU stay exhibited higher circulating PSP/Reg levels than did surviving patients (median, 427.2 ng/mL [IQR, 289–842.1 ng/mL] vs. 208.1 ng/mL [IQR, 135.3–516.2 ng/mL]; $p < 0.001$) (Figure 1D).

Performing the Kaplan–Meier analysis of PSP/Reg values stratified by quartiles revealed that PSP/Reg plasma levels at admission exhibited a strong correlation with the 28-day mortality rate. Furthermore, the survival rate of patients with PSP/Reg levels exceeding the third quartile (246.73 ng/mL) sharply declined during the second week of sepsis (Figure 1E). These findings indicated that the circulating PSP/Reg levels reflected disease severity and that the presence of PSP/Reg might lead to MODS and mortality, especially at high levels.

After adjusting for age and sex, the log regression model showed that the circulating PSP/Reg level was an independent risk factor for progression to MODS 48–72 h after admission and 28-day mortality (odds ratio: 1.012 [1.003, 1.020], $p = 0.005$; odds ratio: 1.006 [1.002, 1.010], $p < 0.001$). The ROC analysis also revealed that it was a predictor of progression to MODS (area under the ROC curve, 0.714; $p = 0.001$) (Figure 1F) and 28-day mortality (area under the ROC curve, 0.734; $p < 0.001$) (Figure 1G).Furthermore, sub-analysis of severe sepsis and septic shock revealed that the predictive value of PSP/Reg level was confirmed (Supplementary Tables S1 and S2).

3.2. PSP/Reg aggravated severity scores and shortened survival in septic mice

To investigate the role of PSP/Reg in inflammation in early-stage sepsis, mice were treated with two doses of PSP/Reg 30 min after successful modeling. It was revealed that 24 h after CLP,the disease severity scores of PSP-40 mice were evidently higher compared with

10.3389/fmed.2023.1172529

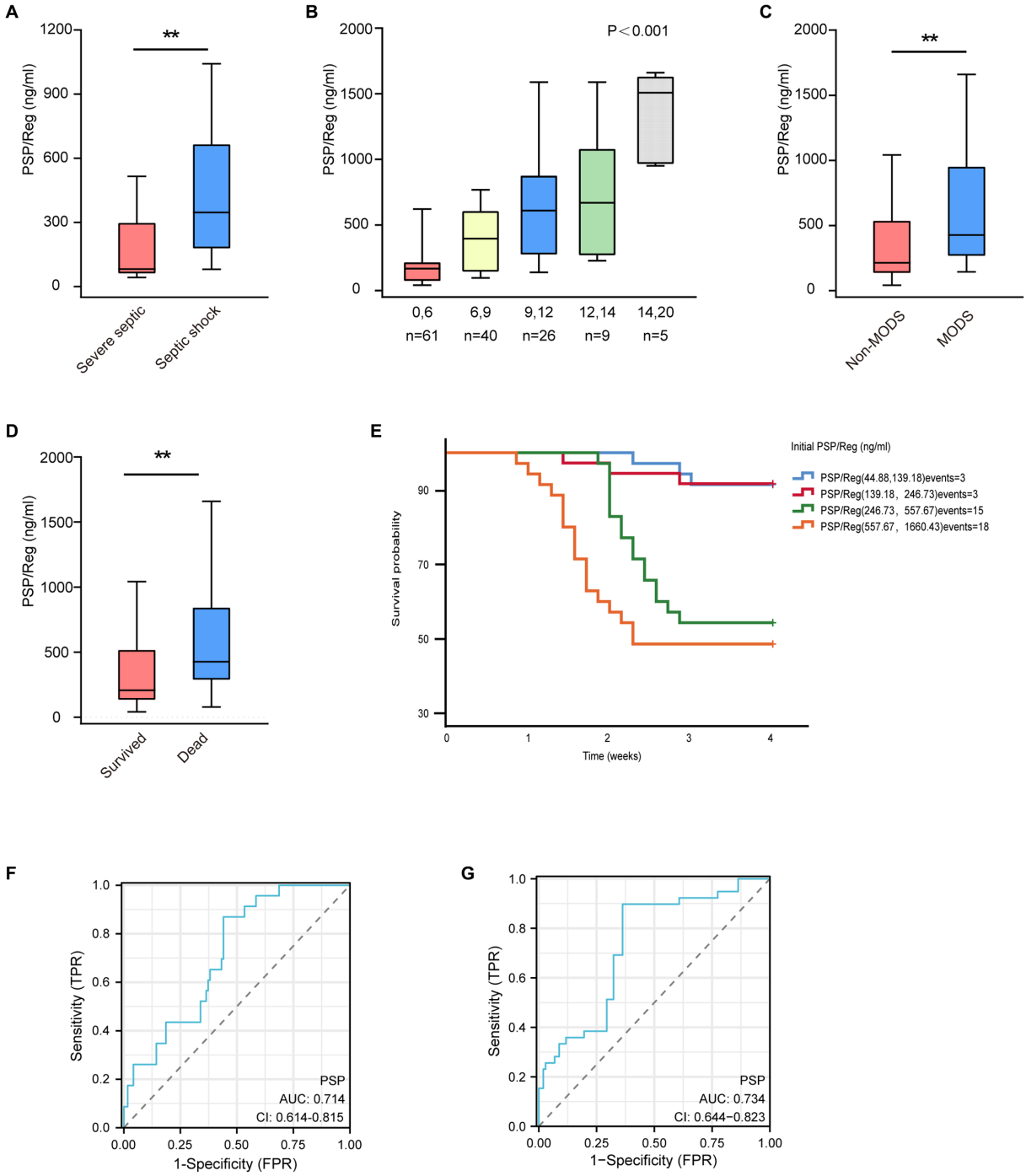

FIGURE 1
Correlation between circulating Pancreatic stone protein/regenerating protein (PSP/Reg) levels and prognosis as well as progression to multiple organ dysfunction syndrome (MODS) in patients with sepsis admitted to an intensive care unit. **(A)** Circulating PSP/Reg levels were compared according to disease severity in patients. Mann–Whitney *U* test showed a significant increase in PSP/Reg levels in patients with septic shock compared with an increase in those with severe sepsis ($p<0.001$). **(B)** PSP/Reg levels were evaluated in patients stratified by Sequential Organ Failure Assessment (SOFA) scores, and Kruskal–Wallis test showed a significant increase in PSP/Reg levels (median and interquartile range) with increasing SOFA scores ($p<0.001$). Mann–Whitney U test indicated significant differences in PSP/Reg levels between patients with and without MODS **(C)** and between survivors and non-survivors of sepsis. **(D)** *$p<0.05$, **$p<0.01$. **(E)** According to the quartile division of PSP/Reg at admission, the Kaplan–Meier survival curve for 28days is shown. The receiver operating characteristic curve analysis of PSP/Reg for the prediction of MODS **(F)** and 28d mortality **(G)**.

those of PBS mice but were visibly lower compared with those of PSP-400 mice ($p<0.01$), suggesting that PSP/Reg increased the disease severity score of the mice in a dose-depended manner (Figure 2A). Survival analyses were performed to further verify the long-term effect of PSP/Reg on animal models, which showed that the median survival time was significantly shorter in PSP-40 mice compared with that in PBS mice (48 h 95% confidence interval [CI]: 41.86–50.13 vs. 52 h 95% CI: 37.59–66.4, $p<0.01$), and PSP-400 mice showed the shortest median survival time (48 h 95% CI: 41.86–50.13 vs. 38 h 95% CI: 33.86–42.13, $p<0.001$) (Figure 2B).

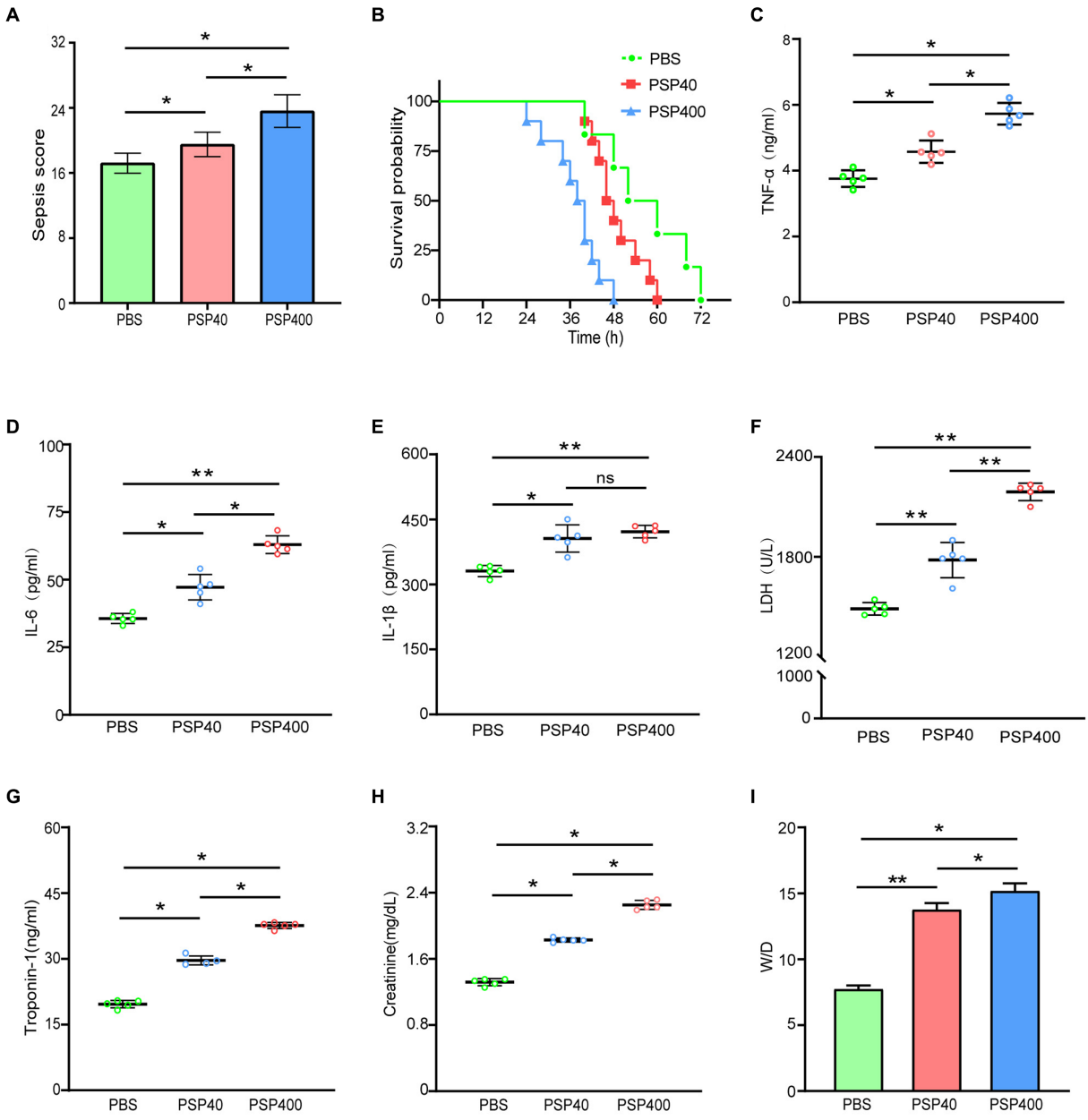

FIGURE 2
Pancreatic stone protein/regenerating protein (PSP/Reg) exacerbates multiple organ failure in a cecal ligation and puncture (CLP) mouse model. Mice were randomly selected to undergo CLP surgery and were intravenously administered with phosphate-buffered saline (PBS), PSP/Reg (40ng/kg), or PSP/Reg (400ng/kg) 30min later. **(A)** Murine sepsis score at 24h after CLP was significantly increased by PSP/Reg treatment by one-way analysis of variance (ANOVA). **(B)** Survival curves and log-rank test showed that compared with PBS, PSP/Reg significantly shortened the survival time of the mice. Serum levels of inflammatory cytokines and organ-damage markers were evaluated at 24h after CLP. **(C)** tumor necrosis factor-α levels (ng/mL), **(D)** interleukin (IL)-6 levels (pg/mL), **(E)** IL-1β levels (pg/mL), **(F)** lactate dehydrogenase (U/L), **(G)** troponin I (ng/mL), **(H)** creatinine (mg/dL), and **(I)** lung wet/dry (W/D) ratio were measured. Data are expressed as the mean±standard error of the mean and analyzed by one-way ANOVA. *p<0.01, **p<0.001, compared with the PBS group.

3.3. PSP/Reg exacerbated systemic inflammation and multiorgan damage in mouse models

Levels of inflammatory factors reflect the level of systemic inflammation. In this study, compared with PBS mice, PSP-40 mice exhibited significantly increased levels of the inflammatory factors tumor necrosis factor-α, IL-6, and Il-1β. High-dose PSP further increased tumor necrosis factor-α and IL-6 levels but did not further exacerbate IL-1β levels (Figures 2C–E).

Key parameters reflecting multiorgan damage were also measured. It was found that the plasma levels of lactate dehydrogenase (1781 ± 105.4 U/L), troponin I (29.65 ± 1.01 ng/mL), and creatinine (1.82 ± 0.02 mg/dL) in PSP-40 mice were indicative of tissue damage in the liver, heart, and kidney, respectively, compared with those in PBS mice (1,488 ± 37.49 U/L; 19.66 ± 0.85 ng/mL; 1.31 ± 0.04 mg/dL,

respectively), and that organ damage was further exacerbated among PSP-400 mice (Figures 2F–H). Additionally, PSP/Reg administration (even at a low dose) resulted in a two-fold increase in the lung wet/dry ratio compared with PBS treatment (Figure 2I). These findings suggested that PSP/Reg aggravated organ damage in a dose-dependent manner in mouse models.

An independent analysis measuring tissue damage was performed on the TUNEL-stained lung, heart, liver, and kidney tissue sections. The lung, heart, liver, and kidney tissues collected from mice injected with PSP/Reg showed a higher TUNEL-positive staining rate than those collected from PBS-treated mice (Figures 3A–D).

3.4. PSP/Reg exacerbated neutrophil tissue infiltration and activation *in vivo*

Given the aggravating effect of PSP/Reg on multiorgan damage in the CLP model, the potential mechanism underlying the exacerbation

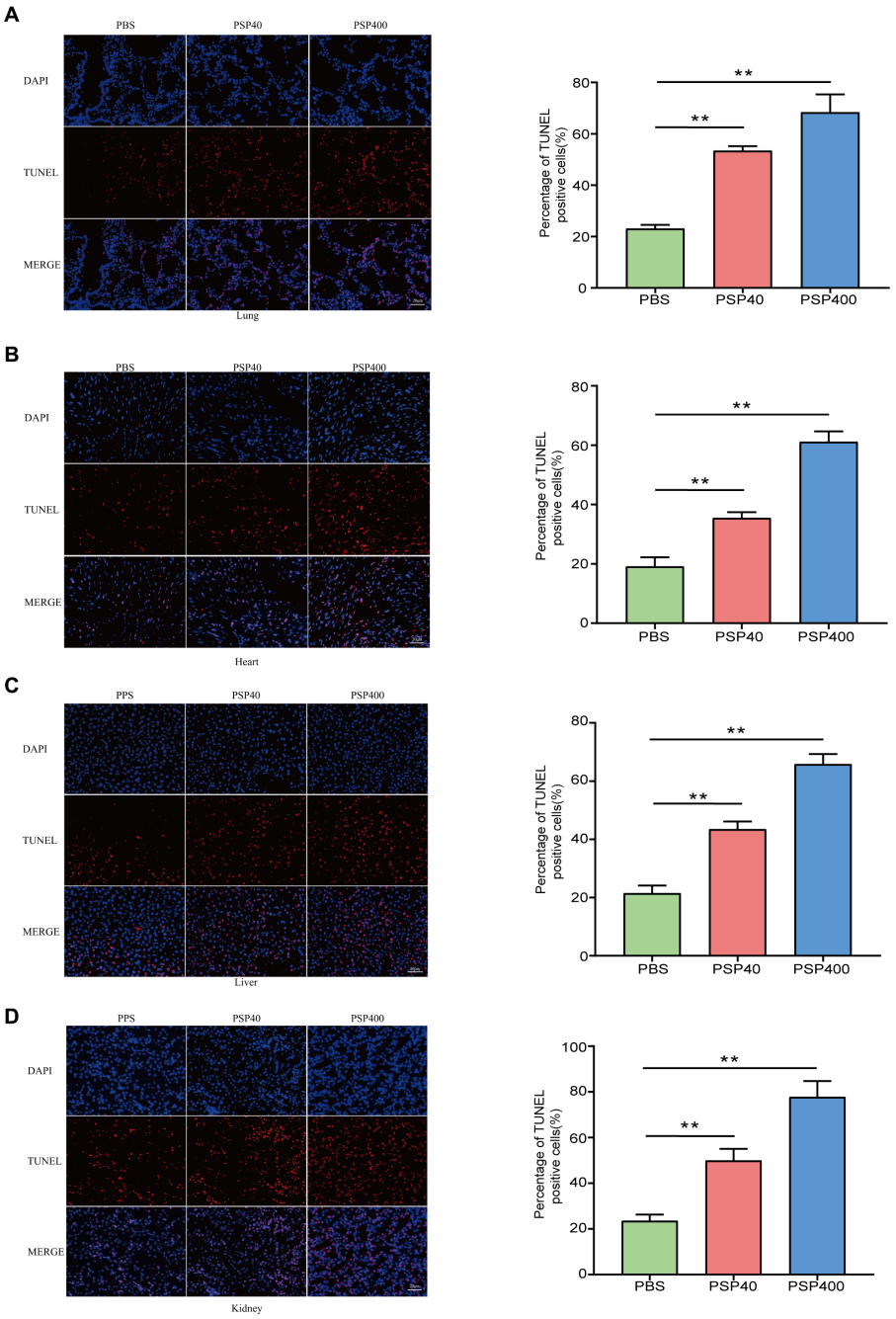

FIGURE 3
Pancreatic stone protein/regenerating protein exacerbated the level of cellular apoptosis in multiple organ tissues of cecal ligation and puncture (CLP) mice. After 24h of CLP surgery, terminal deoxynucleotidyl transferase dUTP nick end labeling (TUNEL) staining was performed to assess the level of cellular apoptosis (represented by red fluorescence) in lung **(A)**, heart **(B)**, liver **(C)**, and kidney **(D)** tissue sections and quantified using the ImageJ software with the TUNEL-positive percentage analyzed by one-way analysis of variance. *p<0.01, **p<0.001 compared with the phosphate-buffered saline group.

was further explored. Neutrophil infiltration in important organs is a crucial cause of multiple-organ dysfunction and is associated with the severity of organ damage. We performed MPO activity tests and immunofluorescence staining of tissue sections 24 h after modeling to determine the effects of PSP/Reg administration on neutrophil tissue infiltration. Then we found that MPO levels in the lungs (1.26 ± 0.06 U/g vs. 2.53 ± 0.07 U/g) and kidneys (0.88 ± 0.02 U/g vs. 1.8 ± 0.16 U/g) increased by over two-fold in PSP-40 mice compared with those in PBS mice, and a similar trend was also observed in the heart (0.81 ± 0.05 U/g vs. 1.22 ± 0.07 U/g) and liver (1.21 ± 0.09 U/g vs. 1.84 ± 0.42 U/g) (Figures 4A–D). Similarly, compared with PSP-40 mice, PSP-400 mice showed increased MPO levels in all four organs ($p < 0.01$). After immunofluorescence staining, neutrophil tissue infiltration was observed in the lungs, kidneys, hearts, and livers of PBS mice, whereas PSP/Reg administration markedly increased PMN tissue infiltration, which was more pronounced in mice injected with a higher dose of PSP/Reg (Figures 4E–H). These findings suggested that PSP/Reg administration enhanced neutrophil infiltration in important organs.

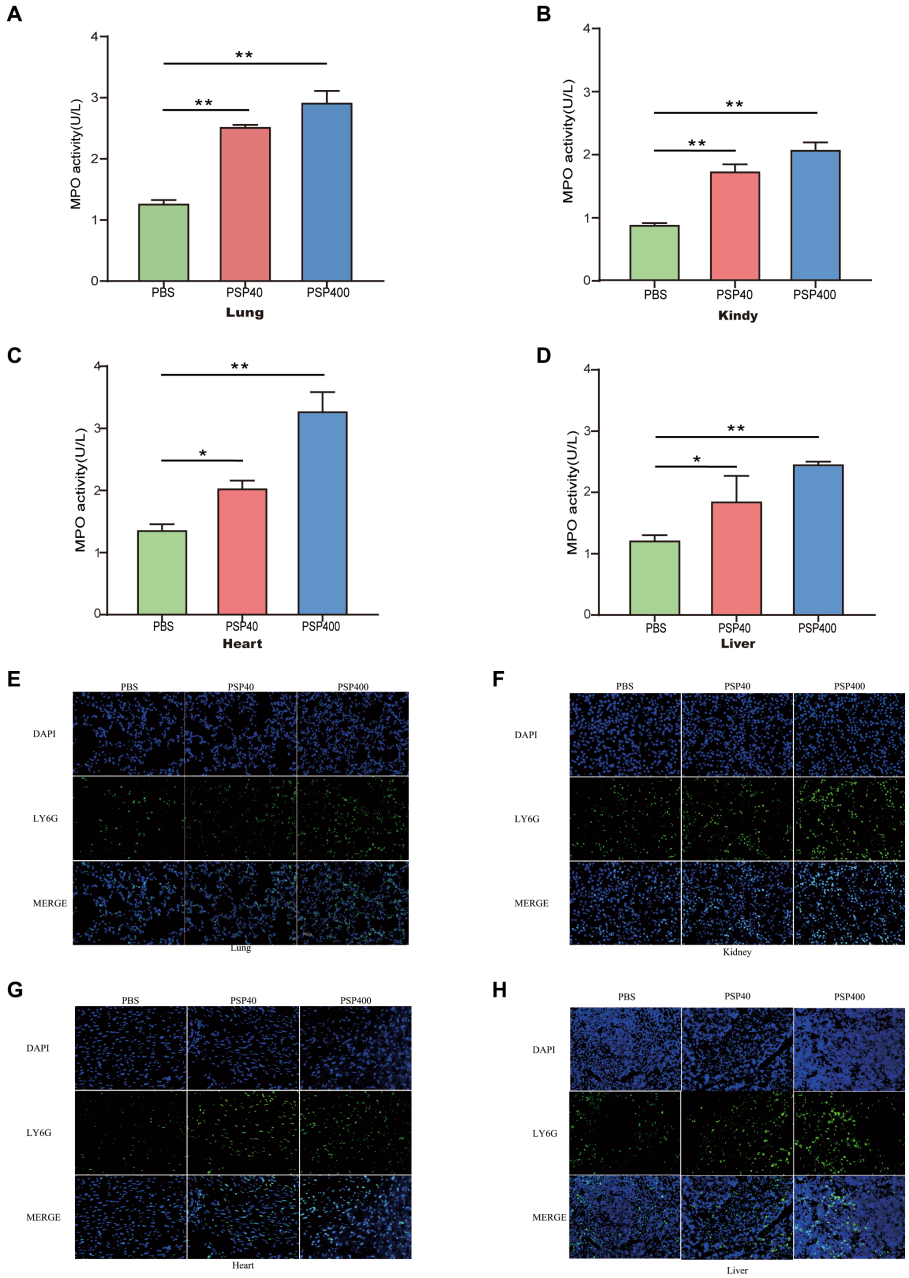

FIGURE 4
Pancreatic stone protein/regenerating protein (PSP/Reg) increased neutrophil infiltration in multiple organs of cecal ligation and puncture (CLP) mice. The level of myeloperoxidase (MPO) activity and neutrophil (Ly6G+) infiltration in multiple organ tissues were measured 24h after CLP in mice treated with PSP/Reg. **(A)**: lung tissue MPO activity, **(B)**: kidney tissue MPO activity, **(C)**: heart tissue MPO activity, and **(D)**: liver tissue MPO activity. The data were analyzed by one-way analysis of variance. *p<0.01, **p<0.001 compared with the PBS group. Representative images of Ly6G+ (green fluorescence) areas in lung **(E)**, kidney **(F)**, heart **(G)**, and liver **(H)** tissues. Scale bar, 20mm.

3.5. PSP/Reg promoted PMN activation induced By CLP *in vivo* and *in vitro*

The effect of PSP/Reg administration on the PMN status of experimental mice was analyzed by isolating neutrophils from the bone marrow of CLP-treated mice. FCM showed that PSP/Reg-injected mice showed significantly increased levels of ICAM-1 and CD29 (integrin 1β) (Figures 5A,B). To further validate the activating effect of PSP/Reg on neutrophils, they were isolated from the bone marrow of wild-type mice, cultured *in vitro*, and injected with equivalent amounts of PSP/Reg (40 or 400 ng/mL) or PBS. PSP/Reg stimulation resulted in increased levels of ICAM-1 and CD29 (Figures 5C,D), consistent with the *in vivo* findings. These results indicated that PSP/Reg administration put neutrophils in a proinflammatory state, exacerbated sepsis-induced high PMN tissue infiltration, and led to aggravated multiorgan damage.

4. Discussion

MODS is a devastating complication in critically ill patients that frequently leads to increased morbidity and mortality in the ICU. Despite the severe effect of MODS on patient outcomes, factors that drive its development into sepsis remain poorly understood. Further in-depth investigations are warranted to gain a better understanding of the mechanisms underlying this condition. Therefore, we designed a prospective clinical study to explore the potential correlation between PSP/Reg and the development of sepsis-induced multiple organ dysfunction. In this study, we established a mouse model of CLP-induced sepsis to investigate the possible involvement of PSP/Reg in the progression of sepsis-induced multiple organ dysfunction via neutrophil activation.

Initially, PSP/Reg was named PSP because it was found to inhibit the precipitation of calcium carbonate crystals in the pancreatic juice within the pancreatic stones of patients with chronic calcific pancreatitis (9). Subsequently, Reg promoted pancreatic tissue repair and regeneration. Because Reg and PSP were later proved to be identical, both of which are encoded by a transcript of the same REG gene and are structurally similar to the C-type lectin-like protein, the protein was renamed PSP/Reg (10). Further research on PSP/Reg has revealed its increased levels in various infectious diseases, including severe infections (11), appendicitis (12), peritonitis (13), pneumonia (14), and sepsis (15). It has also been identified as a potential biomarker for infection and sepsis. Keel et al. demonstrated that (16) PSP/Reg levels increased in 83 patients with severe trauma, but no pancreatic injuries, thus serving as a favorable predictor of infection and sepsis. Moreover, it was confirmed that the onset of sepsis could be predicted earlier via increased PSP/Reg levels than via conventional inflammatory factors, such as C-reactive protein and procalcitonin (15). Similar to previous research, the present study revealed that PSP/Reg levels, which are associated with the severity of sepsis among adult patients, could be utilized to predict patient prognosis and progression to MODS. Notably, PSP/Reg has been identified as a stress protein in both animal models and clinical experiments, indicating its potential as a target for therapeutic interventions against sepsis and related conditions (16, 17). Reding et al. revealed that (18) PSP/Reg, which can respond to injuries in early-stage infections, might be an indicator of systemic stress and a type of secretory stress protein secreted by pancreatic acinar cells after pancreatic perception of distal organ injury and systemic stress. Compelling evidence was provided to confirm that PSP/Reg levels increased during early-stage infections, burns, and traumatic diseases and were visibly associated with the severity of injuries.

In sepsis, it is difficult for neutrophils to be recruited to the site of infection (19), which makes it difficult for invading pathogens to be cleared away from the body in a timely and effective manner, leading to an overactive inflammatory response in the body. In addition, owing to the excessive infiltration of neutrophils in important distal organs, activated PMNs in the organs generate and release proinflammatory cytokines, reactive oxygen species, lysosomal enzymes, neutrophil extracellular traps, and other active substances that trigger organ injury and MODS (20). Therefore, a better understanding of the mechanisms underlying sepsis-induced organ damage caused by PMN activation and recruitment is of great importance for the development of potential therapeutic strategies. In this study, PSP/Reg injection increased the levels of systemic inflammatory factors in mice receiving CLP, exacerbated the apoptosis in their vital organs, and increased levels of organ-damage markers. In the meantime, the infiltration of PMNs in their organs was also found to be enhanced. Although the effect of PSP/Reg has not yet been clarified, its structural homology has been characterized; PSP/Reg is a type of globular polypeptide that adopts the overall folds of C-type lectins (21). C-type lectin-like proteins, calcium-dependent glycan-binding proteins, are known to function as adhesion and signaling receptors in homeostasis and innate immunity and play a crucial role in inflammatory responses as well as leukocyte and platelet trafficking (22). The protein structure of PSP/Reg also supports its interaction with neutrophils. In addition, following the incubation of PSP/Reg with human whole blood, the levels of β-2-integrins (CD11b) in blood PMNs increased, whereas those of L-selectins (CD62L) decreased; PSP/Reg could also directly bind to PMNs after incubation with purified PMNs (16). Therefore, we hypothesized that sharply increased levels of PSP/Reg during sepsis might be involved in the host response to pathogens by activating PMNs, thus playing a role in the progression to MODS.

To further verify the regulatory effect of PSP/Reg on PMN tissue infiltration, we detected the surface activation indicators of bone-marrow PMNs in mice administered with PSP/Reg and discovered that PSP/Reg stimulation increased the levels of the adhesion molecules ICAM-1 and CD29 on the surface of PMNs. The activation and tissue infiltration of neutrophils are strictly regulated by adhesion molecules (23). During inflammation, the increased levels of adhesion molecules mediate the recruitment and activation of PMNs and induce tissue infiltration through the binding of their cytoplasmic domains to actin cytoskeletons (24). Furthermore, it has been reported that the increased level of ICAM-1 in neutrophils in both human and animal models of sepsis induces membrane surface rigidity and impairs cell deformability (25), leading to their decreased ability to migrate to infectious sites, resulting in microvascular and organ dysfunction. Notably, treatment with ICAM-1-specific antibodies can reduce neutrophil migration to distant organs, such as the lungs and spleen (26). The increased level of CD29, also known as integrin beta-1, on the surface of PMNs is associated with the activation and recruitment of neutrophils during inflammation (23). The present study suggested that the activation and induction of neutrophils and inhibition of anti-inflammatory factors by PSP/Reg were partially responsible for the inflammatory responses during

10.3389/fmed.2023.1172529

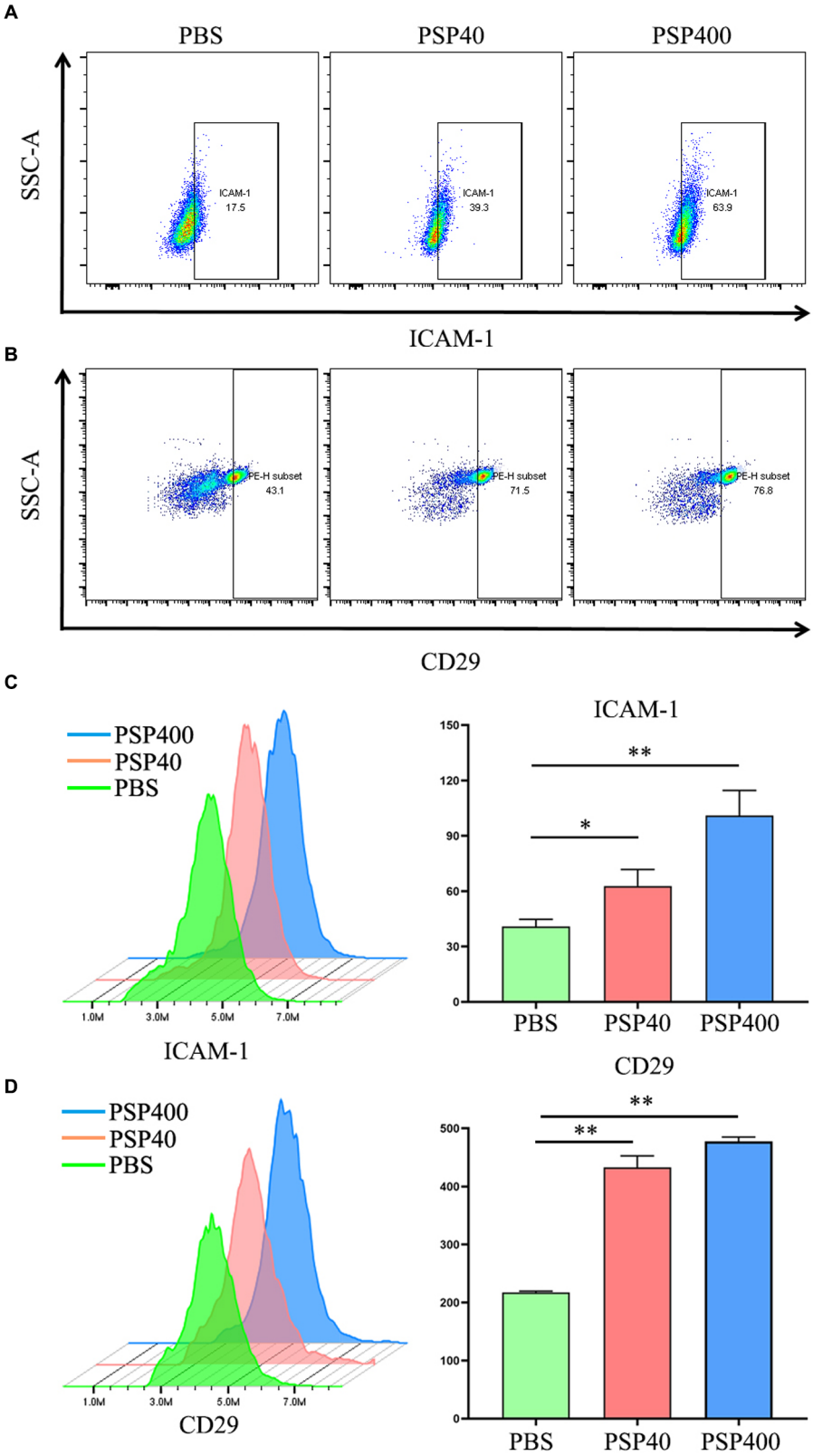

FIGURE 5
Pancreatic stone protein/regenerating protein (PSP/Reg) increased the levels of neutrophil surface adhesion molecules. Cecal ligation and puncture mice were stimulated with PSP/Reg 30min after surgery, and 24h later, flow cytometry was performed to detect the percentage of intercellular adhesion molecule 1 (ICAM-1)-positive **(A)** and CD29-positive **(B)** cells in mouse bone marrow neutrophils. Neutrophils were isolated from the mouse bone marrow and stimulated with 40ng/ml and 400ng/ml of PSP/Reg overnight. **(C)** Representative histograms and MFI quantification analysis of ICAM-1 levels in PMN under 40ng/ml stimulation. **(D)** Representative histograms and MFI quantification analysis of CD29 levels in PMN under 400ng/ml stimulation.The data were analyzed by one-way analysis of variance. *p<0.01, **p<0.001 compared with the PBS group.

early-stage sepsis and multiple organ dysfunction, which also explained the relationship between PSP/Reg levels and progression to MODS in patients with sepsis.

Among the 141 patients with sepsis admitted to the ICU in our study, those with septic shock exhibited significantly higher levels of circulating PSP/Reg. There was a strong correlation between circulating PSP/Reg levels and 7-day survivors requiring organ support, indicating that disease severity was an independent risk factor for progression to MODS 48–72 h after admission and 28-day mortality. Moreover, this study showed that the intravenous injection of PSP/Reg aggravated multiorgan damage in the CLP mouse models and shortened their survival time. At the cellular level, we confirmed that PSP/Reg induced the inflammatory activation of murine neutrophils, further supporting its role in promoting inflammation during sepsis. This indicated that PSP/Reg might facilitate the activation and infiltration of neutrophils in distal organs to intensify the CLP-induced inflammatory cascade, thereby exacerbating multiorgan damage in sepsis.

Sepsis and MODS are multifaceted conditions with highly intricate pathogeneses involving a dynamic and complex immune response that may involve both proinflammatory and anti-inflammatory mechanisms. The effect of PMNs on multiorgan damage in early and late sepsis is not yet fully understood, and further studies are needed to investigate the underlying mechanisms that regulate the immune response during these phases of sepsis. Our study has shed new light on the potential role of PSP/Reg in exacerbating sepsis-induced multiple organ dysfunction by facilitating the activation and infiltration of neutrophils; the underlying regulatory mechanisms involved in this process are likely to be highly complex and multifactorial. Thus, it is necessary to explore these mechanisms in greater detail to identify potential therapeutic targets for the prevention and treatment of sepsis and MODS.

List of abbreviations: PSP/Reg, Pancreatic stone protein/regenerating protein; MODS, multiple organ dysfunction syndrome; ICU, intensive care unit; CLP, cecal ligation and puncture; PBS, phosphate-buffered saline; TUNEL, terminal deoxynucleotidyl transferase dUTP nick end labeling; MPO, myeloperoxidase; SOFA, sequential organ failure assessment; ICAM-1, intercellular adhesion molecule 1; FCM, flow cytometry; IL, interleukin; IQR, interquartile range; ROC curve, receiver operating characteristic curve; CI, confidence interval.

Data availability statement

The original contributions presented in the study are included in the article/Supplementary material, further inquiries can be directed to the corresponding author.

Ethics statement

The studies involving human participants were reviewed and approved by the Ethics Committee of the First Affiliated Hospital of Nanchang University (approval number: NC-2022-1-004), and each patient had signed the informed consent form prior to participation. The patients/participants provided their written informed consent to participate in this study. The animal study was reviewed and approved by Experimental Animal Welfare and Ethics Committee of the First Affiliated Hospital of Nanchang University. Written informed consent was obtained from the individual(s) for the publication of any potentially identifiable images or data included in this article.

Author contributions

PH contributed to the experimentation, analysis, and manuscript preparation. FL contributed to the research concept and oversaw the study. QS and WD contributed to the performance of experiments. LW and WXZ contributed to the immunological evaluation through sample measurements. KQ contributed to the revision of the manuscript. YL contributed to the article by making important revisions and additions. QL contributed to the article by providing assistance with further subgroup analysis of the data. NZ contributed to the article by helping to guide the statistical analysis.

Conflict of interest

The authors declare that the research was conducted in the absence of any commercial or financial relationships that could be construed as a potential conflict of interest.

Publisher's note

All claims expressed in this article are solely those of the authors and do not necessarily represent those of their affiliated organizations, or those of the publisher, the editors and the reviewers. Any product that may be evaluated in this article, or claim that may be made by its manufacturer, is not guaranteed or endorsed by the publisher.

Supplementary material

The Supplementary material for this article can be found online at: https://www.frontiersin.org/articles/10.3389/fmed.2023.1172529/full#supplementary-material

References

1. Balk RA. Systemic inflammatory response syndrome (SIRS): where did it come from and is it still relevant today. *Virulence*. (2014) 5:20–6. doi: 10.4161/viru.27135

2. Marik PE, Taeb AM. SIRS, qSOFA and new sepsis definition. *J Thorac Dis*. (2017) 9:943–5. doi: 10.21037/jtd.2017.03.125

3. Marshall JC. Why have clinical trials in sepsis failed. *Trends Mol Med*. (2014) 20:195–203. doi: 10.1016/j.molmed.2014.01.007

4. Singer M, Deutschman CS, Seymour CW, Shankar-Hari M, Annane D, Bauer M, et al. The third international consensus definitions for sepsis and septic shock (Sepsis-3). *JAMA*. (2016) 315:801–10. doi: 10.1001/jama.2016.0287

5. Capuzzo M, Volta C, Tassinati T, Moreno R, Valentin A, Guidet B, et al. Hospital mortality of adults admitted to intensive care units in hospitals with and without intermediate care units: a multicentre European cohort study. *Crit Care*. (2014) 18:551. doi: 10.1186/s13054-014-0551-8

6. Rittirsch D, Huber-Lang MS, Flierl MA, Ward PA. Immunodesign of experimental sepsis by cecal ligation and puncture. *Nat Protoc*. (2009) 4:31–6. doi: 10.1038/nprot.2008.214

7. Mele TS. Scoring sepsis severity in mice. *Methods Mol Biol*. (2021) 2321:155–9. doi: 10.1007/978-1-0716-1488-4_13

8. Prazak J, Irincheeva I, Llewelyn MJ, Stolz D, García de Guadiana Romualdo L, Graf R, et al. Accuracy of pancreatic stone protein for the diagnosis of infection in hospitalized adults: a systematic review and individual patient level meta-analysis. *Crit Care*. (2021) 25:182. doi: 10.1186/s13054-021-03609-2

9. De Caro A, Lohse J, Sarles H. Characterization of a protein isolated from pancreatic calculi of men suffering from chronic calcifying pancreatitis. *Biochem Biophys Res Commun*. (1979) 87:1176–82. doi: 10.1016/S0006-291X(79)80031-5

10. Graf R, Schiesser M, Reding T, Appenzeller P, Sun LK, Fortunato F, et al. Exocrine meets endocrine: pancreatic stone protein and regenerating protein--two sides of the same coin, Exocrine meets endocrine: pancreatic stone protein and regenerating protein—two sides of the same coin. *J Surg Res*. (2006) 133:113–20. doi: 10.1016/j.jss.2005.09.030

11. Que YA, Guessous I, Dupuis-Lozeron E, Oliveira CF, Graf R, Seematter G, et al. Prognostication of mortality in critically ill patients with severe infections. *Chest*. (2015) 148:674–82. doi: 10.1378/chest.15-0123

12. Raptis DA, Eshmuminov D, Tschuor C, Limani P, Neff T. Prospective diagnostic value of pancreatic stone protein in comparison to white cell count and C-reactive protein in the diagnosis of acute appendicitis – a prospective multicenter diagnostic accuracy trial. *J Surg*. (2019) 10:1201. doi: 10.29011/2575-9760.001201

13. Gukasjan R, Raptis DA, Schulz HU, Halangk W, Graf R. Pancreatic stone protein predicts outcome in patients with peritonitis in the ICU. *Crit Care Med*. (2013) 41:1027–36. doi: 10.1097/CCM.0b013e3182771193

14. Boeck L, Graf R, Eggimann P, Pargger H, Raptis DA, Smyrnios N, et al. Pancreatic stone protein: a marker of organ failure and outcome in ventilator-associated pneumonia. *Chest*. (2011) 140:925–32. doi: 10.1378/chest.11-0018

15. Pugin J, Daix T, Pagani JL, Morri D, Giacomucci A, Dequin PF, et al. Serial measurement of pancreatic stone protein for the early detection of sepsis in intensive care unit patients: a prospective multicentric study. *Crit Care*. (2021) 25:151. doi: 10.1186/s13054-021-03576-8

16. Keel M, Härter L, Reding T, Sun LK, Hersberger M, Seifert B, et al. Pancreatic stone protein is highly increased during posttraumatic sepsis and activates neutrophil granulocytes. *Crit Care Med*. (2009) 37:1642–8. doi: 10.1097/CCM.0b013e31819da7d6

17. Graf R, Schiesser M, Lüssi A, Went P, Scheele GA, Bimmler D. Coordinate regulation of secretory stress proteins (PSP/reg, PAP I, PAP II, and PAP III) in the rat exocrine pancreas during experimental acute pancreatitis. *J Surg Res*. (2002) 105:136–44. doi: 10.1006/jsre.2002.6387

18. Reding T, Palmiere C, Pazhepurackel C, Schiesser M, Bimmler D, Schlegel A, et al. The pancreas responds to remote damage and systemic stress by secretion of the pancreatic secretory proteins PSP/regI and PAP/regIII. *Oncotarget*. (2017) 8:30162–74. doi: 10.18632/oncotarget.16282

19. Alves-Filho JC, de Freitas A, Spiller F, Souto FO, Cunha FQ. The role of neutrophils in severe sepsis. *Shock*. (2008) 30:3–9. doi: 10.1097/SHK.0b013e3181818466

20. Hoesel LM, Neff TA, Neff SB, Younger JG, Olle EW, Gao H, et al. Harmful and protective roles of neutrophils in sepsis. *Shock*. (2005) 24:40–7. doi: 10.1097/01.shk.0000170353.80318.d5

21. Jin CX, Hayakawa T, Ko SB, Ishiguro H, Kitagawa M. Pancreatic stone protein/regenerating protein family in pancreatic and gastrointestinal diseases. *Intern Med*. (2011) 50:1507–16. doi: 10.2169/internalmedicine.50.5362

22. Cummings RD, Chiffoleau E, van Kyook Y, McEver RP. Chapter 34: *C-Type Lectins*. In: A. Varki, R. D. Cummings, J. D. Esko, P. Stanley, G. W. Hart and M. Aebi, et al. editors. Essentials of Glycobiology [Internet]. 4th ed.Cod Spring Harbor Laboratory Press (2022).

23. Ley K, Laudanna C, Cybulsky MI, Nourshargh S. Getting to the site of inflammation: the leukocyte adhesion cascade updated. *Nat Rev Immunol*. (2007) 7:678–89. doi: 10.1038/nri2156

24. Bui TM, Wiesolek HL, Sumagin R. ICAM-1: a master regulator of cellular responses in inflammation, injury resolution, and tumorigenesis. *J Leukoc Biol*. (2020) 108:787–99. doi: 10.1002/JLB.2MR0220-549R

25. Wang JH, Sexton DM, Redmond HP, Watson RW, Croke DT, Bouchier-Hayes D. Intercellular adhesion molecule-1 (ICAM-1) is expressed on human neutrophils and is essential for neutrophil adherence and aggregation. *Shock*. (1997) 8:357–61. doi: 10.1097/00024382-199711000-00007

26. Yang J, Tian H, Huang X. Tephrosin attenuates sepsis induced acute lung injury in rats by impeding expression of ICAM-1 and MIP-2. *Microb Pathog*. (2018) 117:93–9. doi: 10.1016/j.micpath.2018.02.017

frontiers | Frontiers in Medicine

TYPE Original Research
PUBLISHED 02 June 2023
DOI 10.3389/fmed.2023.1162615

OPEN ACCESS

EDITED BY
Dawei Yang,
Fudan University, China

REVIEWED BY
Zhimin Tao,
Jiangsu University, China
Colin E. Evans,
Northwestern University, United States

*CORRESPONDENCE
Daniel O'Toole
✉ daniel.otoole@universityofgalway.ie

RECEIVED 09 February 2023
ACCEPTED 16 May 2023
PUBLISHED 02 June 2023

CITATION
González HE, McCarthy SD, Masterson C, Laffey JG, MacLoughlin R and O'Toole D (2023) Nebulized mesenchymal stem cell derived conditioned medium ameliorates *Escherichia coli* induced pneumonia in a rat model. *Front. Med.* 10:1162615. doi: 10.3389/fmed.2023.1162615

Nebulized mesenchymal stem cell derived conditioned medium ameliorates *Escherichia coli* induced pneumonia in a rat model

Héctor E. González[1], Sean D. McCarthy[1], Claire Masterson[1], John G. Laffey[1], Ronan MacLoughlin[2] and Daniel O'Toole[1]*

[1]REMEDI at CÚRAM Medical Devices Center and Discipline of Anesthesia, University of Galway, Galway, Ireland, [2]Aerogen Ltd., Galway, Ireland

Background: Mesenchymal stem cells (MSC) have shown immense therapeutic promise in a range of inflammatory diseases, including acute respiratory distress syndrome (ARDS), and are rapidly advancing through clinical trials. Among their multimodal mechanisms of action, MSCs exert strong immunomodulatory effects via their secretome, which contains cytokines, small molecules, extracellular vesicles, and a range of other factors. Recent studies have shown that the MSC secretome can recapitulate many of the beneficial effects of the MSC itself. We aimed to determine the therapeutic capacity of the MSC secretome in a rat bacterial pneumonia model, especially when delivered directly to the lung by nebulization which is a technique more appropriate for the ventilated patient.

Methods: Conditioned medium (CM) was generated from human bone marrow derived MSCs in the absence of antibiotics and serum supplements. Post-nebulization lung penetration was estimated through nebulization of CM to a cascade impactor and simulated lung and quantification of collected total protein and IL-8 cytokine. Control and nebulized CM was added to a variety of lung cell culture models and injury resolution assessed. In a rat *E. coli* pneumonia model, CM was instilled or administered by nebulization and lung injury and inflammation assessed at 48h.

Results: MSC-CM was predicted to have good distal lung penetration and delivery when administered by nebulizer. Both control and nebulized CM reduced NF-κB activation and inflammatory cytokine production in lung cell culture, while promoting cell viability and would closure in oxidative stress and scratch wound models. In a rat bacterial pneumonia model, both instilled and nebulizer delivered CM improved lung function, increasing blood oxygenation and reducing carbon dioxide levels compared to unconditioned medium controls. A reduction in bacterial load was also observed in both treatment groups. Inflammatory cytokines were reduced significantly by both liquid and aerosol CM administration, with less IL-1β, IL-6, and CINC1 in these groups compared to controls.

Conclusion: MSC-CM is a potential therapeutic for pneumonia ARDS, and administration is compatible with vibrating mesh nebulization.

KEYWORDS

mesenchymal stem cell, pneumonia, secretome, nebulizer, aerosol—therapeutic

Introduction

Acute respiratory distress syndrome (ARDS) is a severe disease of the lung with a continuing high mortality. It is diagnosed on the basis of acute onset not attributable to background disease, infiltration of blood or tissue derived cells to the airspace and impaired blood oxygenation levels, the last of which can be used to denote severity level (1). The most problematic form of ARDS arises from infectious etiologies, commonly as a result of bacterial or viral infection, termed pneumonia (2). Here the infectious particles trigger an immune response in the lung epithelium and resident alveolar macrophages causing the production of a wide range of soluble signaling factors termed the "cytokine storm," which in turn signals to a wide a variety of tissue and immune effector cells (3). Inflammation and fluid in the airspace eventually impair gas exchange resulting in hypoxemia and possible death. Current standard of care is largely supportive, with hydration, immediate broad-spectrum antibiotics and mechanical ventilation continuing to be mainstays of therapy (4). Of particular concern is the rise in antimicrobial resistant (AMR) strains of bacteria which mean more reliance on the patient's own immune system to clear the infection, which may not be sufficient. Despite many promising preclinical tests, an effective specific therapy for ARDS remains elusive.

Mesenchymal stem/stromal cells (MSCs) have recently risen to prominence in the field of inflammation therapeutics (5). Their multimodal immunomodulatory action has led to investigations in the fields of graft versus host disease (GvHD), diabetic ulcers, critical limb ischemia, and acute kidney injury, to name but a few (6–8). They have also been widely developed for both chronic and acute lung diseases, with promising *in vitro* and preclinical results now graduating to clinical trials (9). While bone marrow is the most studied tissue source of MSCs, they have been prepared from a wide range of tissues by a multiplicity of isolation techniques. However, several issues of practicality have emerged regarding stem cell therapy, including difficulty and expense of human dose manufacture, the requirement of careful cryogenic preservation during storage and transport, and lingering concerns regarding the introduction of a foreign living cell to the patient (10, 11). To alleviate these concerns, recent studies have shown that various MSC products can recapitulate many of the beneficial activities of the MSC itself, including in lung disease model settings (12). While many groups have investigated specific secreted factors such as extracellular vesicles (EV), the total secretome or "conditioned medium" (CM) is also an attractive option for inflammatory, antibacterial and other research and is readily available as a by-product of the MSC manufacturing process.

In light of these emerging possibly superior therapeutic options, our overall hypothesis is that MSC-CM will replicate previous findings with MSC and MSC-EVs in ARDS models and prove a more abundant, more accessible and less expensive source of medicine. We have aimed to build on previous *in vitro* work to apply MSC-CM to cell and animal models of pneumonia. We have also aimed to utilize the novel administration option of vibrating mesh nebulization to the airspace, which is a technique that requires a smaller dose and is likely to produce a stronger and faster effect as it is delivered directly to the affected organ. Of relevance, delivery of MSC themselves intratracheally has previously been shown to be effective in an ARDS model (13, 14), although delivery of volumes of liquid suspensions to the lungs is not considered a viable approach in patients due to an existing dangerous accumulation of fluid. Vibrating mesh nebulization has been previously described to preserve the activity of a broad range of proteins and other soluble factors due the low shear stress applied on solutions during aerosolization, yet it is also capable of providing a mist that penetrates to the distal lung under mechanical ventilation which is the situation in ARDS (15–18).

Methods

Mesenchymal stem cell conditioned medium

Human bone marrow derived MSCs were isolated from healthy donor tissue based on plastic adherence. Briefly, after obtaining informed consent, bone marrow aspirate was sampled from the iliac crest, diluted with minimum essential media alpha (MEMα; Sigma Aldrich, Arklow, Ireland) containing 10% fetal bovine serum (FBS; Gibco, ThermoFisher Scientific, Waltham, MA, United States) and penicillin/streptomycin, and plated to tissue culture flasks (Corning Limited, Dublin, Ireland) at 10^6 cell per cm^2. After 24 h in a humidified incubator at 37°C and 5% CO_2 in air, non-adherent cells were aspirated and remaining cells washed with phosphate buffered saline (PBS). After a further 7 days of incubation with medium refresh on the third day, MSC colonies were trypsinized, counted, and cryopreserved as passage 0. MSC markers were confirmed by flow cytometry as per the minimum criteria for MSC established by Dominici et al. (data not shown) (19). Cryovials of MSCs were then seeded to tissue culture plastic and expanded to 175 cm^2 flasks at passage 3. At 80% confluence, cells were treated with either lipopolysaccharide (LPS) for nebulizer dynamics studies or vehicle for other studies. After 24 h, medium was aspirated, cells washed with PBS and flasks refed with 15 mL of MEMα with no additions, i.e., serum free medium (SFM). After 24 h of further incubation, conditioned medium (CM) was aspirated, centrifuged at 1,000 × *g* for 10 min to remove cells and cell debris. After that, CM was transferred into centrifugal concentrator units (Amicon® Ultra −15 Centrifugal filter Units) with 3 KDa MWCO limit size membrane. Tubes were places in a centrifuge (Epperndorf™ 5810R, Epperndorf, Hamburg, Germany) with swinging rotor at 4,000 × *g* at 4°C until desired final volume. In addition, concentrated CM was transferred into dialysis tubes (Tube-O DIALYZER™ mini dialysis system) with a pore size of 4 KDa MWCO. Dialyzer tubes were placed in closed buckets and exposed to PBS with a ratio of 500 mL of PBS per 100 µL of concentrated CM for 24 h at 4°C. The CM was then collected, aliquoted, and stored at −80°C.

Nebulization and collection of CM

For all experiments where control and nebulized CM were to be compared, in a tissue culture cabinet a vibrating mesh nebulizer (VMN; Aerogen Solo®; Aerogen, Galway, Ireland) was placed so that the lower part fitted into a 50 mL polypropylene tube and the contact points sealed with Parafilm. The controller box was turned on until the CM was passed through and condensed in the tube and a centrifugation (4,000 × *g*, 5 min) settled all the liquid to the bottom.

This process took c. 1 min per mL of CM and recovery was c. 95% by volume.

Nebulized conditioned medium aerosol dynamics

10 mL of LPS-induced CM (LPS-CM) was defrosted, nebulized, and collected. The nebulizer was then washed with PBS and then inverted and washed again with PBS with aerosol collected each time. 10 mL of LPS-CM was then nebulized to a cascade impactor [Next Generation Impactor (NGI); Copley Scientific Ltd., Colwick, United Kingdom] under a normal breathing ventilation regimen (15 L per minute) and each collection plate and connector washed with 10 mL of PBS and collected. Finally, 10 mL of LPS-CM was applied to a simulated lung device (ASL 5000™ Lung Solution; Laerdal, Wappingers Falls, NY, United States), again under normal breathing ventilation, and the various collection filters washed with 10 mL PBS and collected. All samples were then analyzed for total protein content by BCA assay (Pierce BCA Protein Assay Kit; Thermofisher Scientific) and a representative cytokine quantified by ELISA as per manufacturer's instructions (Human IL-8/CXCL8 DuoSet; R&D Systems, Minneapolis, MN, United States).

In vitro lung epithelial model studies

An A549 lung epithelial cell line incorporating an NF-κB driven luciferase reporter construct (A549-κB-luc; Panomics, Fremont, CA, United States) was used for transcription factor assessment and scratch wound assays. A BEAS2B bronchial epithelial cell line (ATCC, Manassas, VA, United States) was used for other injury models. These were both cultured in RPMI-1640 (Sigma) with 10% FBS and penicillin/streptomycin. *Reporter assays:* A549-κB-luc cells were seeded to 96 well plates at 50,000 cells in 100 µL of medium per well and 50 µL of SFM, non-nebulized or nebulized and collected MSC-CM was added 24 h later. An inflammatory activation cocktail (IL-1β 10 ng/mL, TNF-α 50 ng/mL, and IFN-γ 50 ng/mL) was then added for a further 24 h, whereupon medium was aspirated, cells homogenized in luciferase substrate (Bright-Glo™ Luciferase Assay System; Promega, Madison, WI, United States) and luminescence quantified in a Victor™ multilabel plate reader (PerkinElmer, Waltham, MA, United States). *Scratch wound assays:* A549-κB-luc cells were seeded to 24 well plates at 200,000 cells in 1 mL of medium. When confluence was reached, a single scratch wound was performed on the cell monolayer using a 1,000 µL pipette tip, medium aspirated, and cells washed with PBS. 1 mL of fresh medium was then added to each well with 250 µL of SFM, non-nebulized or nebulized MSC-CM. At various timepoints up to 24 h, scratch wounds were imaged under light microscopy (Cytation 5™; BioTek, Shoreline, WA, United States) and total remaining wound size quantified. *Endotoxin inflammation model:* BEAS2B were seeded to 96 well plates at 50,000 cells in 100 µL of medium per well and 50 µL of SFM, non-nebulized or nebulized and collected MSC-CM was added 24 h later. *Escherichia coli* derived lipopolysaccharide (LPS; Sigma) was then added to each well at 1 µg/mL. After another 24 h, media was harvested for cytokine ELISA (Human IL-1β, IL-8/CXCL8 Duoset; R&D Systems) and cell viability assessed through addition of fresh media with 3-(4,5-dimethylthiazol-2-yl)-2,5-diphenyltetrazolium bromide (MTT; Sigma) at a final concentration of 0.5 mg/mL. After 2 h, media was aspirated, formazan crystals solubilized in 100 µL of DMSO, and absorbance read at 630 nm. *Oxidative stress model:* BEAS2B cells were seeded as above and MSC-CM added. Hydrogen peroxide (H_2O_2) was then added to a final concentration of 10 mM for 2 h and an MTT viability assays performed as described above.

In vitro antibacterial activity models

Direct bacterial inhibition: Overnight bacterial cultures were established from cryofrozen beads in 5 mL of Luria Broth (Fannin, Dublin, Ireland) in an orbital shaker at 37°C, 220RPM, overnight. Bacterial strains used were a patient isolate Gram-negative *E. coli* (Department of Clinical Microbiology, University of Galway, Ireland) and a reference Gram-positive *S. aureus* (#5624; ATCC, Manassas, VA, United States). Serial dilution and plating to agar determined these cultures to be c. 5×10^9 and 10×10^9 CFU/mL, respectively. MSC-CM was either used directly or passed through a VMN and added to 96 well V-bottom plates at 200 µL per well. Bacteria was then added in 10 µL of PBS to give final concentrations of 1,000 or 10,000 CFU/µL. Plates were placed in an orbital shaker at 37°C, 220 RPM for 4 h and then centrifuged with a plate adaptor in a benchtop centrifuge at 2,000 × *g* for 10 min. Medium was aspirated, bacteria pellet resuspended in 200 µL and transferred to a flat bottomed 96 well plate. Absorbance was assessed at 650 nm in a multilabel plate reader (Victor™). A linear relationship between absorbance and CFUs has been previously established for these strains (20). *Phagocytosis assay:* THP-1 monocyte cells were seeded to 96 well plates at 100,000 cells per well and differentiated to macrophages with 1 µg/mL of phorbol myristate acetate (PMA) for 72 h. Wells were aspirated and refed with 100 µL of pre-nebulized or control MSC-CM and LPS (100 ng/mL) added to simulate the pneumonia environment. 24 h later, zymosan particles were added (four particles per cell ratio) and phagocytosis allowed to proceed for 4 h. Wells were then imaged under fluorescent microscopy (Leica Biosystems, Clare, Ireland) with two fluorescent particles in a cell being considered positive for phagocytosis activity.

In vivo pneumonia model

All animal experiments were performed under the ethical approval of the Animal Care in Research Ethical Committee (ACREC) at the University of Galway and the regulatory approval of the Health Products Regulatory Agency (HPRA) Ireland.

Adult male Sprague Dawley rats, 350–450 g, were used (Envigo, London, United Kingdom). Animals were anesthetized with inhalational isoflurane (2% in air) and a bolus of clinically isolated *E. coli* delivered intratracheally. Animals were maintained under anaesthesia for 1 h between bacteria administration and treatment and then given IT instillation or attached to a Flexivent small animal ventilator (SciReq, Montral, Canada) for nebulization. Animals were ventilated with room air with 90 breaths per minute, flow rate 500 cc per minute and duty cycle 30%. 300 µL of MSC-CM was delivered to the animals via VMN IT over the course of approximately 5 min. In a separate group, animals were anesthetized and received 300 µL of MSC-CM by direct instillation IT. All animals were allowed to recover and returned to cages for observation.

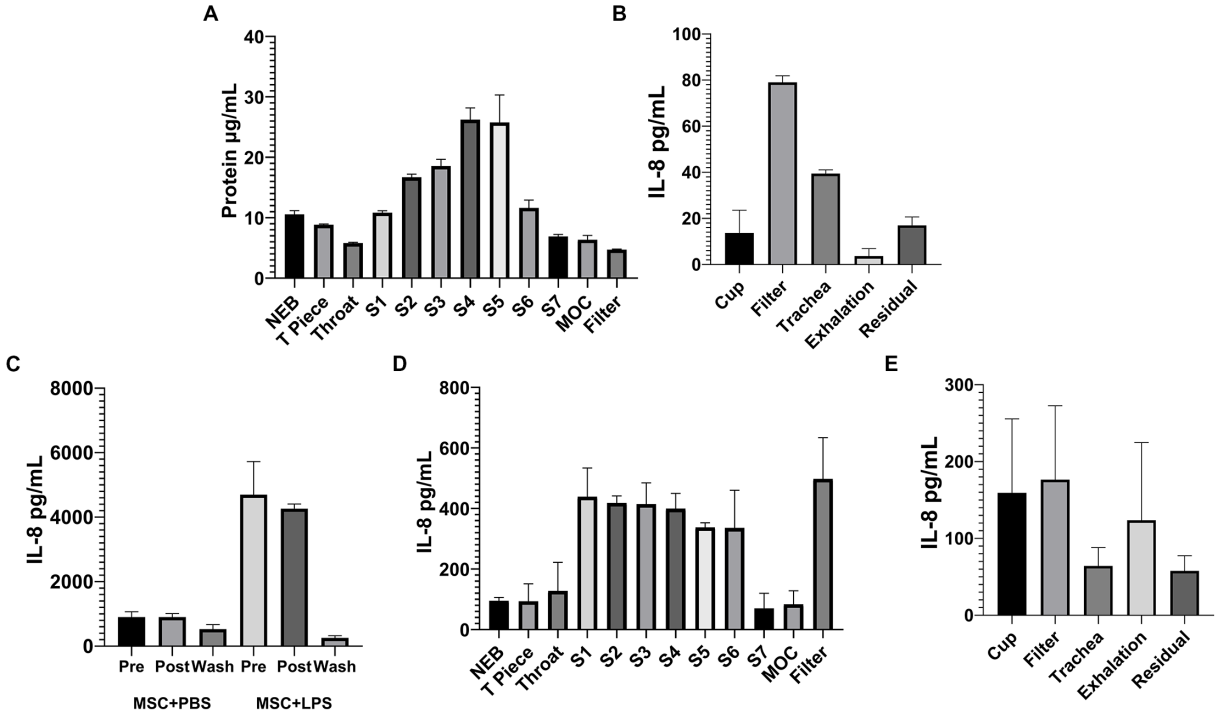

FIGURE 1
Nebulized MSC-CM will penetrate deep into the lung and has preserved protein content. 10mL of MSC-CM was applied by VMN to a cascade impactor with an airflow of 15L/min and protein deposition in the chambers quantified **(A)**. The same MSC-CM was then applied by VMN to a simulated lung and protein deposition to the various parts of the circuit assessed **(B)**. In IL-8 ELISAs as representative of intact protein delivery, naïve and LPS-treated MSC-CM was passed through a VMN and collected **(C)**, and the IL-8 content from the various plates of the cascade impactor **(D)** and points in the simulated lung circuit **(E)** were quantified after delivery of LPS-CM to the devices.

48 h later, animals were reanesthetized with medetomidine 1 mg/kg (1 mg/mL Medetor®; Chanelle Veterinary, Ireland) and ketamine 75 mg/kg (100 mg/mL Ketamidor, RicherPharma AG, Austria), and after confirmation of anesthesia intubated and attached to the ventilator. Ventilation regime was 90 breaths per minute, flow rate 500 cc per minute. Animals were tracheostomized and a canula inserted in the coronary artery for continuous blood pressure and heart rate monitoring. Arterial blood for gas and metabolite analysis was also taken from this canula intermittently (ABL 90 Flex Plus; Radiometer Ireland, Dublin, Ireland). After 1 h, cisatracurium besilate (10 mg·kg^{-1}·h^{-1}; Atricorium besylate, Aspe, Ireland) was administered to induce respiratory paralysis immediately prior to static lung compliance measurement. Animals were then given an anesthetic overdose and sacrificed by exsanguination.

Bronchoalveolar lavage was performed by delivering 5 mL of PBS to the lungs by intratracheal instillation and allowing the fluid to drip into a collection tube. This was repeated twice and all three BAL collections pooled.

Sample analysis

Lung wet:dry ratio: The left lung lobe was separated and weighed. It was then placed in a 37°C oven for 24 h to dehydrate it and reweighed. Wet to dry ratio was then calculated. *Leukocyte differential counts:* 5 mL of BAL was centrifuged at 1,000 × *g* for 10 min and the pelleted cells resuspended in 1 mL of PBS. This was then transferred to a glass slide by centrifugation (Cytospin™; ThermoFisher Scientific), dried and stained with Haema-Gurr for 5 min followed by 5 min of ethanol destain and dried in air. Infiltrating cells were imaged under light microscopy (Leica) and total and neutrophil cell numbers counted. *Cytokine multiplex:* BAL was applied to a bead based cytokine multiplex assay (Bio-Plex Pro™ Rat Cytokine 23-Plex Assay; Accuscience, Naas, Ireland) as per manufacturer's instructions in a multiplex bead reader (Bio-Plex 200 System; Accuscience). *Lung bacterial load:* BAL was serially diluted and plated to Brilliance UTI Clarity agar plates (Fannin). 24 h later *E.coli* presence was confirmed by color of colonies and CFU counted.

Statistical analysis

All data were analyzed using GraphPad Prism Software (GraphPad Software, San Diego, CA, United States). Data were tested for normal distribution and significance determined by ANOVA, with $p < 0.05$ considered significant.

Results

Nebulized MSC-CM has excellent compatibility with VMN delivery

Naïve MSC-CM applied to a cascade impactor by VMN showed delivery to compartments corresponding to airways of diameter 1.39–8.61 mm (Figure 1A) showing deep penetration to the distal lung.

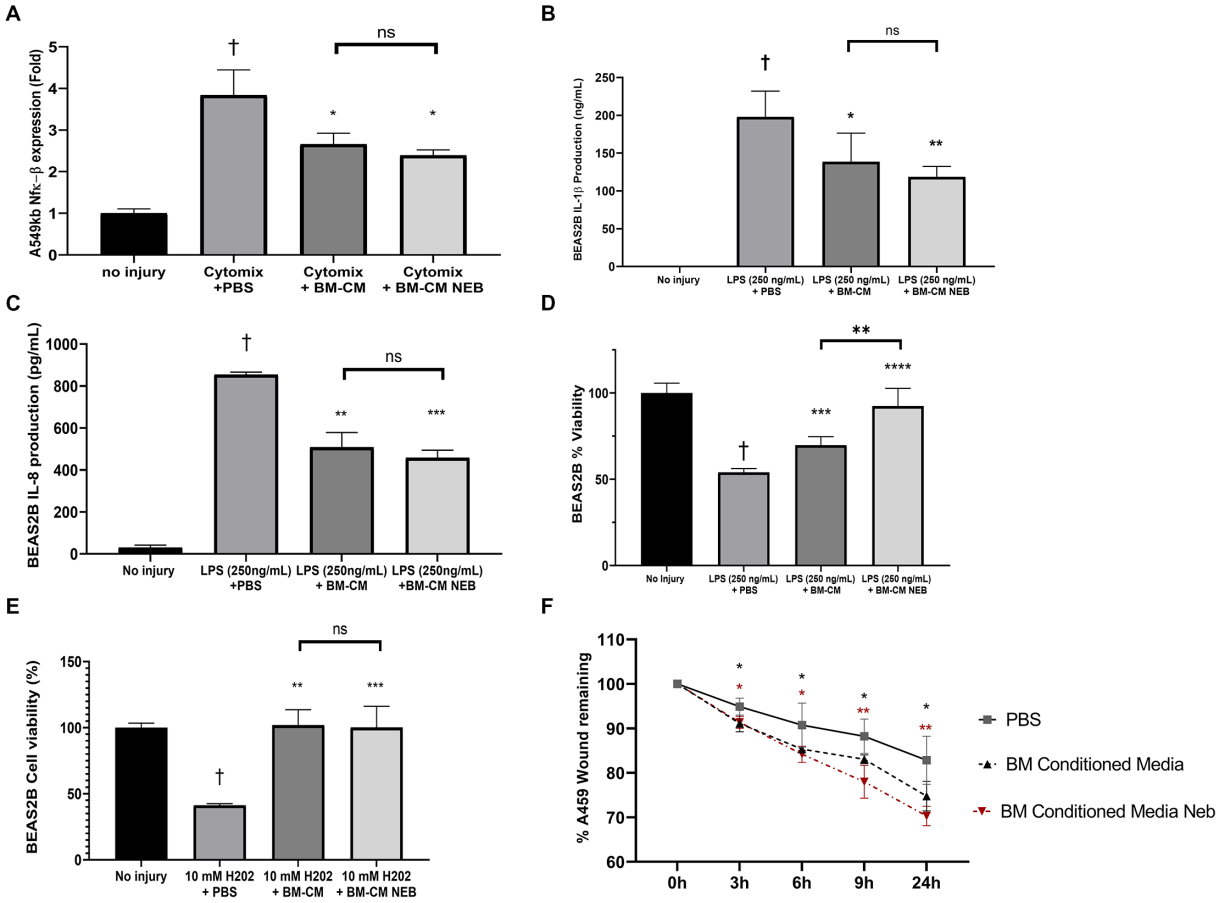

FIGURE 2
Anti-inflammatory and tissue healing capacity of MSC-CM *in vitro* after nebulization. Nebulization of MSC-CM did not attenuate the induction of the pro-inflammatory pathway NF-κB compared with the non-nebulized CM **(A)**. MSC-CM reduced IL-1β **(B)** and IL-8 **(C)** production while attenuating the decrease in BEAS2B cell viability **(D)** after 250ng/mL LPS stimulation, with significant increase of effect after nebulization. MSC-CM also attenuated the viability of BEAS2B after oxidative stress damage **(E)** with no reduction in the effect after nebulization. MSC-CM increased wound closure in A549 monolayers at 6, 9, and 24h after initiation, with no significant reduction in the effect after nebulization (**F**; Data presented mean±SD. †significant between no injury and PBS group, *significant difference between treated group and PBS group, both $p \leq 0.05$. **significant difference between treated group and vehicle $p \leq 0.01$. **significant difference between treated group and vehicle $p \leq 0.00.1$. NS, no significant difference).

Total delivery to a simulated lung was a significant percentage of the sample applied, with 40 μg/mL of protein recovered from the lung compared to only 5 μg/mL in the exhalation filter (Figure 1B), indicating that doses of conditioned medium can be successfully delivered to patient airways. LPS activated MSC-CM contains a high concentration of IL-8 cytokine, which almost completely survived the nebulization process, with little cytokine observed in the filter wash-out (Figure 1C), suggesting that most proteins in the MSC secretome are delivered to the lung intact. However, the profile of IL-8 protein delivered to the airways is somewhat different to that of the total LPS-CM protein (Figures 1D,E). Overall this delivery profile is in line with other aqueous solutions delivered by VMN.

Vibrating mesh nebulization preserves MSC-CM activity *in vitro*

MSC-CM was passed through a VMN, collected, and used in a variety of lung inflammation and injury models. MSC-CM was able to reduce the activity of an NF-κB reporter in alveolar epithelial cells in response to inflammatory cytokine induction and this anti-inflammatory nature persisted after nebulization (Figure 2A). In a bronchial epithelial cell line exposed to *E. coli* LPS induced inflammation, MSC-CM significantly inhibited production of IL-1β (Figure 2B) and IL-8 (Figure 2C) cytokines, and this activity was also preserved after nebulization. This LPS injury model simultaneously resulted in a drop in viability in the bronchial cells, which could be ameliorated by MSC-CM treatment (Figure 2D). Interestingly, nebulized MSC-CM actually performed better than non-nebulized with a significant further increase in cell viability (Figure 2D). In an oxidative stress model, hydrogen peroxide significantly reduced bronchial epithelial cell viability, as measured by MTT assay, and this could be reversed with either control or nebulized MSC-CM (Figure 2E). Finally, in an alveolar epithelial scratch wound model, MSC-CM significantly increased wound closing speed, and pre-nebulization of the MSC-CM actually resulted in an even faster restitution of the epithelial layer (Figure 2F) with representative images available in Supplementary Figure S1.

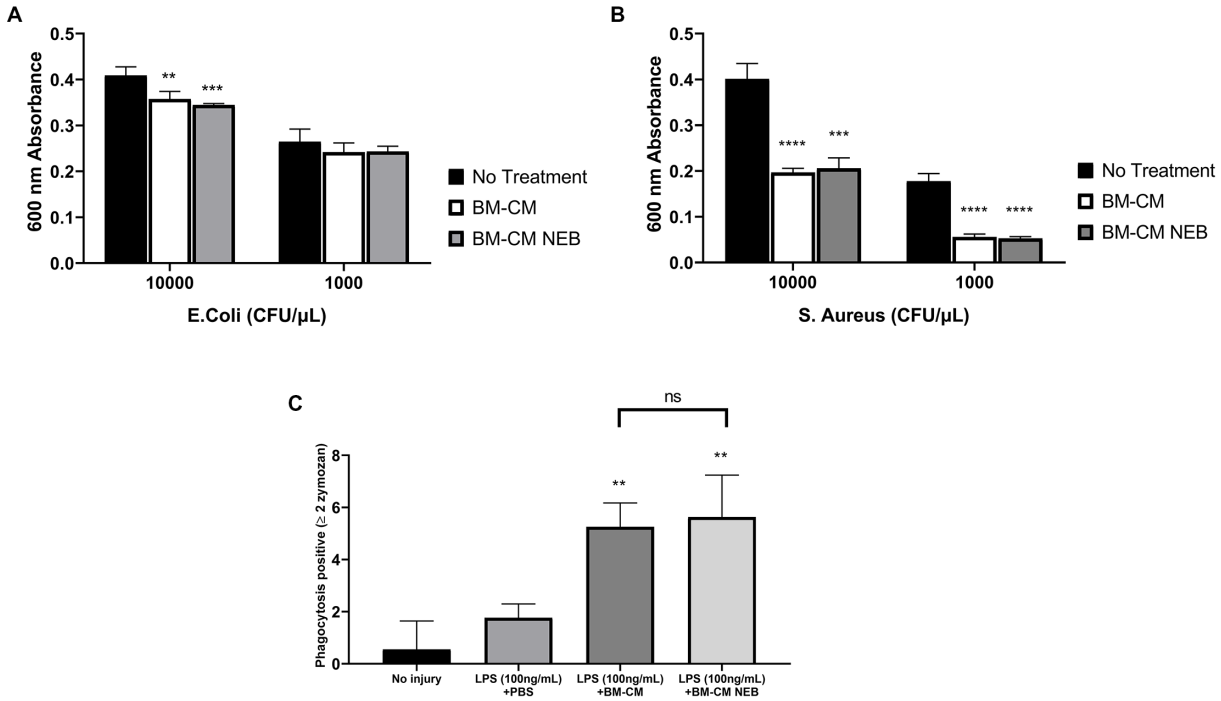

FIGURE 3
Antibacterial capacity of MSC-CM *in vitro* after nebulization. MSC-CM inhibited the growth of *Escherichia coli* **(A)** and *S. aureus* **(B)** cultures before and after nebulization at an initial bacterial concentration of 10,000 or 1,000CFU/μL. MSC-CM increased the phagocytic capacity of LPS-stimulated THP-1 cells compared with vehicle treatment **(B)** with no significant decrease in effect after nebulization (Data presented mean±SD; *significant difference between treated group and no treatment $p \leq 0.05$; **significant difference between treated group and no treatment $p \leq 0.01$; **significant difference between treated group and no treatment $p \leq 0.00.1$; NS, no significant difference).

Antimicrobial activity of nebulized MSC-CM

MSC-CM reduced the proliferation rate of both Gram-negative *E. coli* (Figure 3A) and Gram-positive *S. aureus* (Figure 3B) although this did not reach significance with lower inoculation density of *E. coli* and was particularly pronounced against *S. aureus*. This inhibition was preserved after nebulization in both pathogen strains (Figures 3A,B). In monocyte/macrophages, phagocytosis was enhanced by exposure to both control and nebulized MSC-CM (Figure 3C).

Nebulized MSC-CM ameliorates *Escherichia coli* induced pneumonia

In a rodent model of pneumonia ARDS, instilled MSC-CM reduced the decrease in blood oxygenation observed in injured animals and this therapeutic effect could be reproduced with MSC-CM nebulized to the airspace IT (Figures 4A,B). This benefit did not reach significance for both modes at 21% inspired oxygen (Figure 4A) but did at 100% (Figure 4B). To further explore lung function parameters, blood CO_2 levels were seen to rise with pneumonia injury compared to vehicle control, and this could be reversed by MSC-CM, with no significant difference between instilled or nebulizer delivery modes, however overall significance against vehicle was here lost with nebulization (Figure 4C). The calculated alveolar:arterial (A:a) gradient was also significantly improved by MSC-CM administered by either method (Figure 4D). Respiratory static compliance was improved by instilled MSC-CM alone (Figure 5A), but accumulation of fluid in the lung with pneumonia was reduced by MSC-CM delivered by instillation or nebulization (Figure 5B), an important parameter of lung function. With regard to infiltration of leukocytes to the airspace, significant numbers of total white cells accumulated in the BAL after pneumonia injury, and this was reduced by MSC-CM but only significantly so by direct IT instillation (Figure 5C). However, the percentage of these infiltrating cells that are of the important and more deleterious neutrophil type was significantly attenuated by both IT instilled and nebulized MSC-CM (Figure 5D). Finally, bacteria load in the BAL of animals with pneumonia injury was reduced by both instilled and nebulized MSC-CM although this did not reach significance in either modality (Figure 6).

Nebulized MSC-CM reduced inflammatory cytokines in *Escherichia coli* induced pneumonia

In a 23-plex cytokine assay, almost all cytokines measured were present in BAL in higher concentrations after *E. coli* pneumonia

10.3389/fmed.2023.1162615

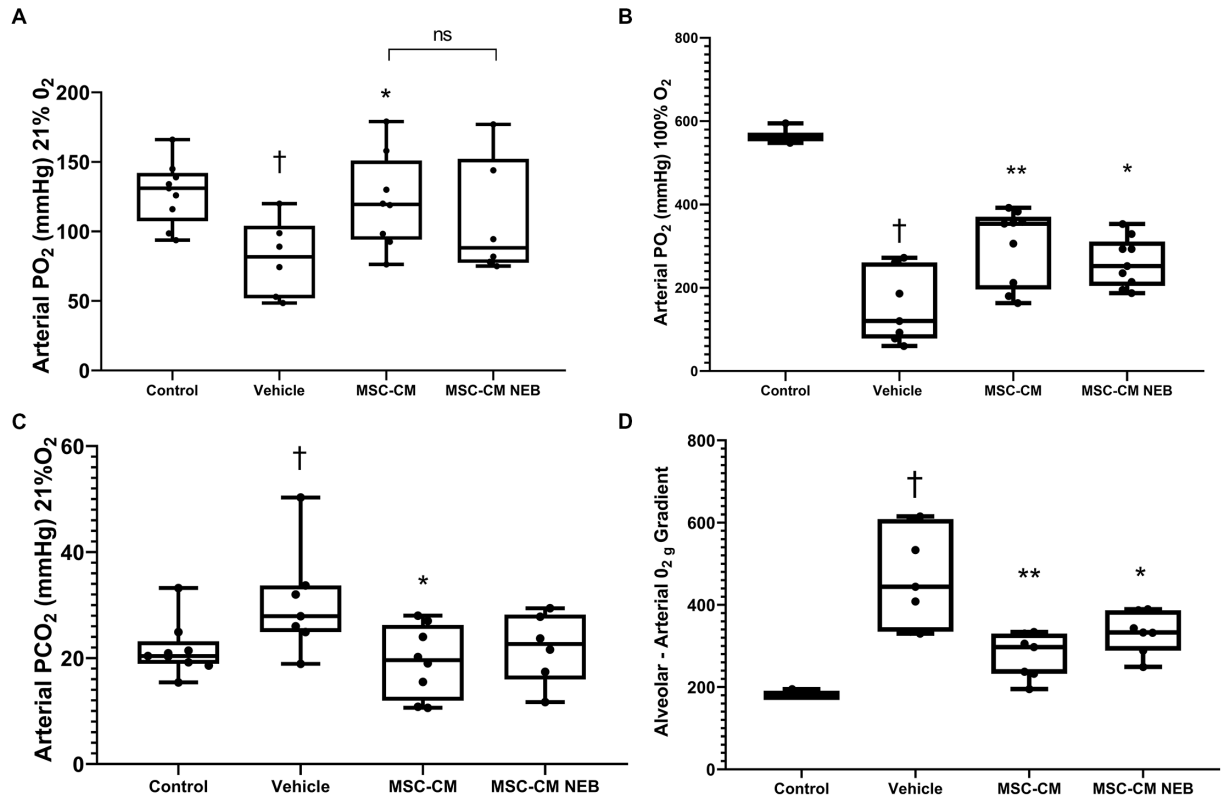

FIGURE 4
MSC-CM ameliorates physiological parameters in bacterial induced lung injury. Nebulization of MSC-CM 1h after *Escherichia coli* installation mitigated the arterial PO_2 decrease on 21% O_2 **(A)** and 100% O_2 **(B)** ventilation and attenuated PCO_2 increase **(C)** at 48h. No difference between delivery methods was observed. MSC-CM attenuated the increase in alveolar-arterial O_2 gradient **(D)** with no statistical difference in effect based on the delivery methods (Data presented mean±SD; †significant between control and vehicle; *significant difference between treated group and vehicle, both $p \leq 0.05$; **significant difference between treated group and vehicle $p \leq 0.01$; and NS, no significant difference between nebulized and instilled delivery method).

compared to healthy control animals (Figure 7). Cytokines reduced by MSC-CM instilled directly to the lung were: IL-1b, IL-2, IL-5, IL-6, IL-12. IL-18, GRO/KC, and M-CSF. Of these, all were also significantly ameliorated by IT nebulized MSC-CM apart from IL-2, IL-12, and M-CSF. The anti-inflammatory/pro-healing cytokines IL-10 and VEGF were both significantly increased by nebulized MSC-CM alone compared to vehicle control.

Discussion

While there are promising preclinical findings and clinical trials are ongoing, there are still challenges associated with cell isolation, production, and administration that need to be solved in order for MSCs to become a feasible treatment for ARDS (10). MSC products are also gaining traction as therapeutics to replace the MSC itself, but these can be expensive and wasteful to isolate. Local administration of MSC conditioned media has been proven effective in the amelioration of lung injury after *E. coli* LPS endotoxin administration (21, 22). However, the intratracheal administration of MSC suspensions could produce a tissue injury due to the additional delivery of vehicle liquid to the lung, where nebulization can overcome local administration issues through delivery of a highly respirable aerosol containing the desired therapeutic over a longer time frame and with a deeper penetration throughout the lung tissue (23).

Supporting this idea, we have observed that nebulization of the MSC-CM allows penetration deep into the lung airways with a minimal waste of the product, confirming the compatibility of this delivery method with MSC cell products. In addition, the nebulization process did not alter the therapeutic capacity of the MSC-CM in reducing inflammatory cytokine concentrations and increasing cell viability after inflammatory damage *in vitro*. In the same vein, as McCarthy et al. (20) demonstrated recently, the direct antibacterial effects were also not adversely affected, with nebulized conditioned medium able to inhibit bacterial growth in live cultures of Gram-positive and Gram-negative bacteria species (20). Ionescu et al. demonstrated that IT delivered MSC-CM reduced the presence of neutrophils in the alveolar space in an LPS lung injury model (21). Similarly, we observed that IT delivery of MSC-CM reduced the immune cell presence in the lungs in a full *E. coli* pneumonia model, with a significant reduction in the percentage of neutrophils as reported in previous studies after whole cell administration (24). Interestingly, nebulization of the same MSC-CM product improved the reduction in infiltrating cells, particularly neutrophils, in the lungs compared with the IT delivery mode. In the same direction, MSC-CM produced a reduction in the fluid infiltration with a lower wet:dry weight ratio in treated animals regardless of the delivery

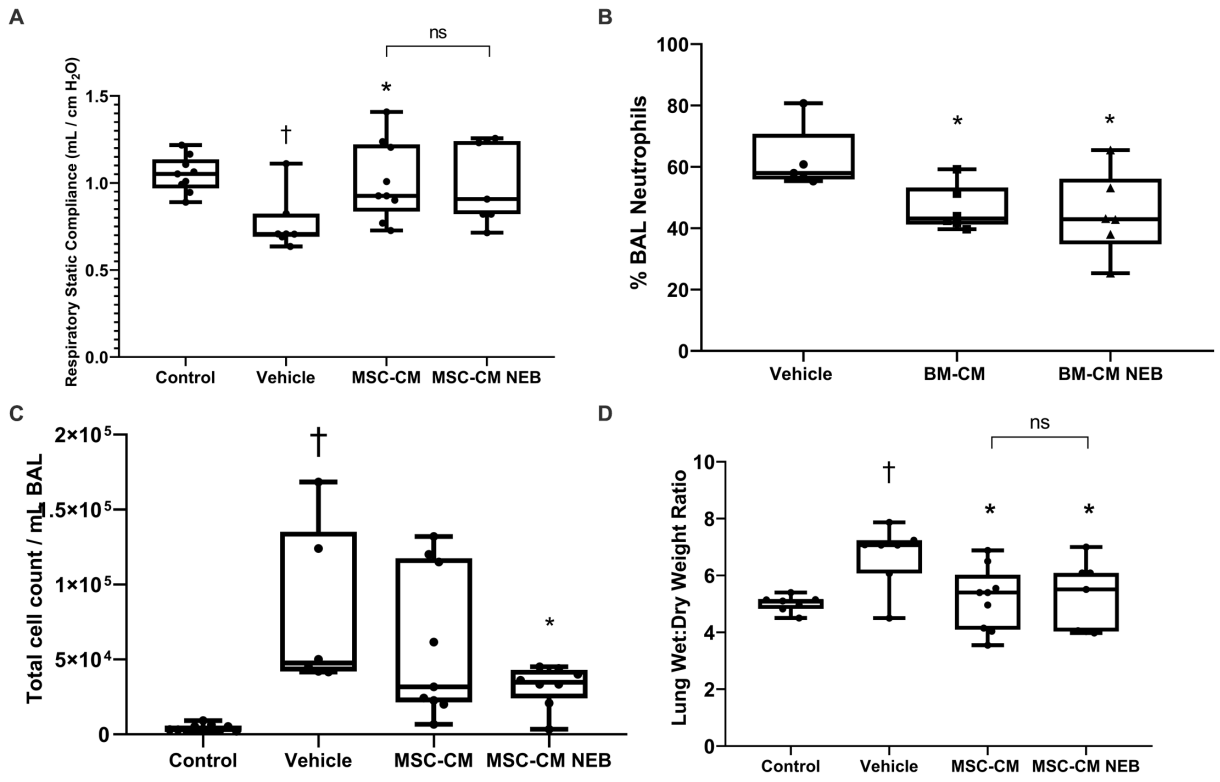

FIGURE 5
MSC-CM ameliorates other injury markers in bacterial induced lung injury. Nebulization of MSC-CM attenuated compliance decrease **(A)** while reducing total infiltrating cell count **(B)**, wet:dry ratio **(C)**, and neutrophils number **(D)** in the lung with no statistical difference between delivery methods (Data presented mean±SD; †significant between control and vehicle; *significant difference between treated group and vehicle, both $p \leq 0.05$; **significant difference between treated group and vehicle $p \leq 0.01$; and NS, no significant difference between nebulized and instilled delivery methods).

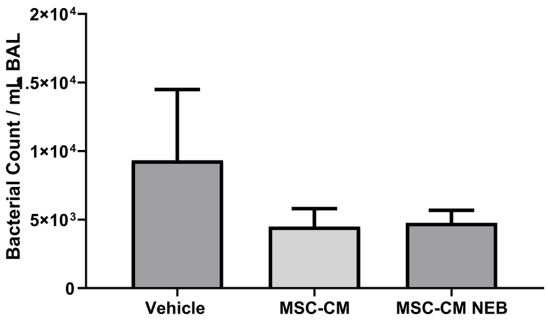

FIGURE 6
MSC-CM reduces bacterial load in bacterial induced lung injury. MSC-CM reduced the presence of *Escherichia coli* colony forming units in lung BAL measured 48h after treatment with no difference between nebulized and non-nebulized CM (Data presented mean±SD).

methods. MSC-CM treated animals showed reduction in pivotal cytokines for the inflammatory process such as IL-1β and IL-6 similar to previous studies where whole MSCs were administrated (25). In addition, there were lower levels of immune cell chemoattractants like GRO/KC, possibly explaining the reduced presence of these cells in the lungs. There was also an increase in the levels of the cytokine IL-10, with an anti-inflammatory effect reminiscent of the findings reported by Gupta et al. after BM-MSC administration in an LPS lung injury model (14). The improvement observed in lung physiology translated into a better organ functionality as proven by the physiological parameters measured in the treated animals. Among these parameters, the alveolar-arterial gradient measurement is a strong indicator of gas exchange efficiency, with a high gradient relating to poor capacity for blood oxygenation (26). The reduction of the alveolar-arterial gradient, added to the reduction in arterial PCO_2 and increase in the PO_2, suggests a recovery of the blood-alveolar barrier and better O_2/CO_2 exchange in animals treated with nebulised MSC-CM.

As observed in previous studies, the MSC secretome modulates macrophage activity, generating an increase in M2 differentiated subpopulations, with anti-inflammatory cytokine production and increased phagocytosis (27). In this sense, we observed that nebulization of MSC-CM did not alter the capacity of MSC-CM to increase phagocytic activity in macrophages-like cells *in vitro*. This mechanism could be partially responsible for the reduction in bacterial presence observed in BAL samples from treated animals.

There are some limitations to this study. Firstly, transformed cell lines can only be considered the first line of *in vitro* investigation and deeper mechanistic studies should utilize

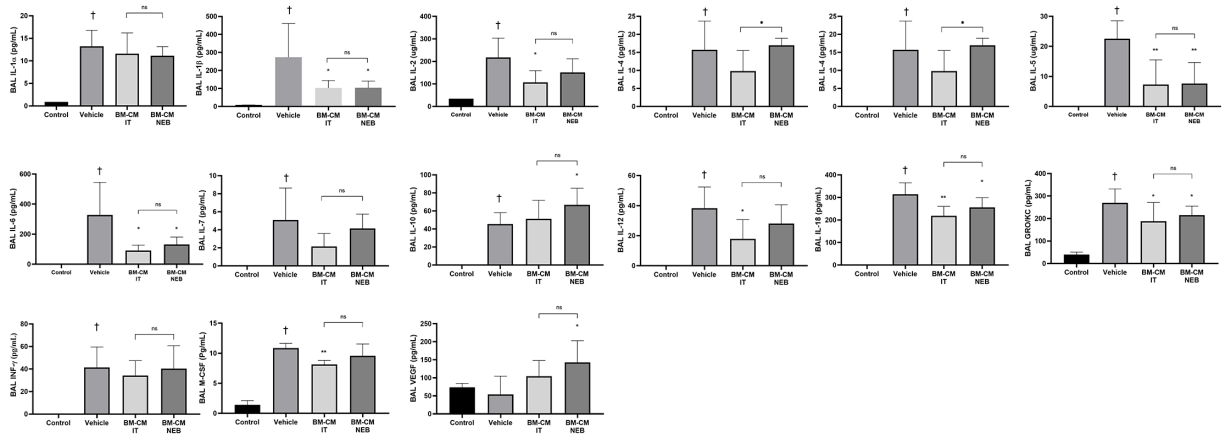

FIGURE 7
MSC-CM reduced inflammatory markers in lung after bacterial infection. Nebulizer administration of MSC-CM mitigated the increase of inflammatory cytokines IL-1α, IL-1β, IL-2, IL-4, IL-5, IL-6, IL-7, IL-12, IL-18, and IFN-γ while increasing anti-inflammatory cytokine IL-10 compared with the vehicle group at 48h after injury induction with significant increase in effect with nebulised MSC-CM in IL-4 and IL-10, and no negative effect in the remaining cytokines. MSC-CM also mitigated the increase in chemoattractant GRO/KC and inflammatory related molecules such as M-CSF and VEGF after *Escherichia coli* administration 48h after injury induction. No significance was observed between delivery routes (Data presented mean±SD; †statistically significant between control and vehicle group; *significant difference between treated group and vehicle, $p \leq 0.05$; and NS, no significant difference between nebulised and IT delivery route).

primary human or animal lung epithelial cells. Secondly, the secretome is an incredibly complex mix of molecules and subcellular constructs, and determining which factors ultimately result in therapeutic effect is ongoing. The absence of a detailed mechanism of action may also have implications for potency assays during larger scale production and eventual trial licensing. Another limitation is that only a single timepoint of therapeutic delivery and injury assessment was possible within the scope of the study. Whether MSC-CM reduces the injurious process of ARDS or enhances the subsequent repair (or indeed both) is not answered. It also remains to be determined in MSC-CM can address a more established pneumonia infection and for the therapeutic window to be calculated.

In summary, the direct nebulization of MSC-CM broadly recapitulated the antibacterial and anti-inflammatory capacity of the MSC itself widely described in the scientific literature. In addition, nebulization enhanced the immune cell and fluid clearance capacity of the MSC-CM, offering a promising delivery route for the MSC secretome in ARDS patients where instillation of liquid therapeutics should be avoided.

Data availability statement

The raw data supporting the conclusions of this article will be made available by the authors, without undue reservation.

Ethics statement

The animal study was reviewed and approved by Animal Care in Research Ethics Committee (ACREC) at University of Galway.

Author contributions

HEG: formal analysis, investigation, data curation, and writing—review and editing. SDM and CM: formal analysis, investigation, data curation, writing—review and editing, and supervision. JL: conceptualization, methodology, formal analysis, resources, writing—review and editing, and supervision. RM: conceptualization, methodology, formal analysis, investigation, resources, data curation, and writing—review and editing. DO'T: conceptualization, methodology, formal analysis, investigation, resources, data curation, writing—original draft, writing—review and editing, supervision, project administration, and funding acquisition. All authors contributed to the article and approved the submitted version.

Funding

DO'T was supported by Health Research Board Ireland (ILP-POR-2017-024) and Science Foundation Ireland (13/RC/2073).

Acknowledgments

We would like to acknowledge the groundwork and contributions made to this study by our former colleague James Devaney.

Conflict of interest

RM is CSO of Aerogen Ltd.

The remaining authors declare that the research was conducted in the absence of any commercial or financial relationships that could be construed as a potential conflict of interest.

Publisher's note

All claims expressed in this article are solely those of the authors and do not necessarily represent those of their affiliated organizations, or those of the publisher, the editors and the reviewers. Any product that may be evaluated in this article, or claim that may be made by its manufacturer, is not guaranteed or endorsed by the publisher.

Supplementary material

The Supplementary material for this article can be found online at: https://www.frontiersin.org/articles/10.3389/fmed.2023.1162615/full#supplementary-material

References

1. Ranieri VM, Rubenfeld GD, Thompson BT, Ferguson ND, Caldwell E, Fan E, et al. ARDS Definition Task Force. Acute respiratory distress syndrome: the Berlin Definition. *JAMA*. (2012) 307:2526–33. doi: 10.1001/jama.2012.5669

2. Bellani G, Laffey JG, Pham T, Fan E, Brochard L, Esteban A, et al. Epidemiology, patterns of care, and mortality for patients with acute respiratory distress syndrome in intensive care units in 50 countries. *JAMA*. (2016) 315:788–800. doi: 10.1001/jama.2016.0291

3. Huppert LA, Matthay MA, Ware LB. Pathogenesis of acute respiratory distress syndrome. *Semin Respir Crit Care Med*. (2019) 40:31–9. doi: 10.1055/s-0039-1683996

4. Gotts JE, Matthay MA. Sepsis: pathophysiology and clinical management. *BMJ*. (2016) 353:i1585. doi: 10.1136/bmj.i1585

5. Shi Y, Wang Y, Li Q, Liu K, Hou J, Shao C, et al. Immunoregulatory mechanisms of mesenchymal stem and stromal cells in inflammatory diseases. *Nat Rev Nephrol*. (2018) 14:493–507. doi: 10.1038/s41581-018-0023-5

6. Lozano Navarro LV, Chen X, Giratá Viviescas LT, Ardila-Roa AK, Luna-Gonzalez ML, Sossa CL, et al. Mesenchymal stem cells for critical limb ischemia: their function, mechanism, and therapeutic potential. *Stem Cell Res Ther*. (2022) 13:345. doi: 10.1186/s13287-022-03043-3

7. Yun CW, Lee SH. Potential and therapeutic efficacy of cell-based therapy using Mesenchymal stem cells for acute/chronic kidney disease. *Int J Mol Sci*. (2019) 20:1619. doi: 10.3390/ijms20071619

8. Li H, Zhu H, Ge T, Wang Z, Zhang C. Mesenchymal stem cell-based therapy for diabetes mellitus: enhancement strategies and future perspectives. *Stem Cell Rev Rep*. (2021) 17:1552–69. doi: 10.1007/s12015-021-10139-5

9. Horie S, Gonzalez HE, Laffey JG, Masterson CH. Cell therapy in acute respiratory distress syndrome. *J Thorac Dis*. (2018) 10:5607–20. doi: 10.21037/jtd.2018.08.28

10. Bunpetch V, Wu H, Zhang S, Ouyang H. From "bench to bedside": current advancement on large-scale production of Mesenchymal stem cells. *Stem Cells Dev*. (2017) 26:1662–73. doi: 10.1089/scd.2017.0104

11. Duan W, Lopez MJ, Hicok K. Adult multipotent stromal cell cryopreservation: pluses and pitfalls. *Vet Surg*. (2018) 47:19–29. doi: 10.1111/vsu.12730

12. Fernández-Francos S, Eiro N, González-Galiano N, Vizoso FJ. Mesenchymal stem cell-based therapy as an alternative to the treatment of acute respiratory distress syndrome: current evidence and future perspectives. *Int J Mol Sci*. (2021) 22:7850. doi: 10.3390/ijms22157850

13. Islam MN, Das SR, Emin MT, Wei M, Sun L, Westphalen K, et al. Mitochondrial transfer from bone-marrow-derived stromal cells to pulmonary alveoli protects against acute lung injury. *Nat Med*. (2012) 18:759–65. doi: 10.1038/nm.2736

14. Gupta N, Su X, Popov B, Lee JW, Serikov V, Matthay MA. Intrapulmonary delivery of bone marrow-derived mesenchymal stem cells improves survival and attenuates endotoxin-induced acute lung injury in mice. *J Immunol*. (2007) 179:1855–63. doi: 10.4049/jimmunol.179.3.1855

15. McGinn KA, Weigartz K, Lintner A, Scalese MJ, Kahn SA. Nebulized heparin with N-Acetylcysteine and albuterol reduces duration of mechanical ventilation in patients with inhalation injury. *J Pharm Pract*. (2019) 32:163–6. doi: 10.1177/0897190017747143

16. Mohamed HS, Meguid MM. Effect of nebulized budesonide on respiratory mechanics and oxygenation in acute lung injury/acute respiratory distress syndrome: randomized controlled study. *Saudi J Anaesth*. (2017) 11:9–14. doi: 10.4103/1658-354X.197369

17. Walther S, Jansson I, Berg S, Lennquist S. Pulmonary granulocyte accumulation is reduced by nebulized corticosteroid in septic pigs. *Acta Anaesthesiol Scand*. (1992) 36:651–5. doi: 10.1111/j.1399-6576.1992.tb03537.x

18. Chimenti L, Camprubí-Rimblas M, Guillamat-Prats R, Gomez MN, Tijero J, Blanch L, et al. Nebulized heparin attenuates pulmonary coagulopathy and inflammation through alveolar macrophages in a rat model of acute lung injury. *Thromb Haemost*. (2017) 117:2125–34. doi: 10.1160/TH17-05-0347

19. Dominici M, Le Blanc K, Mueller I, Slaper-Cortenbach I, Marini F, Krause D, et al. Minimal criteria for defining multipotent mesenchymal stromal cells. The International Society for Cellular Therapy position statement. *Cytotherapy*. (2006) 8:315–7. doi: 10.1080/14653240600855905

20. McCarthy SD, Horgan E, Ali A, Masterson C, Laffey JG, MacLoughlin R, et al. Nebulized Mesenchymal stem cell derived conditioned medium retains antibacterial properties against clinical pathogen isolates. *J Aerosol Med Pulm Drug Deliv*. (2020) 33:140–52. doi: 10.1089/jamp.2019.1542

21. Ionescu L, Byrne RN, van Haaften T, Vadivel A, Alphonse RS, Rey-Parra GJ, et al. Stem cell conditioned medium improves acute lung injury in mice: in vivo evidence for stem cell paracrine action. *Am J Phys Lung Cell Mol Phys*. (2012) 303:L967–77. doi: 10.1152/ajplung.00144.2011

22. Su VY-F, Yang K-Y. Mesenchymal stem cell-conditioned medium induces neutrophils apoptosis via inhibition of NF-kB pathway and increases endogenous pulmonary stem cells in endotoxin-induced acute lung injury. *Int J Mol Sci*. (2015) 46:OA3520.

23. Martin AR, Finlay WH. Nebulizers for drug delivery to the lungs. *Expert Opin Drug Deliv*. (2015) 12:889–900. doi: 10.1517/17425247.2015.995087

24. Gupta N, Krasnodembskaya A, Kapetanaki M, Mouded M, Tan X, Serikov V, et al. Mesenchymal stem cells enhance survival and bacterial clearance in murine *Escherichia coli* pneumonia. *Thorax*. (2012) 67:533–9. doi: 10.1136/thoraxjnl-2011-201176

25. Devaney J, Horie S, Masterson C, Elliman S, Barry F, O'Brien T, et al. Human mesenchymal stromal cells decrease the severity of acute lung injury induced by *E. coli* in the rat. *Thorax*. (2015) 70:625–35. doi: 10.1136/thoraxjnl-2015-206813

26. Avci S, Perincek G. The alveolar-arterial gradient, pneumonia severity scores and inflammatory markers to predict 30-day mortality in pneumonia. *Am J Emerg Med*. (2020) 38:1796–801. doi: 10.1016/j.ajem.2020.05.048

27. Morrison TJ, Jackson MV, Cunningham EK, Kissenpfennig A, McAuley DF, O'Kane CM, et al. Mesenchymal stromal cells modulate macrophages in clinically relevant lung injury models by extracellular vesicle mitochondrial transfer. *Am J Respir Crit Care Med*. (2017) 196:1275–86. doi: 10.1164/rccm.201701-0170OC

frontiers | Frontiers in Medicine

TYPE Original Research
PUBLISHED 23 June 2023
DOI 10.3389/fmed.2023.1181286

OPEN ACCESS

EDITED BY
Shahd Horie,
University of Galway, Ireland

REVIEWED BY
Norma Alva,
University of Barcelona, Spain
Daniel O'Toole,
University of Galway, Ireland

*CORRESPONDENCE
Wantie Wang
✉ wwt@wmu.edu.cn
Fangyan Wang
✉ fangyan_wang@wmu.edu.cn

†These authors have contributed equally to this work and share first authorship

RECEIVED 07 March 2023
ACCEPTED 05 June 2023
PUBLISHED 23 June 2023

CITATION
Liu X, Pan B, Wang X, Xu J, Wang X, Song Z, Zhang E, Wang F and Wang W (2023) Ischemia/reperfusion-activated ferroptosis in the early stage triggers excessive inflammation to aggregate lung injury in rats.
Front. Med. 10:1181286.
doi: 10.3389/fmed.2023.1181286

Ischemia/reperfusion-activated ferroptosis in the early stage triggers excessive inflammation to aggregate lung injury in rats

Xiujie Liu[1,2†], Binhui Pan[3†], Xiaoting Wang[1,2†], Junpeng Xu[1,2], Xinyu Wang[1,2], Zhengyang Song[1,2], Eryao Zhang[4], Fangyan Wang[1,2*] and Wantie Wang[1,2*]

[1]School of Basic Medical Science, Wenzhou Medical University, Wenzhou, China, [2]Institute of Ischemia/Reperfusion Injury, Wenzhou Medical University, Wenzhou, China, [3]Nephrology Department, Wenzhou Central Hospital, Wenzhou, China, [4]Department of Gastroenterology, The Second Affiliated Hospital and Yuying Children's Hospital of Wenzhou Medical University, Wenzhou, China

Objective: Lung ischemia/reperfusion injury (LIRI) is a clinical syndrome of acute lung injury that occurs after lung transplantation or remote organ ischemia. Ferroptosis and inflammation are involved in the pathogenesis of LIRI according to the results of several studies on animal models. However, the interactive mechanisms between ferroptosis and inflammation contributing to LIRI remain unclear.

Methods: HE staining and indicators of oxidative stress were used to evaluated the lung injury. The reactive oxygen species (ROS) level was examined by DHE staining. The quantitative Real-time PCR (qRT-PCR) and western blot analysis were employed to detect the level of inflammation and ferroptosis, and deferoxamine (DFO) was used to assess the importance of ferroptosis in LIRI and its effect on inflammation.

Results: In the present study, the link of ferroptosis with inflammation was evaluated at reperfusion 30-, 60- and 180-minute time points, respectively. As the results at reperfusion 30-minute point shown, the pro-ferroptotic indicators, especially cyclooxygenase (COX)-2 and acyl-CoA synthetase long-chain family member 4 (ACSL4), were upregulated while the anti-ferroptotic factors glutathione peroxidase 4 (GPX4), cystine-glumate antiporter (XCT) and ferritin heavy chain (FTH1) were downregulated. Meanwhile, the increased level of interleukin (IL)-6, tumor necrosis factor alpha (TNF-α) and IL-1β were observed beginning at reperfusion 60-minute point but mostly activated at reperfusion 180-minute point. Furthermore, deferoxamine (DFO) was employed to block ferroptosis, which can alleviate lung injury. Expectedly, the survival rate of rats was increased and the lung injury was mitigated containing the improvement of type II alveolar cells ultrastructure and ROS production. In addition, at the reperfusion 180-minute point, the inflammation was observed to be dramatically inhibited after DFO administration as verified by IL-6, TNF-α and IL-1β detection.

Conclusion: These findings suggest that ischemia/reperfusion-activated ferroptosis plays an important role as the trigger for inflammation to further deteriorate lung damages. Inhibiting ferroptosis may have therapeutic potential for LIRI in clinical practice.

KEYWORDS

ferroptosis, lung, ischemia/reperfusion injury, inflammation cytokines, rat

1. Introduction

Lung ischemia/reperfusion injury (LIRI) is a common risk factor for adverse outcomes occurring when oxygen supply to the lung has been compromised, followed by a period of reperfusion (1–3). The accumulation of lipid reactive oxygen species (ROS) induced by ischemia/reperfusion (IR) and excessive inflammation is considered the main pathogenesis for exacerbating lung tissue damages (4, 5). However, traditional antioxidative and anti-inflammatory properties are unable to completely abrogate the subsequent LIRI. Therefore, it is urgent to explore the underlying mechanisms and targeted treatments for LIRI.

Ferroptosis has been recently identified as an iron- and lipid hydroperoxide-dependent non-apoptotic cell death in numerous clinical pathologies such as intestinal IR injury, myocardial infarction, and renal failure (6, 7). It has been reported that the acyl-CoA synthetase long-chain family member (ACSL4) located in the lipid membrane initiates ferroptosis (8). Some core genes related to the lipid peroxide removal system such as cystine/glutamic acid transporter (XCT) and glutathione peroxidase 4 (GPX4) have been also found to be involved in the suppression of ferroptosis (9, 10). GPX4 is known for its ability to reduce lipid hydroperoxides and other reactive oxygen species (ROS) using glutathione (GSH) as an electron donor. When GPX4 reacts with lipid hydroperoxides, GSH provides the reducing power necessary to convert the hydroperoxide into its corresponding alcohol. This reaction also regenerates the active form of GPX4, allowing it to continue to scavenge ROS and protect the cell from oxidative damage. As evidence shows, lung IR increased the tissue iron content and lipid peroxidation accumulation, along with key protein (GPX4 and ACSL4) expression alteration during reperfusion. Moreover, inhibition of ferroptosis mitigated ferroptotic damage in IR-induced lung injury by reducing lipid peroxidation and increasing the glutathione and GPX4 levels, suggesting that ferroptosis is correlated with LIRI (11). However, the specific role of ferroptosis in LIRI needs further exploration.

Excessive inflammation, another key contributor to LIRI, has been reported to be triggered by necroptosis in several animal models (12–14); however, in fact, ferroptosis is recognized as more immunogenic than necroptosis due to potentiating a series of inflammatory reactions (15). It is well-known that arachidonic acid (AA) is the main component of cell membrane lipids, and AA is metabolized as a precursor of bioactive pro-inflammatory mediators mainly through the cyclooxygenase (COX) and lipoxygenase (LOX) pathways, which are also core pathways for ACSL4, contributing to ferroptosis. In particular, ferroptosis inhibitors have been shown to have anti-inflammatory effects in models of neurological disorders, intracerebral hemorrhage, and acute kidney injury (16–18). IL-6 and TNF-α, playing a key role in the inflammatory reactions through upregulating cytokines, cyclooxygenase, adhesion molecules, and chemokines, were reported to promote the ERK pathway in different organ IR models (19–21). However, the interaction between ferroptosis and inflammation needs further investigation in LIRI.

In this study, we sought to elucidate the specific role of ferroptosis and the interaction between ferroptosis and inflammation in LIRI. To figure out the underlying mechanism, we formulated three different reperfusion points to investigate both ferroptotic and inflammatory indicators and found that key protein GPX4 and ACSL4 expression systems were altered at the 30-min reperfusion point, while interleukin (IL)-6 and tumor necrosis factor-alpha (TNF-α) were upregulated at the 180-min reperfusion point. Furthermore, inhibition of ferroptosis can ameliorate lung injury through inflammation depression. Evidenced by the improvement of lung functions in lung damage, we hypothesize that ferroptosis triggers excessive inflammation in LIRI, and inhibition of ferroptosis would serve as a promising treatment for acute lung diseases.

2. Methods

2.1. Rat model of lung IR injury

Male Sprague–Dawley (SD) rats weighing 220–270 g were purchased from Weitonglihua (Beijing, China), and the rats were fed standard food and water and were acclimated to the environment before use. They were anesthetized and subjected to IR according to the protocols approved by the Animal Care and Use Committee of the University of Wenzhou Medical University (wydw2023-0099).

A total of 60 male SD rats were randomly divided into five groups, including the sham operation group (control group), 30-min lung ischemia–reperfusion (IR) group (IR_{30} group), 60-min lung IR group (IR_{60} group), 180-min lung IR group (IR_{180} group), and deferoxamine (DFO) pretreatment group (IR_{30}+DFO and IR_{180}+DFO group). Rats in the sham operation group did not undergo other procedures, except for opening the left chest. The left hilum of rats in the IR group was clamped with a non-invasive vascular clamp to establish an ischemic model. After 30 min, the vascular clamp was released, and the rats underwent reperfusion for 30, 60, and 180 min. As for rats in the IR_{30}+DFO group and IR_{180}+DFO group, 100 mg/kg of DFO was intraperitoneally injected 1 h before clamping the left hilar (22). Each rat was injected with 500 μl of DFO solution using physiological saline as a solvent, while the control rats were injected with an equivalent volume of physiological saline, and the rest are the same as the IR_{30} or IR_{180} group.

2.2. Survival experiment

A total of 30 male SD rats were randomly divided into three groups, including the control group, IR group, and IR + DFO group. Rats in the control group were opened to the left chest for 30 min and then sutured. The left hilar of rats in the IR group were clamped for 30 min and then sutured. As for rats in the DFO pretreatment group, 100 mg/kg of DFO was intraperitoneally injected 1 h before clamping the left hilar, and the rest are the same as the IR group. All the rats were kept warm on an electric blanket.

2.3. The wet–dry weight ratio experiment

After rats were sacrificed, part of the lungs was cut and weighed as the wet weight. Then, all the lungs were put in a constant temperature oven for 48 h and weighed as the dry weight.

2.4. Hematoxylin–eosin (HE) staining

The lungs were retrieved from indicated animals, and sections were prepared for HE staining. The staining was performed using the standard protocol. The general histopathology examination is under a light microscope (Olympus, Tokyo, Japan).

2.5. Detection of ROS fluorescence levels

Dihydroethidium (DHE) was used to interact with intracellular superoxide anions to create ethidium and 2-hydroxyethidium bromide, a bright red fluorescent complex that may be used to measure the concentration of superoxide anions by measuring the intensity of the fluorescence. DHE (10 mmol/L, Beyotime Institute of Biotechnology, Shanghai, China) was incubated with frozen sections that were sectioned on a cryostat microtome (Leica, Wetzlar, Germany), 5 μm thick, and mounted onto glass slides (CITOTEST, Jiangsu, China), at 37°C, in the dark. The slices mounted by Antifade Solution were examined under an orthographic microscope after being rinsed three times in PBS.

2.6. Measurement of malonaldehyde (MDA), glutathione (GSH), and Fe

Malondialdehyde (MDA) in the degradation products of lipid peroxide can be condensed with thiobarbituric acid (TBA) to form a red product with a maximum absorption peak at 532 nm. The substrate of this method is thiobarbituric acid. According to the manufacturer's instructions, lung samples were homogenized with 0.9% NaCl and centrifuged to extract the supernatant. MDA, GSH, and Fe were quantified in accordance with the detection assays' directions (A006-2-1, A003-1, and A039-2-1, Nanjing Jiancheng Bioengineering Institute, Nanjing, China). MDA, GSH, and Fe levels were standardized to the level of total protein.

2.7. Enzyme-linked immunosorbent assay (ELISA) detection of the level of IL-6 and TNF-α in the lung

ELISA kits were purchased from Elabscience (Wuhan, China), and the level of IL-6 (E-EL-R0015c, Elabscience) and TNF-α (E-EL-R2856c, Elabscience) detection was detected following the instruction provided.

2.8. Transmission electron microscope (TEM) analysis

The rats were sacrificed after reperfusion, and the lung was excised and rinsed with precooled PBS (pH 7.4). A portion of the lung was incubated in 2.5% glutaraldehyde for the whole night. With a vibratome, 50-um thick slices of the lung sample were sliced. Then, 1% osmium tetroxide was used to postfix the targeted lung for 1 h; then, the tissue was dehydrated in a series of graded ethanol and embedded in epoxy resin. The polymerization was performed at 80°C for 24 h. Next, 100-nm thick ultrathin sections were cut, stained with uranyl acetate and lead citrate, and observed under a JEM2000EX TEM (JEOL, Tokyo, Japan). Five fields were randomly selected for each sample to examine mitochondria with ferroptosis features.

2.9. Western blot analysis

Total protein samples were extracted from tissues using RIPA lysis buffer (Yamei, Shanghai, China). Protein concentrations were determined using a BCA protein detection kit (Beyotime Institute of Biotechnology, Shanghai, China). Proteins were separated using 10% SDS-PAGE and transferred to polyvinylidene fluoride membranes. Membranes were blocked in 5% skimmed milk and then incubated with the primary antibodies ACSL4 (ab155282, Abcam, 1:10,000), transferrin receptor 1 (TFR1) (A5865, ABclonal, 1:1,000), ferritin heavy chain (FTH1) (ab65080, Abcam, 1:1,000), XCT (Abcam, ab175186, 1:5000), GPX4 (Abcam, ab125066, 1:5000), and GAPDH (0494-1-AP, Proteintech,1:1,000) at 4°C overnight. After washing three times with tris-buffered saline, the membranes were incubated with appropriate anti-rabbit or anti-mouse secondary antibodies at room temperature for 1 h. Imprinting was observed using chemiluminescence (Yamei, Shanghai, China) and an Odyssey imaging system (Li-Cor-Biosciences, NE).

2.10. Quantitative real-time PCR analysis

Total RNA was extracted with TRIzol reagent (Yamei, Shanghai, China) from the lung tissue and reverse-transcribed to cDNA using a kit (Vazyme, Nanjing, China). The cDNA obtained was subjected to PCR using primers designed for COX-2, solute carrier family 39, member 14 (SLC39A14), ACSL4, GPX4, IL-6, IL-1β, TNF-α, and caspase3. The primer sequences are shown in Supplementary Table 1. Gene expression was determined using the SYBR Green kit (Vazyme, Nanjing, China), according to the instructions. All the results were normalized against β-actin expression using the Thermal Cycler Dice Real Time system (TaKaRa Company, Japan).

2.11. Statistical analysis

GraphPad Prism version 9.0 (GraphPad Software, San Diego, CA) was used for statistical treatment. Experimental data were shown as the mean ± SD. Two-tailed unpaired Student's *t*-test and one-way ANOVA with Tukey's correction were used for all comparisons of rat-related experiments. A *P*-value of <0.05 was considered significant. The sample distribution was determined using a Kolmogorov–Smirnov normality test.

3. Results

3.1. Ferroptosis is activated by ischemia–reperfusion at an early stage in LIRI

Oxidative stress is one of the main pathological mechanisms in LIRI that can induce excessive lipid peroxidation, which is also a characteristic of ferroptosis (23). Therefore, to evaluate ferroptosis sensitivity after reperfusion in the lung, we determined the level of ROS under reperfusion conditions. As shown in Figure 1A, DHE staining has been employed to assess the level of ROS induced after reperfusion at different times. Compared with the control group, the ROS level increased at the 30-min reperfusion point and decreased at the 60- and 180-min reperfusion points in IR group, which strongly suggested that oxidative stress may play a pivotal role in the early stage of LIRI, particularly at the 30-min reperfusion point. Meanwhile, HE staining showed that IR caused the disruption of lung structure, alveolar damage, and red blood cell aggregation. Similar to the above results, MDA, another essential factor for ferroptosis execution, showed a significant increase, while the reduction of the GSH level and increased Fe cytoplasmic accumulation were observed in the early phase (Figure 1B). In addition, the mRNA level of key ferroptotic factors COX-2, SLC39A14, ACSL4, GPX4, and XCT was upregulated at the early reperfusion stage (Figures 1C, D). Meanwhile, Western blot analysis showed that these anti-ferroptotic proteins such as GPX4, XCT, and FTH1 were downregulated, while pro-ferroptotic proteins ACSL4 and TFR1 were upregulated at the early phase after reperfusion (Figure 1E). These findings indicate that ferroptosis induced by IR occurs at an early stage.

3.2. Inflammation erupts following ferroptosis in LIRI

Since ferroptosis is likely to be a trigger of inflammation, we further investigated some inflammation cytokines occurring at different reperfusion stages in LIRI. As results shown in Figure 2A, the gene expression of inflammatory cytokines IL-6, TNF-α, and IL-1β were remarkably increased during prolonged reperfusion along with the upregulated level of caspase 3. To reconfirm the above results, ELISA detection was used to examine the level of IL-6 and TNF-α. As expected, the level of the two key inflammatory cytokines was upregulated at the 180-min reperfusion point (Figure 2B). Furthermore, Western blot analysis of total ERK showed that the ERK increased along with the extension of reperfusion time (Figure 2C). As a result, excessive inflammation erupts following ferroptosis in LIRI.

3.3. DFO attenuates lung damage by inhibiting ferroptosis in LIRI

The survival experiment has been carried out to further elucidate the significance of ferroptosis in LIRI. As the result shown, the survival rate of the IR group was just 40%, but while using the ferroptosis inhibitor DFO, the survival rate significantly increased to 100%, indicating that the ferroptosis plays an important role in LIRI (Figure 3A). In addition, the lung tissue wet–dry ratio showed that DFO relieves pulmonary edema induced by IR (Figure 3B). Additionally, the results of DHE staining showed that IR resulted in an accumulation of ROS, which could be apparently repressed by DFO (Figure 3C). Meanwhile, TEM results at 25,000 magnification showed that IR resulted in rupture of the outer mitochondrial membrane after reperfusion; however, similar features were not observed with DFO treatment (as yellow arrows in Figure 3C). It is reported that MDA and GSH serve key roles in maintaining the balance of oxidation and reduction. Along with the increase of MDA and Fe induced by IR, a decrease of GSH was observed in LIRI which could be reversed by DFO (Figure 3D). The results of Western blot showed that GPX4, FTH1, and XCT were upregulated while TFR1 and ACSL4 were reduced after DFO treatment (Figure 3E). Taken collectively, these results suggest that the ferroptosis inhibitor DFO significantly attenuates the lung injury through inhibiting ferroptosis.

3.4. DFO mitigates lung damage by suppressing inflammation

To investigate whether ferroptosis signals contribute to inflammation, the levels of inflammation cytokines were examined after 180 min of reperfusion in LIRI. The results of qRT-PCR analysis showed that DFO dramatically inhibited the levels of IL-6, TNF-α, IL-1β, and caspase 3 (Figure 4A). Moreover, ELISA detection of IL-6 and TNF-α reconfirmed that DFO can suppress inflammation, suggesting that ferroptosis triggers excessive inflammation in LIRI (Figure 4B). Expectedly, the increased total protein level of ERK was inhibited at the 180-min reperfusion phase (Figure 4C). In addition, MDA, GSH, and Fe levels were improved by DFO (Figure 4D). HE staining also showed that lung damage was relieved after DFO treatment (Figure 4E). Therefore, the results above imply that ferroptosis triggers inflammation and the use of ferroptosis inhibitors can suppress inflammation to mitigate lung damage.

4. Discussion

Given that ferroptosis and inflammation are increasingly reported to play significant roles in acute lung injury pathogenesis (24, 25), however, the link of ferroptosis to inflammation in LIRI is still unclear and needs to further explore the possible mechanisms. It has been reported that DFO, targeting iron excess, which was widely utilized to inhibit ferroptosis in animal research, can significantly mitigate renal injury by restraining inflammation (26). Our study found that ferroptosis was activated by IR in the early stage of reperfusion, and inhibition of ferroptosis can mitigate lung damage by depressing excessive inflammation.

Herein, we showed the time variation of ferroptosis in LIRI, which is almost compatible with a previous study of intestinal ischemia–reperfusion (27). By controlling the level of cellular iron and the state of lipid peroxidation, numerous substances took part in ferroptosis. It has been suggested that ACSL4, a key

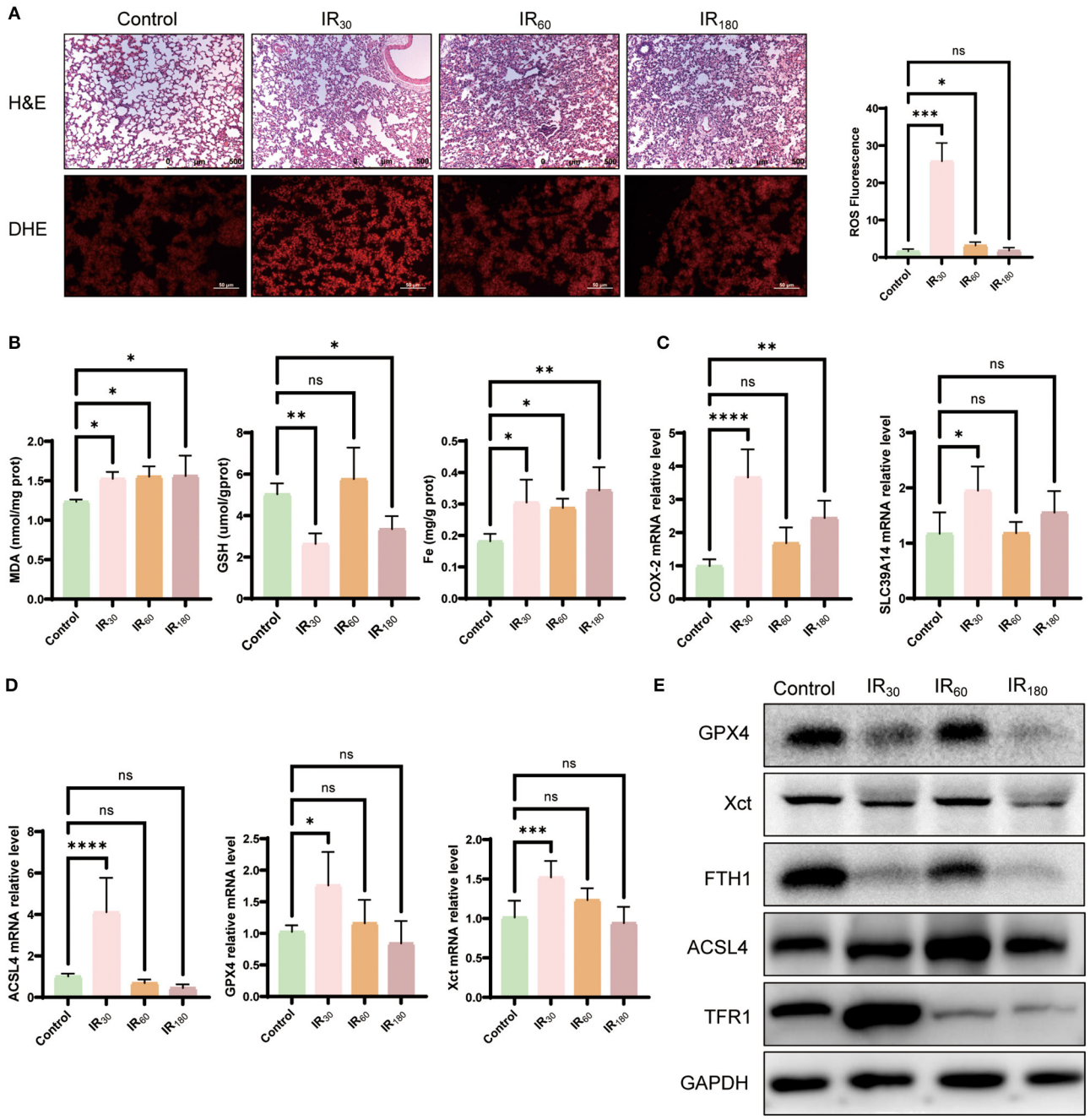

FIGURE 1
Ferroptosis is activated by ischemia–reperfusion at an early stage in LIRI. **(A)** HE and DHE staining of the lung ($n = 3$/group). **(B)** Levels of MDA, GSH, and Fe in the lung tissue ($n = 5$/group). **(C)** qRT-PCR analysis of COX-2 and SLC39A14 in the lung ($n = 5$/group). **(D)** qRT-PCR analysis of ACSL4, GPX4, and XCT ($n = 5$/group). **(E)** Western blot analysis of GPX4, XST, FTH1, ACSL4, and TFR1 in the lung ($n = 3$/group). Data are expressed as mean ± standard deviation. A one-way ANOVA was used to analyze statistical differences; $^{*}P < 0.05$, $^{**}P < 0.01$, $^{***}P < 0.001$, and $^{****}P < 0.0001$.

enzyme involved in the creation of phospholipids that contain polyunsaturated fatty acids, contributes to lipid peroxidation and the ensuing ferroptosis (8). Increased ACSL4 was captured beginning at the 30-min reperfusion point in the current study, declaring that the lung cells were undergoing ferroptosis. In addition, it is well-known that GPX4, a core gene against ferroptosis through lipid hydroperoxides clearance, is influenced by the GSH level in its activity (28). The generation of GSH can be impacted by the glutamate/cysteine antiporter solute carrier family 7 member 11 (SLC7A11), which can influence cysteine absorption (29). Consistently, the reduction of SLC7A11 and GSH, leading to a weakened GPX4 level, was observed, which reconfirmed that ferroptosis happened in the early stage of reperfusion in LIRI. Inhibiting ferroptosis has been proposed as a potential target for several disorders since it is linked to numerous pathophysiological processes. In this study, GPX4 was shown to be significantly

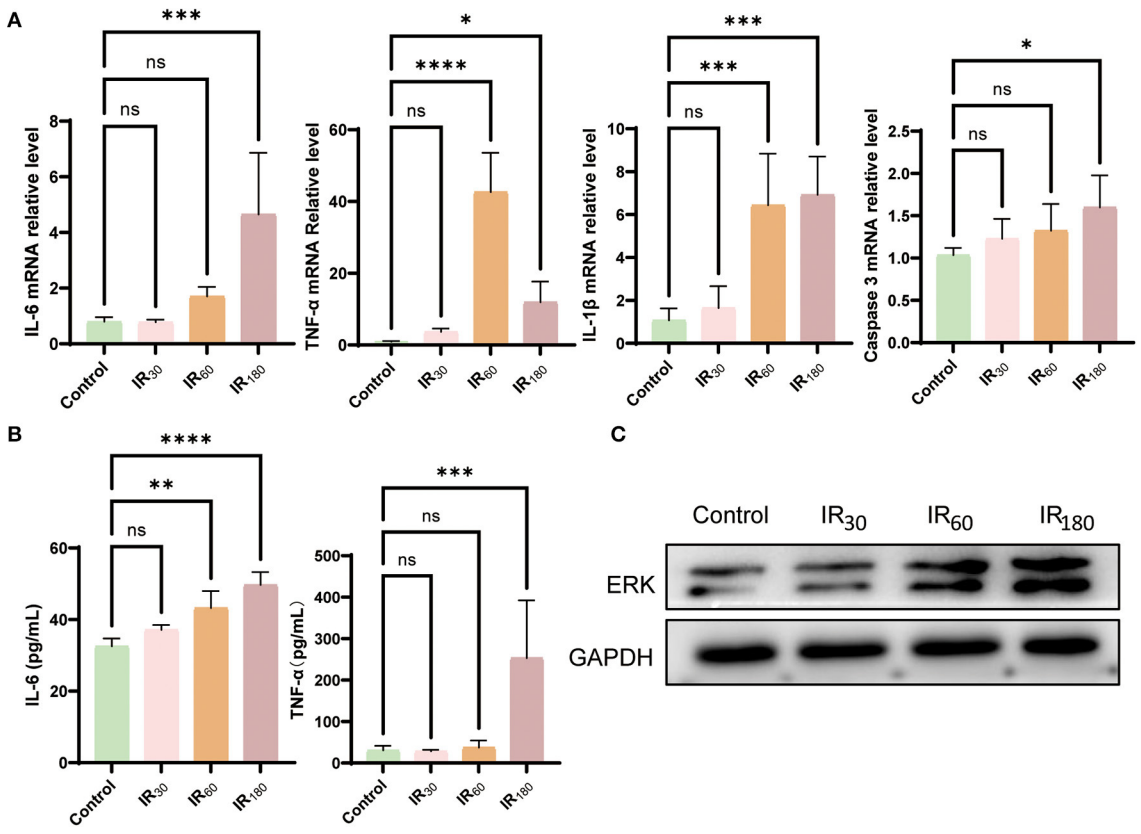

FIGURE 2
Inflammation erupts following ferroptosis in LIRI. **(A)** qRT-PCR analysis of IL-6, TNF-α, IL-1β, and caspase 3 in the lung ($n = 5$/group). **(B)** ELISA detection of IL-6 and TNF-α in the lung ($n = 5$/group). **(C)** Western blot analysis of total ERK in the lung ($n = 3$/group). Data are expressed as mean ± standard deviation. A one-way ANOVA was used to analyze statistical differences; $^{*}P < 0.05$, $^{**}P < 0.01$, $^{***}P < 0.001$, and $^{****}P < 0.0001$.

decreased after reperfusion of 30 min, verified by the level of GSH and XCT. The transient induction of GPX4 at 60 min of reperfusion observed in this study may be induced by the transient profit under a period of compensation response. The decreased GPX4 expression was found in prolonged reperfusion, similarly to other anti-ferroptotic factors FTH1 and XCT. However, the complete impact of ferroptosis on the pathogenesis of LIRI presumably is more complicated, and further research is warranted.

In recent years, accumulating studies demonstrate that inflammation is directly associated with iron and lipid metabolism, which could be triggered by various acute injuries in both humans and animals (30, 31). Ferroptosis is, therefore, believed to play a pathogenic role in LIRI, combining oxidative stress and inflammatory responses linked to iron and lipid metabolism. The well-known ferroptosis biomarker COX-2 accelerates the metabolism of AA and increases inflammation by secreting inflammatory signaling molecules (32), which implies that ferroptosis links inflammation through the activation of cyclooxygenase (33). Moreover, it has been reported that hepatic ferroptosis plays an important role as the trigger for initiating inflammation in non-alcoholic steatohepatitis, showing that the expressions of TNF-α, IL-6, and IL-1β were significantly upregulated following ferroptosis (34). Additionally, evidence exhibited that ferroptosis inhibitors can block inflammatory responses in psoriasis with the reduced production of cytokines including TNF-α, IL-6, IL-1α, IL-1β, IL-17, IL-22, and IL-23 (35). In our study, the inflammatory cytokines, including TNF-α, IL-6, and IL-1β, were also found to be greatly increased in the beginning at the 60-min reperfusion points; however, this increase could be inhibited during DFO administration, which revealed a close connection to the initial ferroptosis.

The ERK signal pathway has been well-researched in various acute injuries covering LIRI (20, 36, 37). As a previous study evidenced, ERK expression was significantly suppressed to attenuate the IR-induced lung injury during the administration of preconditioning anti-vascular endothelial growth factor antibody, which suggests that ERK plays a vital role in LIRI, meaning that there must be a complicated link between ERK and ferroptosis (38). It has been reported that ERK could regulate ferritinophagy and inflammation, contributing to ferroptosis in macrophage (39). However, in the current study, ferroptosis was found to be activated by IR in the early stage of reperfusion, while increased ERK was observed at the following reperfusion. Interestingly, the increased ERK can be inhibited after DFO treatment, revealing that ERK might be triggered by ferroptosis. In brief, the interaction between ERK and ferroptosis needs further exploration.

10.3389/fmed.2023.1181286

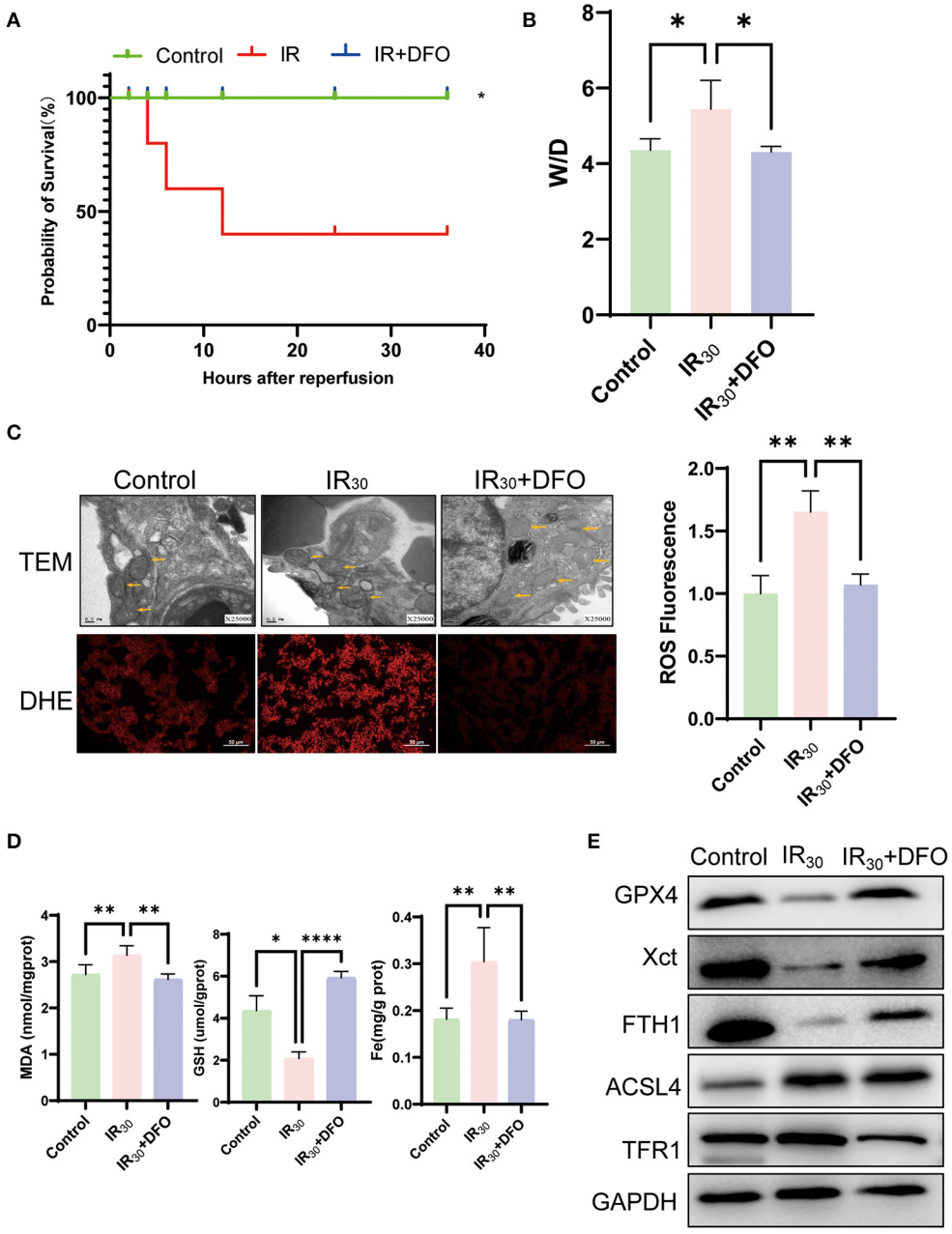

FIGURE 3
DFO attenuates lung damage by inhibiting ferroptosis in LIRI. **(A)** The survival rate of rats after IR operation ($n = 10$/group). **(B)** Wet–dry weight ratio of the lung ($n = 5$/group). **(C)** TEM analysis and DHE staining of the lung ($n = 3$/group), and TEM results were at 25,000 × magnification, and yellow arrows show mitochondria. **(D)** Levels of MDA, GSH, and Fe in the lung tissue ($n = 5$/group). **(E)** Western blot analysis of GPX4, XCT, FTH1, ACSL4, and TFR1 in the lung ($n = 3$/group). Data are expressed as mean ± standard deviation. A one-way ANOVA was used to analyze statistical differences; $^{*}P < 0.05$, $^{**}P < 0.01$, and $^{****}P < 0.0001$.

5. Conclusion

In this study, we established a LIRI model to explore the underlying mechanism. The relationship between inflammation and ferroptosis was evaluated through the related indicators, showing that the pro-ferroptotic markers COX-2 and ACSL4 were upregulated and anti-ferroptotic genes GPX4, XCT, and FTH1 were depressed. Additionally, the level of IL-6, TNF-α, and IL-1β, especially ERK, were observed to be increased following ferroptosis, suggesting that ferroptosis is activated by IR in the early reperfusion stage, which is the initiator of subsequent inflammation in LIRI. Furthermore, DFO significantly ameliorated lung injury, including improvement in type II alveolar cells' ultrastructure and reactive oxygen species (ROS) production, accompanied by a substantial reduction in the levels of IL-6, TNF-α, and IL-1β, which implied that the TNF-α/IL-6-ERK pathway is the crucial role to lung damage. Note that inhibition of ferroptosis with DFO can depress inflammation and thus attenuate LIRI,

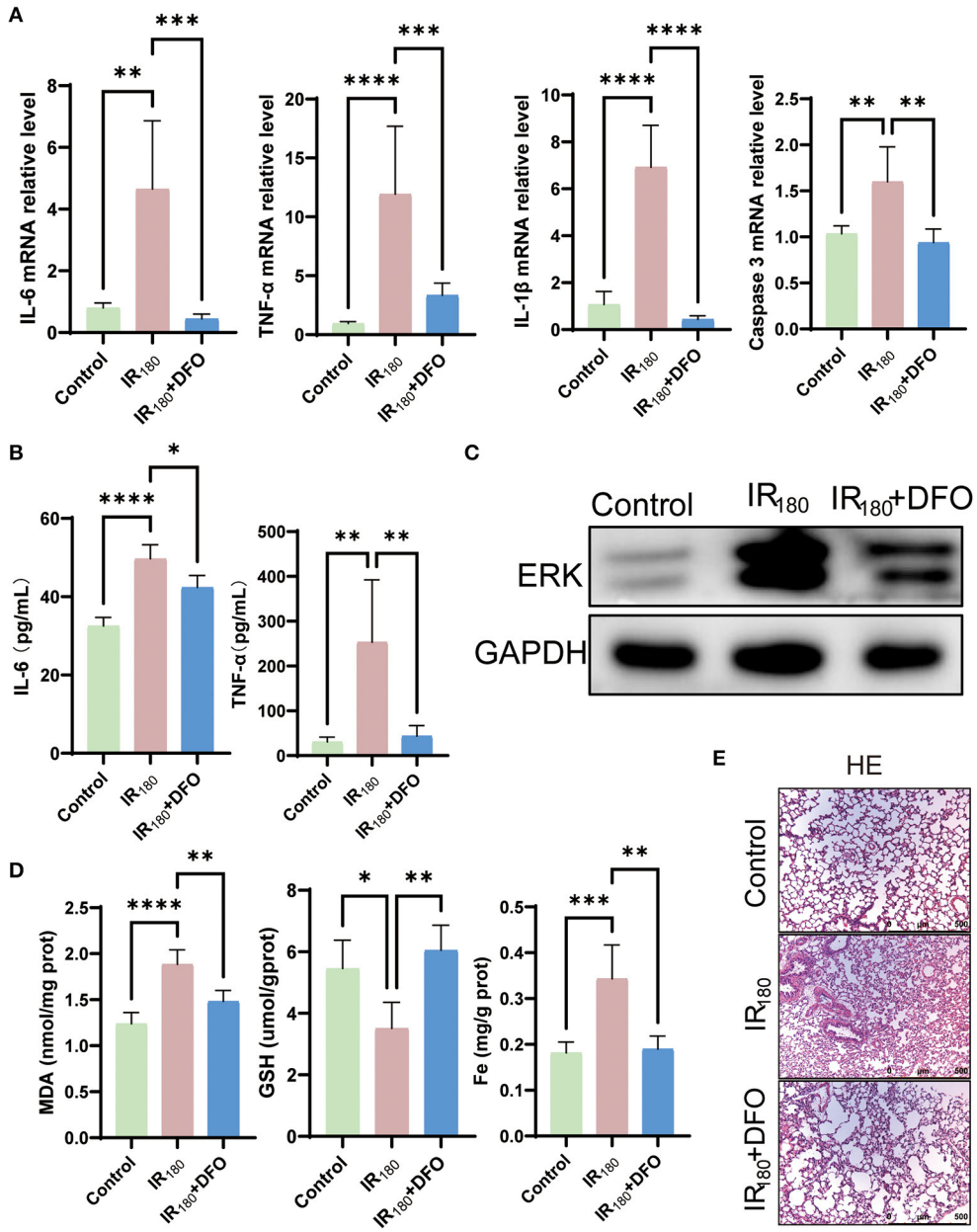

FIGURE 4
DFO mitigates lung damage by suppressing inflammation. **(A)** qRT-PCR analysis of IL-6, TNF-α, IL-1β, and caspase 3 in the lung ($n = 5$/group). **(B)** ELISA detection of IL-6 and TNF-α in the lung ($n = 5$/group). **(C)** Western blot analysis of total ERK in the lung ($n = 3$/group). **(D)** Levels of MDA, GSH, and Fe in the lung tissue ($n = 5$/group). **(E)** HE staining of the lung ($n = 3$/group). Data are expressed as mean ± standard deviation. A one-way ANOVA was used to analyze statistical differences; $^{*}P < 0.05$, $^{**}P < 0.01$, $^{***}P < 0.001$, and $^{****}P < 0.0001$.

which can provide the clinical value for various ferroptosis-related diseases. However, this study only employed male rats, which has limitations, and more experiments need to be carried out in future.

Data availability statement

The original contributions presented in the study are included in the article/Supplementary material, further inquiries can be directed to the corresponding author.

Ethics statement

The animal study was reviewed and approved by Experimental Animal Ethics Committee of Wenzhou Medical University.

Author contributions

WW and FW designed the study. XL and BP analyzed and interpreted data, generated figures and tables, and drafted the manuscript with XiaW. JX and XinW contributed to manuscript drafting. ZS and EZ reviewed and corrected the

manuscript. All authors contributed to the article and approved the submitted version.

Funding

This study was supported by the Medical Health Science and Technology Project of Zhejiang Province of China under Grant No. 2022KY1070 and by Wenzhou Basic Scientific Research Project under Grant No. Y20210083.

Conflict of interest

The authors declare that the research was conducted in the absence of any commercial or financial relationships that could be construed as a potential conflict of interest.

Publisher's note

Supplementary material

The Supplementary Material for this article can be found online at: https://www.frontiersin.org/articles/10.3389/fmed.2023.1181286/full#supplementary-material

References

1. Almeida FM, Battochio AS, Napoli JP, Alves KA, Balbin GS, Oliveira-Junior M, et al. Creatine supply attenuates ischemia-reperfusion injury in lung transplantation in rats. *Nutrients.* (2020) 12:2765. doi: 10.3390/nu12092765

2. Motoyama H, Chen F, Hijiya K, Kondo T, Ohsumi A, Yamada T, et al. Plasmin administration during *ex vivo* lung perfusion ameliorates lung ischemia-reperfusion injury. *J Heart Lung Transplant.* (2014) 33:1093–9. doi: 10.1016/j.healun.2014.06.004

3. Maeda K, Ruel M. Prevention of ischemia-reperfusion injury in cardiac surgery: therapeutic strategies targeting signaling pathways. *J Thorac Cardiovasc Surg.* (2015) 149:910–1. doi: 10.1016/j.jtcvs.2014.11.067

4. Ferrari RS, Andrade CF. Oxidative stress and lung ischemia-reperfusion injury. *Oxid Med Cell Longev.* (2015) 2015:590987. doi: 10.1155/2015/590987

5. Liang S, Wang Y, Liu Y. Dexmedetomidine alleviates lung ischemia-reperfusion injury in rats by activating PI3K/Akt pathway. *Eur Rev Med Pharmacol Sci.* (2019) 23:370–7. doi: 10.26355/eurrev_201901_16785

6. He R, Liu B, Xiong R, Geng B, Meng H, Lin W, et al. Itaconate inhibits ferroptosis of macrophage via Nrf2 pathways against sepsis-induced acute lung injury. *Cell Death Discov.* (2022) 8:43. doi: 10.1038/s41420-021-00807-3

7. Miotto G, Rossetto M, Di Paolo ML, Orian L, Venerando R, Roveri A, et al. Insight into the mechanism of ferroptosis inhibition by ferrostatin-1. *Redox Biol.* (2020) 28:101328. doi: 10.1016/j.redox.2019.101328

8. Doll S, Proneth B, Tyurina YY, Panzilius E, Kobayashi S, Ingold I, et al. ACSL4 dictates ferroptosis sensitivity by shaping cellular lipid composition. *Nat Chem Biol.* (2017) 13:91–8. doi: 10.1038/nchembio.2239

9. Koppula P, Zhuang L, Gan B. Cystine transporter SLC7A11/xCT in cancer: ferroptosis, nutrient dependency, and cancer therapy. *Protein Cell.* (2021) 12:599–620. doi: 10.1007/s13238-020-00789-5

10. Bersuker K, Hendricks JM, Li Z, Magtanong L, Ford B, Tang PH, et al. The CoQ oxidoreductase FSP1 acts parallel to GPX4 to inhibit ferroptosis. *Nature.* (2019) 575:688–92. doi: 10.1038/s41586-019-1705-2

11. Wang Y, Quan F, Cao Q, Lin Y, Yue C, Bi R, et al. Quercetin alleviates acute kidney injury by inhibiting ferroptosis. *J Adv Res.* (2021) 28:231–43. doi: 10.1016/j.jare.2020.07.007

12. Yao D, Zhang S, Hu Z, Luo H, Mao C, Fan Y, et al. CHIP ameliorates cerebral ischemia-reperfusion injury by attenuating necroptosis and inflammation. *Aging.* (2021) 13:25564–77. doi: 10.18632/aging.203774

13. Li W, Terada Y, Tyurina YY, Tyurin VA, Bery AI, Gauthier JM, et al. Necroptosis triggers spatially restricted neutrophil-mediated vascular damage during lung ischemia reperfusion injury. *Proc Natl Acad Sci USA.* (2022) 119:e2111537119. doi: 10.1073/pnas.2111537119

14. Shen B, Mei M, Pu Y, Zhang H, Liu H, Tang M, et al. Necrostatin-1 attenuates renal ischemia and reperfusion injury via meditation of HIF-1alpha/mir-26a/TRPC6/PARP1 signaling. *Mol Ther Nucleic Acids.* (2019) 17:701–13. doi: 10.1016/j.omtn.2019.06.025

15. Tao WH, Shan XS, Zhang JX, Liu HY, Wang BY, Wei X, et al. Dexmedetomidine attenuates ferroptosis-mediated renal ischemia/reperfusion injury and inflammation by inhibiting ACSL4 via alpha2-AR. *Front Pharmacol.* (2022) 13:782466. doi: 10.3389/fphar.2022.782466

16. Qiu W, An S, Wang T, Li J, Yu B, Zeng Z, et al. Melatonin suppresses ferroptosis via activation of the Nrf2/HO-1 signaling pathway in the mouse model of sepsis-induced acute kidney injury. *Int Immunopharmacol.* (2022) 112:109162. doi: 10.1016/j.intimp.2022.109162

17. Kong Y, Li S, Zhang M, Xu W, Chen Q, Zheng L, et al. Acupuncture ameliorates neuronal cell death, inflammation, and ferroptosis and downregulated miR-23a-3p after intracerebral hemorrhage in rats. *J Mol Neurosci.* (2021) 71:1863–75. doi: 10.1007/s12031-020-01770-x

18. Wang C, Chen S, Guo H, Jiang H, Liu H, Fu H, et al. Forsythoside A mitigates Alzheimer's-like pathology by inhibiting ferroptosis-mediated neuroinflammation via Nrf2/GPX4 axis activation. *Int J Biol Sci.* (2022) 18:2075–90. doi: 10.7150/ijbs.69714

19. Xu D, Kong T, Shao Z, Liu M, Zhang R, Zhang S, et al. Orexin-A alleviates astrocytic apoptosis and inflammation via inhibiting OX1R-mediated NF-kappaB and MAPK signaling pathways in cerebral ischemia/reperfusion injury. *Biochim Biophys Acta Mol Basis Dis.* (2021) 1867:166230. doi: 10.1016/j.bbadis.2021.166230

20. Guo J, Yang Y. Parecoxib sodium alleviates ischemia reperfusion-induced pulmonary injury via inhibiting ERK/NF-kappaB and further activating the HIF-1alpha pathway. *Immun Inflamm Dis.* (2022) 10:e684. doi: 10.1002/iid3.684

21. Che H, Lv YF, Liu YG, Hou YX, Zhao LY. Effect of ulinastatin on myocardial ischemia reperfusion injury through ERK signaling pathway. *Eur Rev Med Pharmacol Sci.* (2019) 23:4458–64. doi: 10.26355/eurrev_201905_17957

22. Liu T, Shu J, Liu Y, Xie J, Li T, Li H, et al. Atorvastatin attenuates ferroptosis-dependent myocardial injury and inflammation following coronary microembolization via the Hif1a/Ptgs2 pathway. *Front Pharmacol.* (2022) 13:1057583. doi: 10.3389/fphar.2022.1057583

23. Park MW, Cha HW, Kim J, Kim JH, Yang H, Yoon S, et al. NOX4 promotes ferroptosis of astrocytes by oxidative stress-induced lipid peroxidation via the impairment of mitochondrial metabolism in Alzheimer's diseases. *Redox Biol.* (2021) 41:101947. doi: 10.1016/j.redox.2021.101947

24. Li J, Lu K, Sun F, Tan S, Zhang X, Sheng W, et al. Panaxydol attenuates ferroptosis against LPS-induced acute lung injury in mice by Keap1-Nrf2/HO-1 pathway. *J Transl Med.* (2021) 19:96. doi: 10.1186/s12967-021-02745-1

25. Nie Y, Wang Z, Chai G, Xiong Y, Li B, Zhang H, et al. Dehydrocostus lactone suppresses LPS-induced acute lung injury and macrophage activation through NF-kappaB signaling pathway mediated by p38 MAPK and Akt. *Molecules.* (2019) 24:1510. doi: 10.3390/molecules24081510

26. Vlahakos D, Arkadopoulos N, Kostopanagiotou G, Siasiakou S, Kaklamanis L, Degiannis D, et al. Deferoxamine attenuates lipid peroxidation, blocks interleukin-6 production, ameliorates sepsis inflammatory response syndrome, and confers renoprotection after acute hepatic ischemia in pigs. *Artif Organs.* (2012) 36:400–8. doi: 10.1111/j.1525-1594.2011.01385.x

27. Li Y, Feng D, Wang Z, Zhao Y, Sun R, Tian D, et al. Ischemia-induced ACSL4 activation contributes to ferroptosis-mediated tissue injury in intestinal ischemia/reperfusion. *Cell Death Differ.* (2019) 26:2284–99. doi: 10.1038/s41418-019-0299-4

28. Li K, Lin C, Li M, Xu K, He Y, Mao Y, et al. Multienzyme-like reactivity cooperatively impairs glutathione peroxidase 4 and ferroptosis suppressor protein 1 pathways in triple-negative breast cancer for sensitized ferroptosis therapy. *ACS Nano.* (2022) 16:2381–98. doi: 10.1021/acsnano.1c08664

29. Zhang W, Sun Y, Bai L, Zhi L, Yang Y, Zhao Q, et al. RBMS1 regulates lung cancer ferroptosis through translational control of SLC7A11. *J Clin Invest.* (2021) 131:e152067. doi: 10.1172/JCI152067

30. Johnsson H, Panarelli M, Cameron A, Sattar N. Analysis and modelling of cholesterol and high-density lipoprotein cholesterol changes across the range of C-reactive protein levels in clinical practice as an aid to better understanding of inflammation-lipid interactions. *Ann Rheum Dis.* (2014) 73:1495–9. doi: 10.1136/annrheumdis-2013-203293

31. Pan X, Zhang Z, Liu C, Zhao M, Wang X, Zhai J, et al. Circulating levels of DDIT4 and mTOR, and contributions of BMI, inflammation and insulin sensitivity in hyperlipidemia. *Exp Ther Med.* (2022) 24:666. doi: 10.3892/etm.2022.11602

32. Xu Y, Liu Y, Li K, Yuan D, Yang S, Zhou L, et al. COX-2/PGE2 pathway inhibits the ferroptosis induced by cerebral ischemia reperfusion. *Mol Neurobiol.* (2022) 59:1619–31. doi: 10.1007/s12035-021-02706-1

33. Chen C, Wang D, Yu Y, Zhao T, Min N, Wu Y, et al. Legumain promotes tubular ferroptosis by facilitating chaperone-mediated autophagy of GPX4 in AKI. *Cell Death Dis.* (2021) 12:65. doi: 10.1038/s41419-020-03362-4

34. Tsurusaki S, Tsuchiya Y, Koumura T, Nakasone M, Sakamoto T, Matsuoka M, et al. Hepatic ferroptosis plays an important role as the trigger for initiating inflammation in nonalcoholic steatohepatitis. *Cell Death Dis.* (2019) 10:449. doi: 10.1038/s41419-019-1678-y

35. Shou Y, Yang L, Yang Y, Xu J. Inhibition of keratinocyte ferroptosis suppresses psoriatic inflammation. *Cell Death Dis.* (2021) 12:1009. doi: 10.1038/s41419-021-04284-5

36. Okada M, Yamane M, Yamamoto S, Otani S, Miyoshi K, Sugimoto S, et al. SPRED2 deficiency may lead to lung ischemia-reperfusion injury via ERK1/2 signaling pathway activation. *Surg Today.* (2018) 48:1089–95. doi: 10.1007/s00595-018-1696-x

37. Liu Z, Guan C, Li C, Zhang N, Yang C, Xu L, et al. Tilianin reduces apoptosis via the ERK/EGR1/BCL2L1 pathway in ischemia/reperfusion-induced acute kidney injury mice. *Front Pharmacol.* (2022) 13:862584. doi: 10.3389/fphar.2022.862584

38. Lan CC, Peng CK, Tang SE, Wu SY, Huang KL, Wu CP. Anti-vascular endothelial growth factor antibody suppresses ERK and NF-kappaB activation in ischemia-reperfusion lung injury. *PLoS ONE.* (2016) 11:e0159922. doi: 10.1371/journal.pone.0159922

39. Liu N, Liang Y, Wei T, Zou L, Huang X, Kong L, et al. The role of ferroptosis mediated by NRF2/ERK-regulated ferritinophagy in CdTe QDs-induced inflammation in macrophage. *J Hazard Mater.* (2022) 436:129043. doi: 10.1016/j.jhazmat.2022.129043

frontiers | Frontiers in Medicine

TYPE Review
PUBLISHED 28 June 2023
DOI 10.3389/fmed.2023.1208866

OPEN ACCESS

EDITED BY
Daniel O'Toole,
University of Galway, Ireland

REVIEWED BY
Nektarios Barabutis,
University of Louisiana at Monroe, United States
Nicolas Gendron,
Hôpital Européen Georges Pompidou, France

*CORRESPONDENCE
Melanie Bailey
✉ melanie.bailey@belfasttrust.hscni.net

RECEIVED 19 April 2023
ACCEPTED 05 June 2023
PUBLISHED 28 June 2023

CITATION
Bailey M, Linden D, Guo-Parke H, Earley O, Peto T, McAuley DF, Taggart C and Kidney J (2023) Vascular risk factors for COVID-19 ARDS: endothelium, contact-kinin system.
Front. Med. 10:1208866.
doi: 10.3389/fmed.2023.1208866

Vascular risk factors for COVID-19 ARDS: endothelium, contact-kinin system

Melanie Bailey[1]*, Dermot Linden[1,2], Hong Guo-Parke[2], Olivia Earley[1], Tunde Peto[1,2], Danny F. McAuley[1,2], Clifford Taggart[2] and Joseph Kidney[1]

[1]Mater Infirmorum Hospital, Belfast Health and Social Care Trust, Belfast, United Kingdom, [2]Wellcome - Wolfson Institute for Experimental Medicine, Queen's University Belfast, Belfast, United Kingdom

SARS-CoV-2 binds to ACE2 receptors, expressed within the lungs. Risk factors for hospitalization include hypertension, diabetes, ischaemic heart disease and obesity—conditions linked by the presence of endothelial pathology. Viral infection in this setting causes increased conversion of circulating Factor XII to its active form (FXIIa). This is the first step in the contact-kinin pathway, leading to synchronous activation of the intrinsic coagulation cascade and the plasma Kallikrein-Kinin system, resulting in clotting and inflammatory lung disease. Temporal trends are evident from blood results of hospitalized patients. In the first week of symptoms the activated partial thromboplastin time (APTT) is prolonged. This can occur when clotting factors are consumed as part of the contact (intrinsic) pathway. Platelet counts initially fall, reflecting their consumption in coagulation. Lymphopenia occurs after approximately 1week, reflecting the emergence of a lymphocytic pneumonitis [COVID-19 acute respiratory distress syndrome (ARDS)]. Intrinsic coagulation also induces the contact-kinin pathway of inflammation. A major product of this pathway, bradykinin causes oedema with ground glass opacities (GGO) on imaging in early COVID-19. Bradykinin also causes release of the pleiotrophic cytokine IL-6, which causes lymphocyte recruitment. Thromobosis and lymphocytic pneumonitis are hallmark features of COVID-19 ARDS. In this review we examine the literature with particular reference to the contact-kinin pathway. Measurements of platelets, lymphocytes and APTT should be undertaken in severe infections to stratify for risk of developing ARDS.

KEYWORDS

bradykinin, inflammation, coagulation, endothelium, COVID-19

Introduction

Severe acute respiratory syndrome coronavirus 2 (SARS-CoV-2) has spread around the world rapidly. This novel beta coronavirus, responsible for coronavirus disease of 2019 (COVID-19) may result in a spectrum of illness ranging from asymptomatic infection to severe respiratory failure and death. COVID-19 is extremely contagious and is transmitted *via* respiratory droplets. Viral cell entry is enabled via the SARS-CoV-2 spike protein receptor binding domain (RBD) which attaches to the angiotensin-converting enzyme-2 (ACE2) receptor which is expressed in a wide variety of tissues, including pulmonary epithelial cells and the endothelium. With the help of transmembrane serine protease (TMPRSS2), the virus-receptor complex becomes internalized in cells enabling viral replication within the cell. The principal effects of initial

infection are cough, fever, breathlessness, anosmia, loss of taste and infiltrates on the chest radiograph or computed tomography (CT). These infiltrates are alveolar filling defects, caused initially by oedema. A proportion of patients develop worsening symptoms and require hospitalization, often due to respiratory failure. These patients also develop coagulopathy, abnormal thrombosis, hypotension and acute renal impairment (1). Risk factors for progressive infection and mortality include age, hypertension, diabetes, ischaemic heart disease and obesity (2) suggesting that endothelial pathology may signify a unifying disease mechanism. Pre-existing endothelial dysfunction may cause excessive activation of the contact system in response to SARS-CoV-2 infection. The contact system is a key component of the innate immune response to inflammatory stimuli, tissue injury and infection. It is initiated by the conversion of the circulating zymogen Factor XII (FXII) to its active form FXIIa. This causes synchronous triggering of the intrinsic clotting pathway and the plasma Kallikrein-Kinin System (KKS). Activation of the intrinsic coagulation pathway causes clotting factor consumption (seen as raised APTT) and thrombus formation. Triggering of the KKS leads to the production of bradykinin, resulting in vascular proliferation, vasodilation, oedema, cough and IL-6 release (3). The diverse manifestations of COVID-19 infection could be due to sustained activation of these systems/pathways. Temporal changes in blood markers may reflect the actions of the contact-kinin system.

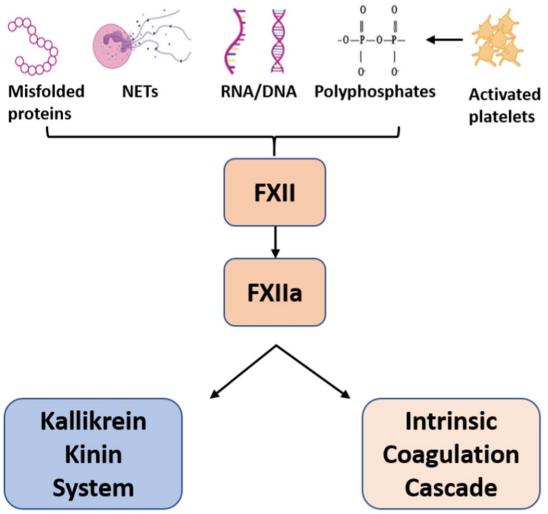

FIGURE 1
Activators of Factor XII. Factor XII is activated upon contact with anionic surfaces leading to dual activation of the Kallikrein-Kinin system and Intrinsic Coagulation cascade.

The contact system and coagulopathy

FXII is a serine protease that circulates in plasma as a single-chain zymogen. After contact with anionic surfaces such as neutrophil extracellular traps (NETs), polyphosphates, activated platelets or DNA released from damaged cells, FXII undergoes autoactivation to FXIIa which triggers the intrinsic clotting cascade via FXI cleavage to generate FXIa.

The subsequent proteolytic cleavage of factors IX and X ultimately leads to thrombin generation, fibrin formation and clotting (Figure 1). Activated partial thromboplastin time (APTT) measures the length of time taken for blood to clot via the intrinsic and common pathways. Prolonged results can indicate factor deficiencies/depletion or the presence of a competing antibody. APTT is often abnormally prolonged in COVID-19 (4). The mechanism behind this is not fully understood. Studies have identified the antiphospholipid antibody, lupus anticoagulant (LA) (5–7). Findings remain controversial as LA assays can be inaccurate in setting of raised C-reactive protein (CRP) or in patients on anticoagulant therapy (8) and these aspects were not always taken into consideration (9). Importantly, APTT prolongation is also found in LA negative COVID-19 patients (10–12). Prothrombin time (PT), fibrinogen and D-dimer levels are often abnormally elevated in COVID-19 (13, 14), and as the incidence of thromboembolism is known to be much higher than hemorrhagic events (15), APTT prolongation may therefore reflect clotting factor depletion.

The contact system and kallikrein kinin system

In addition to triggering the clotting cascade, FXIIa also synchronously activates the KKS; a complex pathway that modulates inflammation, blood pressure control, coagulation and pain (Figure 2). This system is initiated when FXIIa cleaves plasma prekallikrein (PKa) to kallikrein, a serine protease which forms a feedback loop to continue the activation of FXII. Kallikrein then cleaves circulating high-molecular-weight-kininogen (HK), releasing bradykinin and subsequent derivatives. Bradykinin is broken down by ACE receptors. ACE inhibitor drugs are widely used for the treatment of hypertension, heart failure and diabetic nephropathy. Their effects are well established. Between 7 and 25% of people develop a dry cough (3, 16). A lymphocytic alveolitis can also occur (17).

Bradykinin binds to cell receptor B2, a G-protein-coupled receptor which is ubiquitously expressed in most human tissues (18). Further enzymatic processing of bradykinin produces des-Arg-9 bradykinin (DABK), a ligand of receptor B1, which is present on endothelial cells and upregulated in tissue injury and inflammatory states (19). Stimulation of these receptors has a potent effect; inducing vasodilation, vascular proliferation, micro-vascular permeability, oedema and release of pro-inflammatory cytokines including IL-6 and TNF-α (20–22). Nagashima et al. studied lung tissue immunoexpression of B1 and B2 in post mortem lung samples from mechanically ventilated patients with COVID-19 ($n = 24$) and influenza ($n = 10$). Notably, expression of B1 and B2 were significantly increased in both COVID-19 and influenza patients compared to uninfected controls ($n = 11$) (23).

Bradykinin peptides can be generated independently of FXIIa due to the actions of proteases which trigger distal elements of the KKS. Prolylcarboxypeptidase (PRCP), a regulatory protease involved in the renin-angiotensin system (RAS) can cleave PKa to kallikrein (24). However, PRCP activity has been found to be similar in COVID-19 patients and controls (25). Cleavage of HK and kinin generation also occurs by agents other than kallikrein, such as the protease neutrophil elastase (NE), tryptase, cathepsins and proteinase-3 (PR3). These not only cleave HK but liberate bradykinin-like peptides with the ability to act at B2R (26, 27). Neutrophilia occurs frequently in COVID-19 and is associated with poorer

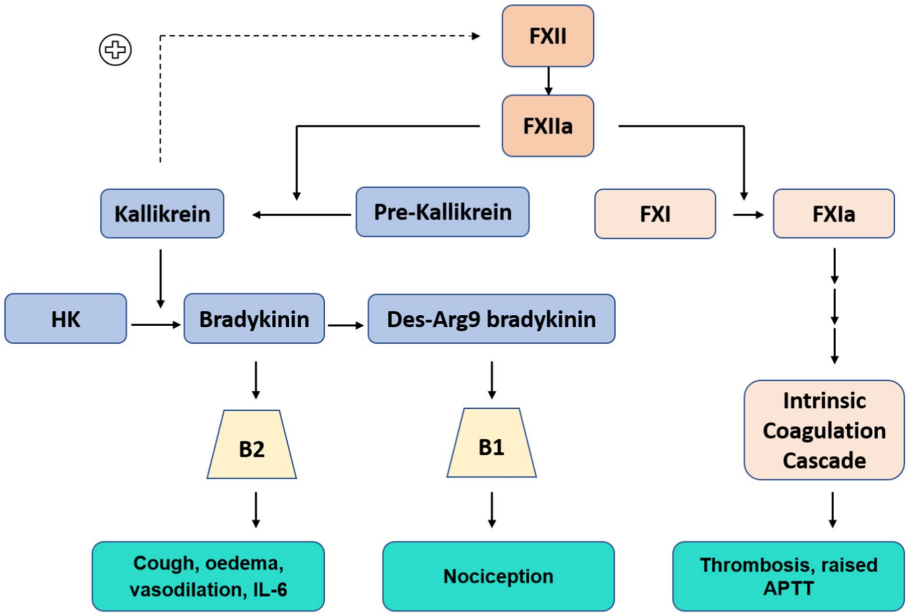

FIGURE 2
Contact Kinin System: Kallikrein-Kinin system (Blue) FXIIa cleaves pre-kallikrein to kallikrein (positive feedback loop to continue FXII activation), kallikrein cleaves high molecular weight kininogen (HK) to produce bradykinin, further processed to Des-Arg9 bradykinin. Bradykinin and Des-Arg9 bradykinin act at receptors B2 and B1, respectively. Intrinsic coagulation cascade (Orange)–abbreviated pathway.

outcomes (28). Neutrophils release a variety of potent enzymes including PR3 and NE (29). PR3 is a destructive protease with microbicidal activity and is capable of extracellular matrix degradation. Furthermore, PR3 can cleave high molecular weight kininogen producing PR3-kinin, which is then processed to bradykinin and des-Arg9-bradykinin in plasma (30). Increased PR3 has been reported in severe COVID-19 (31, 32). NE acts on elastin, collagens and HK - producing E-kinin, which is then cleaved to release bradykinin (26). Compared to healthy controls, progressively increasing NE levels correlated with hospitalization, need for ICU admission and mortality (33).

Factor XII in COVID-19

Wygrecka et al. compared the levels of factor XII (FXII) and its activation products from critically ill COVID-19 patients with samples from influenza patients with severe ARDS (34). FXII was reduced, plasma kallikrein-like activity and HK cleavage products were increased in COVID-19 patients in comparison to influenza ARDS and controls. This shows the decrease in FXII is due to activation (34). A similar pattern of decreased FXII, PKa and HK was reported in a study of 66 intensive care COVID-19 patients (35). Neutrophil extracellular traps (NETS) have been implicated as triggers for the cascade in a study demonstrating the presence of FXIIa alongside NETS in lung parenchyma of COVID-19 patients (36). An increase in serum FXIIa was also seen in a separate group of COVID-19 patients (36). In a study of 128 COVID-19 and 16 healthy controls, admission FXII levels were increased in asymptomatic/ mild/ moderate disease in comparison to controls–possibly reflecting an acute phase response. However, FXII levels were significantly lower in those who progressed to severe disease (37). Importantly this finding is not limited to severely ill COVID-19 patients: reduced FXII levels have also been found in critically ill patients with sepsis (38), likely reflecting increased activation.

Endothelial activity

Pre-existing endothelial pathology may be a priming factor for contact system activation in COVID-19. The endothelium is a complex organ that controls vascular tone, angiogenesis, clotting and the recruitment of leukocytes and platelets. These functions are regulated by expression of cell adhesion molecules such as E-selectin, intracellular adhesion molecule 1 (ICAM-1), vascular cell adhesion molecule 1 (VCAM-1) and thrombomodulin, an anticoagulant glycoprotein. Endothelial cells rapid responses are aided by organelles which function as storage granules called Weibel-Palade bodies. These store P-selectin, Von-Willebrand factor (vWF), eotaxin-3, interleukin-8, tissue-plasminogen activator, angiopoetin-2 (Ang-2), osteoprotegerin and endothelin-1. These are powerful inflammatory and physiological regulators which are rapidly expelled in response to vessel injury or inflammation. Vascular tone is regulated by endothelin-1, a potent vasoconstrictor. Angiopoietin-2, a form of growth factor, can function as a pro or anti-angiogenesis agent depending on inflammatory conditions and the presence or absence of other growth factors (39). P-selectin and vWF promote platelet and leucocyte adhesion. Activated platelets release adhesion molecules, perpetuating endothelial activation and cell recruitment. Von Willebrand factor polymerizes into large multimers that are size regulated by ADAMTS-13 (A Disintegrin And Metalloprotease with ThrombSpondin Motif type 1 motif, member 13), which is reduced in severely ill COVID-19 patients (40–42). This may reflect secondary consumption due to excessive release of vWF–which has been

consistently shown to be markedly raised in the infection (43, 44). In a study examining components secreted from Weibel-palade bodies, blood from 39 patients with moderate/critical/fatal COVID-19 infection had significantly increased levels of plasma vWF, Ang-2 and osteoprotegerin compared to 15 healthy controls (45). When plasma was added to human endothelial cell cultures vWF increased significantly with critical/ fatal case plasma, though not with moderate disease plasma. Furthermore, plasma from fatal cases induced higher intracellular levels, but lower secreted levels of Ang-2, while inducing features of angiogenesis.

COVID-19 infection is also associated with elevated levels of endothelial P-selectin, E-selectin, VCAM-1 and Ang-2 (43, 46–49). At an early stage in the pandemic, Goshua et al. reported a significant increase in vWF factor and P-selectin in both non-ICU and ICU COVID-19 patients compared to controls (46). Notably, disease severity and mortality directly correlated with elevated vWF (46) and this trend has subsequently been shown in further studies (44, 50). Levels of soluble thrombomodulin (sTM) were found to have a mortality correlation (46). Philippe et al. studied results from patients with COVID-19 ($n = 208$) and unaffected controls ($n = 29$) (44). Ang-2, VCAM-1 and E-selectin were included in their analysis. Patients had bloods drawn on admission and were classified into groups (outpatient, non-critical and critical) according to outcomes over next 48 h. Compared to the control group, VCAM-1 was significantly increased in both the critical group and non-critical group. Elevated Ang-2, sTM and E-selectin was only demonstrated in the critical group. None of these markers varied significantly between the non-COVID-19 control group and the outpatient cohort of COVID-19 patients. A markedly different pattern was observed with vWF, with levels significantly elevated in all COVID-19 patients compared to controls. In addition, vWF levels further increased according to disease severity. Both of these results were seen in a smaller study of 50 mild/mod/severe patients and in a study of 28 patients (40, 51).

In a separate hospitalized group, E-selectin levels were raised in severe disease only, but Von Willebrand factor was raised in all patient groups with COVID-19. In 20 of the evaluated patients with mild/mod/severe disease, vWF levels remained elevated in 57% 30 days after admission (52). A larger study of 203 COVID-19 patients found that over 80% had raised vWF levels 3 months after the onset of infection (43). A study of 215 patients investigated endothelial markers in relation to transfer factor (DLCO) 6 months after COVID-19 illness. Patients with the lowest DLCO had higher levels of ICAM-1 and angiopoetin-2 (53). The prolonged lag in normalization may reflect the severity of the endothelial damage occurring during infection. Alternatively, it is possible that patients with persistent, abnormal endothelial markers may have had baseline abnormalities which accentuated their illness.

Viral infection causes oxidative stress and excess protein production in the endoplasmic reticulum. This overwhelms the regulatory unfolded protein response and results in loss of cellular homeostasis (54), which may accentuate the vigorous systemic response to COVID-19 in patients with pre-existing endothelial dysfunction. This includes the known high risk groups of older age, hypertension, ischemic heart disease, obesity, COPD and diabetes. For example, untreated hypertension has been associated with higher levels of vWF and P-selectin (55, 56). Levels improve with treatment though may still remain higher than control results (57). Other studies of hypertensive disorders have also found raised E-selectin (56, 58). Schumacher et al. found that patients with coronary artery disease ($n = 193$) have elevated levels of ICAM-1, VCAM-1 and P selectin compared to healthy controls ($n = 193$) (59). Patients with obesity have elevated levels of chemokines IL-6, TNFα and MCP-1 and increased levels of endothelial ICAM-1, E-selectin, and P-selectin compared to those with a normal BMI (60). Elevated levels of vWF, E-selectin, ICAM-1 and VCAM-1 can be seen in patients with Type II diabetes– and can also precede diagnosis (61–63). Interestingly, increased vWF has also been found in patients experiencing acute COPD exacerbations (64). Hospital admissions due to COPD exacerbations are linked to a markedly increased risk of cardiovascular events (65). Polatli et al. compared levels of vWF in a healthy control group ($n = 16$), patients with stable COPD (n = 33) and patients with acute COPD exacerbations ($n = 26$). They found that the levels were progressively higher between the groups though not reaching statistical significance between stable/acute COPD (66).

Histological features and ACE2

Post-mortem findings from patients with severe COVID-19 lung disease have shown marked endothelial dysfunction, lymphocytic infiltration, intussusceptive angiogenesis and widespread thrombosis with microangiopathy (67). Pathological abnormalities can also be seen in asymptomatic patients. Resected lung samples in patients who were subsequently found to have COVID-19 in the postoperative period have shown alveolar damage, oedema, proteinaceous exudates, vascular congestion, alveolar hemorrhage and interstitial inflammatory infiltrates (68–70). Histological abnormalities are not limited to the respiratory system, demonstrating the systemic nature of the infection. Lymphocytic infiltration, endotheliitis, oedema, microthrombi and vascular proliferation are found in organs such as small bowel, spleen, kidney and liver (67, 70, 71). As neurological symptoms and complications are commonly seen (confusion, delirium, headache, autonomic dysfunction, stroke and meningoencephalitis) histological examination of brain tissue is of significance in this systemic effect. There are ischemic lesions, oedema and microhaemorrhages. Lymphocytic infiltration is seen, affecting the brainstem in particular (72).

These findings are indicative of dysfunction at the epithelial/endothelial interface. Endothelial viral infection and endotheliitis in heart, lung, kidney and liver has been reported (73). A closer look at the mechanism of viral entry may provide an explanation for endothelial disruption. The ACE2 receptor serves as the binding site for SARS-CoV-2. Membrane bound ACE2 undergoes cleavage by ADAM Metallopeptidase Domain 17 (ADAM17) to form soluble ACE2, which plays a critical role in the renin-angiotensin system and the cleavage of numerous bioactive peptides including Des-Arg9-bradykinin (DABK). ACE2 is expressed in lung epithelial cells, the starting point of infection. It is known to be increased in the airways of COPD and current smokers (74). It is found throughout endothelial surfaces in veins, arteries and arterioles and also in arterial smooth muscle cells (75). However, an RNA sequencing study found that ACE2 expression on endothelial cells was low in comparison to epithelial cells from respiratory, gastrointestinal and skin sites (76). Similarly, early in the pandemic ACE2 expression was shown to be highest in small intestine, heart, kidney, adrenal glands, with blood

vessels grouped among tissues with lowest expression (77). However, the endothelium is capable of mounting instant systemic responses and it is possible that low levels of expression are sufficient for damage. Bordoni et al. demonstrated that SARS-CoV-2 viral replication can occur in both airway epithelial and pulmonary endothelial cells (78). They also showed that culture of infected endothelial cells with non-infected pulmonary epithelial cells induced low levels of viral RNA in the pulmonary epithelial cells – though not vice versa. Moreover, viral infection of endothelial cells did not cause an increase in adhesion molecules (E-selectin, ICAM-1 and VCAM-1), but infection of epithelial cells resulted in increased E-selectin and VCAM-1, suggesting that the endothelial damage observed in COVID-19 is initiated by a cytotoxic effect from neighboring infected pulmonary epithelial cells.

Cells infected with SARS-CoV2 undergo pyroptosis leading to cytokines and danger associated molecular patterns (DAMPs). The response to these signals includes the release of neutrophil extracellular traps (NETS) and the activation of platelets. In addition to the damage caused by cell death, internalization of the viral/ACE2 complex leads to a relative ACE2 deficiency, which is significant, as ACE2 plays a vital role in the renin-angiotensin system by converting angiotensin II to angiotensin 1–7 (a vasodilator with anti-inflammatory, anti-thrombotic, antiproliferative and antifibrotic, activity) (79). The beneficial effects of ACE2 have been investigated in mouse models, showing that ACE2 deficient mice with acute lung injury improved following administration of recombinant ACE2 (80). Downregulation of the normal ACE2 function in COVID-19 leads to increased tissue and vessel exposure to angiotensin II, characterized by vasoconstriction, enhanced thrombosis, cell proliferation, increased tissue permeability, and cytokine production (81). Most importantly, a key agent of the contact-kinin pathway is bradykinin. ACE2 metabolizes des-Arg9-bradykinin.

Hematological findings and dynamic changes

Blood results in hospitalized patients with COVID-19 often follow predictable trends, correlating with stage of infection. Blood markers can also indicate severity of disease and aid in predicting outcomes. Lymphopenia is regarded as a cardinal finding, occurring in approximately two-thirds of people with COVID-19 (82). The lowest values occur after 7 days from symptom onset (83), reflecting recruitment to affected tissues. Patients with more severe disease tend to have lower lymphocyte counts at point of admission and have a more prolonged period of lymphopenia than those with mild disease. A retrospective study described admission blood results and subsequent dynamic changes for 548 inpatients (84). In severe disease, average counts were lower than in patients with mild disease. Non-survivors display very low levels on admission without appreciable lymphocyte recovery (84, 85).

Neutrophils usually rise from infection onset (85). Neutrophilia is associated with disease severity and mortality (28). Throughout the pandemic, lymphocyte and neutrophil results have been combined to form the neutrophil/lymphocyte ratio. A score of >11.75 predictive of mortality in hospitalized patients (86). Evidence has suggested that neutrophils may promote organ injury and coagulopathy via direct tissue infiltration and subsequent formation of Neutrophil Extracellular Traps (NETs) (87). NETS are networks of extracellular fibers composed of DNA and histones complexes. Structurally, they play an important role in the entrapment of microbes. They are potent activators of FXII and thus mediators of thromboinflammation. There is evidence to suggest that neutrophils in COVID-19 patients produce higher levels of NETs and also longer complexes in comparison to those from healthy controls (88).

Platelet counts are also affected by COVID-19 infection. Thrombocytopenia is present on admission in over a third of patients (89) although it is typically mild. Studies correlating platelets with day of symptoms have shown that counts begin drop from infection onset and are markedly lower at 7 days post symptom onset. This is often overlooked as the reduction may still fall within normal parameters. The sudden decrease in platelets may reflect depletion due to activation and subsequent consumption. At a later stage in infection, a rebound increase occurs (90, 91)—often meeting criteria for thrombocytosis. This pattern was also observed in the 2002 SARS infection (92). Activated platelets are likely to be a major contributing factor to the disease pathology in COVID-19. Patients with critical disease have increased levels of soluble P-selectin and CD40 ligand (circulating markers of platelet activation) (93). The use of antiplatelet agents has been explored. Anti-platelet therapy has a number of potentially beneficial mechanisms, including inhibition of platelet aggregation, reduction of platelet activation inflammation, and blocking of neutrophil extracellular traps. The RECOVERY trial investigated the use of aspirin in hospitalized COVID-19 patients and found no difference in mortality compared to standard care (94). However, there may be a role for antiplatelet agents in the prevention of disease severity. A cohort study of 984 COVID-19 patients (253 pre-admission aspirin, 751 not on aspirin) reported that that requirement for respiratory support (as defined by non-invasive or invasive ventilation) was significantly lower in the pre-hospital aspirin group: 33% vs. 49%. They also found that this group had a lower neutrophil to lymphocyte ratio on admission ($p = 0.013$) (95). In addition, a large, propensity matched study found there was a 2.6% absolute reduction in mortality with pre-hospital antiplatelet agents (96).

There are limited studies reporting dynamic coagulation changes according to day of symptoms as the majority of studies report findings by day of admission. In a retrospective analysis of 843 COVID-19 inpatients the APTT was significantly higher after 5 days of symptoms, but not after 10 or 13 days (97). This is confirmed by a separate group which reported raised APTT levels from day 5 of symptoms in patients with severe disease which then decreased until day 10 (98). Similarly a significantly higher APTT level was seen in the first week of symptoms compared to the 4th week (99). Studies reporting dynamic changes per day of admission have also demonstrated this trend. A meta-analysis of coagulation factors in COVID-19 reported that APTT levels decreased from point of admission, day 4 and onwards (100). A study of 1,131 hospitalized patients (36 severe) reported a slightly increasing trend in APTT and PT for the severe group and a slightly decreasing trend in the mild group within the first 10 days of admission (4). There was no temporal change in D-dimer for the mild group, but an increasing trend was observed in the severe group, a finding similar to a study of 320 hospitalized patients (101). Smadja et al. studied temporal trends of fibrin monomers, which are generated from the cleavage of fibrinogen from thrombin. They evaluated results from 246 inpatients during

their first 9 days of hospitalization and demonstrated an increasing trend until approximately day 6 of admission in critically ill patients (102).

Interleukin-6

In addition to abnormal hematological parameters, numerous pro-inflammatory cytokines have been detected and associated with the disease evolution of COVID-19. Studies of COVID-19 inpatients have revealed elevated levels of TNF-α, IFN-γ, IL-6, IL-8 and IL-10 (103–105). IL-6 is one of the most widely studied cytokines, leading to the utilization of targeted therapies such as tocilizumab and sarilumab. IL-6 is implicated in multiple processes, however it has a strong lymphotrophic effect, recruiting lymphocytes to the site of inflammation. Studies have consistently shown that elevated levels are predictive of disease severity and mortality (103, 104, 106). A cross sectional observation study of 272 COVID-19 inpatients demonstrated that a value of >79.9 pg./mL was predictive of unfavorable outcomes in terms of respiratory support and mortality (107). Santa Cruz et al. demonstrated that IL-6 levels peaked between 7 and 10 days post symptom onset in hospitalized patients (108). In keeping with risk factors for severe disease, IL-6 levels are higher in men and increase with age (105). This may be the link between high levels and severe lymphopenia and severe disease. It is notable that bradykinin causes release of IL-6.

Radiological features

Chest imaging abnormalities are a signature feature of COVID-19 disease and may even be observed in asymptomatic individuals. Chest radiographs and CT imaging can demonstrate ground glass, oedema, consolidation and fibrotic change. For patients who require hospitalization, these changes also follow trends that can help to distinguish stage of disease. Many studies have correlated imaging findings with days of symptoms. Patients may have imaging changes without symptoms; a meta-analysis of 231 asymptomatic cases reported that 63% had findings on CT imaging–the majority were ground glass opacities (GGO) (109). Within the first 7 days from symptom onset, GGOs are the main radiographic finding (83) and are usually bilateral and favor mid/lower zones (110). After 7 days, consolidation increases and may lead to respiratory failure and ARDS in a proportion of patients. Management involves escalated therapy with ventilatory support *via* NIV/CPAP and may require treatment in intensive care with invasive ventilation, which is associated with a high mortality (111). A meta-analysis of risk factors for COVID-19 severity reported that male sex, hypertension, cardiovascular, cerebrovascular, diabetes and respiratory disease were significantly associated with progression to ARDS (112). Hospitalized patients have a high risk of venous thromboembolic disease. A meta-analysis of hospitalized patients reported a pooled incidence of pulmonary embolism in 14.7% of cases (113). Ackermann et al. carried out high resolution Syncroton imaging on lung samples from 31 COVID-19 patients who had died from respiratory failures, showing partial/total occlusion in sub segmental pulmonary arteries (114).

In addition to parenchymal changes and thrombosis, studies have reported enlargement/dilation of sub segmental blood vessels at an early stage of infection/ on admission to hospital (110, 115). Bianco et al. investigated this phenomenon in COVID-19 patients and compared the findings with CT scans carried out in patients with influenza pneumonia (116). They found that vascular enlargement was present in 90% (45/50) COVID-19 patients, but only seen in 24% (12/50) patients with influenza pneumonia. Poletti et al. carried out an analysis of the thoracic vasculature in COVID-19 patients ($n = 279$), Influenza patients ($n = 159$) and patients with normal CT chest imaging ($n = 634$). Blood vessel volume percentage (BV%) was calculated for small, medium and large vessels. In COVID-19, small vessel BV% were decreased in comparison to normal controls (14% vs. 18%), but larger vessels were significantly bigger (15% vs. 11%) (117). It is possible that these vascular changes develop due to dysregulated release of bradykinin and alterations in the RAS as a consequence of ACE2 downregulation.

Inhibitors of the contact system

The contact system is known to be regulated by several physiological inhibitors. C1-esterase inhibitor (C1-INH) is the main inhibitor of FXIIa and FXIa and also acts to inhibit plasma kallikrein and the complement classical and lectin pathways. C1 inhibitor deficiency is the main cause for hereditary episodic angioedema (HAE); a rare genetic condition characterized by bradykinin mediated episodes of oedema. Consequently, individuals with C1-INH HAE have reduced regulation of the coagulation system and are at an increased risk of thromboembolic disease (118)—a finding recently replicated in a mouse model study (119). There have been differing reports of C1-INH in COVID-19. At the start of the pandemic, a study of admission blood results from 154 COVID-19 inpatients reported elevated levels of C1-INH which correlated positively with peak CRP, LDH and ferritin (120). A smaller study also reported increased C1-INH levels in 5 patients with severe disease (121). Conversely, 27 COVID-19 positive hemodialysis (HD) patients compared with 32 COVID-19 negative HD patients had significantly lower levels of CI-INH in the positive group. However, both HD groups were elevated in comparison to healthy controls (122). Other agents that can inhibit FXIIa (to a lesser extent) include antithrombin, α2-antiplasmin and α2-macroglobulin (123). Antithrombin targets FXIIa, FXIa and plasma kallikrein. Several studies have identified lower antithrombin levels in COVID-19 non-survivors compared to surviving groups (123–126). α2-antiplasmin is the main inhibitor of plasmin and can also inhibit FXIIa. Data on α2-antiplasmin levels in COVID-19 is limited, however similar results have been found between healthy control groups and admission values for COVID-19 patients (127, 128). α2-macroglobulin regulates several proteases including kallikrein and FXIIa. De Laat-Kreemers et al. reported that α2-macroglobulin levels were within normal range in 133 COVID-19 inpatients, but significantly lower levels were noted in patients with thrombosis compared to those without (129).

C1 esterase inhibitor

C1 esterase inhibitor - inhibitor of FXIIa and FXIa and also acts to inhibit plasma kallikrein and the complement classical and lectin pathways. A small case–control study compared the outcomes of 5 COVID-19 patients who received C1-esterase inhibitor with 15

matched controls. The baseline characteristics and admission laboratory parameters were similar between groups. Eight patients (53%) in the matched control group died or required mechanical ventilation compared to only 1 (20%) in the C1-esterase inhibitor group (121). Another study reported the results of a randomized, open label trial of C1-esterase inhibitor, bradykinin B2 receptor antagonist (icatibant) or standard care alone ($n = 9$, 10, 9 respectively) (130). COVID-19 patients with severe infection (radiological pneumonia; $SpO_2 \leq 94\%$ in ambient air or $Pa0_2/FiO_2 \leq 300$ mmHg) were recruited and allocated to treatment arms 1:1:1 up to day 12 of symptoms. There were no significant differences between groups in terms of time to clinical improvement or mortality. There was an improvement in lung CT scores. The size of this study would require a strong signal to identify clinical improvement or mortality.

Plasma kallikrein inhibitors

Plasma kallikrein inhibitors have been developed for use in hereditary episodic angioedema (HAE). Lanadelumab and berotralstat are licensed for the prevention of recurrent attacks. Lanadelumab is administered as a subcutaneous injection every 2–4 weeks, depending on disease stability. Trials in COVID-19 are currently underway. Berotralstat is taken orally once per day. Both medications have been shown to significantly reduce the incidence of attacks compared to placebo (131, 132). Ecallantide is a plasma kallikrein inhibitor used to treat acute HAE attacks (133). Donidalorsen is an antisense oligonucleotide treatment which results in decreased production of PK from the liver. A phase 2 study has demonstrated a reduced rate of angioedema attacks compared to placebo ($p = <0.001$) (134).

Factor XII/FXIIa inhibitors

Garadacimab, a novel FXIIa inhibitor has been recently trialed in a phase 1 study (135). Dose-dependent increases in plasma concentration and pharmacodynamic effects in kinin and coagulation pathways were observed. Trials are currently underway in COVID-19.

B2 receptor blockade in COVID-19

Bradykinin receptor activation may cause the radiological oedema, hypotension and cytokine release seen in early COVID-19 infection. The use of a receptor antagonist may interrupt this pathway and prevent progression to secondary damage, as defined by inflammatory cell infiltrates, thrombosis and vascular injury. Icatibant is a B2 receptor antagonist that has been in use since 2008 for the treatment of oedema caused by hereditary angioedema. It has a rapid onset of action, with median time of 2–2.5 h to symptom relief following a single dose (136, 137). It has a short half-life of 1.48 +/− 0.35 h (138). Published data on the use of icatibant in COVID-19 is limited to four studies and two case reports. Importantly, there have been no safety concerns noted regarding the use of icatibant in COVID-19 in existing reports.

A case report of a single patient with severe COVID-19 infection described a favorable clinical response after icatibant (139). Giol et al. reported radiological improvement in a COVID-19 patient who received icatibant as a treatment for ACE inhibitor induced angioedema (140). Van de Veerdonk et al. described decreased oxygen requirements in COVID-19 patients ($n = 9$) treated with open label icatibant compared to standard care ($n = 18$). After 24 h, 89% of patients receiving Icatibant had a reduction of at least 3 L of oxygen compared to only 17% of controls (141). Mansour et al. carried out a randomized, open-label trial with three treatment arms; icatibant, C1 esterase inhibitor and no trial drug ("usual care") (130). Eligible patients had hypoxia, radiological COVID-19 pneumonia and were within 12 days of symptom onset. Patients in the icatibant arm received 30 mg three times per day for 4 days. The C1 esterase group were administered a dose on days 1 and 4. The main outcomes were time to clinical improvement as defined by the WHO ordinal scale and improvement in lung CT scoring. There were no significant differences between the groups.

Malchair et al. carried out a randomized, open label trial of icatibant 30 mg three times per day for 3 days plus standard care compared to standard care alone. Patients were eligible if requiring supplemental oxygen, but not high flow oxygen or ventilation. Patients were required to have a positive PCR or antigen test within 10 days of randomization although symptom onset was not recorded. The primary outcome was clinical response (defined as category 2 or lower of the WHO ordinal scale, sustained for 48 h) by day 10 or discharge. The primary outcome was assessed for 37 and 36 patients, respectively. 73% of patients in the icatibant arm (27/37) and 53% of standard care patients (20/36) met the clinical response target, although this did not meet statistical significance. However, clinical response was maintained at day 28 by all of the patients in the icatibant arm compared to controls ($p = 0.011$) and icatibant patients had a significantly shorter inpatient admission, 8 days vs. 10 ($p = 0.014$) (142).

A platform study has recently published data for the first seven medications trialed (including icatibant). The trial recruited patients with severe/ critical disease (requiring ≥6 L of oxygen) and an average symptom history of 9–10 days. There were 96 patients enrolled in the icatibant arm. Over half of the patients required ≥15 L of oxygen and a third were on non-invasive or mechanical ventilation. The primary aim was to find a large signal in terms of improved recovery time and mortality. This was not achieved for any of the medications used (143).

Conclusion

Activation of the bradykinin pathway begins at infection onset. In a proportion of cases this process eventually leads to inflammatory cell infiltration and tissue damage. These features are most evident at a later stage of the illness (>7 days post symptom onset). At this point, lymphocyte counts are lowest and neutrophil counts increase. Chest radiological appearances demonstrate progression from initial ground glass appearance (oedema) to dense consolidation. It is acknowledged that widespread vaccine uptake and the emergence of other variants are associated with milder illness in COVID-19. However, patients with vascular co-morbidities remain at risk of infection progression and this may be due to accentuation of the contact-kinin system in setting of endothelial dysfunction.

The study authors are conducting a proof of concept trial of icatibant in hospitalized patients with early COVID-19 infection.

The aim is to trial bradykinin blockade in early, potentially reversible disease, before the onset of secondary damage and acute respiratory distress syndrome (ARDS). Patients who have had symptoms for more than 7 days will not be included. The primary outcome is to determine the effect on the Alveolar-arterial gradient (as measured by arterial blood gas before and after treatment). If an improvement in oxygenation is found, icatibant or alterative medications targeting the KKS could be tested on a larger scale. This could potentially change the management at point of admission for early COVID-19, preventing progression to respiratory failure. There may be wider implications for lung injury, as a study of bradykinin inhibition showed an improvement in the 28-day risk-adjusted survival in patients with SIRS from gram-negative infections (144).

Author contributions

All authors listed have made a substantial, direct, and intellectual contribution to the work and approved it for publication.

Funding

MB is funded by the R&D office for an NIHR adopted COVID-19 study (Grant number: COM/5612/20).

Conflict of interest

The authors declare that the research was conducted in the absence of any commercial or financial relationships that could be construed as a potential conflict of interest.

Publisher's note

All claims expressed in this article are solely those of the authors and do not necessarily represent those of their affiliated organizations, or those of the publisher, the editors and the reviewers. Any product that may be evaluated in this article, or claim that may be made by its manufacturer, is not guaranteed or endorsed by the publisher.

References

1. Lanzani C, Simonini M, Arcidiacono T, Messaggio E, Bucci R, Betti P, et al. Bio angels for COVID-BioB study group. Role of blood pressure dysregulation on kidney and mortality outcomes in COVID-19. Kidney, blood pressure and mortality in SARS-CoV-2 infection. *J Nephrol*. (2021) 34:305–14. doi: 10.1007/s40620-021-00997-0

2. Yang J, Zheng Y, Gou X, Pu K, Chen Z, Guo Q, et al. Prevalence of comorbidities and its effects in patients infected with SARS-CoV-2: a systematic review and meta-analysis. *Int J Infect Dis*. (2020) 94:91–5. doi: 10.1016/j.ijid.2020.03.017

3. Fox AJ, Lalloo UG, Belvisi MG, Bernareggi M, Chung KF, Barnes PJ. Bradykinin-evoked sensitization of airway sensory nerves: a mechanism for ACE-inhibitor cough. *Nat Med*. (1996) 2:814–7. doi: 10.1038/nm0796-814

4. Xu W, Fei L, Huang CL, Li WX, Xie XD, Li Q, et al. Dynamic changes in coagulation parameters and correlation with disease severity and mortality in patients with COVID-19. *Aging (Albany NY)*. (2021) 13:13393–404. doi: 10.18632/aging.203052

5. Taha M, Samavati L. Antiphospholipid antibodies in COVID-19: a meta-analysis and systematic review. *RMD Open*. (2021) 7:e001580. doi: 10.1136/rmdopen-2021-001580

6. Siguret V, Voicu S, Neuwirth M, Delrue M, Gayat E, Stépanian A, et al. Are antiphospholipid antibodies associated with thrombotic complications in critically ill COVID-19 patients? *Thromb Res*. (2020) 195:74–6. doi: 10.1016/j.thromres.2020.07.016

7. Najim M, Rahhal A, Khir F, Aljundi AH, Abu Yousef S, Ibrahim F, et al. Prevalence and clinical significance of antiphospholipid antibodies in patients with coronavirus disease 2019 admitted to intensive care units: a prospective observational study. *Rheumatol Int*. (2021) 41:1243–52. doi: 10.1007/s00296-021-04875-7

8. Devreese KMJ, de Groot PG, de Laat B, Erkan D, Favaloro EJ, Mackie I, et al. Guidance from the scientific and standardization committee for lupus anticoagulant/antiphospholipid antibodies of the international society on thrombosis and haemostasis: update of the guidelines for lupus anticoagulant detection and interpretation. *J Thromb Haemost*. (2020) 18:2828–39. doi: 10.1111/jth.15047

9. Favaloro EJ, Henry BM, Lippi G. Is lupus anticoagulant a significant feature of COVID-19? A critical appraisal of the literature. *Semin Thromb Hemost*. (2022) 48:55–71. doi: 10.1055/s-0041-1729856

10. Reyes Gil M, Barouqa M, Szymanski J, Gonzalez-Lugo JD, Rahman S, Billett HH. Assessment of lupus anticoagulant positivity in patients with coronavirus disease 2019 (COVID-19). *JAMA Netw Open*. (2020) 3:e2017539. doi: 10.1001/jamanetworkopen.2020.17539

11. Ferrari E, Sartre B, Squara F, Contenti J, Occelli C, Lemoel F, et al. High prevalence of acquired thrombophilia without prognosis value in patients with coronavirus disease 2019. *J Am Heart Assoc*. (2020) 9:e017773. doi: 10.1161/JAHA.120.017773

12. Owaidah T, Saleh M, Aguilos AM, Amri AA, Maghrabi K, Owaidah M, et al. Incidence of lupus anticoagulant in hospitalized covid-19 patients. *Am J Blood Res*. (2021) 11:317–24.

13. Zhu J, Pang J, Ji P, Zhong Z, Li H, Li B, et al. Coagulation dysfunction is associated with severity of COVID-19: a meta-analysis. *J Med Virol*. (2021) 93:962–72. doi: 10.1002/jmv.26336

14. Zhang X, Yang X, Jiao H, Liu X. Coagulopathy in patients with COVID-19: a systematic review and meta-analysis. *Aging (Albany NY)*. (2020) 12:24535–51. doi: 10.18632/aging.104138

15. Jiménez D, García-Sanchez A, Rali P, Muriel A, Bikdeli B, Ruiz-Artacho P, et al. Incidence of VTE and bleeding among hospitalized patients with coronavirus disease 2019: a systematic review and meta-analysis. *Chest*. (2021) 159:1182–96. doi: 10.1016/j.chest.2020.11.005

16. Simon SR, Black HR, Moser M, Berland WE. Cough and ACE inhibitors. *Arch Intern Med*. (1992) 152:1698–700. doi: 10.1001/archinte.1992.00400200128023

17. Kidney JC, O'Halloran DJ, FitzGerald MX. Captopril and lymphocytic alveolitis. *BMJ*. (1989) 299:981. doi: 10.1136/bmj.299.6705.981

18. Ma JX, Wang DZ, Ward DC, Chen L, Dessai T, Chao J, et al. Structure and chromosomal localization of the gene (BDKRB2) encoding human bradykinin B2 receptor. *Genomics*. (1994) 23:362–9. doi: 10.1006/geno.1994.1512

19. Qadri F, Bader M. Kinin B1 receptors as a therapeutic target for inflammation. *Expert Opin Ther Targets*. (2018) 22:31–44. doi: 10.1080/14728222.2018.1409724

20. Qin LJ, Gu YT, Zhang H, Xue YX. Bradykinin-induced blood-tumor barrier opening is mediated by tumor necrosis factor-alpha. *Neurosci Lett*. (2009) 450:172–5. doi: 10.1016/j.neulet.2008.10.080

21. Morbidelli L, Parenti A, Giovannelli L, Granger HJ, Ledda F, Ziche M. B1 receptor involvement in the effect of bradykinin on venular endothelial cell proliferation and potentiation of FGF-2 effects. *Br J Pharmacol*. (1998) 124:1286–92. doi: 10.1038/sj.bjp.0701943

22. Lee CH, Shieh DC, Tzeng CY, Chen CP, Wang SP, Chiu YC, et al. Bradykininduced IL-6 expression through bradykinin B2 receptor, phospholipase C, protein kinase Cdelta and NF-kappaB pathway in human synovial fibroblasts. *Mol Immunol*. (2008) 45:3693–702. doi: 10.1016/j.molimm.2008.06.007

23. Nagashima S, Dutra AA, Arantes MP, Zeni RC, Klein CK, de Oliveira FC, et al. COVID-19 and lung mast cells: the kallikrein-kinin activation pathway. *Int J Mol Sci*. (2022) 23:1714. doi: 10.3390/ijms23031714

24. Schmaier AH. The contact activation and kallikrein/kinin systems: pathophysiologic and physiologic activities. *J Thromb Haemost*. (2016) 14:28–39. doi: 10.1111/jth.13194

25. Bracke A, De Hert E, De Bruyn M, Claesen K, Vliegen G, Vujkovic A, et al. Proline-specific peptidase activities (DPP4, PRCP, FAP and PREP) in plasma of hospitalized COVID-19 patients. *Clin Chim Acta*. (2022) 531:4–11. doi: 10.1016/j.cca.2022.03.005

26. Imamura T, Tanase S, Hayashi I, Potempa J, Kozik A, Travis J. Release of a new vascular permeability enhancing peptide from kininogens by human neutrophil elastase. *Biochem Biophys Res Commun*. (2002) 294:423–8. doi: 10.1016/S0006-291X(02)00490-4

27. Coffman LG, Brown JC, Johnson DA, Parthasarathy N, D'Agostino RB, Lively MO, et al. Cleavage of high-molecular-weight kininogen by elastase and tryptase is inhibited by ferritin. *Am J Physiol Lung Cell Mol Physiol*. (2008) 294:L505–15. doi: 10.1152/ajplung.00347.2007

28. Henry BM, de Oliveira MHS, Benoit S, Plebani M, Lippi G. Hematologic, biochemical and immune biomarker abnormalities associated with severe illness and mortality in coronavirus disease 2019 (COVID-19): a meta-analysis. *Clin Chem Lab Med*. (2020) 58:1021–8. doi: 10.1515/cclm-2020-0369

29. Ugonotti J, Chatterjee S, Thaysen-Andersen M. Structural and functional diversity of neutrophil glycosylation in innate immunity and related disorders. *Mol Asp Med*. (2021) 79:100882. doi: 10.1016/j.mam.2020.100882

30. Kahn R, Hellmark T, Leeb-Lundberg LM, Akbari N, Todiras M, Olofsson T, et al. Neutrophil-derived proteinase 3 induces kallikrein-independent release of a novel vasoactive kinin. *J Immunol*. (2009) 182:7906–15. doi: 10.4049/jimmunol.0803624

31. Huang W, Li M, Luo G, Wu X, Su B, Zhao L, et al. The inflammatory factors associated with disease severity to predict COVID-19 progression. *J Immunol*. (2021) 206:1597–608. doi: 10.4049/jimmunol.2001327

32. Akgun E, Tuzuner MB, Sahin B, Kilercik M, Kulah C, Cakiroglu HN, et al. Proteins associated with neutrophil degranulation are upregulated in nasopharyngeal swabs from SARS-CoV-2 patients. *PLoS One*. (2020) 15:e0240012. doi: 10.1371/journal.pone.0240012

33. Ng H, Havervall S, Rosell A, Aguilera K, Parv K, von Meijenfeldt FA, et al. Circulating markers of neutrophil extracellular traps are of prognostic value in patients with COVID-19. *Arterioscler Thromb Vasc Biol*. (2021) 41:988–94. doi: 10.1161/ATVBAHA.120.315267

34. Wygrecka M, Birnhuber A, Seeliger B, Michalick L, Pak O, Schultz AS, et al. Altered fibrin clot structure and dysregulated fibrinolysis contribute to thrombosis risk in severe COVID-19. *Blood Adv*. (2022) 6:1074–87. doi: 10.1182/bloodadvances.2021004816

35. Lipcsey M, Persson B, Eriksson O, Blom AM, Fromell K, Hultström M, et al. The outcome of critically ill COVID-19 patients is linked to Thromboinflammation dominated by the kallikrein/kinin system. *Front Immunol*. (2021) 12:627579. doi: 10.3389/fimmu.2021.627579

36. Englert H, Rangaswamy C, Deppermann C, Sperhake JP, Krisp C, Schreier D, et al. Defective NET clearance contributes to sustained FXII activation in COVID-19-associated pulmonary thrombo-inflammation. *EBioMedicine*. (2021) 67:103382. doi: 10.1016/j.ebiom.2021.103382

37. Ceballos FC, Ryan P, Blancas R, Martin-Vicente M, Vidal-Alcántara EJ, Peréz-García F, et al. Are reduced levels of coagulation proteins upon admission linked to COVID-19 severity and mortality? *Front Med (Lausanne)*. (2021) 8:718053. doi: 10.3389/fmed.2021.718053

38. Collins PW, Macchiavello LI, Lewis SJ, Macartney NJ, Saayman AG, Luddington R, et al. Global tests of haemostasis in critically ill patients with severe sepsis syndrome compared to controls. *Br J Haematol*. (2006) 135:220–7. doi: 10.1111/j.1365-2141.2006.06281.x

39. Akwii RG, Sajib MS, Zahra FT, Mikelis CM. Role of Angiopoietin-2 in vascular physiology and pathophysiology. *Cells*. (2019) 8:471. doi: 10.3390/cells8050471

40. Mancini I, Baronciani L, Artoni A, Colpani P, Biganzoli M, Cozzi G, et al. The ADAMTS13-von Willebrand factor axis in COVID-19 patients. *J Thromb Haemost*. (2021) 19:513–21. doi: 10.1111/jth.15191

41. Delrue M, Siguret V, Neuwirth M, Joly B, Beranger N, Sène D, et al. von Willebrand factor/ADAMTS13 axis and venous thromboembolism in moderate-to-severe COVID-19 patients. *Br J Haematol*. (2021) 192:1097–100. doi: 10.1111/bjh.17216

42. Leisman DE, Mehta A, Thompson BT, Charland NC, Gonye ALK, Gushterova I, et al. Alveolar, endothelial, and organ injury marker dynamics in severe COVID-19. *Am J Respir Crit Care Med*. (2022) 205:507–19. doi: 10.1164/rccm.202106-1514OC

43. Willems LH, Nagy M, Ten Cate H, Spronk HMH, Groh LA, Leentjens J, et al. Sustained inflammation, coagulation activation and elevated endothelin-1 levels without macrovascular dysfunction at 3 months after COVID-19. *Thromb Res*. (2022) 209:106–14. doi: 10.1016/j.thromres.2021.11.027

44. Philippe A, Chocron R, Gendron N, Bory O, Beauvais A, Peron N, et al. Circulating Von Willebrand factor and high molecular weight multimers as markers of endothelial injury predict COVID-19 in-hospital mortality. *Angiogenesis*. (2021) 24:505–17. doi: 10.1007/s10456-020-09762-6

45. Karampini E, Fogarty H, Elliott S, Morrin H, Bergin C, O'Sullivan JM, et al. Endothelial cell activation, Weibel-Palade body secretion, and enhanced angiogenesis in severe COVID-19. *Res Pract Thromb Haemost*. (2023) 7:100085. doi: 10.1016/j.rpth.2023.100085

46. Goshua G, Pine AB, Meizlish ML, Chang CH, Zhang H, Bahel P, et al. Endotheliopathy in COVID-19-associated coagulopathy: evidence from a single-Centre, cross-sectional study. *Lancet Haematol*. (2020) 7:e575–82. doi: 10.1016/S2352-3026(20)30216-7

47. Agrati C, Bordoni V, Sacchi A, Petrosillo N, Nicastri E, Del Nonno F, et al. Elevated P-selectin in severe Covid-19: considerations for therapeutic options. *Mediterr J Hematol Infect Dis*. (2021) 13:e2021016. doi: 10.4084/mjhid.2021.016

48. Karsli E, Sabirli R, Altintas E, Canacik O, Sabirli GT, Kaymaz B, et al. Soluble P-selectin as a potential diagnostic and prognostic biomarker for COVID-19 disease: a case-control study. *Life Sci*. (2021) 277:119634. doi: 10.1016/j.lfs.2021.119634

49. Smadja DM, Guerin CL, Chocron R, Yatim N, Boussier J, Gendron N, et al. Angiopoietin-2 as a marker of endothelial activation is a good predictor factor for intensive care unit admission of COVID-19 patients. *Angiogenesis*. (2020) 23:611–20. doi: 10.1007/s10456-020-09730-0

50. Sinkovits G, Réti M, Müller V, Iványi Z, Gál J, Gopcsa L, et al. Associations between the von Willebrand factor-ADAMTS13 Axis, complement activation, and COVID-19 severity and mortality. *Thromb Haemost*. (2022) 122:240–56. doi: 10.1055/s-0041-1740182

51. Ward SE, Curley GF, Lavin M, Fogarty H, Karampini E, McEvoy NL, et al. Irish COVID-19 vasculopathy study (ICVS) investigators. Von Willebrand factor propeptide in severe coronavirus disease 2019 (COVID-19): evidence of acute and sustained endothelial cell activation. *Br J Haematol*. (2021) 192:714–9. doi: 10.1111/bjh.17273

52. Cugno M, Meroni PL, Gualtierotti R, Griffini S, Grovetti E, Torri A, et al. Complement activation and endothelial perturbation parallel COVID-19 severity and activity. *J Autoimmun*. (2021) 116:102560. doi: 10.1016/j.jaut.2020.102560

53. Sibila O, Perea L, Albacar N, Moisés J, Cruz T, Mendoza N, et al. Elevated plasma levels of epithelial and endothelial cell markers in COVID-19 survivors with reduced lung diffusing capacity six months after hospital discharge. *Respir Res*. (2022) 23:37. doi: 10.1186/s12931-022-01955-5

54. Barabutis N. Unfolded protein response in the COVID-19 context. *Aging Health Res*. (2021) 1:100001. doi: 10.1016/j.ahr.2020.100001

55. Lip GY, Edmunds E, Hee FL, Blann AD, Beevers DG. A cross-sectional, diurnal, and follow-up study of platelet activation and endothelial dysfunction in malignant phase hypertension. *Am J Hypertens*. (2001) 14:823–8. doi: 10.1016/s0895-7061(01)02045-3

56. Petrák O, Widimský J Jr, Zelinka T, Kvasnicka J, Strauch B, Holaj R, et al. Biochemical markers of endothelial dysfunction in patients with endocrine and essential hypertension. *Physiol Res*. (2006) 55:597–602. doi: 10.33549/physiolres.930912

57. Spencer CG, Gurney D, Blann AD, Beevers DG, Lip GY. ASCOT steering committee, Anglo-Scandinavian cardiac outcomes trial. Von Willebrand factor, soluble P-selectin, and target organ damage in hypertension: a substudy of the Anglo-Scandinavian cardiac outcomes trial (ASCOT). *Hypertension*. (2002) 40:61–6. doi: 10.1161/01.hyp.0000022061.12297.2e

58. de La Sierra A, Larrousse M, Oliveras A, Armario P, Hernández-Del Rey R, Poch E, et al. Abnormalities of vascular function in resistant hypertension. *Blood Press*. (2012) 21:104–9. doi: 10.3109/08037051.2011.622983

59. Schumacher A, Seljeflot I, Sommervoll L, Christensen B, Otterstad JE, Arnesen H. Increased levels of markers of vascular inflammation in patients with coronary heart disease. *Scand J Clin Lab Invest*. (2002) 62:59–68. doi: 10.1080/00365102753517217

60. Mulhem A, Moulla Y, Klöting N, Ebert T, Tönjes A, Fasshauer M, et al. Circulating cell adhesion molecules in metabolically healthy obesity. *Int J Obes*. (2021) 45:331–6. doi: 10.1038/s41366-020-00667-4

61. Meigs JB, O'donnell CJ, Tofler GH, Benjamin EJ, Fox CS, Lipinska I, et al. Hemostatic markers of endothelial dysfunction and risk of incident type 2 diabetes: the Framingham offspring study. *Diabetes*. (2006) 55:530–7. doi: 10.2337/diabetes.55.02.06.db05-1041

62. Meigs JB, Hu FB, Rifai N, Manson JE. Biomarkers of endothelial dysfunction and risk of type 2 diabetes mellitus. *JAMA*. (2004) 291:1978–86. doi: 10.1001/jama.291.16.1978

63. Hegazy GA, Awan Z, Hashem E, Al-Ama N, Abunaji AB. Levels of soluble cell adhesion molecules in type 2 diabetes mellitus patients with macrovascular complications. *J Int Med Res*. (2020) 48:030006051989385. doi: 10.1177/0300060519893858

64. Wang M, Lin EP, Huang LC, Li CY, Shyr Y, Lai CH. Mortality of cardiovascular events in patients with COPD and preceding hospitalization for acute exacerbation. *Chest*. (2020) 158:973–85. doi: 10.1016/j.chest.2020.02.046

65. Van der Vorm LN, Li L, Huskens D, Hulstein JJJ, Roest M, de Groot PG, et al. Acute exacerbations of COPD are associated with a prothrombotic state through platelet-monocyte complexes, endothelial activation and increased thrombin generation. *Respir Med*. (2020) 171:106094. doi: 10.1016/j.rmed.2020.106094

66. Polatli M, Cakir A, Cildag O, Bolaman AZ, Yenisey C, Yenicerioglu Y. Microalbuminuria, von Willebrand factor and fibrinogen levels as markers of the severity in COPD exacerbation. *J Thromb Thrombolysis*. (2008) 26:97–102. doi: 10.1007/s11239-007-0073-1

67. Ackermann M, Verleden SE, Kuehnel M, Haverich A, Welte T, Laenger F, et al. Pulmonary vascular Endothelialitis, thrombosis, and angiogenesis in Covid-19. *N Engl J Med*. (2020) 383:120–8. doi: 10.1056/NEJMoa2015432

68. Tian S, Hu W, Niu L, Liu H, Xu H, Xiao SY. Pulmonary pathology of early-phase 2019 novel coronavirus (COVID-19) pneumonia in two patients with lung cancer. *J Thorac Oncol*. (2020) 15:700–4. doi: 10.1016/j.jtho.2020.02.010

69. Pernazza A, Mancini M, Rullo E, Bassi M, De Giacomo T, Rocca CD, et al. Early histologic findings of pulmonary SARS-CoV-2 infection detected in a surgical specimen. *Virchows Arch*. (2020) 477:743–8. doi: 10.1007/s00428-020-02829-1

70. Tabary M, Khanmohammadi S, Araghi F, Dadkhahfar S, Tavangar SM. Pathologic features of COVID-19: a concise review. *Pathol Res Pract*. (2020) 216:153097. doi: 10.1016/j.prp.2020.153097

71. Mikhaleva LM, Cherniaev AL, Samsonova MV, Zayratyants OV, Kakturskiy LV, Vasyukova OA, et al. Pathological features in 100 deceased patients with COVID-19 in correlation with clinical and laboratory data. *Pathol Oncol Res*. (2021) 27:1609900. doi: 10.3389/pore.2021.1609900

72. Matschke J, Lütgehetmann M, Hagel C, Sperhake JP, Schröder AS, Edler C, et al. Neuropathology of patients with COVID-19 in Germany: a post-mortem case series. *Lancet Neurol*. (2020) 19:919–29. doi: 10.1016/S1474-4422(20)30308-2

73. Varga Z, Flammer AJ, Steiger P, Haberecker M, Andermatt R, Zinkernagel AS, et al. Endothelial cell infection and endotheliitis in COVID-19. *Lancet*. (2020) 395:1417–8. doi: 10.1016/S0140-6736(20)30937-5

74. Leung JM, Yang CX, Tam A, Shaipanich T, Hackett TL, Singhera GK, et al. ACE-2 expression in the small airway epithelia of smokers and COPD patients: implications for COVID-19. *Eur Respir J*. (2020) 55:2000688. doi: 10.1183/13993003.00688-2020

75. Hamming I, Timens W, Bulthuis ML, Lely AT, Navis G, van Goor H. Tissue distribution of ACE2 protein, the functional receptor for SARS coronavirus. A first step in understanding SARS pathogenesis. *J Pathol*. (2004) 203:631–7. doi: 10.1002/path.1570

76. McCracken IR, Saginc G, He L, Huseynov A, Daniels A, Fletcher S, et al. Lack of evidence of angiotensin-converting enzyme 2 expression and replicative infection by SARS-CoV-2 in human endothelial cells. *Circulation*. (2021) 143:865–8. doi: 10.1161/CIRCULATIONAHA.120.052824

77. Li MY, Li L, Zhang Y, Wang XS. Expression of the SARS-CoV-2 cell receptor gene ACE2 in a wide variety of human tissues. *Infect Dis Poverty*. (2020) 9:45. doi: 10.1186/s40249-020-00662-x

78. Bordoni V, Mariotti D, Matusali G, Colavita F, Cimini E, Ippolito G, et al. SARS-CoV-2 infection of airway epithelium triggers pulmonary endothelial cell activation and senescence associated with type I IFN production. *Cells*. (2022) 11:2912. doi: 10.3390/cells11182912

79. Passos-Silva DG, Verano-Braga T, Santos RA. Angiotensin-(1-7): beyond the cardio-renal actions. *Clin Sci (Lond)*. (2013) 124:443–56. doi: 10.1042/CS20120461

80. Imai Y, Kuba K, Rao S, Huan Y, Guo F, Guan B, et al. Angiotensin-converting enzyme 2 protects from severe acute lung failure. *Nature*. (2005) 436:112–6. doi: 10.1038/nature03712

81. Gan R, Rosoman NP, Henshaw DJE, Noble EP, Georgius P, Sommerfeld N. COVID-19 as a viral functional ACE2 deficiency disorder with ACE2 related multi-organ disease. *Med Hypotheses*. (2020) 144:110024. doi: 10.1016/j.mehy.2020.110024

82. Li LQ, Huang T, Wang YQ, Wang ZP, Liang Y, Huang TB, et al. COVID-19 patients' clinical characteristics, discharge rate, and fatality rate of meta-analysis. *J Med Virol*. (2020) 92:577–83. doi: 10.1002/jmv.25757

83. Lim AYH, Goh JL, Chua MCW, Heng BH, Abisheganaden JA, George PP. Temporal changes of haematological and radiological findings of the COVID-19 infection-a review of literature. *BMC Pulm Med*. (2021) 21:37. doi: 10.1186/s12890-020-01389-z

84. Chen R, Sang L, Jiang M, Yang Z, Jia N, Fu W, et al. Medical treatment expert group for COVID-19. Longitudinal hematologic and immunologic variations associated with the progression of COVID-19 patients in China. *J Allergy Clin Immunol*. (2020) 146:89–100. doi: 10.1016/j.jaci.2020.05.003

85. Lanini S, Montaldo C, Nicastri E, Vairo F, Agrati C, Petrosillo N, et al. COVID-19 disease-temporal analyses of complete blood count parameters over course of illness, and relationship to patient demographics and management outcomes in survivors and non-survivors: a longitudinal descriptive cohort study. *PLoS One*. (2020) 15:e0244129. doi: 10.1371/journal.pone.0244129

86. Yan X, Li F, Wang X, Yan J, Zhu F, Tang S, et al. Neutrophil to lymphocyte ratio as prognostic and predictive factor in patients with coronavirus disease 2019: a retrospective cross-sectional study. *J Med Virol*. (2020) 92:2573–81. doi: 10.1002/jmv.26061

87. Zuo Y, Yalavarthi S, Shi H, Gockman K, Zuo M, Madison JA, et al. Neutrophil extracellular traps in COVID-19. *JCI Insight*. (2020) 5:e138999. doi: 10.1172/jci.insight.138999

88. Veras FP, Pontelli MC, Silva CM, Toller-Kawahisa JE, de Lima M, Nascimento DC, et al. SARS-CoV-2-triggered neutrophil extracellular traps mediate COVID-19 pathology. *J Exp Med*. (2020) 217:e20201129. doi: 10.1084/jem.20201129

89. Guan WJ, Ni ZY, Hu Y, Liang WH, Ou CQ, He JX, et al. China medical treatment expert Group for Covid-19. Clinical characteristics of coronavirus disease 2019 in China. *N Engl J Med*. (2020) 382:1708–20. doi: 10.1056/NEJMoa2002032

90. Linssen J, Ermens A, Berrevoets M, Seghezzi M, Previtali G, van der Sar-van der Brugge S, et al. A novel haemocytometric COVID-19 prognostic score developed and validated in an observational multicentre European hospital-based study. *Elife*. (2020) 9:e63195. doi: 10.7554/eLife.63195

91. Burke H, Freeman A, O'Regan P, Wysocki O, Freitas A, Dushianthan A, et al. REACT COVID group. Biomarker identification using dynamic time warping analysis: a longitudinal cohort study of patients with COVID-19 in a UK tertiary hospital. *BMJ Open*. (2022) 12:e050331. doi: 10.1136/bmjopen-2021-050331

92. Wong RS, Wu A, To KF, Lee N, Lam CW, Wong CK, et al. Haematological manifestations in patients with severe acute respiratory syndrome: retrospective analysis. *BMJ*. (2003) 326:1358–62. doi: 10.1136/bmj.326.7403.1358

93. Philippe A, Chocron R, Bonnet G, Yatim N, Sutter W, Hadjadj J, et al. Platelet activation and coronavirus disease 2019 mortality: insights from coagulopathy, antiplatelet therapy and inflammation. *Arch Cardiovasc Dis*. (2023) 116:183–91. doi: 10.1016/j.acvd.2023.01.006

94. Recovery Collaborative Group. Aspirin in patients admitted to hospital with COVID-19 (RECOVERY): a randomised, controlled, open-label, platform trial. *Lancet*. (2022) 399:143–51. doi: 10.1016/S0140-6736(21)01825-0

95. Sisinni A, Rossi L, Battista A, Poletti E, Battista F, Battista RA, et al. Pre-admission acetylsalicylic acid therapy and impact on in-hospital outcome in COVID-19 patients: the ASA-CARE study. *Int J Cardiol*. (2021) 344:240–5. doi: 10.1016/j.ijcard.2021.09.058

96. Chow JH, Yin Y, Yamane DP, Davison D, Keneally RJ, Hawkins K, et al. Association of prehospital antiplatelet therapy with survival in patients hospitalized with COVID-19: a propensity score-matched analysis. *J Thromb Haemost*. (2021) 19:2814–24. doi: 10.1111/jth.15517

97. Wang M, Zhang J, Ye D, Wang Z, Liu J, He H, et al. Time-dependent changes in the clinical characteristics and prognosis of hospitalized COVID-19 patients in Wuhan, China: a retrospective study. *Clin Chim Acta*. (2020) 510:220–7. doi: 10.1016/j.cca.2020.06.051

98. Lu H, Chen M, Tang S, Yu W. Association of coagulation disturbances with severity of COVID-19: a longitudinal study. *Hematology*. (2021) 26:656–62. doi: 10.1080/16078454.2021.1968648

99. Xu J, Zhang Y, Li Y, Liao K, Zeng X, Zeng X, et al. Dynamic changes in coagulation function in patients with pneumonia under admission and non-admission treatment. *Front Med (Lausanne)*. (2021) 8:626384. doi: 10.3389/fmed.2021.626384

100. Xiang G, Hao S, Fu C, Hu W, Xie L, Wu Q, et al. The effect of coagulation factors in 2019 novel coronavirus patients: a systematic review and meta-analysis. *Medicine (Baltimore)*. (2021) 100:e24537. doi: 10.1097/MD.0000000000024537

101. Smadja DM, Bory OM, Diehl JL, Mareau A, Gendron N, Jannot AS, et al. Daily monitoring of D-dimer allows outcomes prediction in COVID-19. *TH Open*. (2021) 6:e21–5. doi: 10.1055/a-1709-5441

102. Smadja DM, Gendron N, Philippe A, Diehl JL, Ochat N, Bory O, et al. Fibrin monomers evaluation during hospitalization for COVID-19 is a predictive marker of in-hospital mortality. *Front Cardiovasc Med*. (2023) 10:1001530. doi: 10.3389/fcvm.2023.1001530

103. Liu Y, Tan W, Chen H, Zhu Y, Wan L, Jiang K, et al. Dynamic changes in lymphocyte subsets and parallel cytokine levels in patients with severe and critical COVID-19. *BMC Infect Dis*. (2021) 21:79. doi: 10.1186/s12879-021-05792-7

104. Han H, Ma Q, Li C, Liu R, Zhao L, Wang W, et al. Profiling serum cytokines in COVID-19 patients reveals IL-6 and IL-10 are disease severity predictors. *Emerg Microbes Infect*. (2020) 9:1123–30. doi: 10.1080/22221751.2020.1770129

105. Del Valle DM, Kim-Schulze S, Huang HH, Beckmann ND, Nirenberg S, Wang B, et al. An inflammatory cytokine signature predicts COVID-19 severity and survival. *Nat Med*. (2020) 26:1636–43. doi: 10.1038/s41591-020-1051-9

106. Liu Z, Li J, Chen D, Gao R, Zeng W, Chen S, et al. Dynamic Interleukin-6 level changes as a prognostic indicator in patients with COVID-19. *Front Pharmacol*. (2020) 11:1093. doi: 10.3389/fphar.2020.01093

107. Sakthivadivel V, Bohra GK, Maithilikarpagaselvi N, Khichar S, Meena M, Palanisamy N, et al. Association of Inflammatory Markers with COVID-19 outcome among hospitalized patients: experience from a tertiary healthcare Center in Western India. *Maedica (Bucur)*. (2021) 16:620–7. doi: 10.26574/maedica.2021.16.4.620

108. Santa Cruz A, Mendes-Frias A, Oliveira AI, Dias L, Matos AR, Carvalho A, et al. Interleukin-6 is a biomarker for the development of fatal severe acute respiratory syndrome coronavirus 2 pneumonia. *Front Immunol*. (2021) 12:613422. doi: 10.3389/fimmu.2021.613422

109. Tsikala Vafea M, Atalla E, Kalligeros M, Mylona EK, Shehadeh F, Mylonakis E. Chest CT findings in asymptomatic cases with COVID-19: a systematic review and meta-analysis. *Clin Radiol*. (2020) 75:876.e33–9. doi: 10.1016/j.crad.2020.07.025

110. Larici AR, Cicchetti G, Marano R, Bonomo L, Storto ML. COVID-19 pneumonia: current evidence of chest imaging features, evolution and prognosis. *Chin J Acad Radiol*. (2021) 4:229–40. doi: 10.1007/s42058-021-00068-0

111. Bhatraju PK, Ghassemieh BJ, Nichols M, Kim R, Jerome KR, Nalla AK, et al. Covid-19 in critically ill patients in the Seattle region - case series. *N Engl J Med*. (2020) 382:2012–22. doi: 10.1056/NEJMoa2004500

112. Fang X, Li S, Yu H, Wang P, Zhang Y, Chen Z, et al. Epidemiological, comorbidity factors with severity and prognosis of COVID-19: a systematic review and meta-analysis. *Aging (Albany NY)*. (2020) 12:12493–503. doi: 10.18632/aging.103579

113. Roncon L, Zuin M, Barco S, Valerio L, Zuliani G, Zonzin P, et al. Incidence of acute pulmonary embolism in COVID-19 patients: systematic review and meta-analysis. *Eur J Intern Med*. (2020) 82:29–37. doi: 10.1016/j.ejim.2020.09.006

114. Ackermann M, Kamp JC, Werlein C, Walsh CL, Stark H, Prade V, et al. The fatal trajectory of pulmonary COVID-19 is driven by lobular ischemia and fibrotic remodelling. *EBioMedicine*. (2022) 85:104296. doi: 10.1016/j.ebiom.2022.104296

115. Caruso D, Zerunian M, Polici M, Pucciarelli F, Polidori T, Rucci C, et al. Chest CT features of COVID-19 in Rome, Italy. *Radiology*. (2020) 296:E79–85. doi: 10.1148/radiol.2020201237

116. Bianco A, Valente T, Perrotta F, Stellato E, Brunese L, Wood BJ, et al. Study investigators. Remarkable vessel enlargement within lung consolidation in COVID-19 compared to AH1N1 pneumonia: a retrospective study in Italy. *Heliyon*. (2021) 7:e07112. doi: 10.1016/j.heliyon.2021.e07112

117. Poletti J, Bach M, Yang S, Sexauer R, Stieltjes B, Rotzinger DC, et al. Automated lung vessel segmentation reveals blood vessel volume redistribution in viral pneumonia. *Eur J Radiol*. (2022) 150:110259. doi: 10.1016/j.ejrad.2022.110259

118. Sundler Björkman L, Persson B, Aronsson D, Skattum L, Nordenfelt P, Egesten A. Comorbidities in hereditary angioedema-a population-based cohort study. *Clin Transl Allergy*. (2022) 12:e12135. doi: 10.1002/clt2.12135

119. Grover SP, Kawano T, Wan J, Tanratana P, Polai Z, Shim YJ, et al. C1 inhibitor deficiency enhances contact pathway-mediated activation of coagulation and venous thrombosis. *Blood*. (2023) 141:2390–401. doi: 10.1182/blood.2022018849

120. Charitos P, Heijnen IAFM, Egli A, Bassetti S, Trendelenburg M, Osthoff M. Functional activity of the complement system in hospitalized COVID-19 patients: a prospective cohort study. *Front Immunol*. (2021) 12:765330. doi: 10.3389/fimmu.2021.765330

121. Urwyler P, Moser S, Charitos P, Heijnen IAFM, Rudin M, Sommer G, et al. Treatment of COVID-19 with Conestat alfa, a regulator of the complement, contact activation and kallikrein-kinin system. *Front Immunol*. (2020) 11:2072. doi: 10.3389/fimmu.2020.02072

122. Medjeral-Thomas NR, Troldborg A, Hansen AG, Pihl R, Clarke CL, Peters JE, et al. Protease inhibitor plasma concentrations associate with COVID-19 infection. *Oxf Open Immunol*. (2021) 2:iqab014. doi: 10.1093/oxfimm/iqab014

123. Weidmann H, Heikaus L, Long AT, Naudin C, Schlüter H, Renné T. The plasma contact system, a protease cascade at the nexus of inflammation, coagulation and immunity. *Biochim Biophys Acta Mol Cell Res*. (2017) 1864:2118–27. doi: 10.1016/j.bbamcr.2017.07.009

124. Joshi D, Manohar S, Goel G, Saigal S, Pakhare AP, Goyal A. Adequate antithrombin III level predicts survival in severe COVID-19 pneumonia. *Cureus*. (2021) 13:e18538. doi: 10.7759/cureus.18538

125. Gazzaruso C, Paolozzi E, Valenti C, Brocchetta M, Naldani D, Grignani C, et al. Association between antithrombin and mortality in patients with COVID-19. A possible link with obesity. *Nutr Metab Cardiovasc Dis*. (2020) 30:1914–9. doi: 10.1016/j.numecd.2020.07.040

126. Anaklı İ, Ergin Özcan P, Polat Ö, Orhun G, Alay GH, Tuna V, et al. Prognostic value of antithrombin levels in COVID-19 patients and impact of fresh frozen plasma treatment: a retrospective study. *Turk J Haematol*. (2021) 38:15–21. doi: 10.4274/tjh.galenos.2021.2020.0695

127. Schrick D, Tőkés-Füzesi M, Réger B, Molnár T. Plasma fibrinogen independently predicts hypofibrinolysis in severe COVID-19. *Meta*. (2021) 11:826. doi: 10.3390/metabo11120826

128. Hammer S, Häberle H, Schlensak C, Bitzer M, Malek NP, Handgretinger R, et al. Severe SARS-CoV-2 infection inhibits fibrinolysis leading to changes in viscoelastic properties of blood clot: a descriptive study of fibrinolysis in COVID-19. *Thromb Haemost*. (2021) 121:1417–26. doi: 10.1055/a-1400-6034

129. de Laat-Kremers R, De Jongh R, Ninivaggi M, Fiolet A, Fijnheer R, Remijn J, et al. Coagulation parameters predict COVID-19-related thrombosis in a neural network with a positive predictive value of 98. *Front Immunol*. (2022) 13:977443. doi: 10.3389/fimmu.2022.977443

130. Mansour E, Palma AC, Ulaf RG, Ribeiro LC, Bernardes AF, Nunes TA, et al. Safety and outcomes associated with the pharmacological inhibition of the kinin-kallikrein system in severe COVID-19. *Viruses*. (2021) 13:309. doi: 10.3390/v13020309

131. Banerji A, Riedl MA, Bernstein JA, Cicardi M, Longhurst HJ, Zuraw BL, et al. HELP investigators. Effect of Lanadelumab compared with placebo on prevention of hereditary angioedema attacks: a randomized clinical trial. *JAMA*. (2018) 320:2108–21. doi: 10.1001/jama.2018.16773

132. Zuraw B, Lumry WR, Johnston DT, Aygören-Pürsün E, Banerji A, Bernstein JA, et al. Oral once-daily berotralstat for the prevention of hereditary angioedema attacks: a randomized, double-blind, placebo-controlled phase 3 trial. *J Allergy Clin Immunol*. (2021) 148:164–172.e9. doi: 10.1016/j.jaci.2020.10.015

133. Levy RJ, Lumry WR, McNeil DL, Li HH, Campion M, Horn PT, et al. EDEMA4: a phase 3, double-blind study of subcutaneous ecallantide treatment for acute attacks of hereditary angioedema. *Ann Allergy Asthma Immunol*. (2010) 104:523–9. doi: 10.1016/j.anai.2010.04.012

134. Fijen LM, Riedl MA, Bordone L, Bernstein JA, Raasch J, Tachdjian R, et al. Inhibition of Prekallikrein for hereditary angioedema. *N Engl J Med*. (2022) 386:1026–33. doi: 10.1056/NEJMoa2109329

135. McKenzie A, Roberts A, Malandkar S, Feuersenger H, Panousis C, Pawaskar D. A phase I, first-in-human, randomized dose-escalation study of anti-activated factor XII monoclonal antibody garadacimab. *Clin Transl Sci*. (2022) 15:626–37. doi: 10.1111/cts.13180

136. Lumry WR, Farkas H, Moldovan D, Toubi E, Baptista J, Craig T, et al. Icatibant for multiple hereditary angioedema attacks across the controlled and open-label extension phases of FAST-3. *Int Arch Allergy Immunol*. (2015) 168:44–55. doi: 10.1159/000441060

137. Cicardi M, Banerji A, Bracho F, Malbrán A, Rosenkranz B, Riedl M, et al. Icatibant, a new bradykinin-receptor antagonist, in hereditary angioedema. *N Engl J Med*. (2010) 363:532–41. doi: 10.1056/NEJMoa0906393

138. Leach JK, Spencer K, Mascelli M, McCauley TG. Pharmacokinetics of single and repeat doses of icatibant. *Clin Pharmacol Drug Dev*. (2015) 4:105–11. doi: 10.1002/cpdd.138

139. Pecori D, Della Siega P, Sozio E, Barbano E, Mazzoran L, Zanichelli A, et al. Icatibant in severe acute respiratory syndrome coronavirus 2 infection: a case report. *J Investig Allergol Clin Immunol*. (2021) 31:451–2. doi: 10.18176/jiaci.0659

140. Giol J, Jacob J, Llopis F, Lleonart R, Ruiz Esteve F, Malchair P. Exceptional treatment of COVID-19 pneumonia with icatibant. *Emergencias*. (2022) 34:159–60.

141. Van de Veerdonk FL, Kouijzer IJE, de Nooijer AH, van der Hoeven HG, Maas C, Netea MG, et al. Outcomes associated with use of a kinin B2 receptor antagonist among patients with COVID-19. *JAMA Netw Open*. (2020) 3:e2017708. doi: 10.1001/jamanetworkopen.2020.17708

142. Malchair P, Giol J, García V, Rodríguez O, Ruibal JC, Zarauza A, et al. Three-day Icatibant on top of standard Care in Patients with Coronavirus Disease 2019 pneumonia: a randomized, open-label, phase 2, Proof-of-Concept. *Trial Clin Infect Dis*. (2023) 76:1784–92. doi: 10.1093/cid/ciac984

143. I-SPY COVID Consortium. Report of the first seven agents in the I-SPY COVID trial: a phase 2, open label, adaptive platform randomised controlled trial. *EClinicalMedicine*. (2023) 58:101889. doi: 10.1016/j.eclinm.2023.101889

144. Fein AM, Bernard GR, Criner GJ, Fletcher EC, Good JT, Knaus WA, et al. Treatment of severe systemic inflammatory response syndrome and sepsis with a novel bradykinin antagonist, deltibant (CP-0127). Results of a randomized, double-blind, placebo-controlled trial. CP-0127 SIRS and sepsis study group. *JAMA*. (1997) 277:482–7. doi: 10.1001/jama.1997.03540300050033

Frontiers in Medicine

Translating medical research and innovation into improved patient care

A multidisciplinary journal which advances our medical knowledge. It supports the translation of scientific advances into new therapies and diagnostic tools that will improve patient care.

Discover the latest Research Topics

See more →

Frontiers

Avenue du Tribunal-Fédéral 34
1005 Lausanne, Switzerland
frontiersin.org

Contact us

+41 (0)21 510 17 00
frontiersin.org/about/contact